In Vivo Monitoring of Photodynamic Therapy; from lab to clinic

ISBN: 978-90-9024892-9

Studies presented in this thesis were performed at the center of optical diagnostics and therapy (CODT) of the Erasmus medical center in Rotterdam, The Netherlands.

Publication of this thesis was for a part financially supported by the ErasmusMC.

Cover design: S.A. van Hoof.

Printed by PrintPartners Ipskamp, Enschede

In Vivo Monitoring of Photodynamic Therapy; from lab to clinic

In vivo monitoren van fotodynamische therapie; van lab naar kliniek

Proefschrift

ter verkrijging van de graad van doctor aan de
Erasmus Universiteit Rotterdam
op gezag van de
rector magnificus

Prof.dr. H.G. Schmidt

en volgens het besluit van het College voor Promoties.

De openbare verdediging zal plaatsvinden op

vrijdag 15 januari 2010 om 11.30

door

Bastiaan Kruijt

geboren te Rotterdam

Promotie commissie

Promotor:	Prof.dr. H.J.C.M. Sterenborg
Overige leden:	Prof.dr. P.C. Levendag Prof.dr. B. Heijmen Dr. G.C. van Rhoon
Copromotoren:	Dr. D.J. Robinson Dr. A. Amelink

Contents

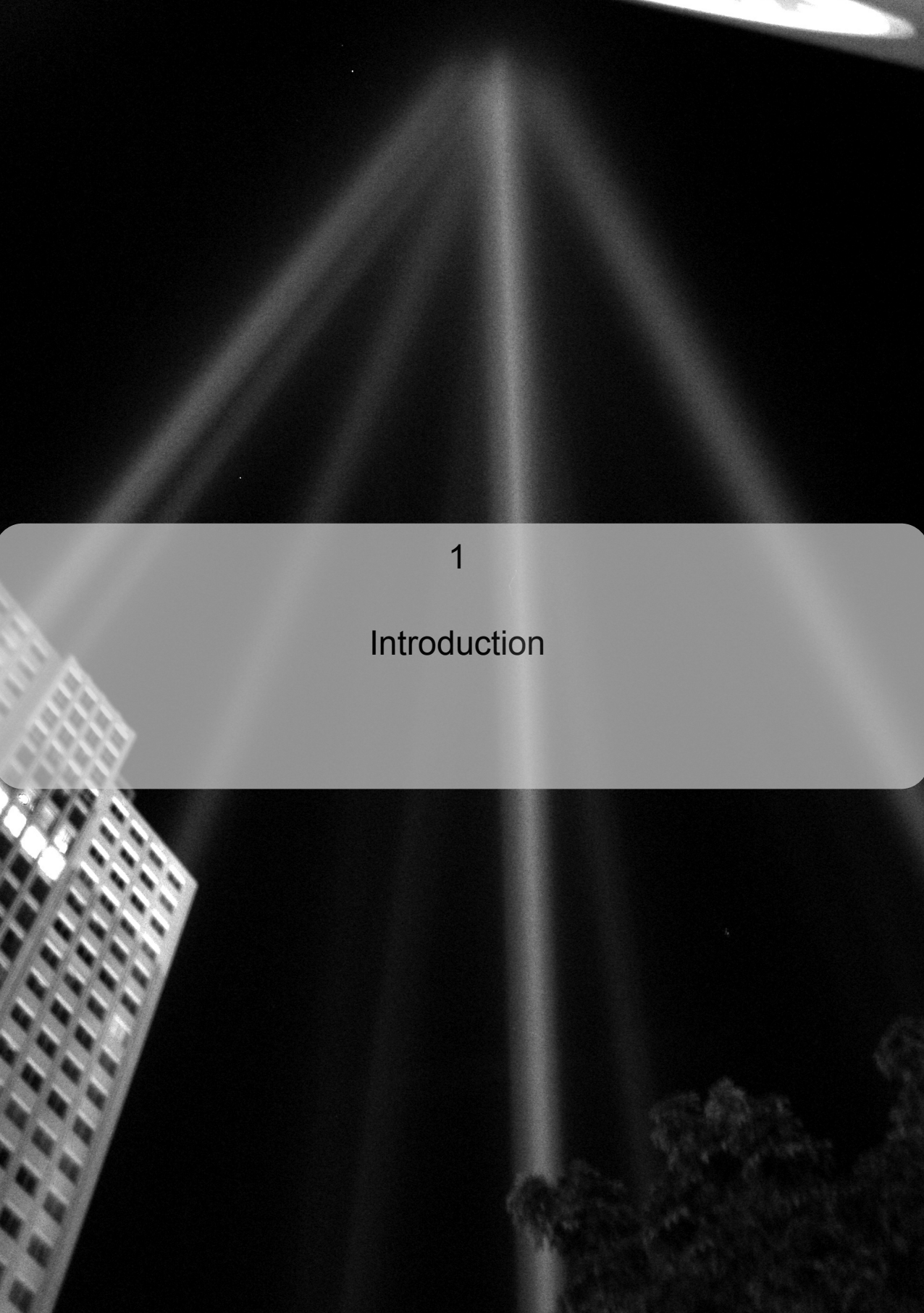

1

Introduction

General introduction

Photodynamic therapy (PDT) is an emerging clinical treatment modality, which utilizes light, oxygen and a light sensitive drug (the photosensitizer), for curative and palliative treatment of a variety of malignant and non-malignant conditions tumors. PDT is frequently used in the clinic for treatment of superficial skin lesions by superficial illumination of the lesion after the topical administration of a photosensitizer or its precursor. However, PDT is also under investigation for treatment of larger tumors volumes in regions such as the head and neck[1,2] and the prostate[3] by inserting optic-fibers in the tumor volume for the delivery of the treatment light.
The therapeutic effect in PDT is induced by the interaction between the tissue and reactive oxygen radicals. These reactive oxygen radicals, predominantly singlet oxygen, are formed by the interaction of photosensitizer, light (of an appropriate wavelength) and oxygen in the tissue. The deposited PDT dose is the amount of light that actually interacts with the photosensitizer that leads to formation of reactive oxygen species responsible for inducing tissue response. Note that this is different from the actual amount of light delivered to the tissue since not all of the light delivered interacts with the photosensitizer scattering and absorption of the tissue. In addition, based on the photosensitizer's ability to form reactive oxygen species (ROS) only a percentage of light that interacts with the photosensitizer lead to formation of ROS. Also there is a difference between the actual delivered light dose and the intended delivered light dose. Where the intended delivered light dose is set by the clinician to be delivered. Only by measuring the amount of light in situ it is possible to determine the actual delivered light dose. So although this intended light dose is kept the same in individuals undergoing treatment, the actual delivered light dose and the deposited PDT dose can vary due to biological variation and the dynamic interaction between light, photosensitizer and oxygen in tissue. Inter individual variations in deposited PDT-dose yield variations in induced tissue response and treatment outcome. For this reason it is necessary to determine and monitor the deposited PDT dose during therapeutic illumination.
Dosimetry is used to monitor parameters during the course of treatment that are of importance to determine the deposited PDT dose. In monitoring dose metric parameters we differentiate between explicit and implicit parameters. Explicit dose metric parameters yield information on the basic parameters necessary for PDT, such as delivered light treatment parameters, administered photosensitizer concentration, and available oxygen concentration. Implicit dose metric parameters implicitly yield information on several or all (explicit) parameters involved during PDT[4] (figure 1). Whereas monitoring the explicit parameters alone does not provide sufficient information on deposited dose due to the complex and dynamic relationship between each of these parameters, the addition of implicit monitoring may give additional information on deposited PDT-dose.

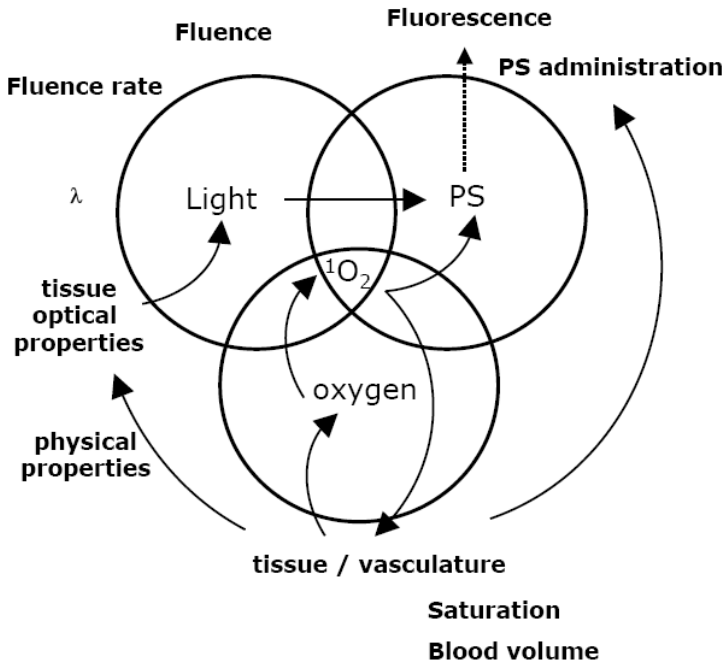

Figure 1. Schematic representation of parameters involved during PDT.

Photosensitizers

The phototoxic effect in PDT is induced by photochemical reactions initiated by the absorption of light of an appropriate wavelength by the photosensitizer. Upon absorption of light by the photosensitizer it is excited from the normal ground state to an excited singlet state (figure 2). This excited singlet state is short-lived and the photosensitizer can return to its initial ground state by releasing the absorbed energy via one of two options. The first option is that the absorbed energy is emitted, via an additional energy state, as light of lower energy and thus higher wavelength than the light used to initially excite the photosensitizer. The second option for the photosensitizer is to transfer its energy via intersystem crossing to an excited triplet state of the photosensitizer. This triplet state decays slower than the singlet state allowing the excited photosensitizer to interact with its environment and transfer its energy via collisions onto other molecular oxygen forming highly reactive singlet oxygen radicals (type II reaction) or on other molecules forming radicals (type I reaction)[5]. Whether a photosensitizer forms radicals via a type I or II reaction (or both) depends on the properties of the photosensitizer and its environment (availability of molecular oxygen). In PDT the type II reaction is preferred over the type I reaction due to the high reactivity of singlet oxygen.

The fluorescence exhibited by a photosensitizer can be used to determine distribution and the relative amount of photosensitizer in tissue. In addition, the degradation of photosensitizer by its formed radicals can be monitored by the decay in exhibited fluorescence during therapeutic illumination and may provide information on radical formation during treatment[6].

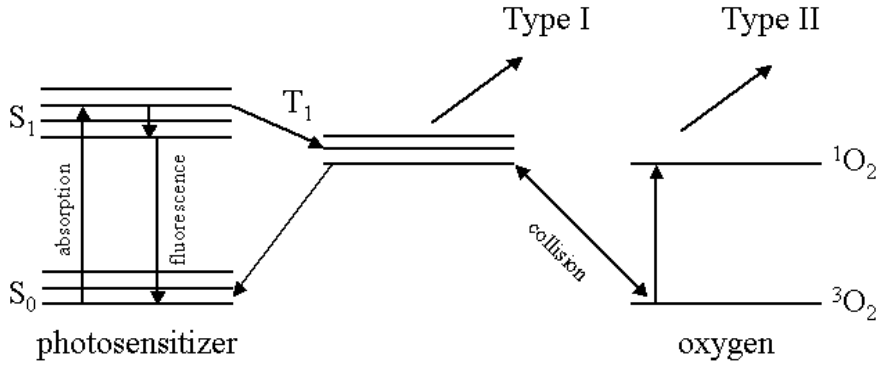

Figure 2. Schematic representation of energy transfer in PDT.

In this thesis the scope is limited to two clinical relevant photosensitizers namely aminolevelunic (ALA) induced protoporphyrin IX (PpIX) and meta-tetrahydroxyphenylchlorin (m-THPC). Both photosensitizers have the ability to fluoresce. Typical fluorescence spectra of PpIX (black solid line) and m-THPC (grey solid line) are shown in figure 3.

The photosensitizer PpIX is formed through the existing haem biosynthetic pathway in cells from the administered pre-cursor ALA which on itself is not a photosensitizer. The exogenous administration of ALA will lead to accumulation of the photosensitizer PpIX in cells yielding maximum concentrations 2-6 hours post administration. The therapeutic effect of PpIX-PDT is predominantly mediated through singlet oxygen. Since singlet oxygen has a short life time[7] and mitochondria are involved in the conversion of ALA to PpIX, these are the main cell structures targeted by singlet oxygen during illumination.

In contrary to ALA induced PpIX, m-THPC is already a pre-formed photosensitizer. M-THPC accumulates in both normal and tumor tissue so this requires selective illumination of the treatment volume. Although a drug light interval of 96 hours yield optimal tumor to normal ratio, other drug light intervals are under investigation for m-THPC-PDT. Localization of m-THPC is dependent on the drug light interval[8,9]. For short drug light intervals m-THPC is predominantly localized in the vasculature. In time, m-THPC diffuses from the vasculature into the cells for longer drug light intervals, 48 to 96 hours. The therapeutic effect of m-THPC-PDT is believed to be mediated by a combination of type I and II reactions.

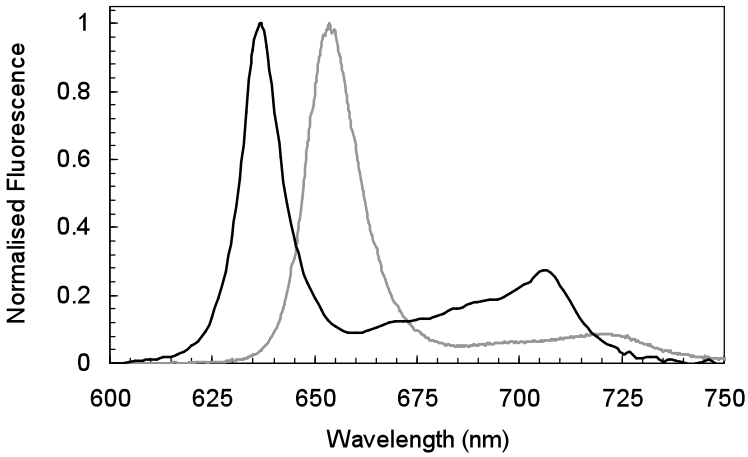

Figure 3. A typical long wavelength PpIX fluorescence spectrum acquired in vivo in the rat esophagus using 405 nm excitation (black solid line) and a typical m-THPC fluorescence spectrum acquired in vivo in the rat abdominal muscle using 514 nm excitation (grey solid line).

Light treatment parameters

There are different methods, depending on the treatment geometry, to deliver light to the treatment volume. For thin superficial lesions, for example skin lesions, a simple flat field illumination technique can be utilized using a lens system or a (lens-tip) fiber. Another possibility is to use a lens-tip fiber or linear diffuser to irradiate superficial lesions in hollow cavities or organs such as the nasopharynx[10], esophagus[11] and anal cavity[12].

A difficulty in these treatments is that the actual fluence rate can vary from the intended fluence rate due to the integrating sphere effect. Here the variation in fluence rate depends on the geometry of the cavity. For optimal light delivery to intra cavital tissue dedicated light delivery applicators are designed to both deliver light as well as for monitoring fluence and fluence rate[10,13].

Large tumors are difficult to treat with PDT using superficial illumination due to the penetration depth of light. A possibility is to interstitially insert optic fibers to deliver the therapeutic light in the tumor volume. Treatment planning is necessary to determine the amount of fibers and the placement of fibers within the treatment volume. The distance between the fibers and the amount of fibers necessary for treatment depend on the penetration depth of the therapeutic light.

The therapeutic wavelength is chosen to have optimal penetration depth and according to the wavelength(s) where the photosensitizer effectively absorbs light. Usually wavelengths beyond the absorption bands of hemoglobin, the main absorber in tissue in the visible wavelength range, are utilized. In case of PpIX this is 635 nm and for m-THPC this is 652 nm.

The therapeutic effect of PDT is mediated by singlet oxygen, in this process oxygen is consumed. The rate by which singlet oxygen is produced and oxygen is consumed

depends on the intensity of light or fluence rate, and on the concentration of photosensitizer. High fluence rates will lead to rapid depletion of available oxygen in the tissue and thereby decreasing the efficacy of the treatment[6,14]. For this reason fluence rates are chosen not to entirely deplete the available oxygen during the treatment. Here the treatment time is dependent on the amount of light, fluence, necessary for a particular photosensitizer to induce sufficient response. Also delivering the fluence in a single or fractionated can influence PDT induced response[15].

Tissue optical properties

Propagation of light in tissue is dependent on the optical properties, light scattering and absorption, of tissue. Both scattering and absorption in tissue are wavelength dependent, meaning that different values for scattering and absorption coefficients can be expected at different wavelengths. Figure 4 shows a typical reflectance spectrum and contains information on absorption and scattering properties of tissue. Absorption due to hemoglobin, the predominant absorber in tissue, is visible by the absorption dips around 420, 540 and 580 nm. In the same figure also the scattering without absorption is shown. Scattering of light is caused by differences of refractive index in tissue on subcellular level. The direction of scattering is reported by the anisotropy factor, where 0 means isotropic scattering and -1 and 1 total backward and forward scattering, respectively. Scattering in tissue is forward directed and has an isotropy factor between 0.7 to 0.95.

Tissue is optically heterogeneous, tissue optical properties can vary between and within different tissue by variations in tissue physiology, such as blood content and saturation. Moreover during therapeutic illumination several studies have shown that the fluence rate can vary due to PDT-induced changes in tissue optical properties[10].

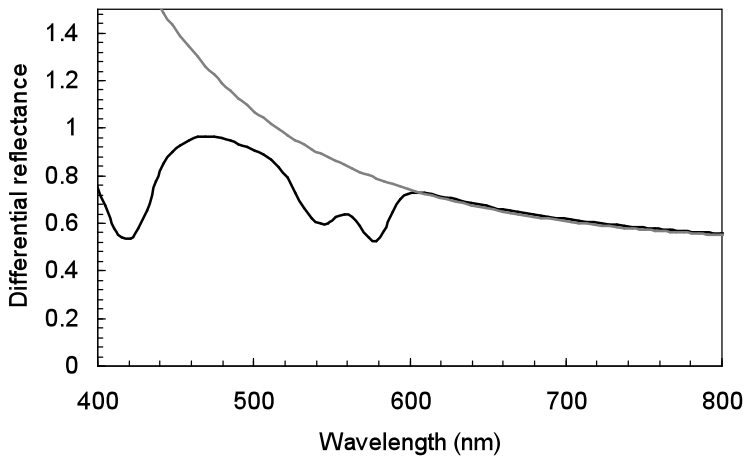

Figure 4. The solid black line represents a typical differential reflectance spectrum containing both scattering and absorption features. The absorption dips due to the presence of oxy- and deoxyhemoglobin at 420, 540 and 580 nm are clearly visible. The gray line represents a differential reflectance spectrum without presence of any absorbers.

Dosimetry

In PDT it is important to have information on the PDT-dose deposited since this yields information on the PDT induced tissue response. It is not only of importance to determine if sufficient PDT dose is delivered to the treatment volume but also to monitor PDT dose delivered in surrounding healthy tissue. Most clinically approved photosensitizers are not tumor specific, they accumulate in both the tumor and the surrounding healthy tissue. This requires specific light delivery during treatment where the aim is to deliver sufficient PDT-dose to the treatment volume while keeping this as low as possible for the surrounding healthy tissue to minimize or avoid adverse side effects. For this reason parameters that yield information on PDT dose deposited are measured in both treatment and surrounding healthy tissue during therapeutic illumination.

Of the three explicit dose metric parameters (fluence (rate) and administered photosensitizer dose), fluence and fluence rate can be monitored by placing calibrated fiber optic probes in or near regions of interest. However this alone is not sufficient to determine PDT dose. High fluence rates increases oxygen consumption and may lead to faster oxygen depletion in comparison to lower fluence rates. PDT efficacy decreases with increasing fluence rate[6,14]. For this reason it is necessary to monitor tissue oxygenation as to prevent fast oxygen depletion by using (too) high fluence rates.

Monitoring tissue oxygenation in vivo is complicated and requires invasive non-optical techniques using small fragile needles. However, it is possible to implicitly monitor oxygenation by measuring the blood saturation using optical techniques. In addition to monitoring oxygen variations due to therapeutic illumination, differences in blood saturation measured during the course of treatment (pre, during and post PDT) can yield information on vascular and or cellular PDT induced response[16].

Several studies apply diffuse reflectance spectroscopy using visible or near infrared light, as an optical method to determine blood saturation during PDT[17,18]. A disadvantage and potential source of error in diffuse reflectance spectroscopy is that the path-length of the photons traveling in tissue is unknown and can vary due to variations in tissue optical properties during therapeutic illumination. To overcome this problem differential path length spectroscopy (DPS) was developed which features spectral measurements over a known path length by subtraction of two signals that contain the same contribution from long path length photons but different contributions from short path length photons[19,20]. This method is insensitive to expected variations in tissue optical properties during illumination. Figure 4 shows a typical DPS spectrum (black line) with absorption due to hemoglobin, the gray line represents tissue scattering without any absorbers.

Another issue with both diffuse and differential reflectance spectroscopy is that it is not possible to monitor with the treatment light on since the intense treatment light overexposes the spectrographs. This limits measurements to before and after illumination[21]. Another possibility is to interrupt the therapeutic illumination at regular intervals to measure reflectance spectra. However, it is unknown whether the regular interruptions of the therapeutic light have an influence on the blood saturation and the tissue response (fractionated illumination). Obviously it is necessary to overcome this

problem so that it will be possible to monitor blood saturation during therapeutic illumination without disturbing the light treatment parameters.
In addition to fluence (rate) and saturation measurements it is possible to use the photosensitizer fluorescence as a relative estimate for photosensitizer concentration. During the therapeutic illumination the photosensitizer concentration will degrade due to interaction with the ROS, which is exhibited by a decrease in photosensitizer fluorescence. Hence the photobleaching may report on ROS produced during therapeutic illumination[6,22]. For PpIX the rate of photobleaching has shown to be indicative for PDT-induced response. However, for both PpIX and m-THPC the most intense fluorescence peak coincides with the therapeutic wavelength (635 and 652 nm, respectively) which makes it difficult to monitor during PDT. A possible option is to monitor fluorescence in the long wavelength region beyond the therapeutic wavelength. Both PpIX and m-THPC exhibit a second, less intense, fluorescence peak in the long wavelength region (figure 3).
Its is therefore potentially very useful to have a quantitative measure of the photosensitizer concentrations in tissue during therapeutic illumination. Several studies have investigated reflectance or absorption spectroscopy to determine photosensitizer concentration, where the amount of absorbed light is a measure for concentration[23,24]. A problem with this method is that the dynamic range of measuring concentration is limited due to limitations on integration time. Long integration times may overexpose the spectrograph in spectral regions where there is no absorption and there is a limit for low integration times for spectrographs. Another source of error is that the white light used in reflectance/absorption spectroscopy excites the photosensitizer that is measured[25]. Hence the detected light consists of both reflected white light and photosensitizer fluorescence. The most important issue is that this method cannot be applied when the treatment light is on.
Fluorescence measurements are clearly not hampered by induced fluorescence or integration time. In order to go from relative to absolute estimates on photosensitizer concentration it is necessary to correct the fluorescence for tissue optical properties[26,27]. In addition it would be useful to monitor fluorescence over the same volume as over which blood saturation is measured with DPS, to determine a possible relationship between variations in blood saturation and absolute photosensitizer concentration during illumination. For this reason we investigated the potential of fluorescence differential path length spectroscopy, based on the principles of DPS[19].
Currently it is also possible to directly monitor singlet oxygen in vivo by its luminescence at 1270 nm using imaging setups[22]. However, the weak luminescence signal combined with the low quantum efficiency of the photomultipliers used in this wavelength region poses a challenge for acquiring sufficient singlet oxygen luminescence signal through an optical fiber.

PDT induced tissue response

In the context of monitoring, optimizing and standardizing PDT it is useful to investigate and quantify PDT-induced tissue response. In pre-clinical models PDT induced tissue damaged is determined at one or multiple time points after therapeutic illumination. There are several methods to determine PDT induced response

dependent on the pre-clinical model, from determination of tumor growth delay[28] and visual scoring[15] on a macroscopical level to histological assessment of the histological response[11].
PDT-induced response based on macroscopical measurements, such as tumor growth delay and visual scoring, have the advantage that the response and healing in the same treated volume can be observed over a long time period. Quantification of PDT-induced response is performed by assessment of the tumor volume in growth delay studies or by visual scoring the tissue on a pre-determined scoring scale[15,28]. However, these methods are limited to already exposed tissue, such as the skin.
To determine PDT response over a histological scale the treated tissue is excised at a pre-determined time point post PDT. This does not allow to monitor the same treated volume over a long time period, although it is possible to excise treated tissue from different individuals at different time points. Histological examination of treated tissue provides insight on the different types of response in PDT, such as inflammation, edema formation, apoptosis, and necrosis[11]. PDT induced response is then quantified by scoring the tissue according to a pre-determined scoring scale for each of the types of response observed.
The treatment geometry in the majority of response studies is two dimensional regarding light treatment parameters, meaning that the fluence rate is constant throughout the treatment volume and the same light dose is delivered throughout this volume[11,15,28]. It becomes more complex when the light treatment parameters in the treatment geometry become dependent on depth or distance from the treatment fiber since the PDT-induced response will also become dependent on depth. This is the case for interstitial PDT in large treatment volumes. For quantifying response in these interstitial environments it becomes necessary to quantify the severity of response as a function of distance from the treatment fiber.

Translation to the clinic
A final step is to transfer the techniques validated in pre-clinical studies to the clinic and translate the data acquired in pre-clinical studies to the clinical situation. The latter part is difficult due to biological differences between humans and animals used in pre-clinical studies. Therefore, when the techniques have been validated, monitoring during clinical treatments is necessary for further understanding the implications of the monitored parameters and the mechanisms of action in clinical PDT. The first step is to continue passive monitoring of parameters to understand the inter individual variations in treatment outcome in clinical PDT. Based on the results of monitoring during therapeutic illumination, clinical PDT can be optimized to yield maximum response and to minimize inter individual variations in response while minimizing the risk on potential adverse side effects.

Aim and outline of this thesis

The aim of this study was to investigate the possibility of determining the deposited PDT dose by explicit and implicit monitoring of parameters during therapeutic illumination and to compare these to PDT-induced response. This required investigation and validation of techniques that might aid in determining the deposited PDT dose and understanding the mechanisms of action in PDT using different photosensitizers. Secondly, it was necessary to investigate possibilities to monitor different parameters, utilizing the investigated and validated techniques, during therapeutic illumination without changing the light treatment protocol. In addition it was necessary to develop pre-clinical models suitable for both monitoring during therapeutic illumination and investigate histological response after PDT.

Chapter 2 investigated the feasibility of laser speckle imaging as a technique of measuring blood flow during PDT. Measuring blood flow in combination with measurements on blood volume and saturation gives an indication on oxygen delivered to the tissue during PDT.

Chapters 3, 4, and 5 describe the validation process of fluorescence differential pathlength spectroscopy (FDPS) to quantify fluorescence and possibly photosensitizer concentration. The first step is to validate quantitative measurements of fluorophores using FDPS in optical phantoms as described in chapter 3. Secondly FDPS is validated in vivo using the exogenous fluorophore mTHPC by comparing the optically measured concentration of mTHPC in tissue against the actual concentration measured by chemical extraction, chapter 5. The method of chemical extraction is described in detail in chapter 4.

Chapter 6 shows the application of FDPS next to fluence rate and fluorescence measurements during PDT in the rat esophagus. The aim of this study was to understand the two phased photobleaching and its implications regarding tissue response for ALA induced PpIX-PDT in the rat esophagus.

Chapter 7 investigates the feasibility of monitoring saturation and blood volume using DPS combined with fluence rate and fluorescence measurements during mTHPC-PDT without interruption to the illumination. For this study a preclinical interstitial PDT model was used.

In chapter 8 we extend our investigations of interstitial m-THPC-PDT in the pre-clinical model. In addition to monitoring parameters during PDT we also quantified tissue response 48 hours after interstitial illumination using clinical relevant fluence rates and doses. For this the animal model presented in chapter 7 was slightly adapted to be able to histologically determine PDT-induced response as a function of distance from the treatment fiber in an interstitial PDT geometry.

Chapter 9 demonstrates the translation of the techniques developed in the lab and used in preclinical studies described in chapters 7 and 8, to the clinical setting.

Saturation, blood volume, fluence rate and fluorescence were monitored during m-THPC-PDT in patients with anal intraepithelial neoplasia grade 3 (AINIII). The fluence rate was set based on in vivo fluence rate measurements and treatment was stopped when the in vivo measured dose was achieved.

In chapter 10 the results and general conclusions of above studies are summarized.

References

1. Copper MP, Tan IB, Oppelaar H, Ruevekamp MC, Stewart FA. Meta-tetra(hydroxyphenyl)chlorin photodynamic therapy in early-stage squamous cell carcinoma of the head and neck. Arch Otolaryngol Head Neck Surg. 2003; 129:709-711.

2. Lou PJ, Jäger HR, Jones L, Theodossy T, Bown SG, Hopper C. Interstitial photodynamic therapy as salvage treatment for recurrent head and neck cancer. Br J Cancer. 2004; 91:441-446.

3. Moore CM, Nathan TR, Lees WR, Mosse CA, Freeman A, Emberton M, Bown SG. Photodynamic therapy using meso tetra hydroxy phenyl chlorin (m-THPC) in early prostate cancer. Lasers Surg Med. 2006; 38:356-363.

4. Wilson BC, Patterson MS, Lilge L. Implicit and explicit dosimetry in photodynamic therapy: a new paradigm. Lasers Med. Sci. 1997; 12:182-99

5. Ochsner M, Photophysical and photobiological processes in the photodynamic therapy of tumours. J Photochem Photobiol B. 1997; 39:1-18.

6. Robinson DJ, de Bruijn HS, van der Veen N, Stringer MR, Brown SB, Star WM. Fluorescence photobleaching of ALA-induced protoporphyrin IX during photodynamic therapy of normal hairless mouse skin: the effect of light dose and irradiance and the resulting biological effect. Photochem Photobiol. 1998; 67:140-149.

7. Moan J, Berg K. The photodegradation of porphyrins in cells can be used to estimate the lifetime of singlet oxygen. Photochem Photobiol. 1991; 53:549-53.

8. Jones HJ, Vernon DI, Brown SB. Photodynamic therapy effect of m-THPC (Foscan) in vivo: correlation with pharmacokinetics. Br J Cancer. 2003; 89:398-404.

9. Cramers P, Ruevekamp M, Oppelaar H, Dalesio O, Baas P, Stewart FA. Foscan uptake and tissue distribution in relation to photodynamic efficacy. Br J Cancer. 2003; 88:283-290.

10. van Veen RL, Nyst H, Rai Indrasari S, Adham Yudharto M, Robinson DJ, Tan IB, Meewis C, Peters R, Spaniol S, Stewart FA, Levendag PC, Sterenborg HJ. In vivo fluence rate measurements during Foscan-mediated photodynamic therapy of persistent and recurrent nasopharyngeal carcinomas using a dedicated light applicator. J Biomed Opt. 2006;11:041107.

11. Boere IA, Robinson DJ, de Bruijn HS, Kluin J, Tilanus HW, Sterenborg HJ, de Bruin RW. Protoporphyrin IX fluorescence photobleaching and the response of rat Barrett's esophagus following 5-aminolevulinic acid photodynamic therapy. Photochem. Photobiol. 2006; 82:1638-1644.

12. van der Snoek EM, Amelink A, van der Ende ME, den Hollander JC, den Hollander JG, Kroon FP, Vriesendorp R, Neumann HAM, Robinson DJ. Photodynamic therapy with topical metatetrahydroxychlorin (fosgel®) is ineffective for the treatment of anal intraepithelial neoplasia, grade III. J Acquir Immune Defic Syndr. in press.

13. Kruijt B, de Bruijn HS, van der Ploeg-van den Heuvel A, de Bruin RWF, Sterenborg HJCM, Amelink A, Robinson DJ. Monitoring ALA-induced PpIX-photodynamic therapy in the rat

esophagus using fluorescence and reflectance spectroscopy. Photochem Photobiol. 2008; 84:1515-1527.
14. Finlay JC, Conover DL, Hull EL, Foster TH. Porphyrin bleaching and PDT-induced spectral changes are irradiance dependent in ALA-sensitized normal rat skin in vivo. Photochem Photobiol. 2001; 73:54-63.
15. de Bruijn HS, van der Ploeg-van den Heuvel A, Sterenborg HJ, Robinson DJ. Fractionated illumination after topical application of 5-aminolevulinic acid on normal skin of hairless mice: the influence of the dark interval. J Photochem Photobiol B. 2006; 85:184-90.
16. Wang HW, Putt ME, Emanuele MJ, Shin DB, Glatstein E, Yodh AG, Busch TM. Treatment-induced changes in tumor oxygenation predict photodynamic therapy outcome. Cancer Res. 2004; 64:7553-7561.
17. Woodhams JH, Kunz L, Bown SG, MacRobert AJ. Correlation of real-time haemoglobin oxygen saturation monitoring during photodynamic therapy with microvascular effects and tissue necrosis in normal rat liver. Br J Cancer. 2004; 91:788-794.
18. Johansson A, Johansson T, Thompson MS, Bendsoe N, Svanberg K, Svanberg S, Andersson-Engels S. In vivo measurement of parameters of dosimetric importance during interstitial photodynamic therapy of thick skin tumors. J Biomed Opt. 2006;11:34029.
19. Amelink A, Kruijt B, Robinson DJ, Sterenborg HJ. Quantitative fluorescence spectroscopy in turbid media using fluorescence differential path length spectroscopy. J Biomed Opt. 2008; 13:054051.
20. Amelink A, Sterenborg HJ. Measurement of the local optical properties of turbid media by differential path-length spectroscopy. Appl Opt. 2004; 43:3048-3054.
21. Weersink RA, Bogaards A, Gertner M, Davidson SR, Zhang K, Netchev G, Trachtenberg J, Wilson BC. Techniques for delivery and monitoring of TOOKAD (WST09)-mediated photodynamic therapy of the prostate: clinical experience and practicalities. J Photochem Photobiol B. 2005; 79:211-222.
22. Niedre MJ, Yu CS, Patterson MS, Wilson BC. Singlet oxygen luminescence as an in vivo photodynamic therapy dose metric: validation in normal mouse skin with topical amino-levulinic acid. Br J Cancer. 2005; 92:298-304
23. Mourant JR, Johnson TM, Los G, Bigio IJ. Non-invasive measurement of chemotherapy drug concentrations in tissue: preliminary demonstrations of in vivo measurements. Phys. Med. Biol. 1999; 44:1397-1417.
24. Kanick SC, Eiseman JL, Joseph E, Guo J, Parker RS. Noninvasive and nondestructive optical spectroscopic measurement of motexafin gadolinium in mouse tissues: comparison to high-performance liquid chromatography. J. Photochem. Photobiol. B. 2007; 88:90-104 (2007).
25. Johansson A, Svensson J, Bendsoe N, Svanberg K, Alexandratou E, Kyriazi M, Yova D, Gräfe S, Trebst T, Andersson-Engels S. Fluorescence and absorption assessment of a lipid mTHPC formulation following topical application in a non-melanotic skin tumor model. J. Biomed. Opt. 2007; 12:034026.
26. Zhang Q, Müller MG, Wu J, Feld MS. Turbidity-free fluorescence spectroscopy of biological tissue. Opt. Lett. 2000; 25:1451-1453.
27. Müller MG, Valdez TA, Georgakoudi I, Backman V, Fuentes C, Kabani S, Laver N, Wang Z, Boone CW, Dasari RR, Shapshay SM, Feld MS. Spectroscopic detection and evaluation of morphologic and biochemical changes in early human oral carcinoma. Cancer. 2003; 97:1681-1692.
28. Sitnik TM, Henderson BW. The effect of fluence rate on tumor and normal tissue responses to photodynamic therapy. Photochem Photobiol. 1998; 67:462-6.

2

Laser speckle imaging of dynamic changes in flow during photodynamic therapy

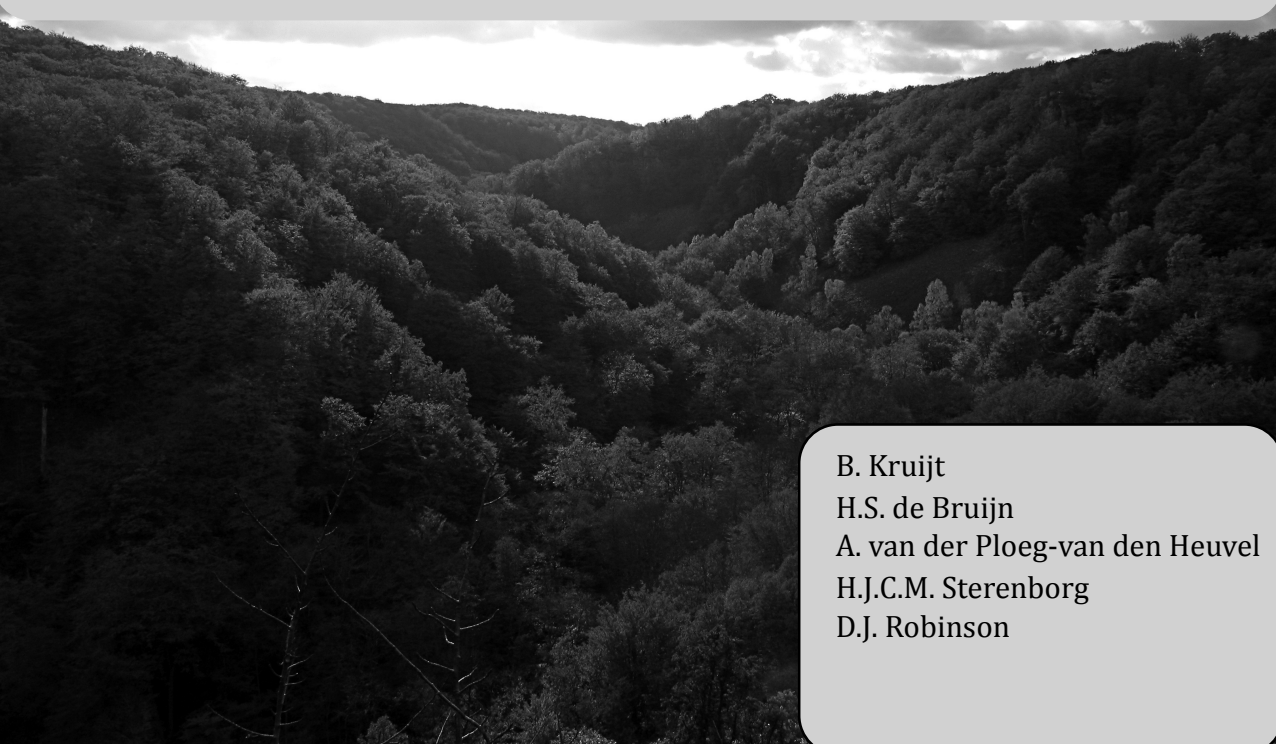

B. Kruijt
H.S. de Bruijn
A. van der Ploeg-van den Heuvel
H.J.C.M. Sterenborg
D.J. Robinson

Abstract
We present a study investigating the use of laser speckle imaging (LSI) for monitoring blood-flow during photodynamic therapy (PDT) utilizing the therapeutic illumination radiation. The coherent nature of a laser source often used in PDT offers the possibility of obtaining information on the blood-flow without interrupting treatment. We have found that in the rat-skin fold observation chamber it is possible to monitor the vasculature response to PDT in individual arteries, veins and in tumor-microvasculature with significantly higher spatial and temporal resolution than current methods. This illustrates the potential for LSI for monitoring PDT in particular for vascular-localizing photosensitizers where current non-invasive methods are difficult because of high absorption due to blood and the specific localization of photosensitizer within the vasculature. However critical problems needs to be further investigated and solved, like the influence of tissue sampling volume, changing of optical properties and movement artifacts from other vessels on the LSI signal. Until then the real potential of LSI for monitoring blood-flow remains of limited value.

Cover: National Park Soderasen, Skåne Sweden (2005).

Published in Lasers in medical science, 2006, 21(4):208-212.

Introduction

The response of tissues to photodynamic therapy (PDT) is dependent on the production of singlet oxygen, $^1O_2$, within the treatment volume. This is determined by the local photosensitizer concentration, light fluence (rate) and tissue oxygenation. While the amount of $^1O_2$ production is important, its localization within the illuminated volume is also an important parameter. Systemically administered photosensitizers accumulate in cellular and vascular compartments of both normal and malignant tissues. They can induce cell death directly via oxidative damage to critical cellular components or indirectly following damage to the vasculature that deprives cells of oxygen. The relative importance of these two mechanisms is dependent on the photosensitizer and the treatment parameters. PDT-dosimetry based on monitoring the $^1O_2$ concentration within the treatment volume is under development[1,2]. The difficulty of this approach, due to the weak luminescence emission of $^1O_2$, has lead investigators to develop other implicit methods of dosimetry[3]. These have been primarily based on properties of the photosensitizer that can be measured optically (i.e. absorption, phosphorescence, fluorescence and photosensitizer triplet state dynamics)[4,5]. For photosensitizers that localize in the vasculature these methods are more challenging because of high absorption coefficient of blood. Also, the specific localization of photosensitizer within the vasculature is an important consideration. The short lifetime of $^1O_2$ [6] means that only $^1O_2$ generated by photosensitizer molecules bound to or very near the vessel wall contributes to the vascular response. Another option is to directly monitor the vascular response to PDT. Blood flow can be monitored non-invasively using Laser Doppler, the closely related diffuse correlation spectroscopy (DCS) and Laser Speckle imaging (LSI)[7-11]. A potential advantage of LSI is that it is a full field method, no scanning is necessary and it has significantly greater spatial and temporal resolution than Laser Doppler or DCS. It may also be possible to utilize the therapeutic light if a laser is being used so that blood-flow information can be recorded without interrupting therapy. The present study reports on the application of LSI for monitoring vascular changes in tissue during PDT in the skin fold observation chamber[12,13] to delineate and discuss problems encountered using LSI *in vivo*.

Materials and Methods

Experimental setup

A schematic diagram of the experimental setup is shown in fig. 1. 514 nm radiation from an Argon Ion laser (Spectra Physics, Darmstadt, Germany) is coupled from an optical fiber using a system of condensing lenses into the base of a heated X-Y stage to produce a uniform distribution of light across the sample. Light transmitted through the sample and collected using an f2.8/105 mm macro lens and imaged onto a peltier-cooled 16-bit, 512 x 512, slow-scan CCD camera (Princeton Instruments Inc. Princeton NJ, USA). The integration time of the camera is 250 ms. The macro lens can be used to zoom in on a specific area within the sample resulting in a square field of view of 4.5 mm. Neutral density filters are used to avoid saturation of the cameras during the acquisition of transmission speckle images.

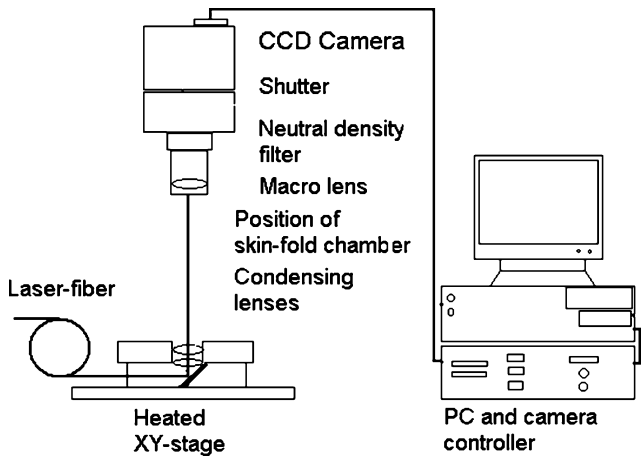

Figure 1. The schematic diagram of the setup

Image analysis

Raw speckle images are processed into blood flow images according to the strict temporal method described by Forrester *et al.* [10]. A reduced speckle image is first calculated based on the average of N_{max} recorded speckle images.

$$I_{ref}(x,y) = \frac{1}{N_{\max}} \sum_{N=1}^{N_{\max}} \left[\frac{1}{2i+1} \sum_{x-i}^{x+i} \left(\frac{1}{2j+1} \sum_{y-j}^{y+j} I_{SP,N}(x,y) \right) \right] \quad (1)$$

Where x and y represent the co-ordinates of the pixel within the image and *i* and *j* represent the boundaries of the chosen region for spatial averaging. *N* is the number of the image in a sequence of N_{max} images. I_{ref} and $I_{SP,N}$ are the reduced speckle image and the N^{th} recorded speckle image respectively. Next the sum of differences in pixel-

intensity between the reduced speckle images and N_{max} recorded speckle images are calculated. The sum of differences is then normalized by the reduced speckle image.

$$I_{SD}(x,y) = \frac{1}{I_{ref}(x,y)} \sum_{N=1}^{N_{max}} \left[\sum_{x-i}^{x+i} \left(\sum_{y-j}^{y+j} \left| I_{SP,N}(x,y) - I_{ref}(x,y) \right| \right) \right] \quad (2)$$

Movement of scatterers causes the speckle pattern to decorrelate when recorded with a finite exposure time. The amount of decorrelation is dependent on the rate of flow of scatterers, i.e. fast flowing scatterers result in more blurring of the speckle pattern than slow flowing scatterers. Equation 2 is therefore an inverse indication of the amount of flow. By taking its inverse we calculate a flow index of the scatterers within the illuminated volume.

$$I_{FI} = \frac{1}{I_{SD}} \quad (3)$$

As stated above using the strict temporal method i and j are set to zero. Laser speckle is normally acquired in reflection, however our illumination geometry means that we measure laser speckle in transmission. It makes relatively little difference whether data is collected in transmission or reflection as long as the tissue is optically thin enough not to completely absorb the incident laser light or has such a high scattering coefficient that the speckle pattern is lost.

Photodynamic therapy

Skin-fold observation chambers were prepared according to a method adapted from van der Veen *et al.*[12] in female Fisher 344 rats. R3230Ac rat mammary carcinoma was implanted 4–7 days before therapy. 5-aminolevulinic acid (ALA) (Medac GmbH, Wedel, Germany) was dissolved in physiological saline and adjusted to pH 5.0 using NaOH and injected to a dose of 200 mg/kg. One hour later PDT was performed using 514 nm radiation at a fluence rate of 50 mW cm^{-2} for 2000 seconds resulting in a fluence of 100 J cm^{-2}. Using an integration time of 250 ms transmission speckle images are acquired at 17-second intervals. This interval was chosen to allow complementary measurements to be acquired during PDT. Before and directly after treatment, vascular damage and changes in blood-flow were visually assessed microscopically.

Results

Figure 2 shows a sequence of blood flow images of an observation chamber containing a tumor (T) approximately 2 mm in diameter, during a PDT to a fluence of 100 J cm^{-2}. The larger arterioles and veins are clearly visible. The tumor is surrounded by numerous micro-vessels with diameters that are smaller than the resolution of the camera that show higher flow than the central areas of the tumor.

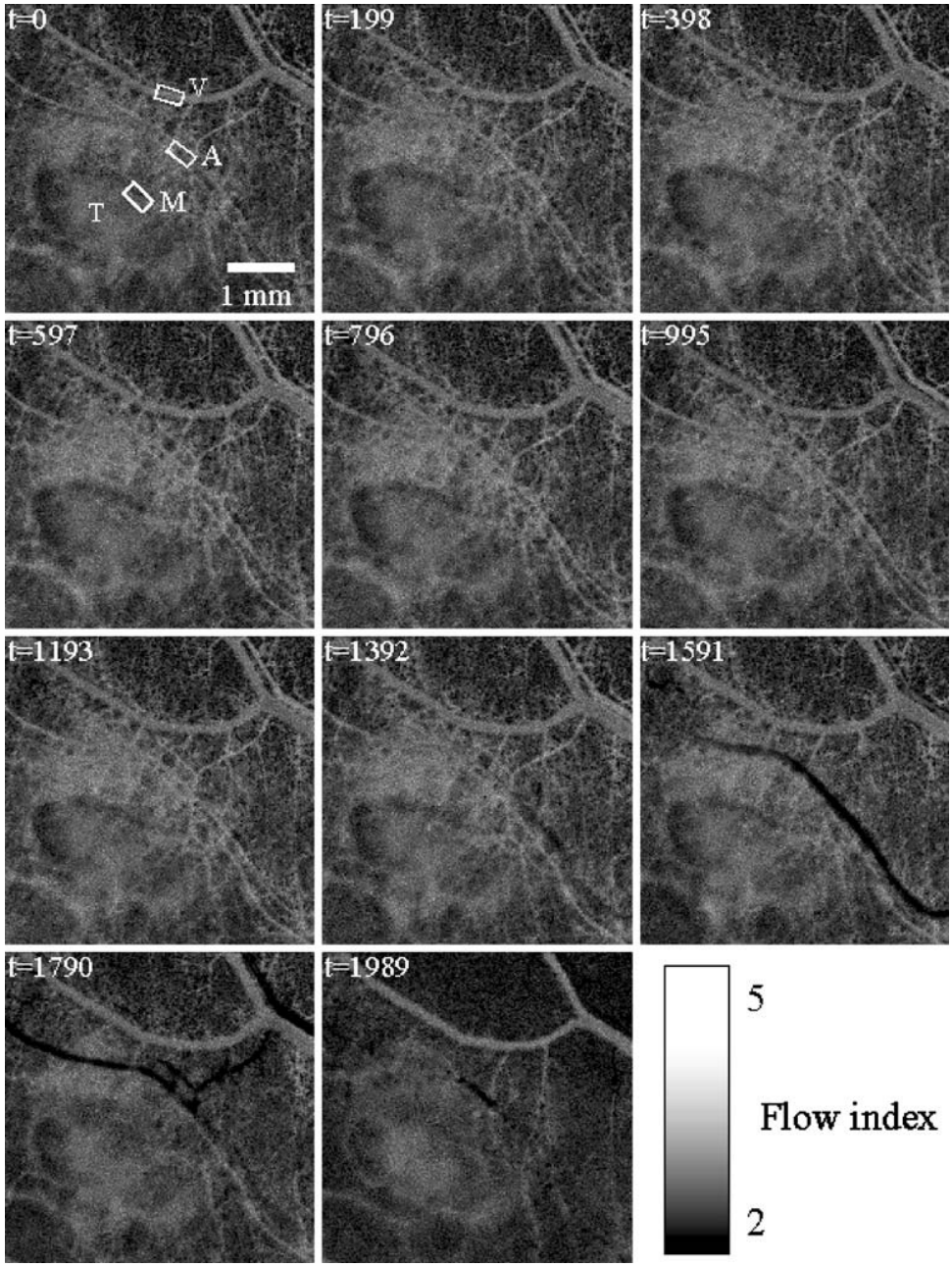

Figure 2. Sequence of images of a skin-fold chamber during ALA- PDT. Three regions of interest are depicted in the first image for a vein (V), an artery (A) and an area of tumor microvasculature (M). T depicts the tumor in the first image. Total width of one image is 4.5 mm. The time indication in the upper left corner is in seconds. First seven images show a slight increase in intensity indicating an increase in flow. Last four images clearly show sudden darkening of vessels indicating drastic change in flow index. Comparing the situation in the last two images with the first, an overall intensity decrease is noticed due to a decrease in flow.

During PDT the image sequence first shows a slight increase in flow in the arteries and in the area surrounding the tumor. After a period of constant flow there is a sudden decrease in flow in the arteries. This response of the arteries is almost immediately followed by an overall decrease in flow mainly in the tumor microvasculature. Venules and arteries in the tumor microvasculature were too small to measure individually. The flow in the large venules is relatively constant compared to the arteries and tumor microvasculature. This is probably due to intrinsically different response of venules to PDT as also observed by van Veen *et al*.[12]. There is a slight increase in flow at the end of the illumination period.

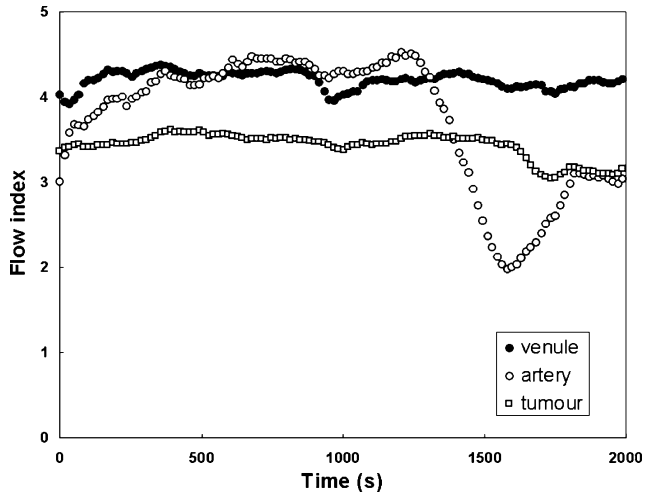

Figure 3. Measured flow index values for the three regions of interest depicted in Fig. 2 as function of delivered dose. Open circles represent the arterial flow, closed circles represent venous flow and open squares represent the microvascular flow within the tumor.

Figure 3 shows relative blood flow index as function of delivered dose to the tissue of three different regions of interest within the chamber. The extent of flow variation in the microvasculature surrounding the tumor is less than in the artery and there is relatively little variation in flow in the vein.

Discussion and Conclusion

We have investigated the use of laser speckle perfusion imaging for monitoring the vascular response of tissues to PDT. For this purpose we have chosen the rat skin fold observation chamber since it is an animal model specially designed for monitoring vascular changes during therapy. Laser speckle perfusion imaging is a technique for measuring relative changes in blood-flow. Directly after PDT blood flow in the chamber was assessed visually, no absolute blood flow values were measured independently of LSI, except for zero flow.

Differences in sample thickness have been shown to affect the degree of blurring of laser speckle when light is transmitted through homogeneous media[14]. In short, an increase in thickness results in an increase in blurring of the speckle pattern, and an increase in blood-flow index value. This is an important factor in the present study since the observation-chamber is not of exact uniform thickness, between 0.1-0.8 mm depending on the location within the chamber.

The coherent nature of a laser illumination source often used in PDT offers the possibility of determining the blood flow without interrupting treatment. This allied with the potential for acquiring data with significantly higher spatial and temporal resolution than existing techniques[7,8] makes LSI an attractive option for monitoring perfusion. This is particularly true for vascular-localizing photosensitizers where current non-invasive methods for monitoring PDT are difficult because of high absorption due to blood and/or the specific localization of photosensitizer within the vasculature[2,3]. The sequence of images in figure 2 and the data from regions of interest within the observation chamber (figure 3) show a significant change in blood flow during illumination. The vascular response during PDT with systemically administered ALA is clearly evident despite the fact that the response to ALA-PDT is dominated by a direct cellular response. Figure 3 shows it is possible to record blood-flow information from individual arterioles and venules and that the temporal resolution of LSI is sufficient to distinguish the different response of arteries, veins and tumor microvasculature to PDT[15]. However there still remain critical questions that need to be investigated in order to determine the applicability of laser speckle perfusion imaging. The presence of an offset in flow index, as seen in figure 3, which has not been addressed in previous studies of LSI[8-11,13,16-18]. This offset is believed to be a combination of several factors that include the tissue optical properties and tissue thickness. In addition the influence of multiple vessels within the detection volume on the actual flow signal from an individual vessel is not determined. Also the influence of these factors on the offset will be different for each pixel of the blood-flow image which means it is difficult to determine an accurate spatial and temporal offset in the present model.

Another complication with speckle algorithms is that they cannot resolve zero flow or very high flow situations, both will generate very high or even infinite calculated perfusion values. However very high or infinite calculated perfusion values due to very high flow can be resolved by reducing the camera integration time, but this can increase the signal to noise ratio of the system and hence influence the calculated perfusion values. Another critical factor is the effect of changing tissue optical properties (μ_s and μ_a) during PDT treatments. A study of Forrester *et al.*[18] already showed significant differences in laser speckle signal between phantoms with different optical properties, no one has yet investigated this influence on speckle signal when both the optical properties and perfusion change within the same tissue volume in time. Considering these difficulties we conclude that the benefit of the information provided by LSI during PDT remains of limited value until flow changes and blood volume changes can be separated.

Acknowledgement

This work was supported by the Dutch Cancer Society NKB 99-1881.

References

1. Niedre M, Patterson MS, Wilson BC. Direct near-infrared luminescence detection of singlet oxygen generated by photodynamic therapy in cells in vitro and tissues in vivo. Photochem Photobiol. 2002; 75:382-391.
2. Niedre M, Patterson MS, Giles A, Wilson BC. Imaging of photodynamically generated singlet oxygen luminescence in vivo. Photochem. Photobiol. 2005; 81:941-943.
3. Wilson BC, Patterson MS, Lilge L. Implicit and explicit dosimetry in photodynamic therapy: a new paradigm. Lasers Med. Sci. 1997; 12:182-199.
4. Sterenborg HJ, Janson ME, van Gemert MJ. A novel frequency domain fluorescence technique for determination of triplet decay times. Phys. Med. Biol. 1999; 44:1419-1426.
5. Sterenborg HJCM, de Wolf JW, Koning M, Kruijt B, van den Heuvel A, Robinson DJ. Phosphorescence-fluorescence ratio imaging for the oxygen status during photodynamic therapy. Opt. Express 2004; 12:1873-1878.
6. Moan J, Berg K. The photodegredation of porphyrins in cells can be used to estimate the lifetime of singlet oxygen. Photochem. Photobiol. 1991; 53:549-33.
7. Essex TJH, Byrne PO (1991) A laser doppler scanner for imaging blood flow in skin. J. Biomed. Eng. 1991; 13:189-194.
8. Chen Z, Milner TE, Wang X, Srinivas S, Nelson JS. Optical Doppler tomography: imaging in vivo blood flow dynamics following pharmacological intervention and photodynamic therapy. Photochem Photobiol. 1998; 67:56-60.
9. Briers JD, Webster S. Laser speckle contrast analysis (LASCA): A nonscanning, full field technique for monitoring capillary blood flow. J. Biomed. Opt. 1996; 1:174-179.
10. Forrester KR, Stewart C, Tulip J, Leonard C, Bray RC. Comparison of laser speckle and laser Doppler perfusion imaging: measurement in human skin and rabbit articular tissue. Med. Biol. Eng. Comput. 2002; 40:687-697.
11. Yu G, Durduran T, Zhou C, Wang HW, Putt ME, Saunders HM, Sehgal CM, Glaststein E, Yodh AG, Busch TM. Noninvasive monitoring of murine blood flow during and after photodynamic therapy provides early assessment of therapeutic efficacy. Clin. Cancer Res. 2005; 11:3543-3552.
12. van der Veen N, van Leengoed HLLM, Star WM. In vivo fluorescence kinetics and photodynamic therapy using ALA-induced porphyrin: increased damage after multiple irradiations. Br. J. Cancer 1994; 70:867-872.
13. Choi B, Kang NM, Nelson JS. Laser speckle imaging for monitoring blood flow dynamics in the in vivo rodent dorsal skin fold model. Microvasc. Res. 2004; 68:143-146.
14. Thompson CA, Webb KJ, Weiner AM. Diffusive media characterization with laser speckle. Appl. Opt. 1997; 36:3726-3734.
15. Leveckis J, Brown NJ, Reed MW. The effect of aminolaevulinic acid-induced, protoporphyrin IX-mediated photodynamic therapy on the cremaster muscle microcirculation in vivo. Br J Cancer 1995; 72:1113-9.
16. Dunn AK, Bolay H, Moskowitz MA, Boas DA. Dynamic imaging of cerebral blood flow using laser speckle. J. Cereb. Blood Flow Metab. 2001; 21:195-201.
17. Durduran T, Burnett MG, Yu G, Zhou C, Furuya D, Yodh AG, Detre J A, Greenberg JH. Spatiotemporal quantification of cerebral blood flow during functional activation in rat somatosensory cortex using laser-speckle flowmetry. J.Cereb.Blood Flow Metab. 2004; 24:518-525.
18. Forrester KR, Tulip J, Leonard C, Stewart C, Bray RC. A laser speckle imaging technique for measuring tissue perfusion. IEEE Trans. Biomed. Eng. 2004; 51:2074-2084.

3

Quantitative fluorescence spectroscopy in turbid media using fluorescence differential path length spectroscopy

A. Amelink
B. Kruijt
D.J. Robinson
H.J.C.M. Sterenborg

Abstract
We have developed a new technique, Fluorescence Differential Path length Spectroscopy (FDPS), that enables the quantitative investigation of fluorophores in turbid media. FDPS measurements are made with the same probe geometry as differential path-length spectroscopy (DPS) measurements. Phantom measurements are performed for 2 fiber diameters (400 μm and 800 μm) and for a wide range of optical properties (μ_s': 0-10 mm^{-1}, μ_a: 0-2 mm^{-1}) to investigate the influence of the optical properties on the measured differential fluorescence signal. The differential fluorescence signal varies by a factor of 1.4 and 2.2 over the biologically relevant scattering range (0.5-5 mm^{-1}) for a given fluorophore concentration for 400 μm and 800 μm fibers, respectively. The differential fluorescence signal is attenuated due to absorption at the excitation wavelength following Lambert-Beer's law with a path length equal to the differential path-length.
Introduction

Cover: Cliffs at Dún Aonghasa on Inis Mór, one of the Arran islands, Ireland (2008)

Published in Journal of biomedical optics, 2008, 13(5):054051

Introduction

Non-invasive quantitative optical measurements of chromophore concentrations in tissue requires knowledge of the optical path length in the tissue. For most fiber-optic measurement geometries the optical path length depends on the scattering coefficient μ_s and on the absorption coefficient μ_a. Since μ_s and μ_a both vary significantly in tissue, quantitative measurements prove to be difficult in tissue unless specific fiber-optic measurement geometries are chosen. For example, the optical pharmacokinetics spectroscopy (OPS) system developed by Mourant *et al.*[1] uses elastic scattering spectra of tissue to calculate the concentration of chromophores in tissue using a fiber-optic probe with a source–detector separation of 1.7 mm. The separation of 1.7 mm was chosen to minimize the dependence of the path-length of the collected photons on scattering properties of tissue. For scattering parameters that are typical of tissue, the path-length varies by less than 20% for a given background absorption. This method has been applied to the measurement of chemotherapy drug concentrations in tissue[2]. A drawback of this method is that the path-length is sensitive to the (background) absorption coefficient of tissue. This means that the amount of measured absorption due to the target chromophore strongly depends on the local blood content and blood saturation. As a consequence a measurement must be made prior to injection of the target chromophore and only changes in concentration can be measured assuming that the background absorption does not change in time. This makes OPS measurements difficult when a background reflectance spectrum cannot be acquired, and even more difficult to interpret when there are changes in the background absorption of tissue. Changes in background absorption can occur for a variety of reasons. Pressure between the measurement probe and the surface of the tissue can influence the blood content. Open surgical procedures can significantly influence both blood volume and saturation. Furthermore, changes in background absorption are a particular problem for *in vivo* photosensitiser concentration measurements during photodynamic therapy (PDT), when the background absorption can change dramatically due to changes in blood volume and saturation resulting from the therapy itself[3].

Another technique that features a known path-length is differential path-length spectroscopy (DPS)[4,5]. The path-length of photons contributing to the differential reflectance signal varies only slightly over a very broad range of both scattering and absorption coefficients. This facilitates quantitative concentration measurements even for strong variations in either absorption or scattering. However, chromophore concentrations calculated from elastic scattering measurements rely on (small) differences between large amounts of detected light with and without the chromophore present. Therefore, the combination of dynamic range and signal-to-noise of the elastic scattering measurement device becomes a limiting factor for accurate measurement of small concentrations of chromophores or measurements of chromophores with low absorption coefficients. This is particularly true for DPS, for which the average path-length of the measured photons is very small (approximately equal to the fiber diameter). In contrast, the dynamic range for fluorescence measurements is much larger than for scattering (absorption) measurements since the fluorescence is measured at a different wavelength than the excitation (scattered) light. For this

reason, we have now developed a technique based on the principles of DPS (subtraction of the diffuse photons to obtain a well-defined measurement volume) but with the enhanced dynamic range of fluorescence measurements: fluorescence-DPS (FDPS).

Fluorescence emission from fluorophores is influenced by their environment. There exists a complex relationship between the concentration of a chromophore and its absorption cross-section and fluorescence emission intensity. In-vivo fluorescence (and to a lesser degree absorption) can be altered by many factors that include changes in quantum yield induced by changes in the microenvironment[6], photobleaching[7], biological compartmentalization, and alteration in binding and aggregation[8,9]. In a turbid sample the amount of fluorescence detected depends not only on the fluorophore concentration and quantum yield, but also on the scattering and absorption coefficients of the medium. Various algorithms and measurement geometries have been developed to correct for the influence of scattering and absorption on a measured fluorescence spectrum. Zhang *et al*.[10] and Muller *et al.*[11] have used photon migration techniques to establish a very general algorithm that corrects for the influence of the optical properties on the measured fluorescence for any measurement geometry and for large variations in scattering and absorption. In this correction algorithm the diffuse reflectance, measured in the same geometry as the fluorescence measurements, is used to correct for differences in tissue optical properties. Unfortunately, elaborate probe specific calibration procedures are required and the correction algorithm is quite complex. Several other authors have developed more simple correction algorithms based on specific probe geometries. Canpolat and Mourant[12] used various source-detector pairs to measure fluorescence and scattered excitation light for small source-detector separations. From Beer's law they determined that their fluorescence-to-excitation reflectance ratio would be proportional to the product of fluorescence quantum yield, path-length and fluorophore absorption coefficient when the background absorption and scattering coefficients are the same at the excitation and emission wavelengths. Weersink *et al.*[13] described a similar measurement technique, except that the fluorescence and reflected excitation light were measured at two different distances. Using a source-detector separation of 0.65 mm for fluorescence and 1.35 mm for reflectance measurements, they showed that it was possible to measure fluorophore concentrations to an accuracy of 15% over a wide range of optical properties using the fluorescence-to-reflectance ratio. In the measurement geometry of Pogue and Burke[14], fluorescence was excited and detected with a single small diameter (100 μm) fiber, but the scattered excitation light was measured with an adjacent fiber. Measurements in phantoms showed that the fluorescence-to-reflectance ratio in this geometry varied by approximately 30% for a given fluorophore concentration over a broad range of optical properties. Diamond *et al.*[15] also used a small diameter (200 μm) single optical fiber to excite and detect the fluorescence, and found that the uncorrected fluorescence signal was insensitive to changes in the scattering coefficient and anisotropy as well as a limited range of absorption coefficients (up to 0.12 mm^{-1}) of the turbid samples, due to the small sampling volume of their technique. However, this single-fiber fluorescence method suffers from the same drawback as Mourants reflectance method: the signal will be sensitive to larger

changes in the (background) absorption coefficient of tissue. For wavelengths below 600 nm the tissue absorption coefficient for most biological tissues is an order of magnitude larger than 0.12 mm^{-1}, mainly due to blood absorption[16]. This limits the applicability of the present techniques to those chromophores that exhibit large absorption (and emission) bands in the red or near-infrared wavelength regions. Therefore, our objective here is to establish an algorithm that can be used to correct FDPS measurements for larger changes in the background absorption coefficient (as high as 2.0 mm^{-1}). Furthermore, we will show that FDPS measurements do not need to be corrected for changes in the reduced scattering coefficient in the range 0.5-5 mm^{-1}, which are values typically encountered in tissue[16-20].

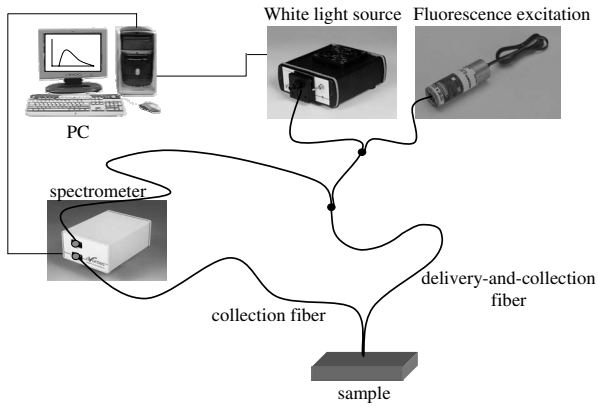

Figure 1. Schematic diagram of the FDPS setup.

Materials and Methods

Experimental Setup

The setup is an adapted version of a Differential Path-length Spectrometer and shown schematically in figure 1. Light from a Tungsten Halogen lamp (Ocean Optics HL-2000) or a blue laser diode (Power Technology PPMT-LD1382, output 5 mW at 405 nm) is led through a 100 µm bifurcated optical fiber, which is at its distal end coupled to a 200 µm bifurcated optical fiber, which is at its distal end coupled to the 400 µm delivery-and-collection (dc) fiber. The distal end of the fiber probe is polished at an angle of 15 degrees to minimize the collection of specularly reflected light at the probe-medium interface, and contacts the sample under investigation. Reflected or fluorescent light collected by the dc fiber is coupled back into the 200 µm bifurcated fiber and coupled to the dc-channel of a 4-channel spectrometer (Ocean Optics MC-2000-4). Light reflected back from the sample into the other arm of the 400 µm bifurcated fiber-optic probe (the collection (c) fiber) is coupled into the c-channel of the 4-channel spectrometer. The c-fiber and dc-fiber are touching to minimize the distance between them. Fluorescence and reflectance measurements were performed consecutively by switching on either the laser or the halogen lamp. An identical setup with twice as large fibers was connected to the third and fourth channels of the 4-channel spectrometer.

Measurements with the 400 μm FDPS probe and the 800 μm FDPS probe were performed consecutively. In the following, the difference of the dc- and c-fiber reflectance signals is called the *differential reflectance signal* ***DR***, where throughout this paper a wavelength-dependent parameter will be presented as a bold faced character and parameters appearing as non-bold are implicitly assumed to be wavelength independent. Similarly, the difference in the fluorescence collected by the dc- and c-fibers is called the *differential fluorescence signal*, ***DF***.

Calibration

The total fluorescence intensity I^F_{sample} measured by the delivery-and-collection fiber in contact with a sample with the laser on can be written as:

$$\boldsymbol{I}^{F}_{\mathbf{sample}} = \boldsymbol{F}^{dc}_{\mathbf{sample}} \cdot \boldsymbol{T}_{\mathrm{dc}} \quad , \tag{1}$$

where F^{dc}_{sample} is the number of fluorescent photons collected by the dc-fiber and T_{dc} is the transmission function of the photons traveling from the tip of the delivery-and-collection fiber to the dc-spectrometer channel. Similarly, the total fluorescence intensity J^F_{sample} measured by the collection fiber is:

$$\boldsymbol{J}^{F}_{\mathbf{sample}} = \boldsymbol{F}^{c}_{\mathbf{sample}} \cdot \boldsymbol{T}_{\mathrm{c}}, \tag{2}$$

where F^c_{sample} is the number of fluorescent photons collected by the c-fiber and Tc is the transmission function of the photons traveling from the tip of the collection fiber to the c-spectrometer channel. The transmission functions T_{dc} and T_c are measured using a calibrated white light source (Ocean Optics HL-2000-CAL) for which the output of the lamp is known. For these measurements the distal end of the probe, which was terminated with an SMA connector, was screwed in the SMA socket of the calibration lamp and we measure $I_{cal} = L_{cal} \cdot T_{dc}$ and $J_{cal} = L_{cal} \cdot T_c$ where L_{cal} is the known output of the lamp.

Finally, day-to-day variations in laser output from the distal end of the dc-fiber are measured by measuring the fluorescence intensity with the probe at a fixed distance from fluorescent spectralon (Labsphere USFS-200-010), which is a stable solid fluorescent standard. Alternatively, the output power of the laser can be directly measured by a power meter.

The differential fluorescence signal ***DF*** is calculated by

$$\boldsymbol{DF} \equiv \boldsymbol{F}^{dc}_{\mathbf{sample}} - \boldsymbol{F}^{c}_{\mathbf{sample}} = \boldsymbol{L}_{\mathbf{cal}} \left(\frac{\boldsymbol{I}^{F}_{\mathbf{sample}}}{\boldsymbol{I}_{\mathbf{cal}}} - \frac{\boldsymbol{J}^{F}_{\mathbf{sample}}}{\boldsymbol{J}_{\mathbf{cal}}} \right). \tag{3}$$

The white light differential reflectance is measured as described previously[4,5]:

$$\boldsymbol{DR} = c\left[\frac{(\boldsymbol{I}-\boldsymbol{I}_{\mathbf{water}})}{(\boldsymbol{I}_{\mathbf{white}}-\boldsymbol{I}_{\mathbf{black}})} - \frac{\boldsymbol{J}}{(\boldsymbol{J}_{\mathbf{white}}-\boldsymbol{J}_{\mathbf{black}})}\right], \tag{4}$$

where (I-I_{water}) represents the dc-fiber signal (I) corrected for internal reflections (I_{water}) using water in a dark reservoir. Fiber transmission characteristics and lamp spectra are accounted for by dividing the (corrected) I and J signals by their reference reflections (I_{white}-I_{black}) and (J_{white}-J_{black}), and calibration constant c depends on the distance between the probe tips and the reference standards.

Phantoms

To characterize the differential fluorescence signal as a function of the optical properties, phantom measurements are performed. We have used liquid phantoms consisting of Intralipid 20% in different dilutions to vary the reduced scattering coefficient from 0 to 10 mm^{-1} at the excitation wavelength of 405 nm. To simulate the presence of an exogenous fluorophore, sulforhodamine 101 was added to the phantoms in concentrations ranging from 0.2 μM to 20 μM. The fluorescence quantum yield of sulforhodamine dissolved in ethanol is 0.9 [21]. Finally, background absorption at the excitation wavelength was varied from 0 to 2 mm^{-1} by addition of Hemoglobin (Sigma-Aldrich, H2500) to the phantoms. Absorption at the Sulforhodamine emission wavelengths (λ > 550 nm) is at least an order of magnitude smaller than at the excitation wavelength.

Results

Fluorophore concentration dependence

The differential fluorescence ***DF*** consists of 2 components: Intralipid fluorescence and sulforhodamine fluorescence. Therefore, for all phantoms the background fluorescence due to Intralipid was measured using phantoms with identical optical properties but without sulforhodamine and was, after normalization to the average differential fluorescence in the wavelength region 500 nm < λ < 550 nm, subtracted from the ***DF*** signal to obtain the sulforhodamine differential fluorescence.

Figure 2a shows ***DF*** for a fixed reduced scattering coefficient of $\mu_s' = 1.5\ mm^{-1}$ at 405 nm and for different fluorophore concentrations c_F, for the 400 μm FDPS system. Figure 2b shows ***DF*** divided by fluorophore concentration c_F. The ***DF***/c_F ratios are constant both in size and spectral shape, which implies that there is a linear relationship between the differential fluorescence and the fluorophore concentration. In the following, the area under the differential fluorescence curves in the wavelength region 550 nm < λ < 700 nm, $\boldsymbol{DF}=\int_{550}^{700} d\lambda \boldsymbol{DF}$, is analyzed as a function of the optical properties.

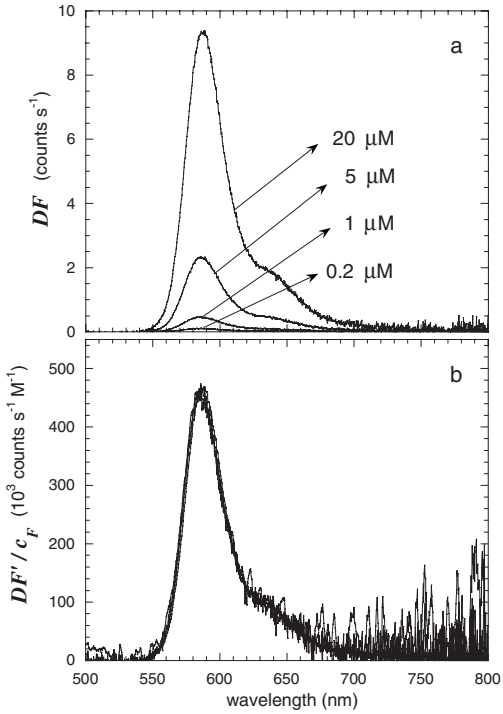

*Figure 2. (a) Measured differential fluorescence **DF** for different fluorophore concentrations c_F for a fixed scattering coefficient (μ_s' = 1.5 mm^{-1}), and (b) ratio of **DF** and c_F for the same measurements.*

Measurement reproducibility

We have tested the measurement reproducibility for phantoms with optical properties corresponding to the median of our measurement range (μ_s' = 1.5 mm^{-1} and μ_a = 1.0 mm^{-1}). Three different sets of phantoms were made with the same optical properties, with and without sulforhodamine (i.e. c_F = 0 µM and c_F = 1 µM). Furthermore, the effect of manual sample homogenization was investigated by measuring the phantoms after i) not shaking, ii) gentle shaking and iii) vigorous shaking. The largest effects on the relative standard deviations of ***DF*** and ***DR*** were found to be due to the differences in shaking: $\Delta DF/DF \approx 7\%$ and $\Delta DR/DR \approx 2\%$ for the 400 µm FDPS system, and $\Delta DF/DF \approx 7\%$ and $\Delta DR/DR \approx 6\%$ for the 800 µm FDPS system. Here the standard deviation in the differential reflectance (ΔDR) was calculated at the excitation wavelength after normalization of the differential reflectance spectra DR in the wavelength region [460 to 500] nm, where hemoglobin absorption is very small compared to the absorption at the excitation wavelength of 405 nm. The relative standard deviation $\Delta DR/DR$ in the absence of hemoglobin, associated with homogenization (shaking) of the phantoms, was found to be 2% for both fiber diameters.

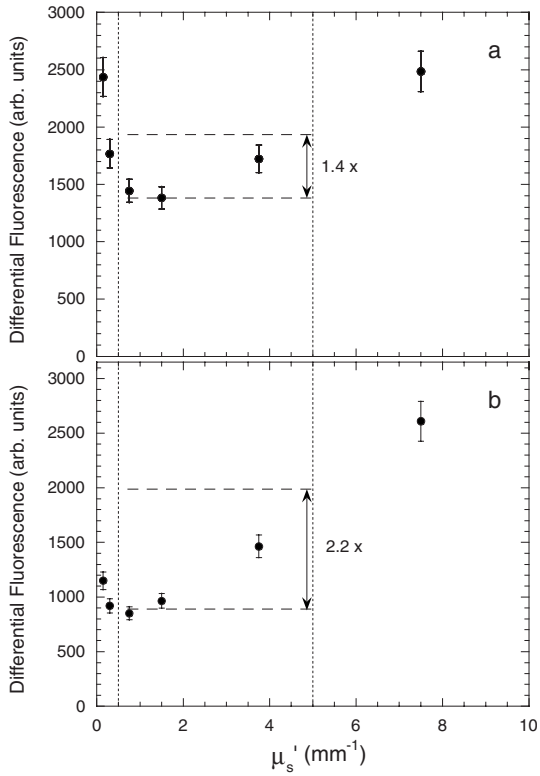

*Figure 3. Measured differential fluorescence **DF** as a function of reduced scattering coefficient for a fixed fluorophore concentration (c_F = 1 μM), (a) for the 400 μm FDPS probe, and (b) for the 800 μm FDPS probe.*

Scattering dependence

Figure 3a shows DF for a fixed fluorophore concentration (c_F = 1 μM) for the 400 μm FDPS system, but now for different reduced scattering coefficients (μ_s' = 0.15, 0.30, 0.75, 1.5, 3.75 and 7.5 mm^{-1} at 405 nm). The error bars represent the 7% standard deviation corresponding to the measurement reproducibility. The differential fluorescence first decreases up to μ_s' = 1.5 mm^{-1}, and then increases with increasing scattering coefficient. In the range relevant for biological tissues (0.5 mm^{-1} < μ_s' < 5 mm^{-1})[14-18] the maximum variation in differential fluorescence ($\boldsymbol{DF}_{max}$ / $\boldsymbol{DF}_{min}$) equals a factor of 1.4. Figure 3b shows the same data for the 800 μm FDPS system, which shows a similar pattern but the increase in differential fluorescence already starts at μ_s' = 0.75 mm^{-1}. In this case the maximum variation in differential fluorescence ($\boldsymbol{DF}_{max}$ / $\boldsymbol{DF}_{min}$) equals a factor of 2.2 in the range relevant for biological tissues.

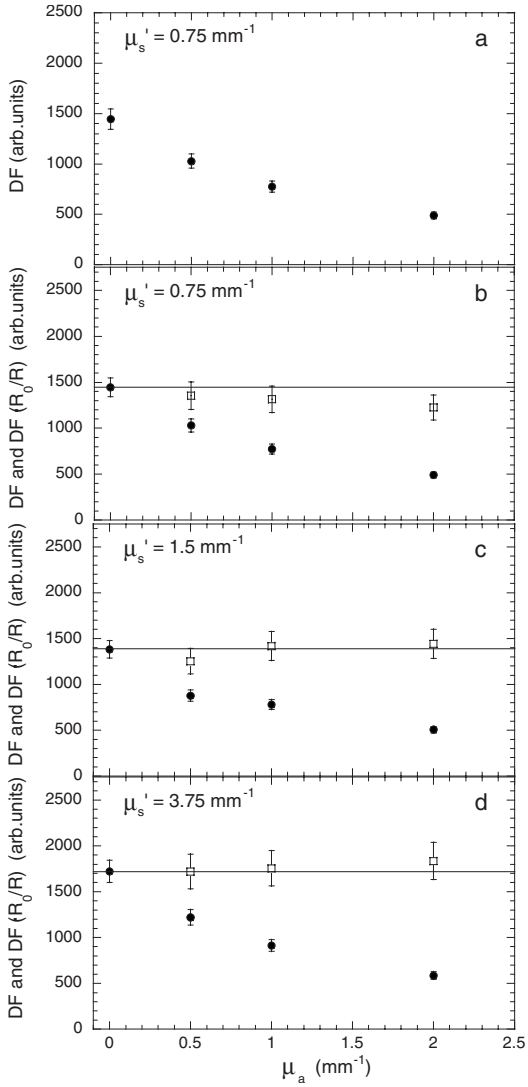

*Figure 4. (a) Measured differential fluorescence **DF** as a function of absorption coefficient for a fixed fluorophore concentration (c_F = 1 μM) and a fixed reduced scattering coefficient (μ_s' = 0.75 mm^{-1}) for the 400 μm FDPS probe. (b) The same including the corrections calculated according to Eq. (7) (open squares). (c) The same for μ_s' = 1.5 mm^{-1}, and d) the same for μ_s' = 3.75 mm^{-1}.*

Background absorption dependence

Figure 4a shows ***DF*** for a fixed fluorophore concentration (c_F = 1 μM) and a fixed scattering coefficient (μ_s' = 0.75 mm^{-1} at 405 nm) for the 400 μm FDPS system as a function of the background absorption coefficient at the excitation wavelength. The error bars represent the 7% standard deviation corresponding to the measurement reproducibility. The differential fluorescence decreases strongly with increasing background absorption. Therefore, it is necessary to correct the measured differential

fluorescence for these high background absorptions. Previously we have shown that the white light differential reflectance is attenuated due to absorption following Beer's law according to Eq. (5)[4,5]:

$$\boldsymbol{DR}(\boldsymbol{\mu}_a) = \boldsymbol{DR}(0)\exp(-\tau_{dps}\boldsymbol{\mu}_a), \tag{5}$$

where τ_{dps} is the differential path-length. Since the differential fluorescence is measured with exactly the same fiber-optic geometry, we will assume that the differential fluorescence is attenuated according to Eq. (6):

$$\boldsymbol{DF}(\mu_{a,x}) = \boldsymbol{DF}(0)\exp(-\tau_{dps}\mu_{a,x}). \tag{6}$$

Combining Eqs. (5) and (6) we can write

$$\boldsymbol{DF}(0) = \boldsymbol{DF}(\mu_{a,x})\frac{DR_x(0)}{DR_x(\mu_{a,x})}, \tag{7}$$

where $\boldsymbol{DR}_x(\mu_{a,x})$ and $\boldsymbol{DR}_x(0)$ are the differential reflectance signals at the excitation wavelength measured with and without background absorber present, respectively. The ratio of $\boldsymbol{DR}_x(0)$ and $\boldsymbol{DR}_x(\mu_{a,x})$ was calculated after normalization of the differential reflectance spectra DR for the different concentrations of hemoglobin in the wavelength region [460-500] nm, where hemoglobin absorption is very small compared to the absorption at the excitation wavelength of 405 nm. The open squares in figure 4b represent the calculations of $\boldsymbol{DF}(0)$ according to Eq.(7). The error bars on the open squares represent the standard deviations corresponding to the measurement uncertainties associated with $\boldsymbol{DF}$, $\boldsymbol{DR}_x(0)$ and $\boldsymbol{DR}_x(\mu_{a,x})$, i.e. $\Delta\boldsymbol{DF}(0)/\boldsymbol{DF}(0) = \Delta\boldsymbol{DF}(\mu_{a,x})/\boldsymbol{DF}(\mu_{a,x}) + \Delta\boldsymbol{DR}_x(0)/\boldsymbol{DR}_x(0) + \Delta\boldsymbol{DR}_x(\mu_{a,x})/\boldsymbol{DR}_x(\mu_{a,x}) = 7\%+2\%+2\% = 11\%$. Good agreement between calculation and measurement is observed, except for the highest absorption coefficient, where a small deviation is observed. Figures 4c and 4d show similar plots for the $\mu_s' = 1.5\ mm^{-1}$ and $\mu_s' = 3.75\ mm^{-1}$ at 405 nm cases, respectively, for the 400 μm FDPS system. Finally, figures 5a, 5b and 5c show similar plots for the $\mu_s' = 0.75\ mm^{-1}$, the $\mu_s' = 1.5\ mm^{-1}$ and the $\mu_s' = 3.75\ mm^{-1}$ at 405 nm cases, respectively, for the 800 μm FDPS system. In this case, the error bars on the open squares are slightly larger (15%) due to the larger measurement uncertainty associated with $\boldsymbol{DR}_x(\mu_{a,x})$.

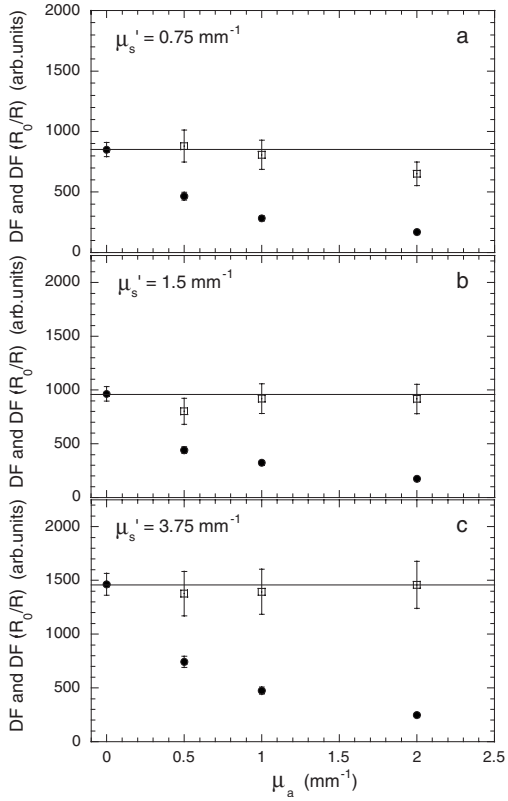

*Figure 5. Measured differential fluorescence **DF** (filled circles) as a function of absorption coefficient for a fixed fluorophore concentration (c_F = 1 μM) and the corrections calculated according to Eq. (7) (open squares) for the 800 μm FDPS probe, for (a) μ_s' = 0.75 mm^{-1}, (b) μ_s' = 1.5 mm^{-1} and (c) μ_s' = 3.75 mm^{-1}.*

DISCUSSION AND CONCLUSION

We have adapted our DPS technique to include fluorescence measurements (FDPS) to enable quantitative fluorescence spectroscopy in turbid media. We showed that the differential fluorescence signal increases linearly with fluorophore concentration for a fixed scattering and background absorption coefficient (figure 2). This facilitates a straightforward interpretation of the fluorescence signals for this range of fluorophore concentrations. We found deviations from linearity for fluorophore concentrations above 50 μM (data not shown). All our subsequent measurements were performed for a concentration of 1 μM, which is well below this value.

We investigated the scattering dependence of the differential fluorescence signal. We found that the differential fluorescence signal decreases up to a reduced scattering coefficient of 1.5 mm^{-1} in case of 400 μm fibers, and then increases with increasing scattering coefficient (figure 3a). Most likely this is due to a combined effect of two counteractive mechanisms. 1) The volume over which the ***DF*** (and ***DR***) is collected is proportional to the differential path-length, which decreases strongly with increasing

scattering for very low reduced scattering coefficients, and becomes roughly constant in the biologically relevant range[4,5]. 2) The fluence rate in the ***DF*** (and ***DR***) collection volume increases with increasing scattering coefficient due to increased backscattering of the excitation light. These 2 effects result in an initial decrease followed by a subsequent steady increase in the differential fluorescence signal. Since the collection volume (or differential path-length) for 800 µm fibers becomes constant for lower scattering coefficients compared to 400 µm fibers[5], the increase in differential fluorescence already starts at a reduced scattering coefficient of 0.75 mm^{-1} for the 800 µm fibers (figure 3b).

In the scattering range relevant for biological tissues the maximum variation in differential fluorescence ($\boldsymbol{DF}_{max}$ / $\boldsymbol{DF}_{min}$) equals a factor of 1.4 for the 400 µm FDPS system and a factor of 2.2 for the 800 µm FDPS system. Note that these factors represent the maximum variation over an order of magnitude change in scattering. For any specific target tissue, the scattering coefficient at the excitation wavelength will vary much less than an order of magnitude; a very conservative estimate would be a twofold variation at the most[16]. Even variations in scattering as large as a factor of 2 result in a maximum variation in differential fluorescence of only a factor of 1.16 for the 400 µm FDPS system and a factor of 1.35 for the 800 µm FDPS system. This implies that FDPS measurements performed on specific target organs can be well compared to each other without correcting for scattering differences, while a more careful interpretation is necessary when FDPS measurements on different organs (with very different scattering coefficients) are to be compared.

The fluence rate in the ***DF*** collection volume will be attenuated due to absorption according to Beer's law similar to the differential reflectance ***DR***, since they are measured in the same geometry. This can be used to account for the effects of absorption on ***DF*** through Eq. (7), which employs the ratio of differential reflectance signals measured with and without absorber present ($\boldsymbol{DR}_x(\mu_{a,x})$ and $\boldsymbol{DR}_x(0)$, respectively). Figures 4 and 5 show that this correction works very well, apart from the combination of very low scattering and very high absorption, where a small deviation can be observed. A possible explanation for this deviation may be that our model does not account for absorption at the emission wavelengths. The largest effect of absorption at the emission wavelengths will be found for the highest concentration of hemoglobin, i.e. for the highest absorption coefficient at the excitation wavelength, combined with the longest differential path-length τ_{dps}, i.e. the lowest scattering coefficient 5.

In this phantom study, we could measure both $\boldsymbol{DR}_x(\mu_{a,x})$ and $\boldsymbol{DR}_x(0)$ directly, while in tissue only $\boldsymbol{DR}_x(\mu_{a,x})$ can be measured. Importantly, in that case $\boldsymbol{DR}_x(0)$ can still be extracted from the measured wavelength dependence of the differential reflectance ***DR*** by fitting the complete DPS spectrum to our previously developed model 22-25, and subsequently calculating what the differential reflectance at the excitation wavelength should be in the absence of blood, as discussed below. Our general model (Eq. 5) can, in case of tissue measurements, be written as[22-25]

$$\boldsymbol{DR}(\mu_a) = \left[a_1 \left(\frac{\lambda}{\lambda_0} \right)^{a_2} + a_3 \left(\frac{\lambda}{\lambda_0} \right)^{-4} \right] \cdot \exp(-\tau_{\mathrm{dps}} \mu_a^{\mathrm{total}}). \quad (8)$$

The scattering function of tissue (in square brackets) is modeled by a combination of Mie scattering and Rayleigh scattering, given by power law functions with amplitudes a_1 and a_3 and wavelength dependencies $(\lambda/\lambda_0)^{a2}$ and $(\lambda/\lambda_0)^{-4}$, respectively. Here λ_0 is a normalization wavelength, which we usually set to 800 nm. The absorption coefficient μ_a^{total} is the sum of the absorption coefficients of all the chromophores present in the interrogation volume, which in the visible wavelength region is typically only blood:

$$\mu_a^{\mathrm{total}} = a_4 \cdot [a_5 \cdot \mu_a^{\mathrm{HbO_2}} + (1 - a_5) \cdot \mu_a^{\mathrm{Hb}}] \cdot \left(\frac{1 - \exp\{- a_6 \cdot [a_5 \cdot \mu_a^{\mathrm{HbO_2}} + (1 - a_5) \cdot \mu_a^{\mathrm{Hb}}]\}}{a_6 \cdot [a_5 \cdot \mu_a^{\mathrm{HbO_2}} + (1 - a_5) \cdot \mu_a^{\mathrm{Hb}}]} \right). \quad (9)$$

Parameter a_4 is the blood volume fraction, a_5 is the blood oxygenation and a6 is the average vessel diameter. Input spectrum μ_a^{HbO2} is the absorption coefficient of fully oxygenated whole blood and μ_a^{Hb} is the absorption coefficient of fully deoxygenated whole blood. When the measured DPS spectrum is fitted to the model (Eqs. 8, 9) using least squares minimization, we obtain best estimates for the fitparameters a_1 – a_6. Using the best estimates of the scattering parameters a_1 – a_3, $\boldsymbol{DR}_x(0)$ can be calculated by

$$DR_x(0) = a_1 \left(\frac{\lambda_x}{\lambda_0} \right)^{a_2} + a_3 \left(\frac{\lambda_x}{\lambda_0} \right)^{-4}. \quad (10)$$

Thus although our correction algorithm (Eq. 7) only utilizes the differential reflectance at the excitation wavelength, measurement of the complete differential reflectance spectrum is required to estimate $\boldsymbol{DR}_x(0)$ accurately. Furthermore, it follows from this analysis that our correction algorithm can in principle correct for background absorption at any excitation wavelength, provided that the absorption coefficients of all the absorbing molecules are known such that $\boldsymbol{DR}_x(0)$ can be estimated accurately using the previously described fitting routine.

In this phantom study, a single exogenous fluorophore was used to study the influence of the optical properties on the FDPS signal. However, our technique can be applied to any number of endogenous as well as exogenous fluorophores. Of particular interest could be the study of native tissue fluorescence of neoplastic epithelial tissues using FDPS, where the small sampling depth of FDPS allows sensitive measurements of potential changes in the concentration of epithelial fluorophores involved in the cellular metabolism such as NADH.

The presence of background absorption is an important parameter to consider both in quantitative fluorescence and elastic scattering spectroscopic measurements. Even when the path length of measured photons varies little with scattering coefficient, the

path length will still depend on the absorption coefficient. In the measurement geometry of Canpolat and Mourant [12] and Diamond *et al.*[15] (fluorescence) or Mourant *et al.*[1] (absorption) the background absorption dependence of the signals reduces the validity range of their approach to only small variations in the background absorption coefficient, and generally to the red and near-infrared wavelength regions. For quantitative fluorescence measurements with excitation in the blue or green wavelength regions, a measurement technique is needed that does not depend so heavily on background absorption, since the absorption coefficient of tissue in these wavelength regions is much higher and may vary significantly within the target tissue. Therefore, the advantage of FDPS over other quantitative fluorescence measurements is its capability to deal with large variations in background absorption using a simple correction algorithm. This makes FDPS especially valuable for in vivo photosensitiser fluorescence spectroscopy during PDT, when the background absorption at these wavelengths can change dramatically. Note that the scattering coefficient is not expected to vary by more than a factor of 2 during PDT[3,26] and will therefore have a small influence on the FDPS signal.

Another advantage of FDPS is that the collection volume can be adjusted to match the relevant dimensions of the application. For absolute fluorescence measurements of photosensitisers or chemotherapy drugs that preferentially localize at specific depths in the tissue, it is essential to selectively interrogate the relevant tissue volume and to avoid averaging drug concentrations over larger/smaller volumes by probing too deep/ shallow in the tissue. With FDPS, this can be achieved by choosing the appropriate fiber diameter since the collection volume is proportional to the fiber diameter[5].

Another potential advantage of FDPS is that, no matter which fiber diameter is used, the measurement volume is always relatively small. Hence multiple FDPS measurements can be used to obtain information on the often heterogeneous distribution of fluorophores in larger tissue volumes[27]. Finally, FDPS is of particular interest for monitoring PDT since a DPS measurement, apart from correcting the differential fluorescence for background absorption changes, also gives information on other important PDT parameters such as the local oxygen saturation, blood volume and changes in scattering. The most appropriate applications of FDPS are likely to be associated with superficial (or intra-luminal) PDT[26]. Here combinations of fiber diameters can also serve to interrogate, and compare different tissue volumes. Therefore, we believe that combining the FDPS and DPS measurements during PDT will give valuable information regarding the PDT process.

Acknowledgement

This research is supported by the Dutch Technology Foundation STW, applied science division of NWO and the Technology Program of the Ministry of Economic Affairs, and by the NIH, grant NIH/NCI U54 CA104677.

References

1. Mourant JR, Bigio IJ, Jack DA, Johnson TM, Miller HD. Measuring absorption coefficients in small volumes of highly scattering media: source–detector separations for which path lengths do not depend on scattering properties. Appl. Opt. 1997; 36:5655–5661.
2. Mourant JR, Johnson TM, Los G, Bigio IJ. Noninvasive measurement of chemotherapy drug concentrations in tissue: preliminary demonstrations of in vivo measurement. Phys. Med. Biol. 1999; 44:1397–1417.
3. Amelink A, van der Ploeg-van den Heuvel A, de Wolf WJ, Robinson DJ, Sterenborg HJCM. Monitoring PDT by means of superficial reflectance spectroscopy. J. Photochem. Photobiol. B: Biol. 2005; 79:243-251.
4. Amelink A, Sterenborg HJCM. Measurement of the local optical properties of turbid media using differential pathlength spectroscopy. Appl. Opt. 2004; 43:3048-3054.
5. Kaspers OP, Sterenborg HJCM, Amelink A. Controlling the optical path-length in turbid media using differential path-length spectroscopy: fiber diameter dependence. Appl. Opt. 2008; 47, 365-371.
6. Wilson BC, Patterson MS, Lilge L. Implicit and explicit dosimetry in photodynamic therapy: a new paradigm. Lasers Med. Sci. 1997; 12:182-199.
7. Robinson DJ, de Bruijn HS, van der Veen N, Stringer MR, Brown SB, Star WM. Fluorescence photobleaching of ALA-induced protoporphyrin IX during photodynamic therapy of normal hairless mouse skin: the effect of light dose and irradiance and the resulting biological effect. Photochem. Photobiol. 1998; 67:140-149.
8. Woodburn K, Chang CK, Lee S, Henderson B, Kessel D. Biodistribution and PDT efficacy of a ketochlorin photosensitizer as a function of the delivery vehicle. Photochem. Photobiol. 1994; 60:154-159.
9. Aveline B, Hasan T, Redmond RW. Photophysical and photosensitizing properties of benzoporphyrin derivative monoacid ring A (BPD-MA). Photochem. Photobiol. 1994; 59:328-335.
10. Zhang Q, Muller MG, Wu J, Feld MS. Turbidity-free fluorescence spectroscopy of biological tissue. Opt. Lett. 2000; 25:1451-1453.
11. Muller MG, Georgakoudi I, Zhang Q, Wu J, Feld MS. Intrinsic fluorescence spectroscopy in turbid media: disentangling effects of scattering and absorption. Appl. Opt. 2001; 40:4633-4646.
12. Canpolat M, Mourant JR. Monitoring photosensitizer concentration by use of a fiber-optic probe with a small source–detector separation. Appl. Opt. 2000; 39:6508-6514.
13. Weersink R, Patterson MS, Diamond K, Silver S, Padgett N. Noninvasive measurement of fluorophore concentration in turbid media with a simple fluorescence/reflectance ratio technique. Appl. Opt. 2001; 40:6389–6395.
14. Pogue BW, Burke G. Fiber-optic bundle design for quantitative fluorescence measurement from tissue. Appl. Opt. 1998; 37:7429–7436.
15. Diamond KR, Patterson MS, Farrell TJ. Quantification of fluorophore concentration in tissue-simulating media by fluorescence measurements with a single optical fiber. Appl. Opt. 2003; 42:2436-2442.
16. Welch AJ, van Gemert MJC, eds., Optical-thermal response of laser irradiated tissue (Plenum, New York, 1995), pp. 280-300
17. Doornbos RMP, Lang R, Aalders MC, Cross FW, Sterenborg HJCM. The determination of in vivo human tissue optical properties and absolute chromophore concentrations using spatially resolved steady-state diffuse reflectance spectroscopy. Phys. Med. Biol. 1999; 44:967-981.
18. Ghosh N, Mohanty SK, Majumder SK, Gupta PK. Measurement of optical transport properties of normal and malignant human breast tissue. Appl. Opt. 2001; 40:176-184.

19. Fishkin JB, Coquoz O, Anderson ER, Brenner M, Tromberg BJ. Frequency-domain photon migration measurements of normal and malignant tissue optical properties in a human subject. Appl. Opt. 1997; 36:10-20.
20. Qu J, MacAulay C, Lam S, Palcic B. Optical properties of normal and carcinomatous bronchial tissue. Appl. Opt. 1994; 33:7397-7405.
21. Birge RR. Kodak Laser Dyes. 1987.
22. Amelink A, Bard MPL, Burgers JA, Sterenborg HJCM. In vivo measurement of the local optical properties of tissue using differential pathlength spectroscopy. Opt. Lett. 2004; 29:1087-1089.
23. Bard MPL, Amelink A, Noordhoek Hegt V, Graveland WJ, Sterenborg HJCM, Hoogsteden HC, Aerts JGJV. Measurement of hypoxia-related parameters in bronchial mucosa by use of optical spectroscopy. Am. J. Respir. Crit. Care Med. 2005; 171:1178-1184.
24. van Veen RLP, Amelink A, Menke-Pluymers M, van der Pol C, Sterenborg HJCM. Optical biopsy of breast tissue using differential path-length spectroscopy. Phys. Med. Biol. 2005; 50:2573-2581.
25. Amelink A, Kaspers OP, Sterenborg HJCM, van der Wal JE, Roodenburg JL, Witjes MJH. Non-invasive measurement of the morphology and physiology of oral mucosa by use of optical spectroscopy. Oral Oncology 2008; 44:65-71.
26. Kruijt B, de Bruijn HS, van der Ploeg-van den Heuvel A, de Bruin RWF, Sterenborg HJCM, Amelink A, Robinson DJ. Monitoring ALA-induced PpIX-photodynamic therapy in the rat esophagus using fluorescence and reflectance spectroscopy. Photochem. Photobiol., in press 2008.
27. Mitra S, Maugain E, Bolotine L, Guillemin F, Foster TH. Temporally and spatially heterogeneous distribution of mTHPC in a murine tumor observed by two-color confocal fluorescence imaging and spectroscopy in a whole-mount model. Photochem Photobiol. 2005; 81:1123-1130.

4

Ex Vivo Quantification of m-THPC Concentration in Tissue: Influence of Chemical Extraction on the Optical Properties

S. Kaščáková
B. Kruijt
H.S. de Bruijn
A. van der Ploeg-van den Heuvel
D.J. Robinson
H.J.C.M. Sterenborg
A. Amelink

Abstract
A method for the quantification of the concentration of the photosensitizer meta-tetra(hydroxyphenyl) chlorin (m-THPC) in tissue samples is presented. The technique is an extension of a previously published method based on alkaline hydrolysis of tissue, using Solvable™ as a tissue solubilizer. m-THPC quantification was achieved by subsequent fluorescence spectroscopy. Since the original extraction method involved multiple steps in which water dilution of the sample was implemented, we studied the spectral characteristics of m-THPC in different Solvable™/water mixtures. Using UV-VIS absorption and fluorescence spectroscopy, it was demonstrated that the spectral characteristics of m-THPC vary for different Solvable™ concentrations. In the range of 20% to 100% Solvable™, the fluorescence intensity of m-THPC did not change, while dramatic changes in the m-THPC fluorescence intensity were observed for lower Solvable™ concentrations (< 20%) due to increasing hydrophilicity of the environment, combined with pH alterations. We also demonstrated that the absorption and fluorescence spectra of the dissolved tissue were time-dependent. Longer incubation of the samples resulted in a significant increase of the native tissue chromophore fluorescence. This implies that for the correct quantification of photosensitizer concentrations, the fluorescence of native tissue chromophores must be accounted for.

Cover: Pointe du Hoc, Calvados-Normandy, France (July 2009).

Published in Journal of photochemistry and photobiology:B, 2008, 91(2-3):99-107

INTRODUCTION

Extraction methods for the determination of photosensitizer concentration in tissue are based on separation of the photosensitizer from the tissue components prior to measurement. The photosensitizer quantification has been achieved by radiolabeling[1,2], chromatographic analysis, such as HPLC chromatography[2,3] or by optical absorption and fluorescence spectroscopy[4-6]. The latter method of quantification is inexpensive and technically simple, although caution is required in combining extraction chemicals with absorption and fluorescence spectroscopy, since the photosensitizer's optical properties (absorption spectra, fluorescence spectra, lifetime and quantum yields) will depend on the tissue solubilizer that is employed. For instance, hydrophobic photosensitizers tend to aggregate in aqueous medium, leading to dramatic changes in the absorption and fluorescence properties[7,8]. For porphyrin-type sensitizers and their related compounds, such as photosensitizers of tetraphenylchlorin series, the arrangement of porphyrins in aggregates is cofacial and two types of porphyrin aggregates are known: J-type (edge-to-edge) and H-type (face-to-face). Compared to the absorption spectra of the monomer, the Soret and Q bands in absorption spectra of J(H)-type aggregates is red (blue) shifted accompanied with band broadening. These changes in the absorption spectra are linked by a strong decrease of the fluorescence intensity[7,9]. Thus when fluorescence spectroscopy is used for the quantification of photosensitizer concentration in tissues, the solvent should be chosen such that complete tissue solubilization is ensured, without creating an environment in which the photosensitizer exhibits a low fluorescence quantum yield. Moreover, extraction methods usually involve multiple steps (solvation, incubation and dilution) and changes in spectroscopic properties of photosensitizers could arise during any of these steps. For these reasons, it is necessary to investigate the spectroscopic properties of the target-photosensitizing drug in the solvent, which is going to be employed to dissolve the tissue.

Several extraction methods have been published, using different solvents to dissolve tissue and thus separate the photosensitizer chemically from the tissue [4, 5, 10-12]. Lilge and associates[4] extensively studied a method first presented by Henderson *et al*.[5], in which Solvable™ was used for tissue solubilization and the photosensitizer (protoporphyrin IX) quantification was measured using fluorescence spectroscopy. Solvable™ is the proprietary name for a mixture of dodecyldimethylamine oxide, secondary alcohol ethoxylate and sodium hydroxide (NaOH) in water. In the method originally described by Henderson *et al*.[5] complete tissue solubilization was reached after the sample was incubated in 1 ml of Solvable for 16 hours at 50 ^{0}C. Prior to the application of fluorescence spectroscopy, the samples were cooled to room temperature and diluted with 1 ml of distilled water, followed by internal spiking for absolute quantification. The described method[5] was tested by Lilge *et al*.[4] for six different photosensitizers in a variety of tissues. For tissue containing photosensitizers dissolved in Solvable they found that for long solubilization times (t > 4 hours), a decrease of the fluorescence signal was evident, and a 2-4 hour time window was subsequently used in all measurements. Hence the most significant difference between the technique originally described[5] and its modified version by Lilge *et al*.[4] was the time of contact between Solvable and the photosensitizer: approximately 16 hours vs. 2-4

hours, respectively. In addition, Lilge *et al*.[4] also highlighted the importance of a low optical density of the sample for fluorometry, which was not addressed in the earlier work. By assuring a low optical density at the excitation wavelength (O.D. < 0.1), one can minimize the self-absorption effect, which causes an undesirable non-linearity between fluorescence intensity and photosensitizer concentration. Thus to ensure a low optical density of the sample for fluorometry, it may be necessary to dilute the solubilized samples further depending on photosensitizer concentration, tissue pigmentation and the excitation wavelength.

The modified solubilization technique for photosensitizer quantification in ex vivo tissue samples, published by Lilge *et al*.[4], consisted of (step (1)) solubilization of tissue sample in 2 ml of Solvable using a shaking water bath at 50 ^{0}C for 1-2 hours. In the second step (2), five 0.2 ml aliquots of the resulting homogenate were each diluted with 1 ml Solvable and 3 ml distilled water and returned to the water bath for another 1 hour. In the third step (3), prior to fluorometry, the sample O.D. at the excitation wavelength was measured and, if required, dilution of the sample with distilled water was performed (sample O.D. at the excitation wavelength was reduced to below 0.1). Thus before fluorescence spectroscopy, in the protocol of Lilge *et al*.[4] the samples changed their environment from 100 % Solvable (step (1)) to 29 % Solvable (step (2)), with an additional decrease of Solvable percentage, if water dilution (to ensure a low optical density) was necessary (step (3)). As discussed above, we believe this change in environment could lead to changes in the spectroscopic properties of the photosensitizer.

Considering that Solvable is an aqueous-based solubilizer with ≤ 2.5 % NaOH content, water dilution will decrease the concentration of NaOH resulting in a drop of pH (the extent of this decrease as a function of dilution factor can be calculated by the pH and pOH definitions[13]). The protonation/deprotonation of ionizable groups within the photosensitizer will also result in modification of drug optical properties. Thus for increasing water dilution factors, an increase in hydrophilicity of the environment as well as pH changes can prevent a reliable interpretation of the obtained fluorescence signals and limit the accuracy and reproducibility of the results.

In our opinion, to improve the accuracy and reproducibility of this method, more attention needs to be paid to the details of the spectroscopic properties of the photosensitizer, the dissolved tissue as well as the photosensitizer/tissue mixtures in Solvable (and in different Solvable/water mixtures). In addition, little is known about the variations in time of the optical properties of tissue in these solubilized environments. The present report therefore describes a modified version of the method of Lilge *et al*.[4] that takes these environment related effects into account. We have applied our method to measure the concentration of the second-generation photosensitizer, 5,10,15,20–tetra(m-hydroxyphenyl)chlorin (m-THPC, proprietary name Foscan®) in liver tissue, which is known to be highly pigmented. Several pharmacokinetics studies demonstrated extremely high concentration of m-THPC in the liver at early time points (1-4 hours) from intravenous injection[1,2,10]. The present method was therefore applied on the liver dissected after 3 hours from m-THPC intravenous injection.

MATERIALS AND METHODS

Chemicals

Solvable™, a mixture of dodecyldimethylamine oxide (2.5-10%), secondary alcohol ethoxylate (2.5-10%) and sodium hydroxide (≤ 2.5%) in water, was purchased ready to use from Perkin Elmer (Groningen, The Netherlands). Polyethylene glycol 400 (PEG400) was obtained from Sigma-Aldrich (Zwijndrecht, The Netherlands) and 96% ethanol (EtOH) was purchased from Merck (Amsterdam, The Netherlands). m-THPC (Foscan®) (c = 4 mg m-THPC/ml dissolved in PEG, EtOH, water free solution) was obtained from Biolitec pharma (Edinburgh, The United Kingdom).

Preparation of m-THPC in Solvable

Stock solutions of m-THPC (c = $1.7x10^{-4}$ M and c = $3x10^{-3}$ M) were prepared by dissolving m-THPC in a solution of PEG400:EtOH:water = 2:3:5 (v/v) (henceforward referred to as the PEG solvent system). These solutions were stored in the dark at 4 ^{0}C for at least 30 minutes prior to use, after which the samples were determined to be stable, i.e. no changes in fluorescence intensity were detected. The solutions of m-THPC in Solvable and/or different Solvable/water ratios were prepared by diluting the stock solution of m-THPC (c = $1.7x10^{-4}$ M) with different Solvable/water mixtures, to reach the final m-THPC concentration of c = 0.51 μM. The fluorescence spectra were recorded immediately after the sample preparation and the measurements were repeated two times. Keeping the quantity of the PEG-solvent system less than 1% excluded the influence of the PEG-solvent system on m-THPC properties in these solutions.

To investigate the potential effects of m-THPC aggregation, the absorption spectra of m-THPC were recorded in the concentration range c = 0.11 – 16.70 μM. The solvents studied were the PEG solvent system as well as 100% and 29% Solvable. The concentration range c = 0.11 – 0.98 μM of m-THPC samples in PEG solvent system and in 100% and 29% Solvable was prepared by diluting the stock solution of m-THPC (c = $1.7x10^{-4}$ M), whereas for the concentration range c = 1.97 – 16.70 μM the m-THPC stock solution (c = $3x10^{-3}$ M) was used. Variations in the wavelength of absorption maxima, spectral peak broadening and deviations from Beer's law were attributed to aggregation[7].

Animals and measurement procedure

The animal experiment committee of the Erasmus Medical Center approved the experimental design for this study. Two weeks before commencing the experiments 4 normal adult male Wistar rats (weight m = 410 ± 23 g) were placed on a diet of chlorophyll free food to minimize the influence of autofluorescence centered at 675 nm due to pheophorbide-a. Two rats were injected with 0.3 mg/kg m-THPC i.v. The control animals (2 rats) were injected with the PEG solvent system alone. Injections were made under isoflurane/O_2/N_2O anesthesia. After the injection, the conscious animals were placed in a dark and warm environment. Three hours after m-THPC or PEG solvent system injection, the rats were anesthetized and the tissue overlying the liver was dissected. The main arteries and veins of the liver were clamped to minimize the loss of blood. Hereafter the liver was excised and snap frozen in liquid nitrogen.

Tissue solubilization

Each tissue sample (approximately 0.1 – 0.2 g wet weight) was chopped into small pieces using a scalpel blade, immersed in 2 ml of Solvable in a plastic tissue culture tube and placed into a shaking water bath at 50 ^{0}C for 2 hours until the solution was clear without any visible tissue residue.

Three 0.15 ml aliquots of the resulting tissue homogenate were each diluted with 3 ml Solvable and returned to the water bath for another 1 hour. For the study of the influence of the incubation time on the spectroscopic properties of tissue alone and tissue containing m-THPC, the incubation time window 1-4 hours was chosen.

Prior to fluorescence measurements, the samples were cooled to room temperature and their optical density (OD) was measured. If required, the sample OD at the excitation wavelength was reduced to below 0.1, by a known dilution factor with Solvable.

The emission spectrum was analyzed as a linear combination of basis fluorescence spectra using a singular value decomposition (SVD) algorithm based on that of Finlay *et al*.[14] implemented in MATLAB (The Mathworks, Inc., Natick, MA). The three basis fluorescence spectra used in the analysis are those of Foscan in Solvable, dissolved control tissue in Solvable and Solvable alone.

After subtracting the contributions of control tissue in Solvable and Solvable itself to the fluorescence spectrum, the m-THPC concentration was calculated according to a calibration curve obtained from mixing of a known concentration of m-THPC with a dissolved control rat liver tissue sample (or, giving the same result, a known concentration of m-THPC mixed with Solvable).

The measurements were repeated as follows: From each liver, three tissue samples (approximately 0.1 – 0.2 g wet weight) were taken and were immersed in Solvable. After two hours, three 0.15 ml aliquots were taken from each of the three tissue homogenates. These aliquots were diluted with Solvable and incubated for another 1 hour. Thus the measurements for each liver sample (0.1 - 0.2 g weight) were repeated three times.

Experimental procedures

Absorption

Absorption spectra were recorded at 20 ^{0}C using a 1 cm quartz cuvette in an UV-VIS spectrophotometer (UV-2101 PC, Shimadzu Deutschland GmbH, Duisburg, Germany) in the wavelength range 240-800 nm with a slit width combination that resulted in a resolution of 2.0 nm.

Fluorescence

Fluorescence spectra were recorded at 20 ^{0}C using the 1 cm quartz cuvette in a LS 50B (Perkin Elmer, Waltham, Massachusetts, USA) spectrofluorometer with the slit width 5.0 nm for excitation and 10.0 nm for emission. Absorption and fluorescence spectra were analysed using Microcal Origin, version 6.0 (Microcal Software, Inc., Northampton, MA).

pH measurements

The pH values of the different Solvable/water ratio samples (prepared separately, by mixing the water and Solvable into the final desired ratio) were measured using a Sentron pH meter (Sentron Europe, Roden, The Netherlands). The pH meter was calibrated with standard buffer solutions under the enclosed instructions of Sentron Europe. All measurements were carried out at room temperature, T = 20 ^{0}C, while continuously stirring the samples. The measurements were repeated 2 times.

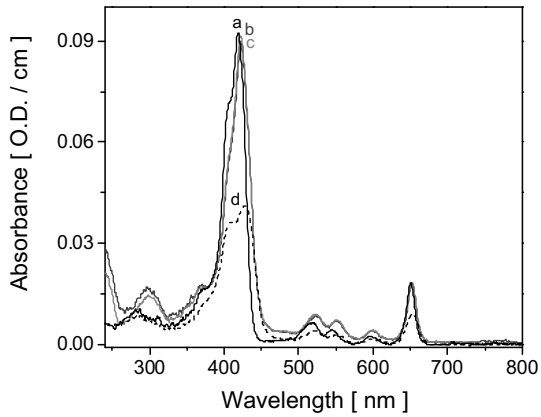

Figure 1. Absorption spectra of m-THPC at a concentration c = 0.49 µM in different solvent conditions: (a = solid black) in PEG400:EtOH:H_20; (b = dark gray) in 100% Solvable; (c = gray) in 29% Solvable; and (d = dashed black in aqueous solution.

RESULTS

In vitro spectroscopic characterization of m-THPC in different media

Absorption spectra. The absorption spectra of m-THPC (c = 0.49 µM) in different solvents are presented in figure 1. In the PEG solvent system (Fig. 1, line a) m-THPC has a characteristic absorption spectrum of chlorin-type compounds with two main peaks centered on 419 nm (Soret band) and 651 nm (Q band). Over the concentration range c = 0.11 – 16.7 µM the spectrum of m-THPC in the PEG solvent system did not change significantly and the solution accurately followed Beer's law (Fig. 2, filled squares) with no evidence of spectral broadening or shifts in absorption maxima (data not shown). Therefore we conclude that the same species of m-THPC, i.e. the monomer, is present throughout this concentration range. Changes, that are consistent with aggregation, were observed after mixing of m-THPC in H_2O (Fig. 1, line d). The aggregated species are characterized by a decrease of extinction in all bands combined with bathochromic shifts. The bathochromic shift of the Soret band to λ = 427 nm is the most pronounced. These features are consistent with the characterization of the J-type structure of aggregates[7]. The spectroscopic properties of m-THPC in the presence of 100% as well as 29% of Solvable displayed transitional features between the PEG solvent system and the aqueous medium (Fig. 1, lines b and c). Compared to the PEG solvent system, the m-THPC Soret absorption band in both 100% and 29% Solvable was characterized by a bathochromic shift to λ = 423

nm. The half height bandwidths of the Soret band in these media were considerably reduced compared to the aqueous medium and are close to the bandwidth in the PEG solvent system (Fig. 1). To determine if there was any evidence for aggregate formation in 100% and 29% Solvable, variations in the wavelength of absorption maxima, spectral peak broadening and deviations from Beer's law were investigated. Over the concentration range c = 0.11 – 16.7 µM the spectrum of m-THPC in 100% and 29% of Solvable did not change (data not shown) and the system accurately followed Beer's law (Fig. 2, open circles and open triangles, respectively).

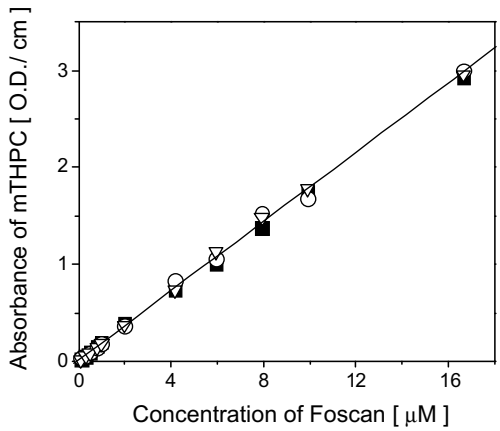

Figure 2. Beer's law plots for the Soret band (λ = 419 nm PEG-solvent system and/or λ = 423 nm Solvable) of m-THPC: (■) in PEG : EtOH : H2O = 2 : 3 : 5 by volume; (○) in 100% Solvable; (△) in 29% Solvable.

Fluorescence spectra The fluorescence emission spectra of m-THPC (c = 0.49 µM) in different surroundings are shown in figure 3. m-THPC exhibited a negligible fluorescence in H2O (Fig. 3, line d). This fact is well documented and has been attributed to the formation of almost nonfluorescent aggregates of m-THPC. The fluorescence spectrum of m-THPC in the presence of 100% or 29% Solvable is the same for both solvent systems (Fig. 3, line b and c), with the maximum slightly shifted from 653 nm (PEG solvent system, Fig. 3, line a) to 656 nm (Solvable). Although in 100 % and 29% of Solvable, the m-THPC fluorescence intensity is two orders of magnitude greater than for m-THPC in aqueous solution, it is still lower compared to monomeric m-THPC in the PEG solvent system (Fig. 3). The absorption spectra over the concentration range (c = 0.11 – 16.7 µM) did not change and no deviations from Beer's law were detected in 100% and 29% Solvable (Fig. 2). Thus the pH value of the solutions was reasonable to consider as an important factor of the detected low fluorescence intensity of m-THPC in 100% and 29% Solvable. Measuring of the pH of m-THPC in 100% and 29% Solvable revealed very similar pH values for both surroundings, i.e. pH = 12.7 for 29% Solvable and pH = 12.8 for 100% Solvable, compared to a pH of 4.3 in the PEG solvent system. Since over the above mentioned concentration range the absorption spectra did not reveal any spectral changes in

100% and 29% Solvable, we conclude that m-THPC is monomeric in these surroundings and its low fluorescence intensity (compared to the PEG solvent system) is related to the basicity of its environment.

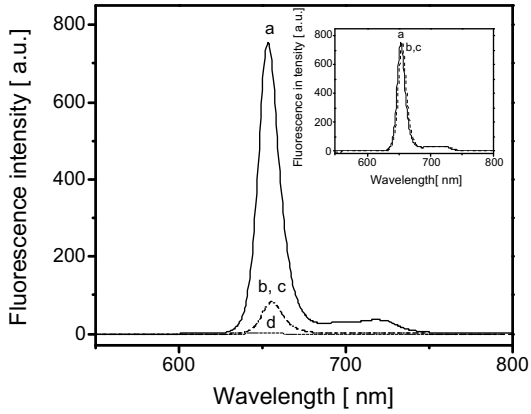

Figure 3. Fluorescence emission spectra (excitation wavelength 422 nm) of m-THPC at a concentration c = 0.49 µM in different solvent conditions: (a) in PEG : EtOH : H2O = 2 : 3 : 5 by volume; (b) in 100% Solvable; (c) in 29% Solvable; and (d) in aqueous solution. The inset shows the normalized fluorescence emission spectra.

The fluorescence intensity of m-THPC (c = 0.51 µM) at its maximum at 656 nm as a function of Solvable concentration is shown in figure 4. Between 100% Solvable and 20% Solvable, the fluorescence intensity of m-THPC does not change significantly. Below a Solvable concentration of 20%, a decrease of m-THPC fluorescence was observed. Below a concentration of 1% Solvable another increase of fluorescence intensity was detected. The intensity increased down to a 0.15% Solvable concentration. Below this concentration the fluorescence intensity of m-THPC steeply declined. The measured pH values of the solutions revealed only minor pH changes from 20-100% Solvable (pH = 12.6-12.8) and from 1-20% Solvable (pH = 12.0-12.6). However, between 0.015-1% Solvable, the pH values ranged between pH = 9.4-12.0. In this range of Solvable/water ratios the fluorescence intensity of m-THPC changed the most.

With respect to sample preparation, no changes in absorption and fluorescence intensity of m-THPC (c = 0.58 µM) were detected in 100% and 29% of Solvable after up to 4 hours incubation in the 50 ^{0}C water bath (data not shown). Thus for times of incubation as long as t = 4 hours, the m-THPC chemical bleaching by Solvable can be excluded.

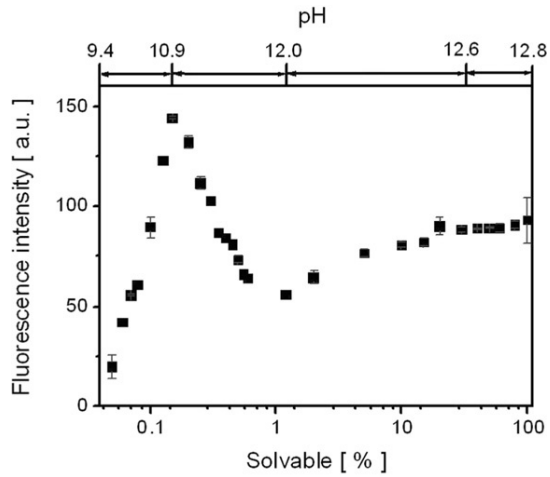

Figure 4. Fluorescence intensity of m-THPC (c = 0.51 μM) (fluorescence maximum at 656 nm, excitation line at 423 nm) in different Solvable/water solutions.

Spectroscopic characterization of dissolved liver tissue samples

The absorption spectra of rat liver tissue sample after in vivo administration of m-THPC (c = 0.3 mg/kg) (dissolved in 100% Solvable followed by dilution in 100% Solvable and further 1 hour incubation) and rat liver sample without m-THPC content are shown in figure 5, lines a and b, respectively. Both spectra show broad absorption bands at 325 nm, 400 nm and in the red wavelength region around 596 nm. There is only a minor difference between the absorption spectra of the liver tissue sample with and without injected m-THPC. Since it is important for accurate photosensitiser concentration measurements to optimize the relative fluorescence of the photosensitiser compared to the tissue/solvent fluorescence background, the excitation wavelength should be chosen such that the ratio of photosensitizer absorbance to tissue/solvent absorbance is at its maximum. Line c in figure 5 shows the absorption spectrum of control liver (dissolved in 100% Solvable followed by dilution in 100% Solvable) mixed with a large concentration of m-THPC (c = 0.26 μM) and further 1 hour incubation. Clearly the ratio of the absorption spectra of lines c and a (or b) is maximal at the Soret band of m-THPC in 100% Solvable, λ = 423 nm.

With regard to the incubation time of the diluted tissue homogenate for 1 hour (step 2 in the sample preparation protocol of Lilge *et al.*[4]), the tissue characteristics in 100% and 29% Solvable were studied as a function of incubation time. The absorption spectra of the control tissue sample (dissolved in 100% of Solvable for 2 hours, diluted with 100% of Solvable) followed by incubation for different time periods are shown in figure 6. With increasing time of incubation, the intensity of the absorption band at 400 nm decreases while there is an increase of the intensity at wavelengths around 325 nm (Fig. 6). Fluorescence excitation of control rat liver tissue samples (dissolved in 100% of Solvable) at λ = 423 nm revealed a fluorescence emission peak around 500 nm (Fig. 7a). Longer periods of incubation of the sample resulted in a significant increase of this control tissue/Solvable chromophore fluorescence emission band (Fig. 7a). The same

spectral characteristics and temporal fluorescence characteristics were observed for absorption and fluorescence spectra of diluted control tissue homogenate in 29% Solvable (data not shown). Compared to tissue homogenate in 100% Solvable, the dilution of the tissue with distilled water to 29% Solvable led to a slight decrease in the fluorescence intensity of the tissue/Solvable mixture (data not shown).

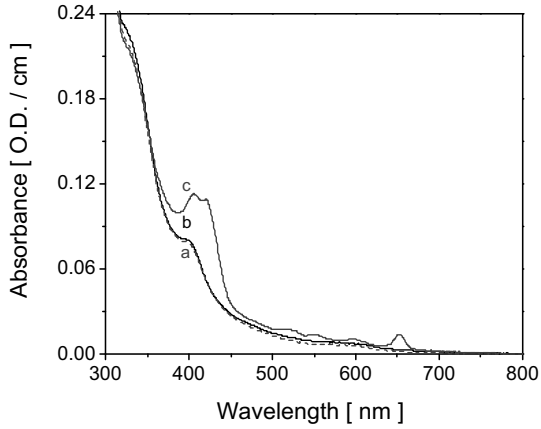

Figure 5. Comparison of absorption spectra of dissolved liver tissue samples: (a = gray) with m-THPC content, (b = dark gray) control liver tissue sample and (c = black) dissolved control liver mixed with m-THPC (c = 0.26 µM) in 100% Solvable.

The dependence of the spectral properties of the liver sample, obtained after in vivo administration of m-THPC (c = 0.3 mg/kg), as a function of total time of incubation in 100 % of Solvable is shown in figure 7b. The temporal dependence was examined by liver solubilization in 100% Solvable for 2 hours, dilution with 100% Solvable, followed by incubation for different time periods. Since the position of m-THPC emission peak was at 656 nm, the steep increase in the fluorescence intensity due to the tissue/ Solvable chromophore around 500 nm wavelength seems to only slightly influence the m-THPC fluorescence (Fig. 7b). However, the tissue/Solvable chromophore does contribute significantly to the fluorescence at 656 nm and should therefore be accounted for in the analysis of the fluorescence signals. After corrections for this tissue/Solvable background using SVD, no significant changes in the fluorescence intensity of the m-THPC for up to 220 min incubation in a 50 ^{0}C water bath were observed (Fig. 7b inset). The gradient of fitted m-THPC fluorescence intensities between the 150 min up to 220 min is not significantly different than 0 ($P > 0.05$). In addition for longer time intervals ($t > 220$ min) the fluorescence intensity of m-THPC decreased (Fig. 7B inset). T-tests revealed significant differences with incubation time for $t = 220$ min; $p < 0.010$ for all time points $t > 255$ min. The same result was obtained for a dissolved control liver tissue sample mixed with a known concentration (c = 0.26 µM) of m-THPC (data not shown). Thus in the case of photosensitizer contact with Solvable for $t > 4$ hours, chemical bleaching of m-THPC was detected (approximately 15% for the 6 hour time point).

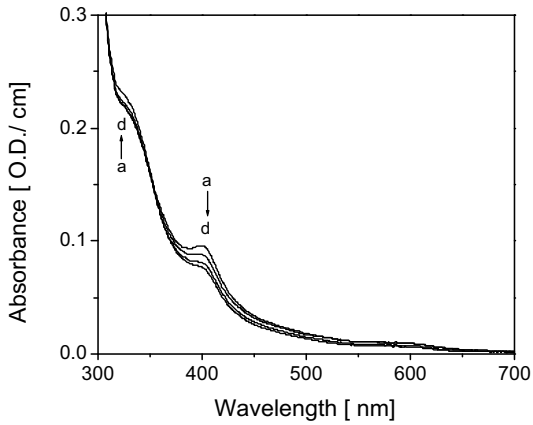

Figure 6. Effect of the total time of incubation on the absorption spectra of dissolved liver tissue samples without m-THPC content (control liver) in 100% Solvable: (a) 190 min; (b) 260 min; (c) 330 min; (d) 410 min. Note that these times include the first incubation step of 120 min.

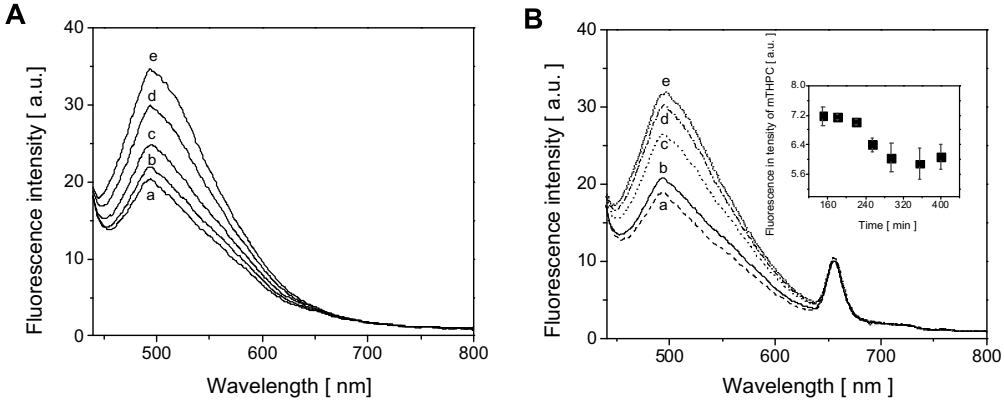

Figure 7. Fluorescence emission spectra (λ_{exc} = 423 nm) of the rat liver tissue sample a) without m-THPC content followed for periods of incubation (contact with Solvable): a) 120 min; (b) 160 min; (c) 190 min; (d) 260 min; (e) 360 min. b) with m-THPC content as a function of total time of incubation in 100% Solvable: (a) 150 min; (b) 180 min; (c) 220 min; (d) 255 min; (e) 295 min. The inset shows the dependence of the m-THPC fluorescence on the total time of incubation after correction for tissue/solvent fluorescence background using SVD. Note that these times include the first incubation step of 120 min.

Degree of tissue solubilization

The capacity of Solvable for solubilization of liver tissue samples was also studied. The dissolved homogenate of control liver tissue sample was mixed with a known concentration of m-THPC (c = 0.37 μM) followed by another incubation for t = 4 h in a 50 ^{0}C water bath. After the incubation, the absorption spectrum of the control liver homogenate in 100% Solvable was subtracted from the absorption spectrum of dissolved control liver mixed with m-THPC and compared with the m-THPC absorption spectrum in 100% Solvable (Fig. 8). The agreement in the absorption spectra (no wavelength shifts in the absorption maxima) indicates totally dissolved tissue and therefore no binding of m-THPC with any resulting tissue residual.

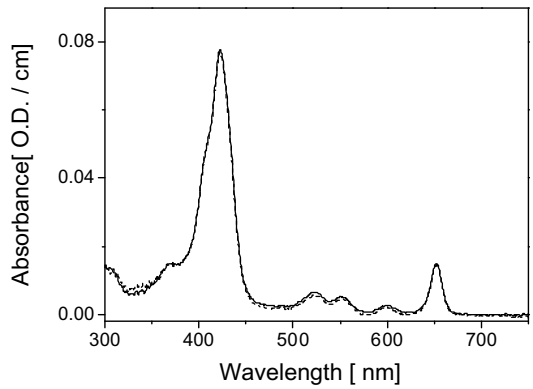

Figure 8. Comparison of the absorption spectra of m-THPC in 100% Solvable (black) with the absorption spectra of m-THPC obtained after the subtraction of tissue absorption from the dissolved liver tissue mixed with m-THPC (gray). Incubation of dissolved liver sample in 100% Solvable was for t = 4 hours.

DISCUSSION

In several studies[15-18] Solvable was used as tissue solvent, following the solubilization technique published by Lilge *et al*.[4]. Since in the original method used by Henderson *et al*.[5] as well as in its modified version[4] the solubilized samples (in 100% Solvable) are further diluted with distilled water to different extents, the measurements presented here were intended to investigate the influence of water dilution on the fluorescence intensity of m-THPC.

It has been demonstrated that the fluorescence intensity of m-THPC changes in different environments, i.e. Solvable/water mixtures (Fig. 4). Between 100% Solvable and 20% Solvable, the fluorescence intensity of m-THPC is stable. However, below 20% Solvable significant changes (both increases and decreases) in the fluorescence intensity of m-THPC were observed. Our interpretation of these data is that monomerization of m-THPC becomes important in aqueous Solvable environments for concentrations above 1% Solvable. Thus for 1% Solvable, aggregation of m-THPC molecules decreases the fluorescence, and increasing monomerization leads to increased fluorescence for increasing Solvable concentrations up to 20% Solvable,

after which monomerization is complete. However, between 0% and 1% Solvable, the fluorescence intensity of m-THPC showed dramatic changes and was at 0.2% Solvable even higher than at 100% (Fig. 4). This is most likely the consequence of the fact that Solvable can act not only as a solubilizer for m-THPC, but due to its composition (Solvable is a very basic solution) is likely to cause protonation/ deprotonation of m-THPC as well. This hypothesis is supported by the observation of measured pH values of the studied solutions (Fig. 4). In 0.015–1.000% Solvable solutions the pH values change in the range of pH = 9.4–12.0, while only minor pH changes are detected from 1-100% Solvable (pH = 12.0-12.8). Thus both processes (aggregation and pH changes) are present throughout the studied Solvable concentration range, but their contribution in the studied range differed. In the work of Bonnet *et al*.[7] the influence of the pH on the absorption spectroscopic properties of m-THPC was studied. The absorbance of the Soret band increased in the pH range 4-8, followed by a decrease between pH = 10-12. It is likely that a change in absorbance is accompanied by a change in fluorescence, although the relationship between absorbance and fluorescence is not trivial. In Cunderlikova *et al*.[19] the fluorescence spectral properties of m-THPC were studied as well, but the studied pH region was lower than that of our interest, i.e. pH = 1-10. To our knowledge from the literature, detailed studies concerning the influence of the pH on fluorescence spectral properties of m-THPC for the region pH = 9-13 are missing.

Due to the large influence of water dilution on the fluorescence intensity of the m-THPC in Solvable (for Solvable/water mixtures < 20%), we decided to exclude water dilution of the tissue from our protocol. Thus we modified the protocol of Lilge *et al*.[4] by only diluting the samples with 100% Solvable, thereby always keeping the tissue and photosensitizer in the same environment, i.e. 100% of Solvable.

Furthermore, we have demonstrated that there is only a small difference between the absorption spectra of control liver tissue sample and the sample containing m-THPC (Fig. 5, line a and b). Thus native tissue chromophore absorption in 100% Solvable seems to be much higher than absorption of m-THPC itself. Therefore, prior to the fluorescence measurements the excitation wavelength was selected to optimize the photosensitizer-tissue chromophore absorption ratio. Excitation at λ_{exc} = 423 nm revealed to be the best for detection of m-THPC in the liver homogenate. In this case, the excitation wavelength (λ_{exc} = 423 nm) corresponded to the wavelength at which m-THPC in 100% Solvable absorbed the most (Fig. 8). However, for other photosensitizers and for different types of tissue, this situation is not necessarily the same and one should carefully consider the absorption and fluorescence properties of the tissue/solvent mixture when selecting the optimal excitation wavelength for the fluorescence measurements.

In the absorption spectra of the liver tissue homogenate one should expect to find features of blood. Comparison of the absorption spectra of control liver tissue homogenate in 100% Solvable (Fig. 5 and 6) with absorption spectra of hemoglobin in 100% Solvable revealed consistent characteristics, i.e. absorption bands at 400 nm and broad absorption band around 596 nm. However, the character of these spectra does not correspond to the well-known absorption spectra of blood [20]. Considering the properties of Solvable (Solvable is an aqueous-based solubilizer with NaOH

content), the biological tissue is decomposed by the process of alkaline hydrolysis, i.e. proteins are denaturated and hydrolyzed. Thus it is not surprising that the optical properties of blood change upon mixing with Solvable.

In addition, we observed that liver tissue homogenates in Solvable exhibit broad fluorescence band in the wavelength region 450-650 nm with a maximum around 500 nm when excited with blue light (λ_{exc} = 423 nm) (Fig. 7). Also we have found that the absorption and fluorescence spectroscopic properties of dissolved liver tissue change with the incubation time (Fig. 6, 7). Longer incubation of the samples resulted in a significant increase of the tissue chromophore characteristics, i.e. the fluorescence emission band at 500 nm increased (Fig. 7). If the fluorescence of the photosensitizer is in the same wavelength region as the native tissue fluorescence, then these temporal fluorescence characteristics of tissue homogenates in Solvable influence the measured photosensitizer fluorescence as well. This may well explain the unreproducibility of the results of Lilge *et al*.[4] with Photofrin. In the work of Lilge *et al*.[4], the excitation of the tissue homogenates containing the photosensitizers was perfomed using blue light (for detection of protoporphyrin IX λ_{exc} = 400 nm; tin-ethyl-etiopurpurin λ_{exc} = 447 nm; tri/tetra-sulfonated chloroaluminum phthalocyanine λ_{exc} = 480 nm; non-sulfonated chloroaluminum phthalocyanine λ_{exc} = 480 nm and photofrin λ_{exc} = 405 nm) with exception for benzoporphyrin derivative monoacid ring A, where the wavelength λ_{exc} = 584 nm was used for excitation. Except for Photofrin, all photosensitizers had emission bands well above 600 nm, where the temporal changes in the fluorescence of the tissue related to incubation time are only minor (Fig. 7a). Photofrin, however, was measured in the 550-625 nm wavelength region where the incubation time does influence the tissue fluorescence. It appears that in their analysis, photosensitizer fluorescence intensity was quantified by integrating the signal within its emission band. Unfortunately, when this approach is used, information concerning the contribution of native tissue fluorescence properties could be missed. In our opinion, even when the tissue/solvent fluorescence is stable, it is important to correct for this background fluorescence to obtain accurate photosensitizer concentrations. Therefore, full spectroscopic analysis of tissue/solvent fluorescence background is necessary to exclude the influence of the tissue/solvent component on the fluorescence intensity of the photosensitizer.

In summary, the accuracy and reproducibility of the technique of Lilge *et al*.[4] for photosensitizer quantification can be improved by: (i) accounting for the tissue/solvent fluorescence background using spectroscopy and by (ii) keeping the same environment during the extraction procedure by diluting only with Solvable.

We would like to emphasize that our study represents the protocol for m-THPC quantification. If a different photosensitizer is administrated and Solvable will be used for tissue solubilization, the spectroscopic properties of this photosensitizer in Solvable and in different Solvable/water mixture should be carefully considered.

Acknowledgements

This research was supported by the Dutch Technology Foundation STW, applied science division of NWO and the Technology Program of the Ministry of Economic Affairs, and by the NIH grant NIH/NCI U54 CA104677.

References

1. Jones HJ, Vernon DI, Brown SB. Photodynamic therapy effect of m-THPC (Foscan) in vivo: correlation with pharmacokinetics. British Journal of Cancer 2003; 89:398-404.
2. Cramers P, Ruevekamp M, Oppelaar H, Dalesio O, Baas P, Stewart FA, Foscan uptake and tissue distribution in relation to photodynamic efficacy. British Journal of Cancer 2003; 88:283-290.
3. Morlet L, Vonarx-Croinsmann V, Lenz P, Foultier MT, Xavier de Brito L, Stewart C, Patrice T. Correlation between meta(tetrahydroxyphenyl)chlorine (m-THPC) biodistribution and photodynamic effects in mice. J. Photochem. Photobiol. B: Biology 1995; 28:25-32.
4. Lilge L, O'Carroll C, Wilson B. A solubilization technique for photosensitizer quantification in ex vivo tissue samples. J. Photochem. Photobiol. B: Biology 1997; 39:229-235.
5. Henderson BW, Vaughan L, Bellnier DA, H. van Leengoed, Johnson PG, Oseroff AR. Photosensitization of murine tumor, vasculature and skin by 5-aminolevulinic acid-induced porphyrin. Photochem. Photobiol. 1995; 62:780-789.
6. Bellnier DA, Dougherty TJ. A preliminary pharmacokinetic study of intravenous Photofrin in patiens. J. Clin. Laser Med. Surg. 1996; 14:311-314.
7. Bonnet R, Birgul DD, Nguyen A. Physical and chemical studies related to the development of m-THPC (Foscan) for the photodynamic therapy (PDT) of tumours. J. Porphyrins and Phthalocyanines 2001; 5:652-661.
8. Falk H, Meyer J. On the homo- and the heteroassociation of hypericin. Monatsh. Chem. 1994; 125:753-762.
9. van Esch JH, Feiters MC, Peters AM, Nolte RJM. UV-VIS, fluorescence and EPR studies of Porphyrins in Bilayers of Dioctadecyldimethylamomonium surfactans. J. Phys. Chem. 1994; 98:5541-5551.
10. Rovers JP, Saarnak AE, Molina A, Schuitmaker JJ, Sterenborg HJCM, Terpstra OT. Effective treatment of liver metastases with photodynamic therapy, using the second-generation photosensitizer meta-tetra(hydroxyphenyl)chlorine (m-THPC), in a rat model. British Journal of Cancer 1999; 81:600-608.
11. Triesscheijn M, Ruevekamp M, Aalders M, Baas P, Stewart FA. Outcome of m-THPC mediated photodynamic therapy is primarily determined by the vascular response. Photochem. Photobiol. 2005; 81:1161-1167.
12. Maugain E, Sasnouski S, Zorin V, Merlin JL, Guillemin F, Bezdetnaya L. Foscan-based photodynamic treatment in vivo: correlation between efficacy and Foscan accumulation in tumor, plasma and leukocytes. Oncology reports 2004; 12:639-645.
13. Atkins P, Jones L. Chemical Principles: The quest for insight, 3rd Ed.. New York: WH Freeman, 2005.
14. Finlay JC, Conover DL, Hull EL, Foster TH. Porphyrin Bleaching and PDT-induced spectral changes are irradiance dependent in ALA-sensitized normal rat skin in vivo. Photochem. Photobiol. 2001; 73:54-63.
15. Rovers JP, Saarnak AE, de Jode M, Sterenborg HJCM, Terpstra OT, Grahn MF. Biodistribution and bioactivity of Tetra-pegylated Meta-tetra(hydroxyphenyl)chlorine compared to native Meta-tetra(hydroxyphenyl)chlorine in a rat liver tumor model. Photochem. Photobiol. 2000; 71:210-217.
16. Diamond KR, Malysz PP, Hayward JE, Patterson MS. Quantification of fluorophore concentration in vivo using two simple fluorescence-based measurement techniques. J. Biomed. Optics 2005; 10:024007.
17. Jiang F, Lilge L, Grenier J, Li Y, Wilson MD, Chopp M. Photodynamic therapy of U87 human glioma in nude rat using liposome-delivered Photofrin. Lasers Surg. Med. 1998; 22:74-80.
18. Jiang F, Lilge L, Belcuig M, Singh G, Grenier J, Li Y, Chopp M. Photodynamic therapy using Photofrin in combination with Buthionine Sulfoximine (BSO) to treat 9L gliosarcoma in rat brain. Lasers Surg. Med. 1998; 23:161-166.
19. Cunderlikova B, Bjorklund EG, Pettersen EO, Moan J. pH-dependent spectral properties of HpIX, TPPS2a, mTHPP and m-THPC. Photochem. Photobiol. 2001; 74:246-252.
20. Optical absorption of hemoglobin by Scott Prahl, Oregon Medical Laser Center http://omlc.ogi.edu/spectra/hemoglobin/index.html

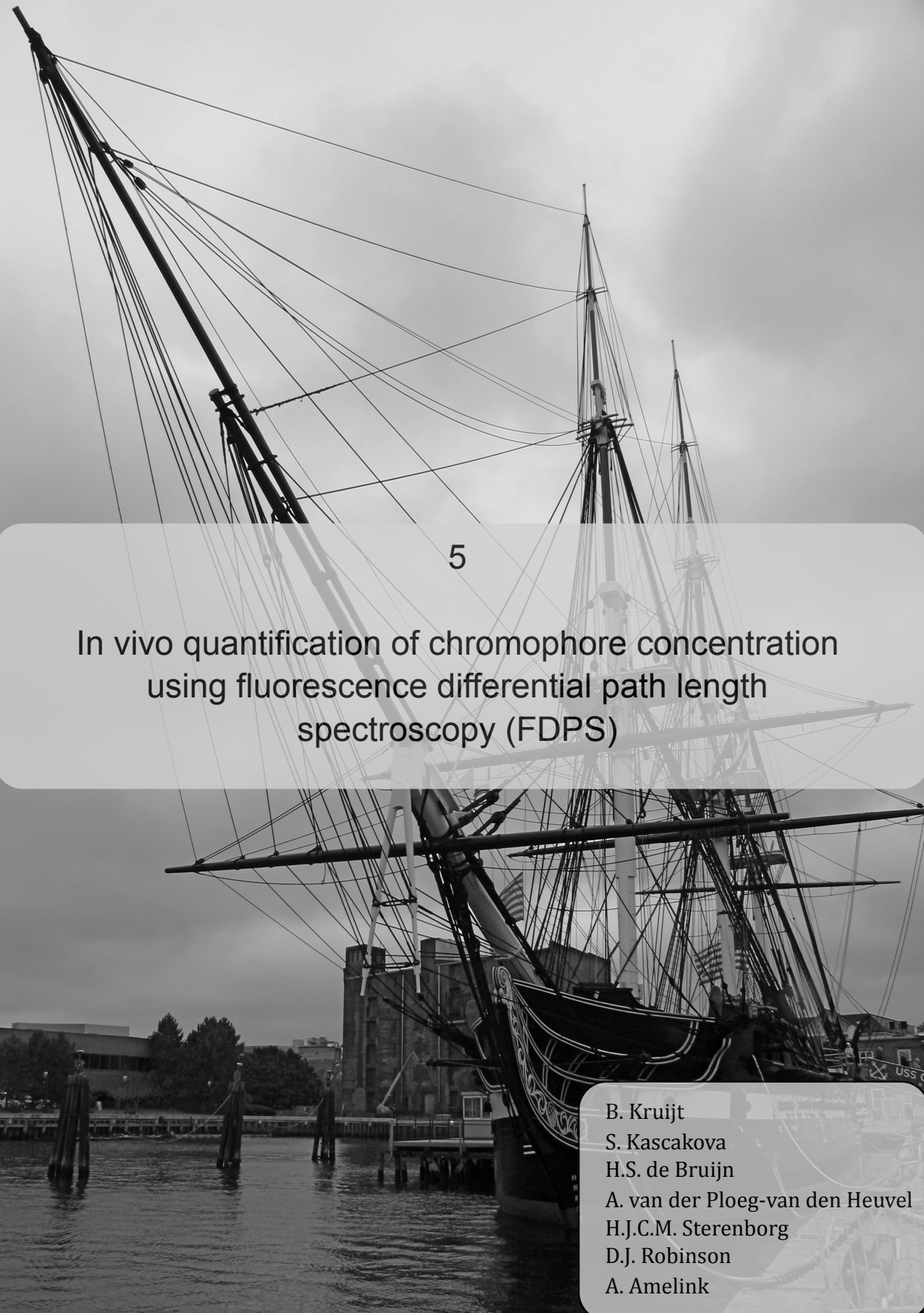

5

In vivo quantification of chromophore concentration using fluorescence differential path length spectroscopy (FDPS)

B. Kruijt
S. Kascakova
H.S. de Bruijn
A. van der Ploeg-van den Heuvel
H.J.C.M. Sterenborg
D.J. Robinson
A. Amelink

Abstract
We present an optical method based on fluorescence spectroscopy for measuring chromophore concentrations *in vivo*. Fluorescence differential path length spectroscopy (FDPS) determines chromophore concentration based on the fluorescence intensity corrected for absorption. The concentration of the photosensitizer m-THPC (Foscan®) was studied in vivo in normal rat liver, which is highly vascularized and therefore highly absorbing. Concentration estimates of m-THPC measured by FDPS on the liver are compared with chemical extraction. Twenty-five rats were injected with 0.3 mg/kg m-THPC. *In vivo* optical concentration measurements were performed on tissue 3, 24, 48, and 96 h after m-THPC administration to yield a 10-fold variation in tissue concentration. After the optical measurements, the liver was harvested for chemical extraction. FDPS showed good correlation with chemical extraction. FDPS also showed a correlation between m-THPC fluorescence and blood volume fraction at the two shortest drug-light intervals. This suggests different compartmental localization of m-THPC for different drug-light intervals that can be resolved using fluorescence spectroscopy. Differences in measured m-THPC concentration between FDPS and chemical extraction are related to the interrogation volume of each technique; ~0.2 mm^3 and ~10^2 mm^3, respectively. This indicates intra-animal variation in m-THPC distribution in the liver on the scale of the FDPS sampling volume.

Cover: The USS Constitution in Boston Harbor,
this work was presented at the NTROI symposium
in Boston, 2007.

Published in Journal of biomedical optics, 2009, 14:034022.

INTRODUCTION

Noninvasive optical methods for measuring tissue concentrations of endogenous and exogenous substances have several benefits over invasive techniques. Most importantly, optical concentration measurements allow nondestructive *in vivo* monitoring of drug pharmacokinetics at various tissue sites[1-5]. Two different sources of optical contrast are routinely used for target compound concentration measurements in tissue: absorption and fluorescence.

Methods based on absorption (reflectance) spectroscopy have the advantage that the measurement setup is relatively simple compared to fluorescence measurements. A typical setup consists of a fiber-optic probe, a broadband light source, and a spectrometer. The signal analysis is based on attenuation of elastically scattered light. Integration times are generally small, which enables measurements in the presence of ambient lighting (e.g., endoscopic illumination) and allows continuous measurements with a high temporal resolution. The optical contrast depends on the product of path length and target compound absorption coefficient, where the latter is the product of molar extinction coefficient and concentration. This implies that the absorption contrast might become too low for accurate concentration measurements for short path lengths, small molar extinction coefficients, and small target compound concentrations. An additional problem arises when the absorption band of the target compound overlaps the absorption bands of highly absorbing endogenous chromophores such as blood. In that case, the attenuation of the scattered light due to blood might prevent accurate concentration estimates of the target compound as well.

For most fiber-optic measurement geometries, the optical path length depends on the scattering coefficient μ_s and on the absorption coefficient μ_a of the tissue. Since μ_s and μ_a both vary significantly in tissue, quantitative measurements prove to be difficult in tissue unless specific fiber-optic measurement geometries are chosen. For example, the optical pharmacokinetics spectroscopy (OPS) system developed by Mourant *et al.*[1] uses elastic scattering spectra of tissue to calculate the concentration of chromophores in tissue using a fiber-optic probe with a source–detector separation of 1.7 mm. The separation of 1.7 mm was chosen to minimize the path length dependence of the collected photons on scattering properties of tissue. For scattering parameters that are typical of tissue, the path length varies by less than 20% for a given background absorption. Another technique that features a known path length is differential path length spectroscopy (DPS)[6-9]. The path length of photons contributing to the differential reflectance signal varies by less than 20%, over a very broad range of both scattering and absorption coefficients[6,7]. This facilitates quantitative concentration measurements even for strong variations in either background absorption or scattering. However, as explained earlier, chromophore concentration measurements based on attenuation of elastically scattered light rely on (small) differences between large amounts of detected light with and without the target chromophore present. Therefore, accurate measurement of small concentrations of chromophores or measurements of chromophores with low absorption coefficients are difficult. This is particularly true for DPS, for which the average path length of the measured photons is very small, approximately equal to the fiber diameter[6-9]. Moreover, for fluorescing compounds such as photosensitizers, the concentration can be underestimated due to the presence of

fluorescence, induced by the lower wavelengths of the white-light source, in the reflection spectra[4]. For example, Johansson *et al*.[4] used the OPS technique to estimate m-THPC concentration in a nonmelanotic skin tumor model and found a factor 2 underestimation in m-THPC concentration when not accounting for the presence of m-THPC fluorescence.

In contrast, measurements based on fluorescence contrast rely on the induced fluorescence of the fluorescing compound. Furthermore, the dynamic range for measurements based on fluorescence contrast is much larger than for scattering (absorption) measurements since the fluorescence is measured at a different wavelength than the excitation (scattered) light. Therefore, fluorescence-based concentration measurements are more sensitive and better capable of measuring very low fluorophore concentrations simply by increasing the integration time. However, there exists a complex relationship between the concentration of a chromophore and its absorption cross section and fluorescence emission intensity. *In vivo* fluorescence can be influenced by many factors that include changes in quantum yield induced by changes in the microenvironment[10], photobleaching[11], biological compartmentalization, and alteration in binding and aggregation[12,13]. In a turbid sample, the amount of fluorescence detected depends not only on the fluorophore concentration and quantum yield, but also on the scattering and absorption coefficients of the sample at the excitation and emission wavelengths. Various algorithms and measurement geometries have been developed to correct for the influence of tissue optical properties on a measured fluorescence spectrum. Photon migration techniques have been used to establish a general algorithm, applicable to any measurement geometry and for a broad range of scattering and absorption variations, to correct the measured fluorescence for the influence of tissue optical properties[14,15]. For this algorithm, the diffuse reflectance is measured in the same geometry as the fluorescence measurements and used to correct for differences in optical properties. However, elaborate probe-specific calibration procedures are required and the correction algorithm itself is quite complex. Several other more simple correction algorithms based on specific probe geometries have been developed[16-19]. We have recently developed fluorescence differential path length spectroscopy (FDPS), which is based on the principles of DPS (the difference of two signals that contain the same contribution from long path length photons but different contributions from short path length photons, to obtain a well-defined, small measurement volume) but with the enhanced dynamic range of fluorescence measurements[5]. The advantage of FDPS over other quantitative fluorescence measurements is its capability to deal with large variations in background absorption using a simple correction algorithm.

In this paper, we compare an optical concentration measurement technique based on quantitative fluorescence spectroscopy, FDPS, with chemical extraction[20]. The photosensitizer m-THPC was chosen as the target chromophore to test the concept of FDPS in vivo. To test the strength of FDPS in vivo, we performed the measurements on highly absorbing tissue, the liver. Variations in m-THPC concentration in the liver are achieved by choosing different drug-light intervals based on the known pharmacokinetics of m-THPC in liver[21,22]. The distribution of m-THPC at the different time points within the liver was investigated using fluorescence microscopy.

MATERIALS AND METHODS

Animal and Measurement Procedures

The experimental design for this study was approved by the animal experiment committee of the Erasmus MC. Two weeks before the start of the experiments, 25 normal adult male Wistar rats were placed on a diet of chlorophyll-free food to minimize the influence on autofluorescence centered at 675 nm due to pheophorbide-α. All rats were injected with 0.3 mg/kg m-THPC i.v., except for the control animals (n=5), which were injected with the solution (PEG400:ethanol:water, 2:3:5) not containing m-THPC. At either 3h, 24h, 48h or 96h after injection (n=5 animals per time point), the tissue overlying the liver was dissected, and optical concentration measurements were conducted on 10 randomly chosen positions across different lobes of the liver. Directly after the optical measurements, the main arteries and veins of the liver were clamped, to minimize the loss of blood. The liver was then excised and snap-frozen in liquid nitrogen.

Concentration Measurements

Concentration of Foscan in the liver was measured in vivo using FDPS and *ex vivo* using chemical extraction. FDPS determines a concentration estimate based on the emitted photosensitizer fluorescence. Figure 1 shows a schematic diagram of the measurement setup. The concentration estimates measured by FDPS were compared to the concentration values determined by chemical extraction. Both methods, FDPS and chemical extraction, are described in more detail in the following sections.

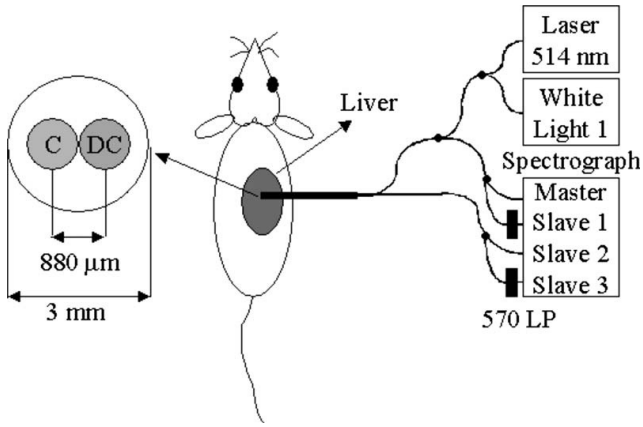

Figure 1. Schematic diagram of the FDPS measurement setup. The probe tip with a diameter of 3 mm contains two 800 µm fibers at a core-to-core distance of 880 µm.

FDPS

The probe contained two 800-µm fibers placed at minimum core-to-core distance, 880 µm, in a specially adapted subminiature version A (SMA) connector. The SMA connector configuration ensured a reproducible fixed distance when calibrating the setup using a calibration lamp, as described elsewhere[5]. The probe surface was polished under an angle of 15 degrees to minimize specular reflections at the probe-

medium interface during FDPS measurements. The 800-µm delivery-and-collection (dc) fiber is coupled into a 400-µm bifurcated fiber, which contains a delivery and a collection leg. The delivery leg is coupled into a 200-µm bifurcated fiber, of which one end is coupled into a xenon light source (HPX-2000, Ocean Optics, Duiven, The Netherlands) and the other end to a 514-nm argon laser (Spectra Physics, Eindhoven, The Netherlands). The collection leg is also coupled into a 200-µm bifurcated fiber, of which one end directly leads to the first channel of a temperature-regulated four-channel spectrograph setup (MC-2000-4-TR2, Ocean Optics, Duiven, The Netherlands) and the other end leads to a filter block containing a 570-nm long-pass filter before being coupled into the second channel of the spectrograph. The 800-µm collection (c) fiber is coupled to a 400-µm bifurcated fiber, of which one end directly leads to the third channel and the other is again first filtered by the same 570-nm long-pass filter before being coupled in to the fourth spectrograph channel.

Tissue Extraction

Tissue extraction was performed according to the chemical extraction method recently described by Kascakova *et al*.[20]. This is a modification of the original method described by Lilge *et al*.[23]. In short, small liver tissue samples (~0.1 grams or ~ 100 mm^3) were randomly acquired from the liver. Note that we did not attempt to colocate the optical measurement sites with the tissue extraction sites. Instead, we avoided complicated experimental procedures associated with co-locating the sites by averaging multiple random locations in both the optical and chemical concentration measurements. The liver samples were dissolved in 2 ml of the ready-to-use tissue solvent Solvable™ (Perkin Elmer, Groningen, the Netherlands), which is a mixture of dodecyldimethylamine oxide (2.5 to 10%), secondary alcohol ethoxylate (2.5 to 10%), and sodium hydroxide (≤ 2.5%) in water. Subsequently the tissue sample in Solvable™ was placed in a water bath of 50 degrees and agitated regularly for 2 h. The solubilized liver solution was then diluted with Solvable™ to an OD<0.1, to minimize absorption artifacts and to ensure homogenous illumination of the sample in 1 cm path length quartz cuvettes in a fluorimeter (Perkin Elmer, Groningen, the Netherlands). The diluted samples were analyzed by using an excitation wavelength of 423 nm (corresponding to the wavelength at which m-THPC in 100% Solvable™ absorbs the most (20)) and a spectral detection band of 450 to 800 nm with a resolution of 0.5 nm.

Fluorescence Microscopy

Frozen tissue samples of control and m-THPC administered animals were handled under subdued light conditions. Liver sections of 20-µm thickness were sectioned and mounted on glass slides (Menzel, Braunschwig, Germany). Fluorescence images were acquired at a 50 X magnification using a CCD camera (ORCA-ER, Hamamatsu, Herrsching am Ammersee, Germany) mounted on a fluorescence microscope (Leica, Leiden, The Netherlands) equipped with an N2.1 filter block with an additional bandpass detection filter, 670 ± 50 nm.

Data Processing

FDPS

Before every measurement the FDPS system was calibrated as described previously[5]. A differential reflectance spectrum (DPS) is obtained by subtracting the spectral signal from the c-fiber, which collects long path length photons only, from the dc-fiber, which collects photons of both long and short path length. Hence, the differential spectrum contains the spectral contribution from short path length photons only. Differential reflectance spectra were fitted according to the following model[6-9, 24]:

$$R = \left[a_1 \left(\frac{\lambda}{\lambda_0} \right)^{a2} + a_3 \left(\frac{\lambda}{\lambda_0} \right)^{-4} \right] \cdot \exp\{ - d_{fiber} \cdot \rho \cdot [StO_2 \cdot \mu_a^{HbO_2}(\lambda) + (1 - StO_2) \cdot \mu_a^{Hb}(\lambda)] \cdot C_{cor}(D_{ves}) \cdot C_{cor}(\mu_a^{total}) \} \quad . \tag{1}$$

The scattering function is modeled by a combination of Mie scattering and Rayleigh scattering, given by power law functions with amplitudes a_1 and a_3 and wavelength dependencies $(\lambda/\lambda_0)^{a2}$ and $(\lambda/\lambda_0)^{-4}$, respectively. Here, λ_0 is a normalization wavelength where the signal is predominantly dependent on scattering, which we usually set to 800 nm. d_{fiber} is the fiber diameter (0.8 mm), ρ is the blood volume fraction, StO_2 is the microvascular blood oxygenation, $\mu_a^{HbO2}(\lambda)$ is the absorption coefficient of fully oxygenated whole blood, and $\mu_a^{Hb}(\lambda)$ is the absorption coefficient of fully deoxygenated whole blood[25]. $C_{cor}(D_{ves})$ is a correction factor that accounts for the inhomogeneous distribution of blood in tissue and depends on the vessel diameter D_{ves}, and $C_{cor}(\mu_a^{total})$ is a correction factor that accounts for the absorption dependence of the path length for highly vascularized tissue such as liver[26]. A differential fluorescence spectrum (DF_{meas}) is obtained by subtracting the fluorescence spectral signal measured by the c-fiber from the fluorescence spectral signal measured by the dc-fiber. The measured differential fluorescence signal is corrected for absorption by multiplying DF_{meas} by the ratio of the reflectance at the excitation wavelength without and with absorption present, as follows[5]:

$$DF_{corr} = DF_{meas} \frac{DR_x(0)}{DR_x(\mu_{a,x})} \quad , \tag{2}$$

where $DR_x(\mu_{a,x})$ and $DR_x(0)$ are the differential reflectance signals at the excitation wavelength measured with and without background absorber present, respectively. $DR_x(\mu_{a,x})$ is the DPS signal at the excitation wavelength measured *in vivo*. The DPS signal at the excitation wavelength without absorption present, $DR_x(0)$, cannot be measured, but is calculated from the fit of the in vivo DPS spectrum to Eq. (1), using the best estimates of the parameters a_1 to a_3 and setting the exponent for the exponential term to 0. It was previously shown that the differential fluorescence signal is relatively insensitive to variations in scattering[5], and consequently no corrections

were performed to account for scattering differences between tissue samples. The absorption-corrected FDPS spectra were analyzed as a linear combination of basis spectra and fitted using a singular value decomposition (SVD) algorithm [24,27]. The fluorescence was described by a combination of autofluorescence and m-THPC fluorescence. Basis spectra for these two components were extracted from spectra acquired *in vivo*. The autofluorescence basis-spectrum is the normalized average of the control animals. For m-THPC, a basis-spectrum, based on the spectra acquired in vivo corrected for the autofluorescence, is determined for each of the four time points to account for possible spectral changes in m-THPC fluorescence due to changes in environment and/or binding.

Chemical Extraction

Fluorescence spectra acquired by the fluorimeter could be described as a linear combination of autofluorescence, Solvable™ fluorescence, and m-THPC fluorescence. The Solvable™ fluorescence basis spectrum was measured in the fluorimeter using pure Solvable™. m-THPC was dissolved in Solvable™ and measured in the fluorimeter; the basis spectrum for m-THPC was acquired by subtracting the Solvable™ component. Last, the autofluorescence basis spectrum is the normalized average fluorescence spectrum of spectra acquired from dissolved liver samples of control animals after subtraction of the Solvable™ component. The absolute m-THPC concentration of the liver samples was derived from a calibration curve, which was constructed from measurements of known m-THPC concentrations mixed with dissolved control liver samples in Solvable™ [20].

Statistics and Correlation

Confidence intervals on the individual parameters for the individual measurements were determined based on the covariance matrix generated for each fit as described by Amelink *et al*.[28]. Differences between groups were determined using the nonparametric Mann-Whitney test.

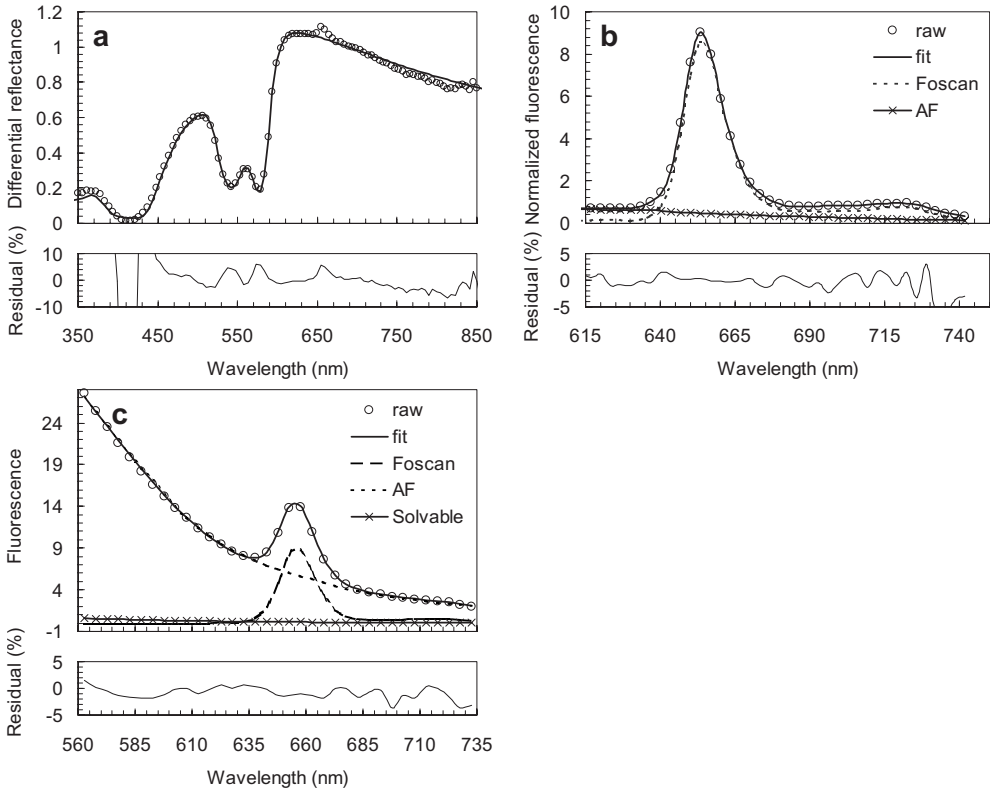

Figure 2. Typical Levenberg-Marquardt fit of the DPS signal (a) and SVD fit for the FDPS signal (b) acquired under 514 nm excitation. (c) SVD fit for the fluorescence signal of the liver after chemical extraction measured using a fluorimeter.

RESULTS

Figure 2 shows the data and fit for the three spectra acquired per animal for the different methods: DPS, FDPS, and chemical extraction. Figure 2(a) shows a typical differential reflectance spectrum acquired in vivo from rat liver with its fit and residual between fit and data from an animal 3 h after m-THPC injection. Figure 2(b) shows the fit of a differential fluorescence spectrum acquired *in vivo* under 514-nm excitation of the rat liver 24 h after m-THPC injection. In addition to the fit and residual between fit and data, the individual components are also shown. Figure 2(c) shows a typical fluorescence spectrum and its fit and the individual components (m-THPC, autofluorescence, and Solvable™ fluorescence) of extracted liver tissue 3 h after m-THPC injection measured using the fluorimeter at 423-nm excitation.

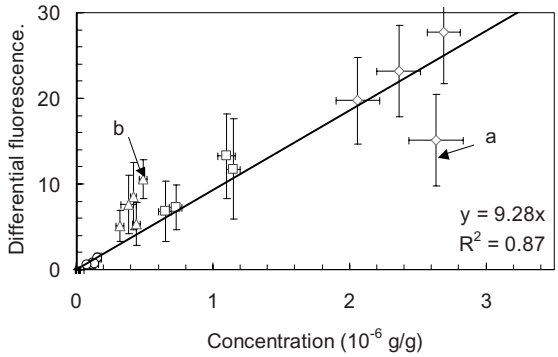

Figure 3. Optically measured m-THPC concentration using FDPS versus true m-THPC concentration measured by chemical extraction for the 4 different time points, 3h (◇), 24h (□), 48h (△) and 96h (○) together with the regression line.

Figure 3 shows the m-THPC component of the absorption-corrected FDPS fluorescence versus the actual m-THPC concentration determined with chemical extraction. For the control animals, the FDPS spectrum was fully described by the autofluorescence component with negligible contribution from the m-THPC component, as expected. The smallest nonzero amount of m-THPC fluorescence (measured at the 96-h time point) corresponded to an actual m-THPC concentration of 160 ng/g. Fitting a straight line forced through the origin shows an R^2 value of 0.87. Every measurement point represents the average of multiple fluorescence measurements at randomly chosen locations on the liver in a single animal. For these animals, the average blood volume fraction, measured with DPS, was 11.1 ± 3%. The two most prominent average deviations from the straight line, indicated by arrows a and b in Fig. 3, had an average blood volume fraction of 7.6 ± 0.02% and 14.5 ± 0.05%, respectively. Furthermore, all animals in the 48-h group are above the regression line in Fig. 3. The 3 animals within this group that deviate from the regression line by more than one times the standard deviation show an increased blood volume fraction (14.9 ± 2%) compared to the total average blood volume fraction for all animals (11.1 ± 3%). These observations indicate a possible relationship between measured m-THPC fluorescence and blood volume fraction. In Fig. 4, therefore, we have plotted the m-THPC fluorescence intensity as a function of blood volume fraction for each animal. Indeed a strong correlation between m-THPC fluorescence and blood volume fraction is observed for the early time points, 3 and 24 h. A decrease in correlation coefficients between m-THPC fluorescence and blood volume fraction with increasing drug-light intervals is observed.

Another interesting feature to be noticed in Fig. 3 is the difference in standard deviations between FDPS intensity and m-THPC concentration determined through chemical extraction. The large standard deviations in FDPS intensity are caused by intra-animal variations in m-THPC fluorescence in the liver, most likely related to a heterogenous distribution of m-THPC on a scale resolved by the FDPS technique but averaged out in the extraction. Therefore, we investigated the m-THPC fluorescence distribution at the different time points in liver sections using fluorescence microscopy.

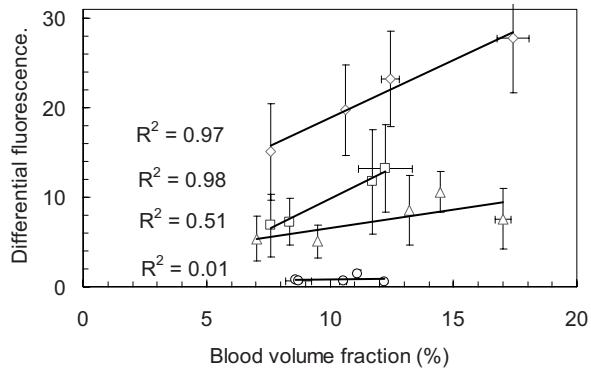

Figure 4. Optically measured concentration using FDPS as a function of DPS-measured blood volume fraction averaged per animal for the four different time points 3h (◇), 24h (□), 48h (△) and 96h (○).

Figure 5 shows representative fluorescence microscopy images at 50 X magnification of liver sections for the 3-, 24-, 48- and 96-h time points. The 3-h time point clearly shows intense clusters of m-THPC fluorescence randomly spread throughout the section. At 24-h m-THPC fluorescence is measured in the whole section, and more intense m-THPC fluorescence is observed around the bigger vessels, which appear black in the image due to blood absorption. The 48-h animal shows similar m-THPC fluorescence distribution as on the 24-h time point, with the difference that the overall m-THPC fluorescence intensities are lower. The 96-h time point shows m-THPC fluorescence more evenly distributed throughout the section than on the other time points.

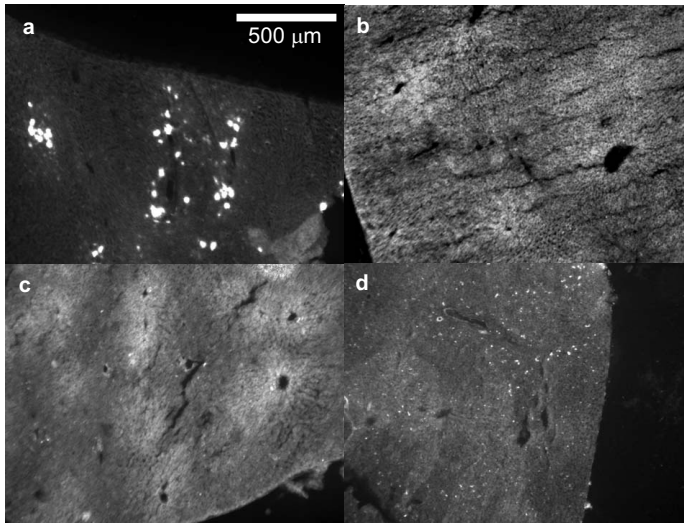

Figure 5. Fluorescence microscopy performed on 20 μm thick liver sections at 50 X magnification for the (a) 3, (b) 24, (c) 48 and (d) 96 hour time points.

DISCUSSION

The aim of this study was to test the concept of optical concentration measurements based on quantitative fluorescence spectroscopy (FDPS) *in vivo*. We have chosen to validate the FDPS concentration measurements in an *in vivo* environment on highly vascularized and thus highly absorbing tissue (liver) using m-THPC as an exogenous chromophore. Different drug-light intervals were chosen based on the pharmacokinetics of m-THPC in the liver[21,22] to vary the *in vivo* tissue concentrations by an order of magnitude. FDPS concentration estimates for the different time points were compared with chemical extraction.

Based on our measurements, we found that FDPS is capable of measuring m-THPC concentrations as low as 160 ng/g in the liver at the 96-h drug-light interval. We expect to be able to measure even lower concentrations by optimizing the setup and increasing the integration time. The measured m-THPC concentration with FDPS showed good linear correlation with the extracted m-THPC concentration, $R^2 = 0.87$. The correlation coefficient could be improved to 0.96 when the outliers from the linear regression line in Fig. 3, identified as a and b, are omitted. However, these outliers yield important information about in vivo m-THPC localization. The animals with the two most prominent deviations from the straight line, indicated by arrows a and b, were shown to have blood volume fractions of 7.6 ± 0.02% and 14.5 ± 0.05%, respectively. These are significantly different from the average blood volume fraction of the m-THPC animals, 11.1 ± 3% (the blood volume fraction of the control animals was 9.1 ± 4%, which is not significantly different from the m-THPC animals). Based on this observation, we investigated the correlation between m-THPC concentration measured using FDPS and blood volume fraction. For the two shortest drug-light intervals, we found a strong correlation (R^2 values of 0.97 and 0.98 for the 3-and 24-h drug-light intervals). For longer drug-light intervals, there was a decrease in the correlation between m-THPC fluorescence intensity and blood volume fraction. The drug-light interval dependence of the correlation between fluorescence and blood volume suggests that m-THPC is predominantly localized in or near the tissue vasculature for short drug-light intervals and less so for longer drug-light intervals. This is in agreement with a range of m-THPC pharmacokinetic studies in rats showing high concentrations of m-THPC in the plasma directly after i.v. injection, followed by an initial rapid exponential decrease followed by one or two exponential decays with lower elimination rates[21,22].

Another interesting observation is that the intra-animal variations in FDPS signals are up to a factor of 5 larger than those of chemical extraction. The source for these larger variations in FDPS concentration estimates is potentially related to (intra-animal) differences in tissue scattering, since the FDPS signal is dependent on scattering. The scattering dependence of the FDPS signal depends on the probe geometry. For an 800-µm FDPS probe, it has been shown in a phantom study that within biological relevant scattering values, the FDPS signal can vary by a factor of 2.2 [5]. Since in these experiments the overall variation in the scattering parameter (a_1) was small, 16%, it is safe to assume that scattering had no significant influence on the FDPS signal and hence does not contribute to the variation in the data, inter- or intra-individual. It is most likely that the differences in standard deviations between FDPS and chemical

extraction are related to intra-animal variability in m-THPC concentration on a microscopic scale and are a result of the different interrogation volumes of the techniques. For chemical extraction, tissue samples of ~10^2 mm^3 are used, whereas FDPS probes only ~0.2 mm^3 of tissue [corresponding to the volume of a cylinder with a diameter equal to the fiber (0.8 mm) and height of half the path length (0.4 mm)]. Fluorescence microscopy on sections at 50 X magnification for the four different time points (Fig. 5) shows a heterogeneous m-THPC fluorescence distribution throughout the sections. This heterogeneous distribution of m-THPC is on a submillimeter spatial scale and can be picked up only by techniques that sample small tissue volumes. Obviously, the tissue volumes used for chemical extraction are too large to pick up this sub-millimeter spatial heterogeneity, and standard deviations in m-THPC concentrations are small since multiple regimes of high and low fluorescence are present in each individual tissue volume used for chemical extraction. However, the measured m-THPC fluorescence intensity using FDPS depends heavily on probe placement on the liver; some measurements will contain bright spots of fluorescence, and other measurements on the same liver will contain smaller amounts of m-THPC, leading to large intra-animal variations in fluorescence intensity.

The spatial m-THPC distribution in the liver at different time points using fluorescence microscopy [Fig. 5(a)] illustrates the wide variations in spatial distribution of m-THPC in rat liver 3 h after the administration of m-THPC. It is clear that the localization of m-THPC is not coincident with the whole liver vasculature and that depending on probe placement, the volume interrogated by our optical technique contains areas of very high or low m-THPC fluorescence intensities. The spatial distribution of m-THPC is likely to be dominated by the role of the liver in the elimination of m-THPC[29,30]. A number of studies have illustrated the complexity of m-THPC pharmacokinetics *in vivo*[21,31,32]. These studies have shown the formation of m-THPC aggregates and the importance of binding to plasma proteins. Jones *et al*.[21] postulated that m-THPC could disaggregate and redistribute to lipoproteins in the liver before further distribution to other tissues. It is therefore not surprising that m-THPC fluorescence is not homogeneously distributed within the liver vasculature 3 h after the administration of m-THPC. In the liver, we observe increased m-THPC fluorescence around the vasculature at both intermediate (24 h) and long drug-light intervals (48 h and 96 h). Note that m-THPC fluorescence is observed throughout the whole section, although in a lower intensity than around the vasculature.

Another important consideration is that the measured fluorescence signal by FDPS is the product of the photosensitizer concentration and the quantum yield. The quantum yield of a photosensitizer can change due to changes in environment and binding[10,12,13] and might give a possible indication on (sub)cellular localization of the photosensitizer. We find a linear correlation between FDPS measured fluorescence and extracted concentration, which suggests that the quantum yield is relatively constant over the drug-light intervals that we have investigated. This observation is in agreement with the fact that we found only small differences in the shape of the basis spectra for different m-THPC drug-light intervals (data not shown). It seems that these binding effects are not sufficiently large to affect the m-THPC concentration estimate. We note that there may be subtle differences in quantum yield with respect to drug-light interval in the liver

and that other organs might show significant variations in quantum yield. It should also be noted that steady-state fluorescence measurements are rather insensitive to the effects of binding and variations in quantum yield and that time-resolved spectroscopy would be much more appropriate to determine the magnitude of these effects[33,34]. The possible subtle differences in fluorescence quantum yield and the differences in scattering properties for different tissue types strongly suggest the necessity to determine a calibration curve (such as Fig. 3 for liver) for each tissue type separately. This is a topic currently under investigation.

In conclusion, we compared an optical concentration measurement technique based on quantitative fluorescence spectroscopy (FDPS) with chemical extraction in an in vivo model. FDPS showed good correlation with chemical extraction and an ability to measure m-THPC values as low as 160 ng/g. Moreover, for short drug-light intervals, a correlation was observed between blood volume fraction and measured m-THPC fluorescence. A larger intra-animal variability was measured with FDPS compared to chemical extraction due to its smaller interrogation volume and heterogenous distribution of m-THPC on the scale of the FDPS sampling volume.

References

1. Mourant JR, Johnson TM, Los G, Bigio IJ. Noninvasive measurement of chemotherapy drug concentrations in tissue: preliminary demonstrations of in vivo measurements. Phys. Med. Biol. 1999; 44:1397-1417.
2. Kanick SC, Eiseman JL, Joseph E, Guo J, Parker RS. Noninvasive and nondestructive optical spectroscopic measurement of motexafin gadolinium in mouse tissues: comparison to high-performance liquid chromatography. J. Photochem. Photobiol. B. 2007; 88:90-104.
3. Reif R, Wang M, Joshi S, A'Amar O, Bigio IJ. Optical method for real-time monitoring of drug concentrations facilitates the development of novel methods for drug delivery to brain tissue. J. Biomed. Opt. 2007; 12:034036.
4. Johansson A, Svensson J, Bendsoe N, Svanberg K, Alexandratou E, Kyriazi M, Yova D, Gräfe S, Trebst T, Andersson-Engels S. Fluorescence and absorption assessment of a lipid mTHPC formulation following topical application in a non-melanotic skin tumor model. J. Biomed. Opt. 2007; 12:034026.
5. Amelink A, Kruijt B, Robinson DJ, Sterenborg HJ. Quantative fluorescence spectroscopy in turbid media using fluorescence-DPS. in press.
6. Amelink A, Sterenborg HJ. "Measurement of the local optical properties of turbid media by differential path length spectroscopy. Appl. Opt. 2004; 43:3048-3054.
7. Amelink A, Sterenborg HJ, Bard MP, Burgers SA. In vivo measurement of the local optical properties of tissue by use of differential path length spectroscopy. Opt. Lett. 2004; 29:1087-1089.
8. van Veen RL, Amelink A, Menke-Pluymers M, van der Pol C, Sterenborg HJ. Optical biopsy of breast tissue using differential path length spectroscopy," Phys. Med. Biol. 2005; 50:2573-2581.
9. Amelink A, Kaspers OP, Sterenborg HJ, van der Wal JE, Roodenburg JL, Witjes MJ. Noninvasive measurement of the morphology and physiology of oral mucosa by use of optical spectroscopy. Oral. Oncol. 2008; 44:65-71.
10. Wilson BC, Patterson MS, Lilge L. Implicit and explicit dosimetry in photodynamic therapy: a new paradigm. Lasers Med. Sci. 1997; 12:182-199.
11. Robinson DJ, de Bruijn HS, van der Veen N, Stringer MR, Brown SB, Star WM. Fluorescence photobleaching of ALA-induced protoporphyrin IX during photodynamic therapy of normal hairless mouse skin: the effect of light dose and irradiance and the resulting biological effect. Photochem. Photobiol. 1998; 67:140-149.
12. Woodburn K, Chang CK, Lee S, Henderson B, Kessel D. Biodistribution and PDT efficacy of a ketochlorin photosensitizer as a function of the delivery vehicle. Photochem. Photobiol. 1994; 60:154-159.
13. Aveline B, Hasan T, Redmond RW. Photophysical and photosensitizing properties of benzoporphyrin derivative monoacid ring A (BPD-MA). Photochem. Photobiol. 1994; 59:328-335.
14. Zhang Q, Müller MG, Wu J, Feld MS. Turbidity-free fluorescence spectroscopy of biological tissue. Opt. Lett. 2000; 25:1451-1453.
15. Müller MG, Valdez TA, Georgakoudi I, Backman V, Fuentes C, Kabani S, Laver N, Wang Z, Boone CW, Dasari RR, Shapshay SM, Feld MS. Spectroscopic detection and evaluation of morphologic and biochemical changes in early human oral carcinoma. Cancer. 2003; 97:1681-1692.
16. Canpolat M, Mourant JR. Monitoring photosensitizer concentration by use of a fiber-optic probe with a small source–detector separation. Appl. Opt. 2000; 39:6508-6514.
17. Weersink R, Patterson MS, Diamond K, Silver S, Padgett N. Noninvasive measurement of fluorophore concentration in turbid media with a simple fluorescence/reflectance ratio technique. Appl. Opt. 2001; 40:6389–6395.
18. Pogue BW, Burke G. Fiber-optic bundle design for quantitative fluorescence measurement from tissue. Appl. Opt. 1998; 37:7429–7436.
19. Diamond KR, Patterson MS, Farrell TJ. Quantification of fluorophore concentration in tissue-simulating media by fluorescence measurements with a single optical fiber. Appl. Opt. 2003; 42:2436-2442.
20. Kascáková S, Kruijt B, de Bruijn HS, van der Ploeg-van den Heuvel A, Robinson DJ, Sterenborg HJ, Amelink A. Ex vivo quantification of mTHPC concentration in tissue: influence of chemical extraction on the optical properties. J. Photochem. Photobiol. B. 2008; 91:99-107.
21. Jones HJ, Vernon DI, Brown SB. Photodynamic therapy effect of m-THPC (Foscan) in vivo: correlation with pharmacokinetics. Br. J. Cancer. 2003; 89:398-404.

22. Cramers P, Ruevekamp M, Oppelaar H, Dalesio O, Baas P, Stewart FA. Foscan uptake and tissue distribution in relation to photodynamic efficacy. Br. J. Cancer. 2003; 88:283-290.
23 Lilge L, O'Carroll C, Wilson BC. A solubilization technique for photosensitizer quantification in ex vivo tissue samples. J. Photochem. Photobiol. B. 1997; 39:229-35.
24. Kruijt B, de Bruijn HS, van der Ploeg-van den Heuvel A, de Bruin RW, Sterenborg HJ, Amelink A, Robinson DJ. Monitoring ALA-induced PpIX photodynamic therapy in the rat esophagus using fluorescence and reflectance spectroscopy," Photochem. Photobiol. 2008; 84:1515-1527.
25. Finlay JC, Foster TH. Hemoglobin oxygen saturations in phantoms and in vivo from measurements of steady-state diffuse reflectance at a single, short source-detector separation. Med. Phys. 2004; 31:1949-1959.
26. Kaspers OP, Sterenborg HJ, Amelink A. Controlling the optical path length in turbid media using differential path length spectroscopy: fiber diameter dependence. Appl. Opt. 2008; 47:365-371.
27. Finlay JC, Mitra S, Foster TH. In vivo mTHPC photobleaching in normal rat skin exhibits unique irradiance-dependent features. Photochem. Photobiol. 2002; 75:282-288.
28. Amelink A, Robinson DJ, Sterenborg HJ. Confidence intervals on fit parameters derived from optical reflectance spectroscopy measurements. J Biomed Opt. 2008; 13:054044.
29. Alian W, Andersson-Engels S, Svanberg K, Svanberg S. Laser-induced fluorescence studies of meso-tetra(hydroxyphenyl)chlorin in malignant and normal tissues in rats. Br. J. Cancer. 1994; 70:880-885.
30. Whelpton R, Michael-Titus AT, Jamdar RP, Abdillahi K, Grahn MF. Distribution and excretion of radiolabeled temoporfin in a murine tumor model. Photochem. Photobiol. 1996; 63:885-891.
31. Hopkinson HJ, Vernon DI, Brown SB. Identification and partial characterization of an unusual distribution of the photosensitizer meta-tetrahydroxyphenyl chlorin (temoporfin) in human plasma. Photochem. Photobiol. 1999; 69:482-488.
32. Triesscheijn M, Ruevekamp M, Out R, Van Berkel TJ, Schellens J, Baas P, Stewart FA. The pharmacokinetic behavior of the photosensitizer meso-tetra-hydroxyphenyl-chlorin in mice and men. Cancer Chemother. Pharmacol. 2007; 60:113-122.
33. Kress M, Meier T, Steiner R, Dolp F, Erdmann R, Ortmann U, Rück A. Time-resolved microspectrofluorometry and fluorescence lifetime imaging of photosensitizers using picosecond pulsed diode lasers in laser scanning microscopes. J Biomed Opt. 2003; 8:26-32.
34. Diamond KR, Malysz PP, Hayward JE, Patterson MS. Quantification of fluorophore concentration in vivo using two simple fluorescence-based measurement techniques. J. Biomed. Opt. 2005; 10:024007.

6

Monitoring ALA-induced PpIX photodynamic therapy in the rat esophagus using fluorescence and reflectance spectroscopy.

B. Kruijt
H.S. de Bruijn
A. van der Ploeg-van den Heuvel
R.W. de Bruin
H.J.C.M. Sterenborg
A. Amelink
D.J. Robinson

ABSTRACT

The presence of phased protoporphyrin IX (PpIX) bleach kinetics has been shown to correlate with esophageal response to ALA-PDT in animal models. Here we confirm the existence of phased PpIX photobleaching by increasing the temporal resolution of the fluorescence measurements using the therapeutic illumination and long wavelength fluorescence detection. Furthermore fluorescence differential pathlength spectroscopy (FDPS) was incorporated to provide information on the effects of PpIX and tissue oxygenation distribution on the PpIX bleach kinetics during illumination.

ALA at a dose of 200 mg/kg was orally administered to 15 rats, 5 rats served as control animals. PDT was performed at an *in-situ* measured fluence rate of 75 mW cm^{-2} using a total fluence of 54 J cm^{-2}. Forty eight hours after PDT the esophagus was excised and histologically examined for PDT-induced damage. Fluence rate and PpIX photobleaching at 705 nm were monitored during therapeutic illumination with the same isotropic probe. A new method, FDPS, was used for superficial measurement on saturation, blood volume, scattering characteristics and PpIX fluorescence. Results showed two-phased PpIX photobleaching that was not related to a (systematic) change in esophageal oxygenation but was associated with an increase in average blood volume. PpIX fluorescence photobleaching measured using FDPS, in which fluorescence signals are only acquired from the superficial layers of the esophagus, showed lower rates of photobleaching and no distinct phases. No clear correlation between two-phased photobleaching and histological tissue response was found. This study demonstrates the feasibility of measuring fluence rate, PpIX fluorescence and FDPS during PDT in the esophagus. We conclude that the spatial distribution of PpIX significantly influences the kinetics of photobleaching and that there is a complex interrelationship between the distribution of PpIX and the supply of oxygen to the illuminated tissue volume.

Cover: Golden gate bridge in San Francisco,
this work was presented at photonics West
in San Jose, 2008

Published in Photochemistry and photobiology, 2008, 84(6):1515-1527.

INTRODUCTION

Barrett's esophagus is a pre-malignant condition defined as intestinal metaplasia of the epithelium[1]. Currently 5-aminolevulinic acid based photodynamic therapy (ALA-PDT) of Barrett's esophagus is under investigation as an alternative to esophageal resection[2]. The administration of ALA induces, through a number of intermediates in the heme biosynthetic pathway of cells, accumulation of endogenous protoporphyrin IX (PpIX). Interaction of PpIX with light of an appropriate wavelength and oxygen leads to the generation of reactive oxygen species, notably singlet oxygen[3]. In the esophagus, where PpIX predominantly localizes in the epithelial layer and submucosa[4], sufficient formation of singlet oxygen leads to epithelial ablation. Despite the relatively high clinical response of Barrett's esophagus to ALA-PDT, there remain a significant number of patients that show incomplete epithelial ablation[5].

There are a number of often interdependent parameters that determine the efficacy of PDT which include PpIX concentration and distribution, treatment wavelength, fluence, fluence rate (distribution) and availability of oxygen within the treatment volume. We have been investigating several of these parameters and how they relate to biological response in pre-clinical rat models[6,7]. Despite standardizing light treatment parameters (e.g. fluence and fluence rate) based on in situ measurements, large variations in response were observed. In a step further we combined standardized light treatment with fluorescence spectroscopy using 405 nm excitation during short interruptions to the therapeutic light source[6]. These measurements of PpIX photobleaching showed a higher rate of photobleaching and total amount of bleaching in animals that showed complete epithelial ablation than in animals that showed no or partial response of the esophageal epithelium. Furthermore, in animals that showed complete epithelial ablation two distinctive phases in PpIX photobleaching were observed. Here an initial high rate of photobleaching was followed by a phase in which the rate of photobleaching was lower. These observations are supported by the recent results of Sheng *et al*.[8].

A theoretical analysis of the kinetics of PpIX photobleaching shows that the kinetics of photobleaching can be described by a second-order function in which the concentration of oxygen determines the rate of photobleaching[9-11]. We have previously attributed differences in rate of photobleaching between phases and between animals to differences in tissue oxygenation. It is important to consider that, in addition to the oxygen concentration, the second-order function also implies that the initial photosensitizer concentration and distribution may have an influence on the rate of photobleaching. In the present study we have three aims: I) to more closely investigate the phased photobleaching kinetics by increasing temporal resolution of fluorescence measurements by measuring fluorescence above 660 nm during the therapeutic illumination[12]; II) to determine the source of these different phases of PpIX photobleaching by incorporating superficial fluorescence measurements and monitoring physiological parameters such as saturation and blood volume using fluorescence differential pathlength spectroscopy (FDPS) (manuscript submitted) during therapeutic illumination; and III) to compare the above methods of monitoring ALA-PDT with the histologically observed response of esophageal tissue 48 hours after treatment and the microscopical distribution of PpIX over the different layers of the

esophagus, performed on tissue of non-treated control and ALA-administered animals, using fluorescence microscopy.

MATERIALS AND METHODS

Animal and treatment procedure

The experimental design for this study was approved by the animal experiment committee of the Erasmus Medical Center. Two weeks before commencing the experiments 20 normal adult male Wistar rats were placed on a diet of chlorophyll free food to minimize the influence on autofluorescence centered at 675 nm due to pheophorbide-α. 200 mg/kg ALA, dissolved in saline, was orally administered to 15 animals two hours before PDT. Five rats in the control group were administered saline only. Just before PDT the rats were intramuscular (i.m.) anaesthetized with 60 mg/kg ketamine and 5 mg/kg xylazine (Rompun, Bayer, Germany).

Figure 1a shows a schematic outline of the illumination and measurement setup. Homogeneous illumination of the esophagus was achieved by a rigid, optically clear, double lumen balloon, length 40 mm and 3 mm diameter (inflated), on the distal end of a catheter (opta pro, Cordis, Roden, The Netherlands). A 20 mm cylindrical linear diffuser was placed in the catheter to illuminate the esophagus using 635 nm light from an argon ion pumped dye laser (Spectra Physics, Eindhoven, The Netherlands). An isotropic probe was placed on the outer wall of the balloon to measure fluence rate and long wavelength fluorescence (> 660 nm) with high temporal resolution during illumination from the esophageal mucosa. An additional FDPS-probe was placed on the adjacent wall of the balloon to measure physiological parameters, (oxygen saturation and blood volume) and tissue scattering characteristics using the DPS technique and local fluorescence under 405 nm excitation using the FDPS technique, described in section 2.3. The balloon and probes, figure 1b, were inserted into the esophagus and the balloon was fully inflated to its fixed diameter with between 2 and 2.5 ml of air, keeping the pressure between the specified nominal and burst pressure of 6 and 10 atmospheres, respectively. As in our previous studies the in-situ fluence rate measured at the esophagus wall was adjusted to 75 mW cm^{-2}. The adjustment procedure took between 5 and 10 seconds during which a 10% neutral density filter was used to minimize light fluence delivered to the esophagus. Before starting PDT up to three FDPS spectra were acquired. Thereafter, during PDT, the treatment was interrupted for 3 seconds every 30 seconds to acquire FDPS spectra. Fluence rate at 635 nm and fluorescence above 660 nm were measured continuously with the isotropic probe. PDT was stopped when a total delivered dose of 54 J cm^{-2} was reached. In 9 animals immediately after PDT the effect of balloon pressure on blood volume and saturation was measured by completely deflating and inflating the rigid balloon. Directly after PDT 0.05 mg/kg Temgesic (Schering-Plough, Utrecht, The Netherlands) was administered i.m. as analgesic.

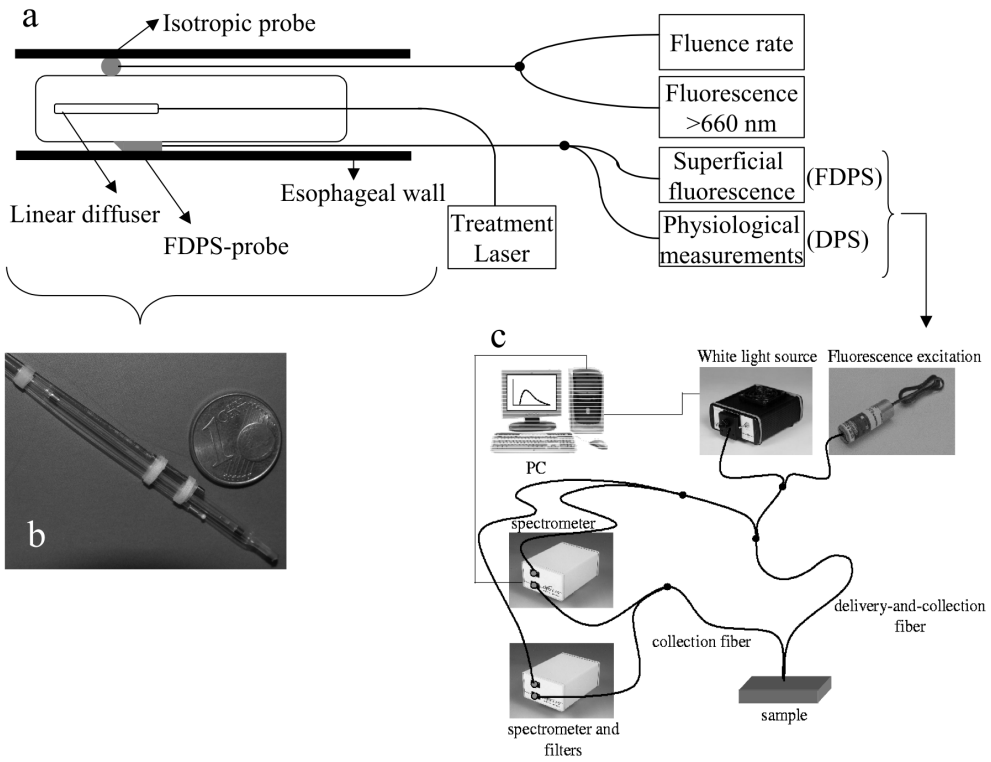

Figure 1. a) Shows a schematic diagram of the experimental setup; b) Photo of the balloon with the isotropic and DPS probe attached to the balloon; c) schematic diagram of the FDPS system.

Light dosimetry and fluorescence

Fluence rate and long wavelength tissue fluorescence were measured using the same 1 mm isotropic probe at the distal end of either a 200 or 400 µm optical fiber. Depending on this optical fiber diameter the fiber-probe is coupled into a 100/200 or 200/400 µm bifurcated fiber. These types of fiber bifurcations were chosen to give an optimal signal through the large fiber diameter of the bifurcation used for fluorescence measurements. A smaller fraction of the excitation light was led to a modular based multi-channel dosimetry device and was sufficient for accurate fluence rate measurements (13). The larger fiber diameter of the bifurcation is led to a spectrograph (USB4000, Ocean Optics, Duiven, The Netherlands) containing a 660 nm long pass filter to block the reflected and scattered light from the excitation light source and detect tissue fluorescence above 660 nm. Integration times were restricted to a maximum of 5 seconds to allow monitoring of fluorescence photobleaching kinetics with high temporal resolution.

Fluorescence Differential Pathlength Spectroscopy

Fluorescence differential pathlength spectroscopy (FDPS) is an extension to DPS[14,15] which is based on the principles of DPS. Figure 1c shows the schematic diagram of the

combined DPS and FDPS configuration. A DPS/FDPS probe was made containing two 400 micron fibers with a minimal core-to-core distance (440 microns) and polished at an angle of 35 degrees to minimize specular reflectance at the probe-medium interface. Figure 1b shows the balloon with the tip of the FDPS probe. This angle was chosen to ensure and optimize contact with the esophageal wall and is slightly greater than used in previous DPS studies[14,15]. For DPS one fiber acts as both delivery and collection fiber (dc-fiber) and the second as a collection fiber (c-fiber). The dc fiber delivers white light to the tissue and collects both superficially and deeply scattered photons, while the c-fiber only collects deeply scattered photons. Hence the differential signal is based on superficially scattered photons of which the pathlength is known and depends only on the probe fiber diameter[16]. For FDPS, like DPS, one fiber is designated as a dc-fiber and the second as a c-fiber. The dc-fiber collects superficially as well as deeply excited fluorescence while the c-fiber only collects deeply excited fluorescence. Thus the difference in fluorescence measured in the dc-fiber and c-fiber, the differential fluorescence signal, only takes into account the superficial fluorescence. Phantom measurements have shown that the differential fluorescence signal is independent of the scattering coefficient of the sample under investigation. Moreover, since both the DPS and FDPS measurement are performed with the same probe and having the same measurement geometry, the differential fluorescence can be corrected for the effects of absorption of excitation light by multiplication of the differential fluorescence signal by the ratio of the differential reflectance signals with and without absorption at the excitation wavelength. The FDPS system was calibrated before the start of each measurement series (manuscript submitted).
During each 3 second interruption, first the differential reflectance is measured, after which the differential fluorescence signal is acquired using a 405 nm excitation laser light source (PPMT-LD1382, Power Technology, Little Rock, USA). The 405 nm source was allowed to stabilize before each measurement session and was kept on continuously and controlled using an external shutter (Uniblitz LS-series, Vincent Associates, Rochester, USA). The total laser output power at the fiber-tip was 0.04 mW, and resulted in a light fluence of 32 μJ cm^{-2} per measurement. Hence no significant contribution to the PDT effect from the 405 nm light source is expected. No detection filter was necessary since initial measurements showed negligible contribution from the 405 nm laser source above 420 nm.

Histology and PDT response
Animals were sacrificed after 48 hours by intracardiac exsanguination under isoflurane anesthesia. 30 minutes before exsanguination 0.05 mg/kg temgesic was administered i.m. as additional analgesic. The thoracic and abdominal cavities were opened and macroscopically examined for PDT damage. Thereafter the esophagus was excised, opened longitudinally and macroscopically assessed for PDT-damage and abnormalities. Then the esophagus was swiss rolled from distal to proximal, fixed in formalin, embedded in paraffin, sectioned and stained using hemeatoxylin and eosin. Damage to the individual esophageal layers was examined microscopically as described by Boere *et al*.[6,7]. Particular attention was paid to determine if there was a complete or incomplete ablation of the epithelium.

Fluorescence microscopy

Frozen tissue samples of untreated control and ALA-administered animals were handled under subdued light conditions. Esophageal cross sections of 20 µm thickness were sectioned and mounted on glass slides (Menzel, Braunschwig, Germany). Fluorescence images were acquired at a 50 times magnification using a CCD camera (ORCA-ER, Hamamatsu, Herrsching am Ammersee, Germany) mounted on a fluorescence microscope (Leica, Leiden, The Netherlands) equipped with an N2.1 filter block with an additional bandpass detection filter, 635 ± 10 nm. Fluorescence spectra were acquired from individual esophageal layers using spot sizes of either 12.5 or 67.5 µm, and 200 times magnification using a spectrograph (USB4000, Ocean Optics, Duiven, The Netherlands). Fluorescence was induced with a mercury lamp using a 405 nm band pass filter in combination with a 460 nm short pass filter. Light from the sample was filtered using a 460 nm long pass filter before collected by the spectrograph. Appropriate autofluorescence spectra were acquired and subtracted using methods similar to those described in section 2.6.2.

Data analysis

FDPS data

The DPS part of the setup is calibrated as described previously[14,15]. Calibration of the fluorescence signals for the dc- and c-fibers is done based on the transmission functions measured using a calibrated white light source (HL-2000-CAL, Ocean Optics, Duiven, The Netherlands) (manuscript submitted). The day-to-day variations in output from the laser excitation source were accounted for by measuring the fluorescence intensity with the probe at a fixed distance from fluorescent spectralon (USFS-200-010, Labsphere purchased from Laser 2000, Vinkeveen, The Netherlands). Hence the differential fluorescence (DF), corrected for the absorption, can be described by:

$$\mathrm{DF} = \frac{L_{\mathrm{cal}}}{L_{\mathrm{laser}}}\left(\frac{I^{\mathrm{F}}}{I_{\mathrm{cal}}} - \frac{J^{\mathrm{F}}}{J_{\mathrm{cal}}}\right)\left(\frac{R(0)}{R}\right) \quad . \tag{1}$$

Here L_{cal} is the true output of the calibrated white light source and L_{laser} is the measured laser intensity using fluorescent spectralon. I_F and J_F are the tissue fluorescence intensities measured by the dc- and c-fibers, respectively. Ical and J_{cal} are the calibration lamp intensities as measured by the dc- and c-fibers, respectively. Correction for the tissue absorption is performed by taking the ratio of the calculated differential reflectance without absorption present (R(0)), i.e. the Mie and Rayleigh scattering intensities at the excitation wavelength, and the measured differential reflectance of the tissue (R) at that wavelength.

DPS data

Differential reflectance spectra were fitted according to a model described by Amelink *et al*.[14] including an additional scattering term, see equation 2. In addition to Mie-scattering we observed Rayleigh scattering in the rat esophagus, as has been observed previously in skin[17]. The inclusion of the Rayleigh scattering term in the fit-

model resulted in a significant better fit of the data ($P < 0.05$). The differential reflectance, R, is written,

$$R = \left(a_1 \left(\frac{\lambda}{\lambda_0} \right)^{-b} + a_2 \left(\frac{\lambda}{\lambda_0} \right)^{-4} \right) \cdot \exp\left\{ -0.38 \cdot C_{cor}(\lambda) \cdot \rho \cdot \left[StO_2 \cdot \mu_a^{HbO_2}(\lambda) + (1 - StO_2) \cdot \mu_a^{Hb}(\lambda) \right] \right\} \quad (2)$$

in which the scattering function is modeled by a combination of Mie scattering and Rayleigh scattering, given by power law functions with amplitudes a_1 and a_2 and wavelength dependencies λ^{-b} and λ^{-4}, respectively. C_{cor} is a correction factor that accounts for the inhomogeneous distribution of blood in tissue and depends on the vessel diameter D_{vessel}, ρ is the blood volume fraction, StO_2 is the microvascular blood oxygenation, $\mu_a^{HbO2}(\lambda)$ is the absorption coefficient of fully oxygenated whole blood, and $\mu_a^{Hb}(\lambda)$ is the absorption coefficient of fully deoxygenated whole blood.

Fluorescence spectroscopy

As we and others have described previously[6,11,12] fluorescence spectra were analyzed as a linear combination of basis spectra and fitted using a singular value decomposition algorithm. The fluorescence can be described by a combination of tissue autofluorescence, PpIX and its photoproducts (pPpIX). Basis spectra for the individual components were extracted from the in vivo measured fluorescence spectra. For both of the fluorescence spectroscopy methods, each with its own excitation wavelength and detection wavelength band, a separate set of basis spectra was obtained. All animals in this study, including the light-only controls, showed PpIX fluorescence.

Differential fluorescence spectra were fitted using 7 components (equally weighted) over the wavelength region of 435 to 750 nm. Three basis spectra were used to fit PpIX and its 2 photoproducts centered at 675 nm and 652 nm with a full width half maximum (FWHM) of 27 nm and 15 nm, respectively. Though this second photoproduct at 652 nm is not included nor observed in our previous PpIX photobleaching analysis in the esophagus[6], it is consistent with the analysis of Finlay *et al*.[11]. To obtain a representative autofluorescence basis spectrum for the region where PpIX fluorescence is dominant, we used a scaled curve of elastin and collagen from the literature[18]. Other endogenous non-porphyrin fluorophores show a spectrally similar shaped monotonic decrease above 600 nm[18].

In a small number of animals a distinctive narrow peak centered at 623 nm was observed in the FDPS spectra. A fluorophore expressing a similar peak was also observed in the rat skin[11]. We included a Lorentzian centered at 623 nm with a FWHM of 17.5 nm to our fit model to account for the presence of this (unidentified) fluorophore.

Below 600 nm the differential autofluorescence spectra between individual animals varied considerably. Besides a general monotonic decrease in autofluorescence

intensity as observed previously in the rat esophagus and which is attributed to elastin and collagen, two distinct peaks at 480 FWHM 160 nm and 530 nm FWHM 100 nm were observed in a number of animals. The basis spectra for these peaks are average spectra acquired from animals in which either of the two peaks was dominating. Since there was no direct relation between the intensities or the presence of the 480 nm and 530 nm peaks and fluorescence attributed to elastin and collagen, they were considered to originate from different fluorophores. The presence of two individual peaks indicate the presence of two additional fluorophores in the rat esophagus. Note that the presence or absence of these peaks has no influence on the PpIX amplitude above 600 nm.
The long wavelength fluorescence spectra acquired in the wavelength region from 660 to 825 nm using the isotropic probe were fitted using three components: tissue autofluorescence, PpIX and its photoproduct (pPpIX) centered on 675 nm with a FWHM of 27 nm.

PpIX photobleaching
In previous ALA-PDT experiments on mouse skin and rat esophagus we have shown that PpIX photobleaching can be described by a second-order function [7,19],

$$[S_0]_t = [S_0]_{t=0}\left(1 + \frac{[S_0]_{t=0}\left[^3O_2\right]_t \alpha\phi_t\sigma\kappa_{os}}{\kappa_d + \kappa_{oa}[A]}D\right)^{-1}. \quad (3)$$

Here $[S0]_t$ and $[S0]_{t=0}$ are the photosensitizer concentration and the initial photosensitizer concentration, respectively. Fluence rate per time unit or dose is represented by the parameter D. The local concentration of oxygen, $[^3O_2]$, is a free parameter that is determined by the balance between the supply of oxygen from the tissue vasculature and the photodynamic and metabolic demand for oxygen. In this approach it is assumed that the concentration of biological substrate, [A], remains constant during treatment. If it is further assumed that parameters α, fraction of interactions between triplet state sensitiser and ground state oxygen that lead to formation of singlet oxygen, φ_t, triplet quantum yield of of the sensitiser, σ, the photosensitizer absorption cross section, κ_d, monomolecular decay rate of singlet oxygen, κ_{os}, bimolecular rate of chemical reaction between singlet oxygen and ground state photosensitizer, κ_{oa}, the chemical reaction between singlet oxygen and tissue, remain constant, equation 3 can be simplified to:

$$[S_0]_t = \frac{[S_0]_{t=0}}{1 + C[^3O_2]_t[S_0]_{t=0}D} = \frac{[S_0]_{t=0}}{1 + P[S_0]_{t=0}D}. \quad (4)$$

Here P is proportional to the local concentration of molecular oxygen. During illumination the concentration of oxygen is influenced by the decreasing photodynamic demand for oxygen caused by PpIX photobleaching and variations in the vascular

supply of oxygen. It is possible that the supply of oxygen to the illuminated volume will change throughout the illumination (19). In previous experiments in the esophagus (6, 7) we have observed that a high initial PpIX rate of photobleaching (below 2 J cm^{-2}) is followed by a lower rate of photobleaching for the remainder of the treatment. This was further demonstrated by arbitrarily splitting the analysis of kinetics of photobleaching into two parts, up to 2 J cm^{-2} and from 2 J cm^{-2} onwards, and fitting these separately. In this approach it was assumed (and emphasized) that variations in rate of photobleaching were likely to be due to the availability of oxygen. In the present study we have not made this arbitrary choice but analyzed the whole of the measured photobleaching kinetics and fitted the data with one or more functions of the form of equation 4, where both initial photosensitizer concentration and the oxygen dependent parameter were regarded as free parameters.

Statistical analysis

Spectra are smoothed by binning pixels (n=10) and calculating the average value and standard error of the mean. The smoothed spectra were then fitted using the standard error of the mean as weight factor. The 68% confidence interval (or fitting accuracy) of each of the fitted parameters is given by the square root of the diagonal elements of the covariance matrix. The covariance matrix is the inverse of the second derivative matrix of χ^2 with respect to its free parameters and is exact if and only if the weight factors used in the minimization routine are exact. However, in our case the standard errors of the mean of the individual data points are not real measurement uncertainties but mainly reflect spectrometer noise. In this case, the true variance of the data must be estimated from the data itself. The covariance matrix is then estimated by multiplying the inverse of the second derivative matrix of χ^2 with respect to its free parameters by χ^2/v, with v the number of degrees of freedom. The 68% confidence interval (or fitting accuracy) of each of the parameters is then given by the square root of the diagonal elements of the estimated covariance matrix under the assumption that the model (Eq. (2)) is correct.

The significance level for the differences in fitting of the rate of photobleaching kinetics with a single and double second-order model were tested with an F-test. Differences between groups were tested with the non-parametric Mann-Whitney test.

RESULTS

General observations and histological response to PDT

Catheter placement in the rat esophagus can trigger a reflex that causes respiratory arrest. We encountered this in a small number of animals and one animal died during the procedure. One animal also died one day after PDT. No histological examination was performed in these animals. In a further two animals a poor signal to noise ratio, caused by incomplete contact between one or more of the probes and the mucosa, did not allow a comparison between fluorescence photobleaching data and histological analysis.

At 48 hours post PDT histology showed no PDT related response in the light-only controls while in the ALA-PDT group 9 out of 13 animals showed complete epithelial ablation. In addition to the epithelial layer, severe damage up to ablation was seen in the submucosa and *muscularis propria*. Of the 4 non- or partially responding animals, one did not show any response, one had partial response in the epithelial layer and two others showed damage in all layers except the epithelial layer which remained viable.

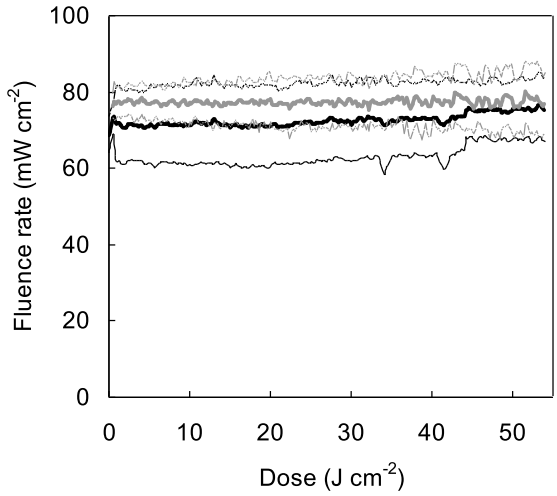

Figure 2. Mean measured fluence rates during illumination (thick lines) and their standard deviations (thin lines) for both the control group (gray) and ALA-PDT group (black).

Fluence rate

Figure 2 shows the average fluence rates as a function of dose, measured during illumination, for the control and ALA-PDT groups together with the standard deviations. There was no change in fluence rate during PDT. The control group received a mean fluence rate of 77.9 ± 6.9 mW cm^{-2} and total dose of 54.4 ± 0.2 J cm^{-2}. The mean fluence rate and fluence delivered in the ALA-PDT group was 75.2 ± 6.0 mW cm^{-2} and 54.6 ± 0.3 J cm^{-2}, respectively. There was no significant difference in either the mean fluence rate or fluence delivered for the control and ALA-PDT group.

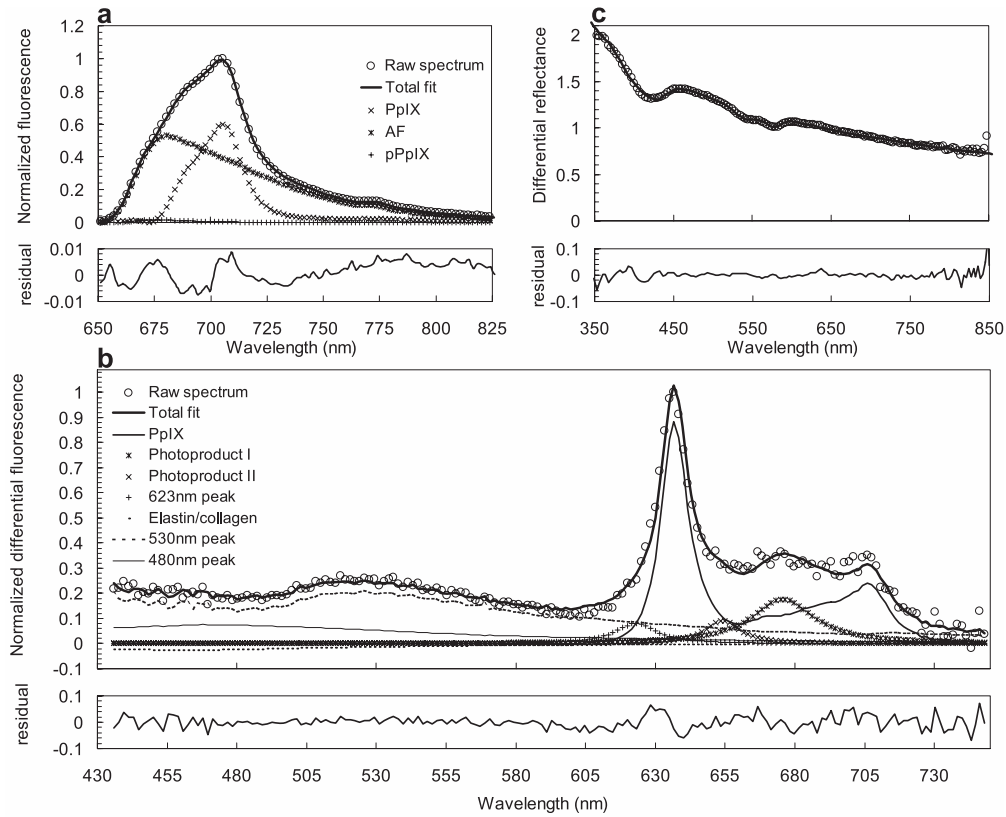

Figure 3. Typical SVD component fit for a) long wavelength fluorescence acquired with an isotropic probe under 635 nm excitation and b) a fluorescence spectrum as acquired with the FDPS probe under 405 nm excitation in the short interruptions during PDT. c) shows a typical Levenberg-Marquardt fit of the DPS signal.

Fluorescence and reflectance spectroscopy

Figure 3a shows a typical long wavelength fluorescence spectrum acquired approximately 1.5 J cm^{-2} after treatment commenced. The spectrum was acquired during PDT, using the 635 nm excitation light from the therapeutic light source. Fitting was done based on three individual components, autofluorescence, PpIX and its photoproduct centered on 675 nm. Also plotted is the residual between the total fit and the acquired spectrum. Figure 3b shows a typical differential fluorescence spectrum acquired under 405 nm excitation at 21 J cm^{-2} after treatment commenced. Also shown are the individual components on the total fit and the residuals between the total fit and the acquired spectrum. Figure 3c shows a typical differential reflectance spectrum acquired during PDT with its fit and residual between fit and data, approximately 7 J cm^{-2} after treatment commenced. The characteristic absorption bands of blood, around 415 nm, 540 nm and 575 nm, are seen which are of importance in determining the blood volume, saturation and the scattering characteristics.

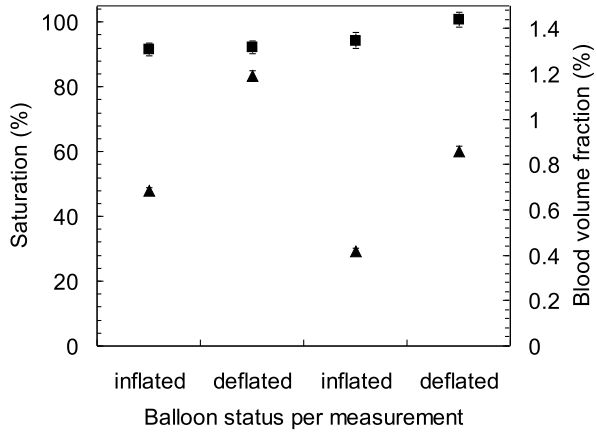

Figure 4. The blood saturation (closed squares) and blood volume (closed triangles) and their standard deviations measured in one animal when the balloon was completely inflated and deflated in two cycles.

Figure 4 shows an example of the variation in saturation and blood volume for 2 inflation and deflation cycles of the balloon in one animal. During PDT with an inflated balloon a constant saturation was observed throughout the treatment in the esophagus and showed no evidence for delayed saturation changes due to possible vasoconstriction of vessels. This means time between inflation and deflation on the saturation is not an important factor and was on average 30 seconds. These inflation/ deflation measurements were conducted directly after PDT in 9 animals. In 4 out of 9 animals there was a significant decrease in blood volume when the balloon is deflated while the saturation remains relatively constant. There was no significant change in either blood volume or saturation in 3 animals. Two animals showed the opposite effect; a high blood volume when the balloon is inflated and low blood volume when deflated. In conclusion, there can be a significant change in blood volume when pressure is exerted on the esophagus wall while the blood saturation remains constant.

Monitoring esophageal PDT

To correct for small variations in fluence rate, the fitted PpIX component of the long wavelength fluorescence emission above 660 nm was divided by the fluence rate, measured at 635 nm with the same isotropic probe at the corresponding time point. The corrected PpIX fluorescence decreases rapidly during the therapeutic illumination. Figure 5(a-f) shows PpIX photobleaching, physiological parameters and tissue optical properties monitored during PDT in two animals. The left column (panels a, b, c) shows data from an animal that showed significant two phased photobleaching. The right column (panels d, e, f) shows data from an animal that also showed two phased photobleaching, although this effect is not statistically significant. The photobleaching kinetics shown in figures 5 a and d are both fitted with a single as well as the sum of 2 second order functions. The corresponding residuals for both fits are shown in each figure. The residuals for the sum of 2 second order functions are smaller and more

evenly distributed around 0. In the ALA-PDT group as a whole the sum of 2 second order functions resulted in a better fit to the measured photobleaching kinetics curve than a single second order fit. In one animal this reached statistical significance as determined by an F-test statistic ($p<0.05$). The transition point between the two phases is defined as the point at which the calculated fractional bleaching for both phases are equal and this is at a fluence of 2.8 ± 0.9 J cm^{-2}, range 1.7 - 4.8 J cm^{-2}. The overall extent of photobleaching measured in these animals is representative of all of the animals in the ALA-treatment group, which was between 70% and 80%.

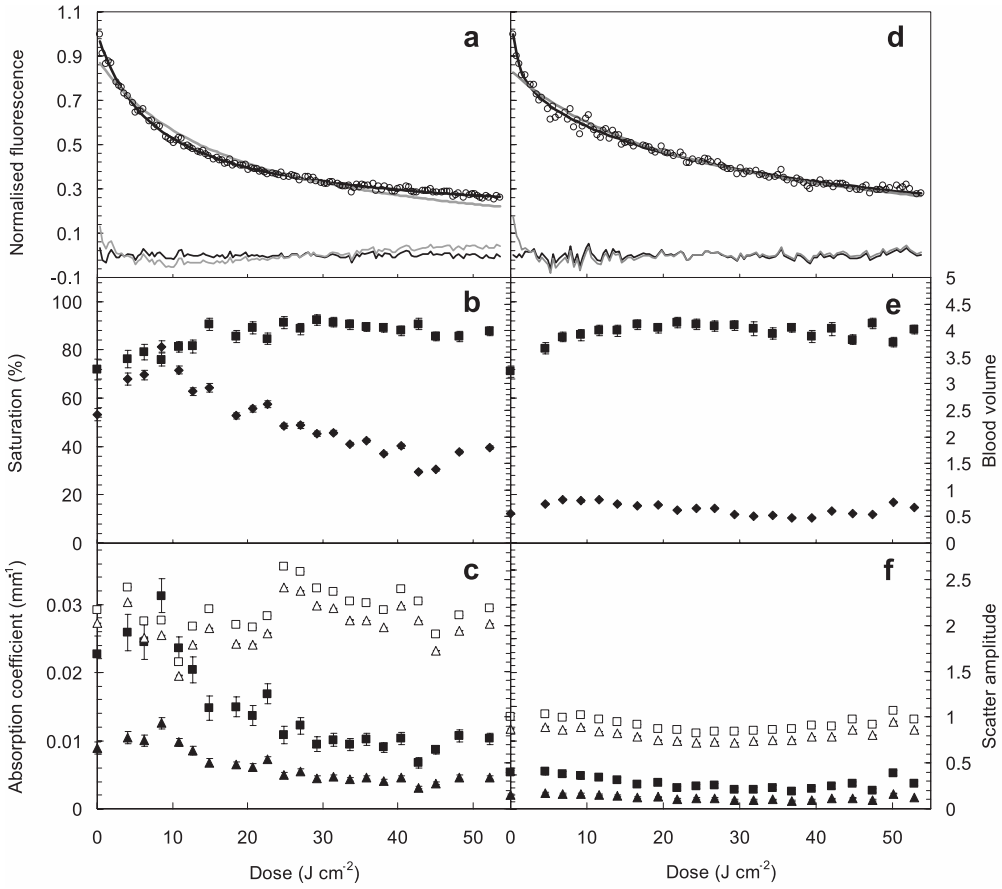

Figure 5. Measured long wavelength fluorescence together with DPS measured physiological and tissue optical parameters plotted against in vivo measured dose for two animals of which one shows statistically significant two phased bleaching (panels a, b and c). a) and d) long wavelength fluorescence (open circles) fitted with a single second order model (thick gray line) and a double second order model (thick black line). Also plotted are the residuals of the individual fits with the data (thin lines). b) and e) DPS measured saturation (closed squares), left axis, and blood volume (closed diamonds), right axis, with confidence intervals during illumination. c) and f) absorption coefficients at 630 nm (closed squares) and 705 nm (closed triangles) with confidence intervals and scattering amplitude at 630 nm (open squares) and 705 nm (open triangles) both with confidence intervals.

Figures 5 b and e show the esophageal saturation and blood volume for the two animals plotted as a function of the delivered fluence. The saturation in both animals at the start of treatment is approximately 71% which increases to 90 % during the first 15-20 J cm^{-2} and remains relatively constant for the remainder of treatment. The absolute blood volume for each animal at the start of treatment is 2.4% and 0.6% respectively (the range within the treatment group is 3.7% to 0.1%). The blood volume increases by approximately 35% during the first 10 J cm^{-2} and subsequently decreases by 30% and 17%, respectively (compared to the starting value). In figures 5 c and f the calculated absorption coefficient (closed symbols) and scatter amplitude (open symbols) at 635 (squares) and 705 nm (triangles) are plotted as a function of the delivered fluence. The absorption coefficient was calculated based on the blood volume percentage and the ratio of oxy- and deoxyhemoglobin and is dependent on variations in the saturation and blood volume, assuming that hemoglobin is the main absorber in tissue. Based on the extinction coefficients of oxy- and deoxyhemoglobin in the 600-800 nm wavelength range it is expected that variations in the ratio between oxy- and deoxyhemoglobin causes higher variability in the absorption coefficient at 635 nm than at 705 nm. The scatter amplitude at 635 nm and 705 nm was calculated as the value of the differential reflectance signal at those particular wavelengths. Figure 5 c shows a relatively high scatter amplitude compared to figure 5 f and has a sudden increase of 26% at 25 J cm^{-2} after which it decreases to its initial value during the remainder of treatment. The scatter amplitude in figure 5f shows a decrease of 28% with a minimum at approximately 27 J cm^{-2}, followed by an increase to its initial value.

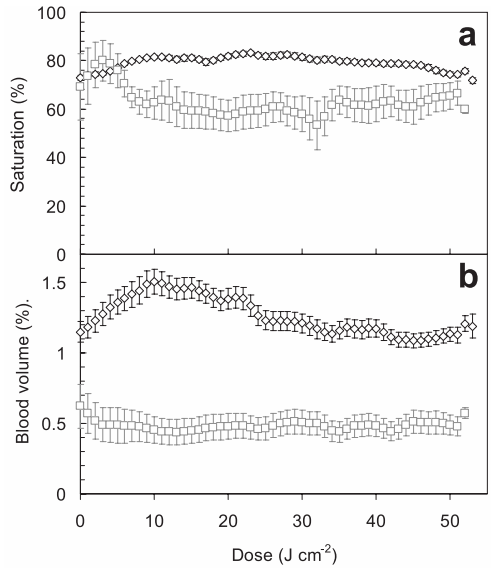

Figure 6. a) mean saturation with standard error of the mean (SEM) against dose for the control (gray) and ALA-PDT animals (black); b) mean blood volumes with SEM against dose for the control (gray) and ALA-PDT animals (black).

Figure 6a shows the average saturation for all of the animals in the control (□) and ALA-PDT (◇) groups. In the ALA-PDT group the saturation is relatively constant during illumination, while in the control group the saturation first decreases over the first 10 J cm^{-2} and then stays constant. There is no significant difference in the average saturation during illumination for the ALA-PDT and control animals, 79 ± 8% and 63 ± 20%, respectively (P>0.1). Figure 6b shows the average blood volumes for the ALA-PDT animals (◇) and the control animals (□). In the ALA-PDT group the average blood volume increases during the first 10 J cm^{-2}, stays relatively constant for the next 8 J cm^{-2} followed by a slight decrease which stabilizes after a dose of 35 J cm^{-2}. In the control group the average blood volume is relatively constant. On the overall treatment there was a significant difference in blood volume during illumination between ALA-PDT and control animals, 1.28 ± 0.65% and 0.43 ± 0.22%, respectively (P<0.05).

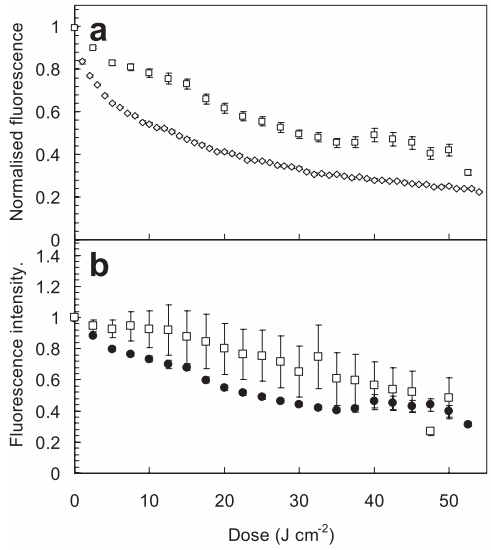

Figure 7. a) Mean normalized fluorescence with SEM against dose for the ALA-PDT animals for the long wavelength fluorescence using 630 nm excitation (open diamonds) and FDPS measured using 405 nm excitation (open squares). b) average PpIX fluorescence photobleaching and SEM of the responders (closed circles) and non-responders (open squares).

Figure 7a shows the average PpIX fluorescence kinetics for all ALA-PDT animals during PDT for the long wavelength fluorescence data (◇) and the differential fluorescence data (□). There are clear differences in the kinetics of PpIX photobleaching measured using the two different fluorescence detection techniques. There is a statistically significant higher rate of photobleaching measured (during the first 4 J cm^{-2}) using the long wavelength fluorescence compared to the differential fluorescence (P<0.01). The average rate of photobleaching in both FDPS and the second phase of the long wavelength fluorescence measurements are not significantly different. Figure 7b shows the FDPS photobleaching data for animals that showed complete epithelial ablation (■) and animals in which the epithelium remained intact

(□). There is a clear difference between the average kinetics of photobleaching for animals that showed ablation and animals that did not respond. Animals that show epithelial ablation show higher rates of photobleaching and this is particularly evident over the first 20 J cm^{-2} of the illumination period.

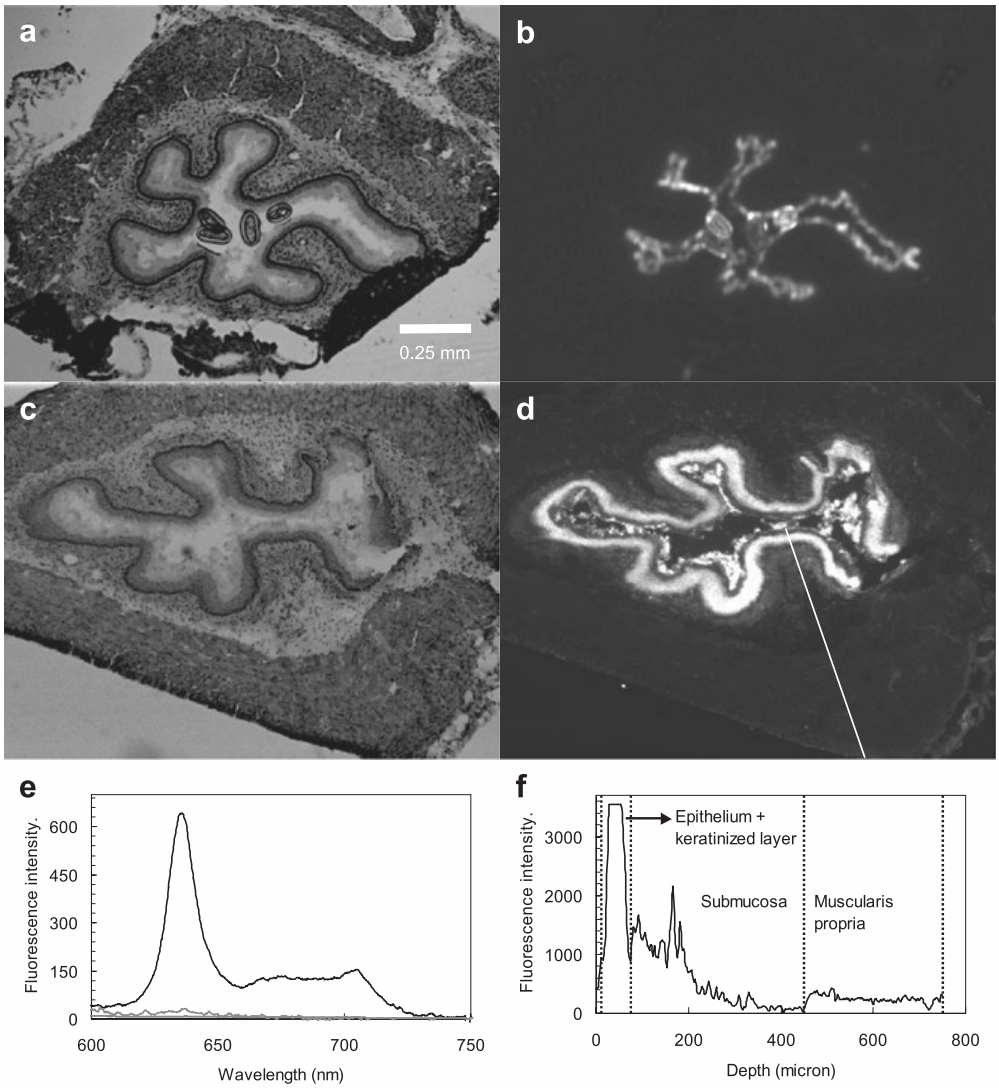

Figure 8. a) H&E stained section from the esophagus of a control rat and b) its corresponding PpIX fluorescence image at a 50 X magnification. c) H&E stained section of an ALA-administered rat and d) the PpIX fluorescence image, at a 50 X magnification. e) fluorescence spectra from the superficial keratinized esophageal layer (black) and epithelium, submucosa and muscularis propria (all gray), acquired at a 400 X magnification. f) PpIX fluorescence line profile of the esophagus in an ALA-administered rat across the line depicted in figure 8d. The epithelium and keratinized layer were allowed to saturate as to show the more subtle PpIX fluorescence in the other esophageal layers.

Fluorescence microscopy

Figures 8 a and b show an H&E stained section and a fluorescence image of a non-treated control animal. Figures 8 c and d show a fluorescence and H&E stained image of a non-treated ALA administered animal. The superficial keratinized layer of the esophagus of a control animal shows a weak autofluorescence emission that we were able to attribute to PpIX autofluorescence using spectral imaging, see figure 8e. A similar fluorescence signal was also present in the residual contents of the esophagus. All other layers, including the squamous epithelium showed no presence of PpIX. Fluorescence spectra confirmed the presence of PpIX in all esophageal layers in the ALA-PDT animals. Figure 8f shows a PpIX fluorescence intensity line profile, depicted in figure 8d, across all esophageal layers. For graphical purposes the epithelial and keratinized layer were allowed to saturate in order to have a better signal to noise ratio for the mucosal and muscular layers.

DISCUSSION

The aim of the present study was to investigate the existence of phased PpIX fluorescence photobleaching and whether this effect was due to the spatial distribution of PpIX and/or tissue oxygenation. This was accomplished by extending our previous attempts to monitor ALA-PDT in the esophagus by combining monitoring long wavelength PpIX fluorescence photobleaching with the simultaneous measurement of blood saturation, blood volume and tissue optical properties using differential pathlength spectroscopy (DPS)[14], and by combining these measurements with fluorescence differential pathlength spectroscopy (FDPS) of PpIX photobleaching (manuscript submitted).

Monitoring the kinetics of PpIX photobleaching

The acquisition and interpretation of PpIX photobleaching measurements in-vivo is a complex task and studies in the literature addressing these issues are somewhat conflicting[6-8,10,11,20-22]. The intrinsic mechanism of photobleaching has been shown to be photosensitizer specific[23-27]. This has important consequences for the general interpretation of photobleaching as a dose metric for PDT[28]. If we only consider PpIX, which has been shown to undergo self-sensitised photobleaching mediated by the production of $^1O_2$ [11], there remain critical issues regarding how fluorescence signals are acquired and how they are interpreted[27]. Of particular importance are the effects of the specific measurement geometry, the influence of tissue optical properties and the relationship between the microscopic distribution of PpIX, molecular oxygen and the treatment volume.

Here one of our specific aims was to determine the mechanism underlying the kinetics of PpIX photobleaching in the esophagus. In both normal and Barrett's esophagus we have previously measured large differences in rates of photobleaching during PDT in animals that showed complete epithelial ablation[6]. Our previous attempts to monitor the multiple phases of PpIX photobleaching were hampered by the low temporal resolution of our spectral measurements acquired under 405 nm excitation during short interruptions to the therapeutic illumination. In the present approach we have repeated these types of measurement (with the incorporation of FDPS) and utilized the

therapeutic illumination at 635 nm to monitor the long wavelength emission of PpIX above 660 nm. The advantage of this detection strategy, besides the increase in temporal resolution of monitoring photobleaching, is that there is no need for interruption of therapeutic illumination. This type of spectrally resolved long wavelength photobleaching measurements has been performed previously in the skin[12]. Recently Sheng *et al*. have also used the therapeutic illumination to monitor PpIX photobleaching in the esophagus using a photomultiplier in combination with a 690 nm long pass filter[8]. However, measurements with a filtered photomultiplier do not provide sufficient information to account for differences in tissue autofluorescence and to correct for the influence of fluorescent photoproducts of PpIX on the fluorescence emission. Data, presented in figure 3a, shows a substantial influence of autofluorescence on the total measured fluorescence. Although the autofluorescence stays relatively constant during PDT (data not shown) its intensity varies between animals. Moreover, during PpIX photobleaching a fluorescent photoproduct, centered around 675 nm, is formed which in turn is also photobleached. The influence of the variation in intensity of the photoproduct is significant above 690 nm. In our opinion these intra- and inter animal variations in intensity of the different components, necessitate the use of spectral decomposition to determine the actual PpIX intensity and recover an accurate rate of photobleaching during PDT. Notwithstanding these findings, it is interesting that Sheng *et al*.[8] were able to show different phases of PpIX photobleaching as we have shown here (figures 5a and d) and in our previous studies[6,7].

The fluorescence excitation and detection 'mode', (i.e. short wavelength excitation with relatively long time intervals between measurements or long wavelength detection without interruptions) presents an interesting trade off between high temporal resolution and signal to noise ratio. It is important to recognize that in order to actually determine the kinetics of photobleaching (whether they contain one or more phases) it is necessary to have sufficient temporal resolution and signal to noise ratio. For example based on our previous experiments[6] we require sufficient data over at least the first 5 J cm^{-2}, thus acquiring data during the therapeutic illumination is advantageous. However, measuring at longer wavelengths where PpIX fluorescence is less intense means that the fit accuracy and fit confidence intervals per parameter become more dependent on the signal to noise ratio of the detector/measurement. The fact that we made only a crude estimate of the relative importance of these effects probably explains why we were only able to show a statistically significant separation between the initial and later phases of photobleaching in one animal in the present study. Furthermore, since the number of data points in the second phase is much greater than in the first phase, the chi-square (the goodness-of-fit parameter) of the fit will change little when fitting the second order model compared to the single second order model. This means that the standard statistical tests to determine significance between two groups, like the F-test, might be too strict for our data. It is possible that similar issues have led to some of the confusion on the exact kinetics of photobleaching of PpIX postulated by a number of authors[8,21,22]. Specifically, with good evidence for the second order function as a physical model for PpIX photobleaching it remains unclear why exponentials and double exponentials are used to describe the

photobleaching process, in particular as there is no underlying physical background for this type of analysis. Parameter values of (double) exponential functions have limited value even when there is no significant difference between the (double) exponential and (the sum of two) second order fits. Another critical issue that is closely related to the choice of excitation and detection mode is the volume (depth) over which fluorescence is excited and collected, which is discussed in detail below.

The mechanism underlying phased PpIX photobleaching in the esophagus

As described previously our intention was to determine the mechanism underlying the differences in rate of photobleaching between the observed first and second phase. By using differential pathlength spectroscopy tissue physiological parameters, such as blood volume and saturation, can be monitored and combined with the data from PpIX fluorescence photobleaching. Our data (illustrated in figure 5) clearly indicates the phases of photobleaching are not simply due to a change in the tissue saturation. Indeed both saturation and blood volume increase over the period in which the rate of photobleaching decreases between the initial and later phase in PpIX photobleaching. We did not find a systematic correlation between overall extent of photobleaching and the average esophageal saturation and/or blood volume. Interestingly, we found a significant difference in blood volume between the control and ALA administered animals which might be correlated to blood pressure effects due to the administration of systemic ALA[29]. Importantly, significant differences between photobleaching kinetics are observed when 405 nm excitation FDPS data are compared with those measured using the therapeutic illumination combined with long wavelength detection (Figure 7).

We believe that these results are consistent with a heterogeneous spatial distribution of PpIX and tissue oxygenation. The heterogeneous spatial distribution of fluorescence is immediately evident from the microscopic distribution of PpIX shown in figure 8. The esophagus consists of a number of layers that surround the lumen; squamous epithelium, submucosa and the muscularis propria. In the rat, and most animals, the most superficial layer of the epithelium is keratinized. The submucosa can be divided into two layers separated by the muscularis mucosa. The muscularis propria also consists of two layers of muscle fibers orientated perpendicularly. Our results show that after the administration of ALA, PpIX accumulates in different amounts in all of these layers. We have also shown that PpIX accumulates in the most superficial keratinized cell layer of the squamous epithelium in control animals, that have not received ALA. This is most likely due to endogenous porphyrins from the Harderian gland that are adsorbed as a result of grooming behavior. These porphyrins are however restricted to the most superficial cell layer and do not result in any PDT induced damage in the epithelium. In contrast, the human esophagus does not show significant levels of endogenous PpIX[30]. For the present discussion we consider 4 layers; a thin layer of keratinized epithelium, the epithelial layer, the submucosa and the muscularis propria. Previous research concluded that PpIX accumulation in the rat is predominantly epithelial and submucosal and negligible (at or very near background levels) amounts of PpIX are present in the muscle layers[4,31]. However in the present study, using fluorescence microscopy we observe PpIX in all esophageal layers including the muscularis propria. We believe that this inhomogeneous distribution of PpIX

fluorescence explains the phased bleaching that has been observed and that this has important consequences for the interpretation of fluorescence photobleaching signals for monitoring ALA-PDT. There is unlikely to be a significant variation in depth distribution of fluence rate using 635 nm illumination in the rat esophagus. In this case, assuming sufficient biological substrate, the rate of photobleaching is dependent on the ratio of photosensitizer concentration and the local tissue oxygen concentration. For example at the same oxygen concentration, with increasing photosensitizer concentrations, the rate of photobleaching will decrease. In an opposite way low photosensitizer concentrations combined with (more than) sufficient oxygen supply will yield an increase in the rate of photobleaching. It is obvious that these processes are dynamic and that there is a photosensitizer concentration below which the total deposition of singlet oxygen limits local PDT response. It is also clear that the deep lying muscularis propria shows low PpIX concentrations but is probably well perfused, whereas the squamous epithelium shows high PpIX concentration but is dependent on the diffusion of oxygen from vessels in the submucosa. Microscopy showed that on average, the first vessels are encountered at a depth of 100 µm below the esophageal surface. These effects accompanied with the relative thicknesses of the epithelium and submucosa and the fact that in the long wavelength excitation and collection mode PpIX fluorescence is collected from all of the esophageal layers means that a substantial quantity of fluorescence is collected from areas of low PpIX concentration and high oxygen saturation. Considering these effects we believe that the spatial distribution of PpIX and tissue oxygenation are responsible for phased PpIX bleaching kinetics we observe. PpIX is essentially partitioned between two locations, the epithelium and the deeper layers, and this results in two phases of photobleaching where the signals from the epithelium are reported by the second slower phase of photobleaching. This second slower phase predominates because PpIX is preferentially localized in the squamous epithelium and the relative contribution of the deeper layers is small. An interesting observation in the present study is that the fluence at which the kinetics of photobleaching transitions between phases is not fixed, this may be a consequence of different inter-animal PpIX distribution.

Optical spectroscopy and tissue optical properties

The incorporation of a correction for the influence of tissue optical properties on the measured fluorescence photobleaching kinetics is an important issue that we and other have addressed previously[6,12,24]. The long wavelength fluorescence data is divided by the fluence rate as a first approximation for correction in optical properties, though figures 5 c and f show changes in optical properties during PDT which are somewhat different in magnitude between the excitation wavelength at 635 nm and the long wavelength emission peak of PpIX at 705 nm. We note that the magnitude of these variations in the optical properties appear to have a small impact on the kinetics of photobleaching for the long wavelength fluorescence measured with the isotropic probe (figure 5). Hence no attempts were made to correct the long wavelength fluorescence data for variations in optical properties as measured with DPS.

The fluorescence photobleaching data from FDPS (figure 7) strongly supports our hypothesis regarding the heterogeneous depth distribution of PpIX and tissue oxygen.

As described FDPS is a quantitative measure of fluorescence independent of optical properties that interrogates a small volume of tissue that is approximately equal to the fiber diameter. Therefore instead of collecting signal from all esophageal layers it measures fluorescence photobleaching predominantly within the squamous epithelium and submucosa. In this configuration the rate of PpIX photobleaching measured with FDPS is significantly less than that of the long wavelength mode and shows no distinctive phases in the photobleaching kinetics. It is important to note that while the FDPS pathlength is known and the variation of the differential signal with tissue optical properties is well understood, these dependencies have, to date, only been investigated in homogenous tissue phantoms (manuscript submitted). It is therefore difficult to be absolutely certain about the actual depth probed in layered tissues. In particular effects that relate to the specific probe geometry we have used in the present study have yet to be fully elucidated and is clearly an area for future study.
FDPS of the esophagus showed significant differences in tissue autofluorescence between 430-600 nm between individual animals. Peaks observed at 480 nm and 530 nm are somewhat similar to NaDH and FAD[18], respectively. Some animals showed systematic variations in autofluorescence components during PDT. While it would be interesting to investigate this in greater detail, the animal numbers in the present study that showed these variations were too small to correlate with the effects of PDT. Further investigation is required to determine the exact origin of these peaks, inter-animal differences in autofluorescence and if there is a correlation between the variation in autofluorescence components and PDT.

Monitoring PDT using fluorescence and reflectance spectroscopy
The kinetics of PpIX photobleaching that we observe in the esophagus are significantly different from those in the skin of pre-clinical models. Here different phases of PpIX photobleaching have not been observed. This is almost certainly a consequence of the use of topical ALA application and the thickness of the skin of normal animal models[32,33]. It is notable that a recent study investigating PpIX photobleaching measured in thicker non-melanoma skin tumors reported phased photobleaching kinetics[21]. It is unclear if these data were considered in the same way we have done in the present study and it seems that there remain issues surrounding the use of an appropriate model for PpIX photobleaching and the correction for changes in tissue optical properties during therapy[11,12]. It is important to highlight the fact that the phased PpIX photobleaching kinetics we observe in the esophagus should be separated from observations of phased photobleaching with other photosensitizers, such as mTHPC[24] and AlPc4[26] where it is evident that more complicated processes are occurring. A recent in vitro study using different cancer cell lines showed mono and bi-exponential bleach kinetics which were attributed to different intracellular localisation of ALA-induced PpIX[34]. While there remains very little in-vivo evidence of large variations in intracellular PpIX distribution at early time points after the administration of ALA, these effects cannot be discounted. We would like to emphasize, however, the use of appropriate physical models for the mechanism underlying PpIX photobleaching and that fitting parameters and measurement errors be incorporated in the analysis of photobleaching kinetics.

The use of reflectance spectroscopy to monitor changes in blood content and saturation during PDT is not new[15,21,35]. A significant advantage of DPS is that it provides a quantitative measure of the physiological constituents of tissue. This is important since, for example, the absolute blood saturation and volume measured in-vivo have the potential to be linked to singlet oxygen deposition, fluorescence photobleaching and tissue response. This is difficult if only relative measurements are possible. We have previously demonstrated the feasibility of DPS type measurements during topical ALA-PDT in mouse skin[19]. The mouse ear was chosen because the thickness of skin at this location facilitated both the measurement procedure and the analysis of reflectance spectra. We observed correlations between the rate of PpIX photobleaching and microvascular saturation modulated by variations in fluence rate. Not surprisingly we found that the microvasculature of the mouse ear was very sensitive to ALA-PDT such that at a fluence rate of 50 mW cm^{-2} the saturation decreased from 30% to 0% within 50 seconds after the start of the illumination. In the present study a fluence rate of 75 mW cm^{-2}, in the esophagus, did not result in oxygen depletion. While the differences in response to PDT are clearly related to differences in the physiology of each tissue, data from the mouse ear does illustrate an important phenomenon. DPS measurements at moderate fluence rate showed low saturations combined with large increases in blood volume. This illustrates that blood supply (flow) is also an important consideration that is not addressed in our present approach.

PpIX photobleaching and the local response to therapy

As in our previous studies, we investigated the relationship between PpIX photobleaching and tissue response in histological sections 48 hours after therapy. This approach was also adopted in the recent study by Sheng *et al*. However, we examined the degree of ablation in individual cell layers, mainly in the epithelial layer, using histological sections, whereas Sheng *et al*. determined the area of edema measured in histological sections stained with H&E. The relationship between these two methods of quantifying PDT response is not immediately clear. The formation of edema is a complex process that may or may not be associated with tissue ablation. We have previously observed that the relation between the amount of edema and local tissue ablation can change with the light treatment parameters[36]. In the current study we were careful to adopt exactly the same treatment parameters, i.e. fluence (rate), treatment regime, balloon size and pressure as we have used previously[6]. We observed compete epithelial ablation in 9 of 13 animals and this was accompanied by severe damage that included ablation in the submucosa and in the muscularis propria. Apparently even in the submucosa and muscularis there is sufficient PpIX and oxygen present to induce complete ablation. This observation is supported by our fluorescence microscopy data (figure 8). Of the 4 non or partially responding animals, one did not show any response, one had partial response in the epithelial layer and two others showed damage in all layers except the epithelial layer which remained viable. All of the animals, including the non-responders, exhibited phased photobleaching kinetics when the long wavelength fluorescence mode was employed. As described previously this was a statistically significant effect in one animal. This result is somewhat different from our previous findings in normal rat esophagus where we observed that the

presence of a rapid initial phase in photobleaching was predictive of tissue response[6,7], although it is difficult to compare these studies since fluorescence excitation and collection geometry were significantly different in our previous studies.
Figure 7b shows the relationship between epithelial ablation and fluorescence photobleaching measured using FDPS. While the error bars are large, the rate of photobleaching is greater in animals that show epithelial ablation and this difference is greatest over the first 20 J cm^{-2} of the illumination. Again this supports our hypothesis that the local rate of photobleaching is correlated with local tissue response and that in some circumstances the supply of oxygen from the submucosa to the epithelium (or the high local concentration of PpIX) may limit the local response to therapy. It is clear that further studies are required to investigate the concepts surrounding the use of FDPS in layered media. In particular there are significant uncertainties that surround the correction of fluorescence spectra in which the fluorophore is heterogeneously distributed and when this distribution is significantly different from the background absorber.

Clinical therapeutic monitoring
Although the rat esophagus is an interesting model to develop techniques to monitor PDT dosimetry, the diameter of the esophagus is prohibitively small and the thickness of esophageal layers is much less than those encountered in clinical PDT of Barrett's esophagus. While the ablation of muscle layers is an interesting effect in the rat this is not a significant effect after ALA-PDT in larger animals or in humans. It is however very likely that a heterogeneous distribution of photosensitizer remains an important issue. An advantage of FDPS and DPS measurements is that the interrogation depth can be adjusted to match the relevant dimensions of the application by changing the diameter of the fibers within the FDPS-probe. In this way photobleaching signals can be used to selectively interrogate the relevant tissue volume and to avoid averaging photosensitizer concentrations over larger/smaller volumes by probing too deeply or too superficially in tissue. In addition there is the obvious opportunity of combining the advantages of the continuous data acquisition mode of the long wavelength fluorescence with FDPS by guiding a fraction of the therapeutic illumination through the excitation channel of the FDPS probe. This would allow uninterrupted and unshielded therapeutic illumination. As we have discussed previously[6] our attempts to monitor PDT in the esophagus remains to be point measurements and there are significant challenges in acquiring measurements from a sufficient area of the tissue to make these types of measurements clinically relevant.

Conclusion
In conclusion we have observed phased bleaching kinetics in the rat esophagus during therapeutic illumination. The results obtained from the long wavelength fluorescence measurements, FDPS, fluorescence microscopy and the histological damage assessment show that there is a complex relationship between PDT response and phased photobleaching kinetics in the rat esophagus. The data suggests that phased bleaching is due to a combination of spatial distribution of PpIX and tissue oxygenation.

References

1. Altorki NK, Oliveria S, Schrump DS. Epidemiology and molecular biology of Barrett's adenocarcinoma. Semin. Surg. Oncol. 1997; 13:270-280.
2. Barr H, Shepherd NA, Dix A, Roberts DJ, Tan WC, Krasner N. Eradication of high-grade dysplasia in columnar-lined (Barrett's) oesophagus by photodynamic therapy with endogenously generated protoporphyrin IX. Lancet 1996; 348:584-585.
3. Ochsner M. Photophysical and photobiological processes in the photodynamic therapy of tumours. J. Photochem. Photobiol. B 1997; 39:1-18.
4. van den Boogert J, Houtsmuller AB, de Rooij FW, de Bruin RW, Siersema PD, van Hillegersberg R. Kinetics, localization, and mechanism of 5-aminolevulinic acid-induced porphyrin accumulation in normal and Barrett's-like rat esophagus. Lasers Surg. Med. 1999; 24:3-13.
5. Siersema PD. Photodynamic therapy for Barrett's esophagus: not yet ready for the premier league of endoscopic interventions. Gastrointest. Endosc. 2005; 62:503-507.
6. Boere IA, Robinson DJ, de Bruijn HS, van den Boogert J, Tilanus HW, Sterenborg HJ, de Bruin RW. Monitoring in situ dosimetry and protoporphyrin IX fluorescence photobleaching in the normal rat esophagus during 5-aminolevulinic acid photodynamic therapy. Photochem. Photobiol. 2003; 78:271-277.
7. Boere IA, Robinson DJ, de Bruijn HS, Kluin J, Tilanus HW, Sterenborg HJ, de Bruin RW. Protoporphyrin IX fluorescence photobleaching and the response of rat Barrett's esophagus following 5-aminolevulinic acid photodynamic therapy. Photochem. Photobiol. 2006; 82:1638-1644.
8. Sheng C, Hoopes JP, Hasan T, Pogue PW. Photobleaching-based Dosimetry Predicts Deposited Dose in ALA-PpIX PDT of Rodent Esophagus. Photochem. Photobiol. 2007; 83:738-748.
9. Forrer M, Glanzmann TM, Braichotte D, Wagnieres GA, van den Bergh H, Savary JF, Monnier P. In-vivo measurement of fluorescence bleaching of meso-tetra hydroxy phenyl chlorin (mTHPC) in the esophagus and the oral cavity. Proc. Soc. Photo-Opt. Inst. Eng. 1995; 2627:33-39.
10. Robinson DJ, de Bruijn HS, van der Veen N, Stringer MR, Brown SB, Star WM. Fluorescence photobleaching of ALA-induced protoporphyrin IX during photodynamic therapy of normal hairless mouse skin: the effect of light dose and irradiance and the resulting biological effect. Photochem. Photobiol. 1998; 67:140-149.
11. Finlay JC, Conover DL, Hull EL, Foster TH. Porphyrin bleaching and PDT-induced spectral changes are irradiance dependent in ALA-sensitized normal rat skin in vivo. Photochem. Photobiol. 2001; 73:54-63.
12. Cottrell WJ, Oseroff AR, Foster TH. Portable instrument that integrates irradiation with fluorescence and reflectance spectroscopies during clinical photodynamic therapy of cutaneous disease. Rev. Sci. Instrum. 2006; 77:064302.
13. van Veen, RL, Nyst H, Rai Indrasari S, Adham Yudharto M, Robinson DJ, Tan IB, Meewis C, Peters R, Spaniol S, Stewart FA, Levendag PC, Sterenborg HJ. In vivo fluence rate measurements during Foscan-mediated photodynamic therapy of persistent and recurrent nasopharyngeal carcinomas using a dedicated light applicator. J. Biomed. Opt. 2006; 11:041107.
14. Amelink A, Sterenborg HJ, Bard MP, Burgers SA. In vivo measurement of the local optical properties of tissue by use of differential path-length spectroscopy. Opt. Lett. 2004; 29:1087-1089.
15. Amelink A, van der Ploeg van den Heuvel A, de Wolf WJ, Robinson DJ, Sterenborg HJ. Monitoring PDT by means of superficial reflectance spectroscopy. J. Photochem. Photobiol. B 2005; 79:243-251.
16. Kaspers OP, Sterenborg HJ, Amelink A. Controlling the optical path length in turbid media using differential path-length spectroscopy: fiber diameter dependence. Appl. Opt. 2008; 47:365-371.
17. Saidi IS, Jacques SL, Tittel FK. Mie and Rayleigh modeling of visible-light scattering in neonatal skin. Appl. Opt. 1995; 34:7410-7414.
18. DaCosta RS, Andersson H, Wilson BC. Molecular fluorescence excitation-emission matrices relevant to tissue spectroscopy. Photochem. Photobiol. 2003; 78:384-392.
19. Robinson DJ, de Bruijn HS, van der Veen N, Stringer MR, Brown SB, Star WM. Protoporphyrin IX fluorescence photobleaching during ALA-mediated photodynamic therapy of UVB-induced tumors in hairless mouse skin. Photochem. Photobiol. 1999; 69:61-70.

20. Sorensen R, Iani V, Moan J. Kinetics of photobleaching of protoporphyrin IX in the skin of nude mice exposed to different fluence rates of red light. Photochem. Photobiol. 1998; 68:835-840.
21. Johansson A, Johansson T, Thompson MS, Bendsoe N, Svanberg K, Svanberg S, Andersson-Engels S. In vivo measurement of parameters of dosimetric importance during interstitial photodynamic therapy of thick skin tumors. J. Biomed. Opt. 2006; 11:34029.
22. Moan J, Ma L, Iani V, Juzeniene A. Influence of light exposure on the kinetics of protoporphyrin IX formation in normal skin of hairless mice after application of 5-aminolevulinic acid methyl ester. J. Invest. Dermatol. 2005; 25:1039-1044.
23. Georgakoudi I, Foster TH. Singlet oxygen- versus nonsinglet oxygen-mediated mechanisms of sensitizer photobleaching and their effects on photodynamic dosimetry. Photochem. Photobiol. 1998; 67:612-625.
24. Finlay JC, Mitra S, Foster TH. In vivo mTHPC photobleaching in normal rat skin exhibits unique irradiance-dependent features. Photochem. Photobiol. 2002; 75:282-288.
25. Finlay JC, Mitra S, Patterson MS, Foster TH. Photobleaching kinetics of Photofrin in vivo and in multicell tumour spheroids indicate two simultaneous bleaching mechanisms. Phys. Med. Biol. 2004; 49:4837-4860.
26. Kunz L, Connelly JP, Woodhams JH, MacRobert AJ. Photodynamic modification of disulfonated aluminium phthalocyanine fluorescence in a macrophage cell line. Photochem. Photobiol. Sci. 2007; 6:940-948.
27. Wang KK, Wilson JD, Kenney ME, Mitra S, Foster TH. Irradiation-induced enhancement of Pc 4 fluorescence and changes in light scattering are potential dosimeters for Pc 4-PDT. Photochem. Photobiol. 2007; 83:1056-1062.
28. Wilson BC, Patterson MS, Lilge L. Implicit and Explicit Dosimetry in Photodynamic Therapy: A New Paradigm. Lasers Med. Sci. 1997; 12:182-199.
29. Schleyer V, Radakovic-Fijan S, Karrer S, Zwingers T, Tanew A, Landthal M, Szeimies RM. Disappointing results and low tolerability of photodynamic therapy with topical 5-aminolaevulinic acid in psoriasis. A randomized, double-blind phase I/II study.J. Eur. Acad. Dermatol. Venereol. 2006; 20:823-828.
30. Regula J, MacRobert AJ, Gorchein A, Buonaccorsi GA, Thorpe SM, Spencer GM, Hatfield AR, Bown SG. Photosensitisation and photodynamic therapy of oesophageal, duodenal, and colorectal tumours using 5 aminolaevulinic acid induced protoporphyrin IX--a pilot study. Gut 1995; 36:67-75.
31. van den Boogert J, van Hillegersberg R, de Rooij FW, de Bruin RW, Edixhoven-Bosdijk A, Houtsmuller AB, Siersema PD, Wilson JH, Tilanus HW. 5-Aminolaevulinic acid-induced protoporphyrin IX accumulation in tissues: pharmacokinetics after oral or intravenous administration. J. Photochem. Photobiol. B 1998; 44:29-38.
32. van der Veen N, de Bruijn HS, Berg RJ, Star WM. Kinetics and localisation of PpIX fluorescence after topical and systemic ALA application, observed in skin and skin tumours of UVB-treated mice. Br. J. Cancer 1996; 73:925-930.
33. Kristiansson S, Juzeniene A, Juzenas P, Iani V, Löfgren L, Moan J. Kinetics of protoporphyrin IX formation in rat oral mucosa and skin after application of 5-aminolevulinic acid and its methylester. Photochem Photobiol. 2005; 81:394-397.
34. Ji Z, Yang G, Vasovic V, Cunderlikova B, Suo Z, Nesland JM, Peng Q. Subcellular localization pattern of protoporphyrin IX is an important determinant for its photodynamic efficiency of human carcinoma and normal cell lines. J. Photochem. Photobiol. B 2006; 84:213-220.
35. Finlay JC, Foster TH. Hemoglobin oxygen saturations in phantoms and in vivo from measurements of steady-state diffuse reflectance at a single, short source-detector separation. Med. Phys. 2004; 31:1949-1959.
36. de Bruijn, HS, Meijers C, van der Ploeg-van den Heuvel A, Sterenborg HJCM, Robinson DJ. Microscopic localisation of protoporphyrin IX in normal mouse skin after topical application of 5-aminolevulinic acid or methyl-aminolevulinate. J. Photochem. Photobiol. B 2008 (in press).

7

Monitoring interstitial m-THPC-PDT in vivo using fluorescence and reflectance spectroscopy.

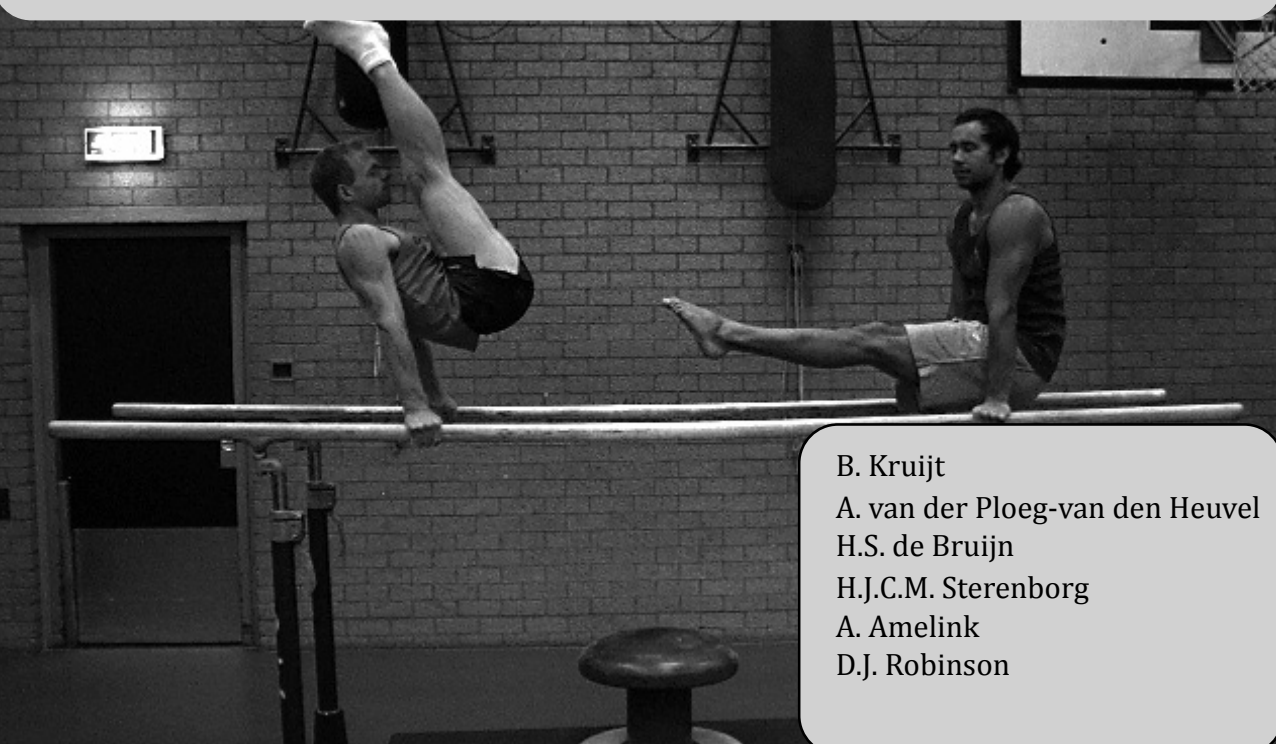

B. Kruijt
A. van der Ploeg-van den Heuvel
H.S. de Bruijn
H.J.C.M. Sterenborg
A. Amelink
D.J. Robinson

Abstract

In order to understand the mechanisms of photodynamic therapy (PDT) it is important to monitor parameters during illumination that yield information on deposited PDT-dose. The aim of this study is to investigate the possibility of monitoring implicit parameters, such as photobleaching, in addition to monitoring explicit parameters (fluence (rate), oxygenation, photosensitizer concentration) directly or indirectly. These parameters are monitored during PDT without interrupting the therapeutic illumination.

Rats were injected with 0.3 mg kg^{-1} m-THPC. Sixteen hours after administration the abdominal muscle in rats was irradiated for 1500 seconds using clinically relevant fluence rates of 50, 100 and 250 mW cm^{-1} of diffuser length at 652 nm. In addition to the linear diffuser for delivering treatment light, isotropic fiber-optic probes and fiber-optic probes for differential path length spectroscopy (DPS) were placed on both sides of the muscle to monitor tissue physiological parameters, fluence rate and fluorescence.

The m-THPC treatment groups show a decrease in fluence rate throughout PDT of 16%, 19% and 27% for the 50, 100 and 250 mW cm^{-1} groups, respectively. Both during and post PDT differences in vascular response between treatment groups and animals within the same treatment group are observed. Furthermore we show fluence rate dependent bleaching of m-THPC up to a measured fluence rate of 100 mW cm^{-1}.

The data presented in this study show the possibility of simultaneously monitoring fluence (rate), fluorescence, hemoglobin oxygen saturation and blood volume during PDT without interruptions to the therapeutic illumination. Differences in saturation profiles between animals and treatment groups indicate differences in vascular response during illumination. Furthermore the relationship between fluence rate and m-THPC fluorescence photobleaching is complex in an interstitial environment.

Cover: using the abdominal muscles in gymnastics (top: Dineke Huson, Niki van de Loo, Anneloes Geerts; Bottom: Oliver Lemans, Thomas Weber)

Published in lasers surgery and medicine, 2009,

INTRODUCTION

In order to optimize and standardize clinical photodynamic therapy (PDT) it is necessary to understand the mechanisms of action surrounding the deposition of PDT dose. The dose delivered during PDT is determined by the amount of reactive oxygen species that are generated. The generation of reactive oxygen species is dependent on the photosensitizer, its concentration, the local fluence (rate) and the availability of oxygen. However the dynamic nature of PDT means that things change continuously and the fact that there is a complex relationship between each of these parameters makes it difficult to determine the PDT dose deposited. This has led a number of investigators to explore, in addition to explicit dosimetry (fluence rate, oxygenation and photosensitizer concentration), methods of implicit dosimetry, such as fluorescence photobleaching, with the aim of standardizing and optimizing therapy[1,2]. Therefore a combination of both explicit and implicit parameters, monitored during PDT, would be valuable tools for understanding mechanisms underlying PDT. Preferably these parameters are monitored during PDT without disturbing the light treatment protocol.

Fluence rate and fluence are relatively simple explicit parameters to monitor *in vivo* and can be adapted during PDT if necessary. High fluence rates lead to faster depletion of tissue oxygen which is not favorable since it decreases PDT efficacy[2,3]. For this reason monitoring tissue oxygenation in combination with fluence (rate) may be a step forward in optimizing therapy. In addition a number of authors have suggested that monitoring tissue oxygenation during the course of treatment might yield information on vascular response (vasodilatation or constriction) and/or possible mechanisms of cell death[4,5]. Although there are a variety of methods for measuring oxygenation in cells which can be applied *in vivo*[5,6], these methods are relatively difficult and often invasive to apply. Another (non-invasive but more indirect) way to determine the availability of oxygen is to monitor blood saturation using non-invasive optical techniques.

Tissue oxygenation is dependent on the supply of oxygen by the vasculature, therefore saturation may be an indicator of tissue oxygenation. Several studies have used diffuse reflectance spectroscopy using visible or near infrared light to determine the saturation during superficial[4,7,8] or interstitial PDT[9,10,11]. A difficulty of this approach is that the therapeutic illumination interferes with the measurements by overexposing the spectrograph so that measurements can only be acquired during interruptions to PDT[9] unless the therapeutic wavelength is outside the spectral range of the detector[7]. Another important consideration is that diffuse reflectance spectroscopy is hampered by the lack of knowledge of the optical path-length of light *in vivo*[12,13]. This is particularly important since the path-length of light in tissue depends on the tissue optical properties which are known to change during PDT as a result of variations in saturation, blood volume and tissue scattering. To avoid these problems we have developed differential path-length spectroscopy (DPS) which measures saturation and blood volume by subtracting two signals that contain the same contribution from long path-length photons but different contributions from short path-length photons, to obtain a well-defined path-length that is insensitive to changes in tissue optical properties[13-15]. It is however, still necessary to filter out the light at the therapeutic wavelength. As a solution to this problem a notch filter centered at the therapeutic

wavelength is placed in front of the spectrographs used for acquiring reflectance spectra.

In addition to fluence (rate) and tissue oxygenation the amount of photosensitizer present is clearly an important factor in the deposition of PDT dose. The photosensitizer concentration can potentially be monitored using its fluorescence emission. The direct relationship between the concentration of photosensitizer and therapeutic outcome is complicated by the dynamic nature of the therapeutic dose delivered during PDT. Nonetheless in certain specific circumstances it can be advantageous to monitor the degradation of photosensitizer (photobleaching) as an implicit parameter. This is due to the fact that for some photosensitizers photobleaching is mediated by reactive oxygen species and can be related to the local therapeutic dose delivered during PDT[2,3]. Most photosensitizers investigated exhibit the most intense fluorescence peak at or near the clinical therapeutic wavelength. To date in most studies monitoring photosensitizer photobleaching the treatment is either interrupted at regular intervals[16] or, mostly in pre-clinical studies, a different treatment wavelength is chosen[2]. Another possibility is to monitor photosensitizer fluorescence at longer wavelengths, beyond the therapeutic wavelength[17,18].

Meta-tetrahydroxyphenylchlorin (m-THPC) or Foscan® is a potent second generation photosensitizer. Therefore m-THPC-PDT is currently under investigation as a potential treatment modality in addition to radiotherapy and surgery[19-21]. Especially good results in the head and neck region using (interstitial) PDT in combination with m-THPC[19-22] have been observed. This approach to PDT is not limited to the head and neck region. Various studies are underway investigating the use of m-THPC-PDT for the treatment of other malignancies in the prostate[23], vulva[24], lungs[25], skin[26] and anal canal[27]. Despite overall positive results there are still a number of patients that show no or partial response. A first step in understanding these variations lies in the understanding of the mechanisms underlying m-THPC-PDT. To our knowledge, no monitoring of explicit and/or implicit parameters are currently performed in interstitial m-THPC-PDT that can aid in standardizing and optimizing clinical m-THPC-PDT. For this reason in the current study our first aim is to investigate the possibility of monitoring explicit (fluence(rate)) and implicit parameters (photobleaching, blood volume and saturation) during PDT in an interstitial environment to provide clinicians in the near future with tools to standardize and optimize clinical m-THPC-PDT.

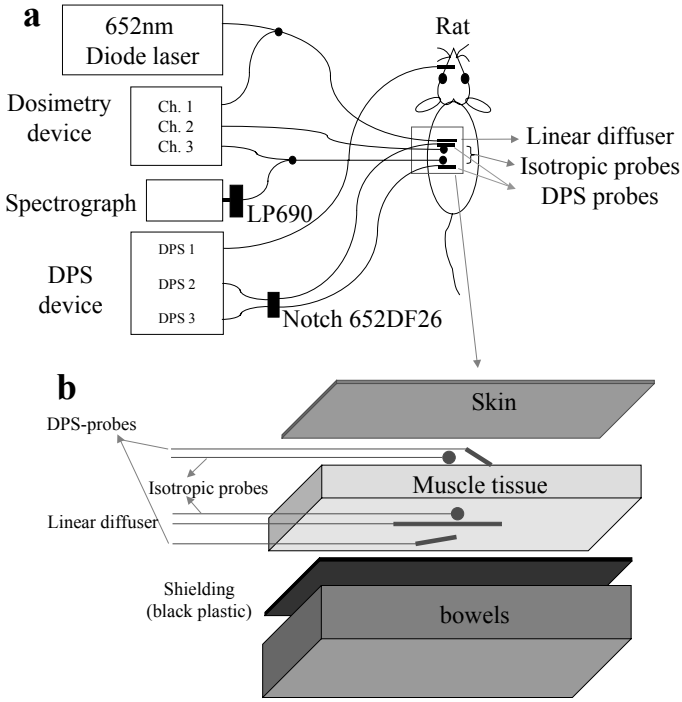

Figure 1. a) Schematic outline of the experimental setup showing the therapeutic 652 nm laser, the 3-channel dosimetry device, the 690 nm long pass filtered spectrograph and the 3-channel DPS device of which two channels are filtered using a 650 nm notch filter. The two channels of the DPS device that are filtered detect (reflected) light via fiber-optic probes within the treatment area. The third DPS probe is used to monitor physiological parameters outside the treatment area; b) Shows a exploded schematic close up of the treatment area in its different layers with the in vivo placement of the illumination fiber (linear diffuser), the two isotropic probes and the two DPS probes. The shielding is layer is black plastic and prevents illumination of the intestines.

MATERIALS AND METHODS

Animals and treatment procedure

The experimental design for this study was approved by the animal experiment committee of the Erasmus University Medical Center. Two weeks prior to the experiments, 31 normal adult male Wistar rats were placed on a diet of chlorophyll free food (AB Diets, Woerden, the Netherlands) to minimize the influence of autofluorescence centered at 675 nm due to pheophorbide-α. The drug-light interval of the present study was chosen based on the pharmacokinetics of m-THPC in muscle. Between 12 and 120 hours after administration, the concentration of m-THPC remains relatively constant[28,29]. Sixteen hours before treatment rats were injected with 0.3 mg/kg m-THPC i.v., except for control animals which were injected with the injection vehicle (PEG400:ethanol:water, 2:3:5) not containing m-THPC.

The m-THPC administered rats were divided into three groups of 7 animals each receiving fluence rates that are typical of interstitial PDT. Fifty, 100 and 250 mW cm^{-1}

diffuser length were delivered over a time period of 1500 seconds. The 10 remaining animals were divided into two control groups of 5 animals receiving fluence rates of 50 and 250 mW cm^{-1}, respectively.
At the time of treatment animals were anaesthetized using isoflurane and oxygen. A vertical incision was made through the skin and the abdominal muscle layer at the *linea alba*. Figure 1 shows the schematic outline of the different tissue layers and the probe placement. Skin overlying the muscle layer was separated from the muscle layer. A sheet of black plastic was placed between the muscle layer and the intestines of the animal to prevent PDT induced damage to the intestines. Next a linear diffuser (length 1 cm, diameter 1 mm) (CeramOptec, Jena, Germany), DPS probe and isotropic probe were placed underneath the muscle layer, which is approximately 2.5-3 mm thick. The DPS and isotropic probe were positioned at the centre of the linear diffuser and as close to it as possible. This measurement location will be referred to as adjacent to the illumination fiber. A second isotropic probe and DPS probe were placed at the top side of the muscle layer, this second isotropic probe is bifurcated to measure both fluence rate and fluorescence. Again the DPS-probe was placed as close to the isotropic probe as possible. This measurement location will be referred to as on the top of the muscle. The skin flaps overlying the abdominal muscle were drawn together and the incision in the muscle was closed as far as practicable. With the illumination and optical monitoring fibers fixed in position the local blood physiological parameters were measured prior to, during, and after the therapeutic illumination. A third DPS probe was placed outside the PDT illumination field, on the tongue of the animal, to monitor the systemic saturation and possible effects of anaesthesia during the treatment procedure. For a period of time after light source and probe positioning (between 10 and 15 minutes) the local blood physiological parameters measured using DPS varied significantly. On average these changes were characterised by a decrease in blood volume and variations in blood saturation. In each animal these parameters were allowed to stabilise before the start of the illumination. PDT was performed using 652 nm laser light from a diode laser (CeramOptec, Jena, Germany). During PDT light dosimetry, reflectance and fluorescence spectroscopy were performed continuously as described below. For a period after the end of the illumination physiological parameters were measured at regular time intervals to monitor changes induced after PDT. After these measurements each animal was sacrificed using an overdose of pentobarbital.

Light dosimetry and fluorescence spectroscopy
Fluence rate was measured at each location; adjacent to the treatment fiber and on the top of the muscle, using a 1 mm isotropic probe on the distal end of a 400 micron fiber (Cardiofocus, formerly Rare Earth Medical, West Yarmouth MA, USA). The isotropic probe on top of the muscle layer had a fiber bifurcation (200/400 micron) in order to measure both fluence rate and m-THPC fluorescence. Fluorescence was measured in the long wavelength region, between 690 and 750 nm, using a spectrograph (USB 4000, Ocean Optics, Duiven, The Netherlands) in combination with a 690 nm long pass filter. Fluence rate was measured with a modular based multi-channel dosimetry device that has been described in detail previously[22]. The spectrometer for measuring fluorescence was incorporated in the dosimetry system

and both devices were controlled using the same LabView (National Instruments, Austin Texas, USA) based program. Fluorescence was measured directly after a fluence rate measurement. Typical integration times for the spectrograph ranged between 2500 and 5000 ms. This allows a maximum sampling frequency of 24 measurements a minute using an integration time of 2500 ms.

Differential path-length spectroscopy

Differential path length spectroscopy (DPS) was used to obtain local information on physiological parameters, such as saturation and blood volume[13,14,17]. DPS was measured at two different locations on the abdominal muscle layer, adjacent to the treatment fiber and on top of the muscle, using two probes each containing two 400 μm fibers placed at a core-to-core distance of 440 μm. Both probes were polished at an angle of 15 degrees to minimize specular reflectance at the probe-tissue interface. The DPS system was modified to enable white light differential reflectance measurements during therapeutic illumination at 652 nm. This was achieved by coupling the end-fibers of the two individual DPS-probes, leading to the 4 spectrographs, first into a 4-channel filter block containing a 650 ± 13 nm notch filter (03FIN149, Melles Griot, Didam, the Netherlands). We would like to note that we observed a second blocking region of the notch filter around 450 nm. No contribution due to the 652 nm light from the therapeutic light source was measured in the reflectance spectra. There was no measurable cross talk between the channels within the filter block. The white light used for acquiring reflectance spectra can interfere with the fluorescence signal acquired by the isotropic probe making the fluorescence spectra unsuitable for fitting. To allow acquisition of sufficient uncontaminated fluorescence spectra during PDT the sampling rate of the DPS system was set to acquire 4 reflectance spectra per minute at an maximum integration time of 100 milliseconds. The third DPS probe positioned on the tongue of the animal, used to monitor systemic saturation, contained 800 micron fibers.

Data processing

Fluorescence spectroscopy

To correct for variations in fluence rate during PDT the fitted long wavelength fluorescence was divided by the measured fluence rate[17]. Both fluence rate and fluorescence were monitored using the same isotropic probe. The corrected fluorescence spectra were described as a linear combination of basis spectra and fitted with a singular value decomposition algorithm[3,17,30]. Here the fluorescence was attributed to the combination of m-THPC fluorescence and tissue autofluorescence. The basis spectrum for the autofluorescence component was the normalized average fluorescence spectrum acquired in the control animals. The m-THPC fluorescence component was the normalized average of fluorescence measured in the m-THPC administered animals with subtraction of the autofluorescence signal.

One of the aims of the present manuscript is to investigate the suitability of performing fluorescence spectroscopy in combination with DPS measurements during illumination for interstitial PDT. It is important to note that considerable effort has centered on understanding the mechanism by which m-THPC photobleaches and how these processes can be monitored using *in vivo* spectroscopy (31-35). A complete analysis of

these mechanisms lies outside the scope of this manuscript and will be presented elsewhere. It is however necessary to perform a preliminary analysis of the kinetics of photobleaching so that it is possible to present the data collected in the present study. M-THPC has previously been shown to undergo self sensitized photobleaching via a mechanism mediated by singlet oxygen[32,33]. This has led investigators to fit *in vivo* m-THPC photobleaching with second order decay kinetics, an approach that we and others have adopted for other photosensitizers such as PpIX[2,17]. In the present manuscript we have continued with this approach. However the second order decay kinetics could not be used to fit the m-THPC bleach kinetics over the entire dose range measured. For this reason we used the second order decay kinetics to fit m-THPC photobleaching kinetics over the dose range of 0 – 10 J cm^{-2} under the assumption that the oxygenation of the tissue over this dose range is sufficient for m-THPC to undergo photobleaching predominantly via a singlet oxygen mediated mechanism. In a simplified formulation the second order model is given by[19]:

$$[S_0]_t = \frac{[S_0]_{t=0}}{1 + C[^3O_2]_t[S_0]_{t=0}D} \tag{1}$$

Here $[S_0]_t$ and $[S_0]_{t=0}$ are the photosensitizer concentration and the initial photosensitizer concentration, respectively. The delivered light dose is represented by the parameter D and $[^3O_2]$ is the local concentration of oxygen determined by the balance between the supply of oxygen from the tissue vasculature and the photodynamic and metabolic demand for oxygen. The constant C, as described previously[17], consists of a group of parameters assumed to be constant.

Differential pathlength spectroscopy

Differential reflectance spectra were fitted according to a model described by Kruijt *et al*.[17]:

$$R = \left(a_1\left(\frac{\lambda}{\lambda_0}\right)^{-b} + a_2\left(\frac{\lambda}{\lambda_0}\right)^{-4}\right) \times \exp\{-0.38C_{\mathrm{cor}}(\lambda)\rho[\mathrm{StO_2}\mu_a^{\mathrm{HbO_2}}(\lambda) + (1-\mathrm{StO_2})\mu_a^{\mathrm{Hb}}(\lambda)]\} \tag{2}$$

The scattering function is modelled by a combination of Mie scattering and Rayleigh scattering, given by power law functions with amplitudes a_1 and a_2 and wavelength dependencies λ^{-b} and λ^{-4}, respectively. C_{cor} is a correction factor that accounts for the inhomogeneous distribution of blood in tissue and depends on the vessel diameter D_{vessel}, ρ is the blood volume fraction, StO_2 is the microvascular blood oxygenation, $\mu_a^{HbO2}(\lambda)$ is the absorption coefficient of fully oxygenated whole blood, and $\mu_a^{Hb}(\lambda)$ is the absorption coefficient of fully deoxygenated whole blood.

Note that before fitting the reflectance spectra are spectrally binned, meaning that, the average and standard deviation are calculated over bins containing a number of spectral data points, in this case 10 spectral data points. This binning procedure is necessary to provide standard deviations for the fit procedure. The fit procedure uses

the standard deviation of the average data points as a weighing factor in the fit[36]. Outliers and poor signal to noise ratio lead to average data points with high standard deviations which are given a lower weight in the fitting procedure. For this reason it is possible to accurately fit the data despite the spectral blocking regions of the applied notch filter around 450 nm and 650 nm, where spectral points contain high standard deviations and thus are given low weights in the fit.

Statistics

Confidence intervals on the individual parameters for the individual measurements were determined based on the covariance matrix generated for each fit as described by Amelink *et al.*[36]. Differences between animals and groups were tested using the non-parametric Mann-Whitney test.

RESULTS

Directly after the surgical procedure DPS measurements showed significant changes in local blood volume and saturation of the abdominal muscle structure. PDT was started when both saturation and blood volume signals had stabilized after the surgical procedure, on average this took approximately 10 minutes. The third DPS probe, placed on the tongue, showed no blood volume or saturation variations in either the control or m-THPC administered groups before, during and after PDT.

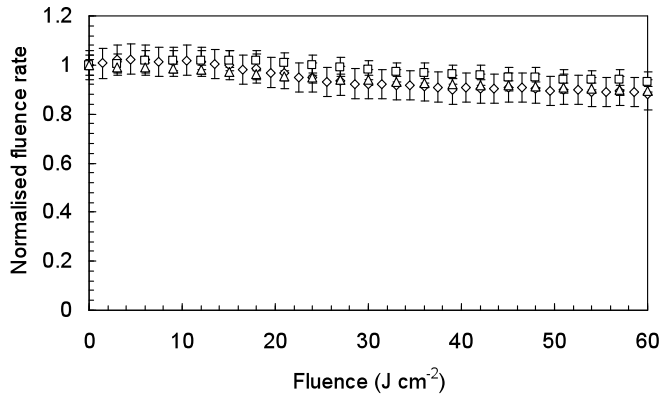

Figure 2. Normalised average fluence rates measured at the detection side as function of fluence (over a range of 0-60 J cm^{-2}) for the 50 mW cm^{-1} m-THPC (◇), 100 mW cm^{-1} m-THPC (□) and 250 mW cm^{-1} m-THPC (△) treatment groups. The error bars represent standard error of the mean (SEM).

Figure 2 shows the variation in normalised fluence rate as a function of fluence over a range of 0-60 J cm^{-2}, measured at the top surface of the muscle for all groups. The absolute measured fluence rate at this side is dependent on the thickness of muscle tissue which varies between animals. Average measured fluence rates at the top surface of the muscle for the experiment groups were 17 ± 9, 42 ± 14 and 117 ± 68 mW cm^{-2} for the 50, 100 and 250 mW cm^{-1} groups, respectively. The control groups show a constant fluence rate during therapeutic illumination, whereas the m-THPC treatment groups show a decrease in fluence rate of 10% over 0-60 J cm^{-2} for all treatment groups, respectively. Fluence rates measured with the isotropic probe adjacent to the linear diffuser show average measured fluence rates of 45 ± 13, 93 ± 20 and 211 ± 32 mW cm^{-2} for the 50, 100 and 250 mW cm^{-1} groups, respectively. The m-THPC treatment groups show a decrease in fluence rate of 7% (data not shown) over 0-60 J cm^{-2} for the 50 and 100 mW cm^{-1} groups. The 250 mW cm^{-1} group shows constant fluence rate over the range of 0-60 J cm^{-2}.

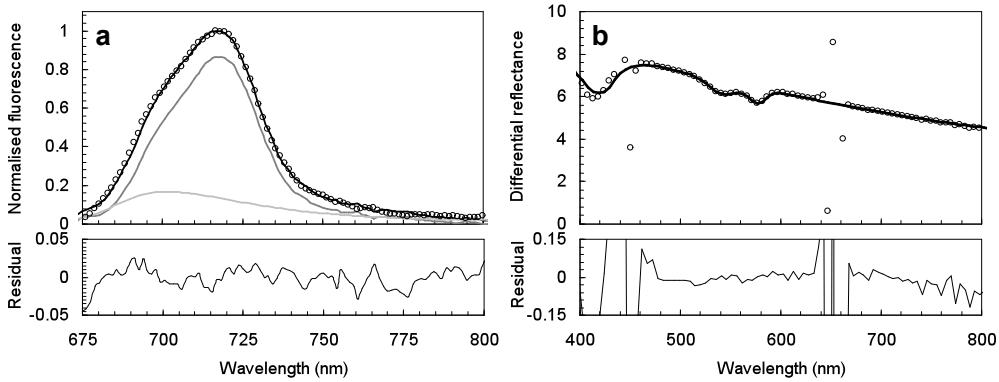

Figure 3. a) Typical SVD component fit (black solid line) of long wavelength fluorescence acquired using an isotropic probe under 652 nm excitation (open circles). Also the individual components for m-THPC (dark grey line) and autofluorescence (light grey line) are shown. The residual between fit and data is plotted separately underneath. Note that the fluorescence signal was not corrected for the transmission of the optical system. b) typical fit (solid black line) of the differential reflectance signal (open circles) using a Levenberg-Marquardt fit algorithm with Eq.2 as model to fit the data. The residual between fit and data is plotted separately underneath. Note the discontinuities in the spectrum at 652 nm and 450 nm due to the notch filter.

Figure 3a shows a typical fitted long wavelength fluorescence spectrum with the residual and the individual components, m-THPC and tissue autofluorescence, acquired approximately 2 J cm^{-2} after the start of treatment. These fluorescence spectra were acquired during illumination using the 652 nm therapeutic light as excitation. Especially the autofluorescence shows an increase in fluorescence followed by a decrease as a function of wavelength since these fluorescence spectra (and basis spectra) are not corrected for the system transmission. For this reason the basis spectra utilized can only be used to fit fluorescence data acquired with the current system.

Figure 3b shows a typical differential reflectance spectrum acquired during PDT with its fit and residual between fit and data, approximately 2 J cm^{-2} after treatment commenced. The presence of the notch filter is observed by the measured noise in the reflectance spectrum around 450 and 650 nm.

Figure 4 shows the fluorescence and physiological parameters, saturation and blood volume, as a function of treatment time. Figure 4a shows the normalized fluorescence against time over the whole treatment time. Figures 4b and c show the measured saturation for the control and m-THPC-groups as a function of time for the probes located adjacent to the linear diffuser and on top of the muscle, respectively. As expected the control groups maintain constant high saturation throughout treatment at both sides. The 50 mW cm^{-1} m-THPC-group shows high saturation during PDT but has more variation at both measurement sides as compared to the control groups. The saturation in the 100 mW cm^{-1} m-THPC-group also starts at 90-100% saturation but shows a gradual decrease in saturation during illumination measured on top of the muscle. Adjacent to the fiber the decrease in saturation is more rapid until halfway into

the treatment where it maintains low saturation until the end of treatment. In the 250 mW cm^{-1} m-THPC-group the saturation shows a rapid decrease at both measurement locations immediately after the start of illumination and remains low until the end of treatment.

Figures 4d and e show the normalized blood volumes for all groups again measured both on top of the muscle and adjacent to the linear diffuser, respectively. Blood volumes for all groups at both measurement sides are relatively constant during PDT. Only on top of the muscle for the 50 mW cm^{-1} m-THPC-group an increase in blood volume is observed over the first 270 seconds.

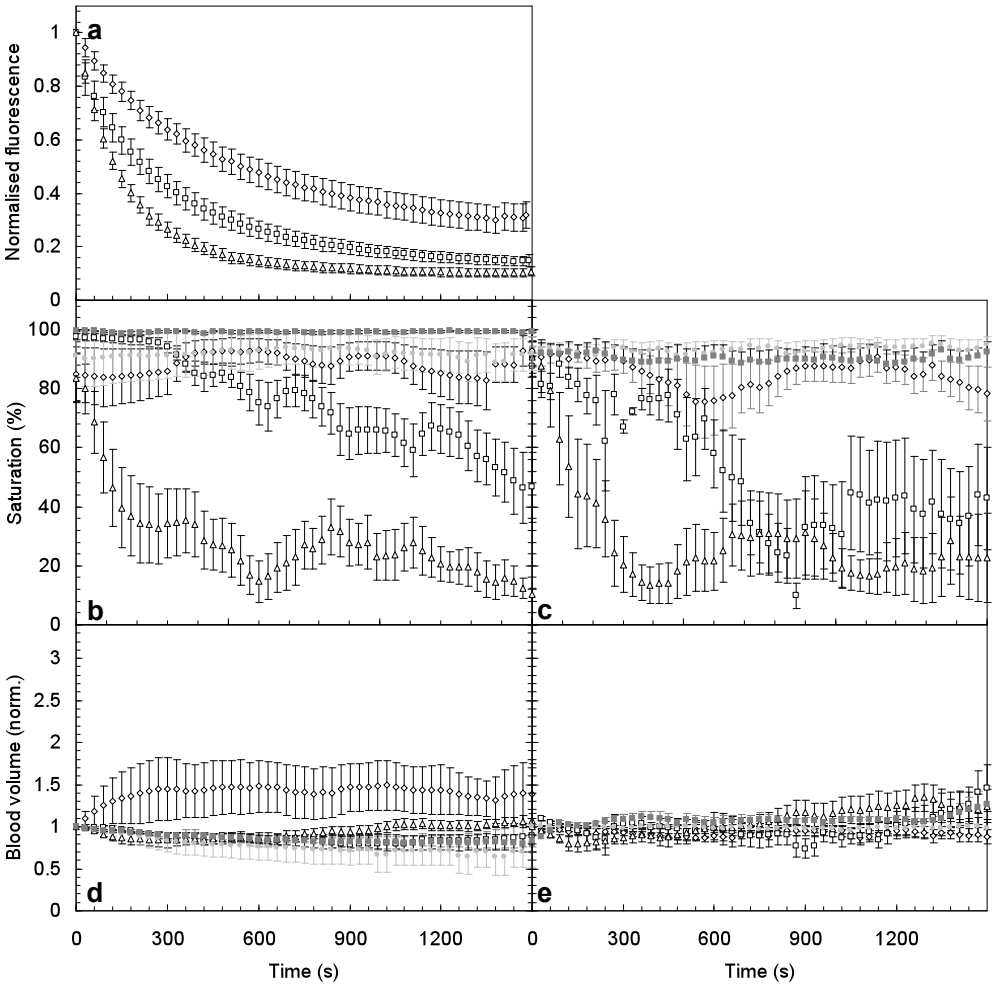

Figure 4. Normalised average fluorescence, measured at the detection side, as function of treatment time for the 50 mW cm^{-1} (◇), 100 mW cm^{-1} (□) and 250 mW cm^{-1} (△) m-THPC groups (a). Average saturation for the three m-THPC groups and the control groups, 50 mW cm^{-1} (◆) and 100 mW cm^{-1} (■), as a function of treatment time for the two measurement locations, the detection side (b) and the illumination side (c). Average blood volume fractions for the same groups as a function of treatment time also for both the detection side (d) and illumination side (e). The error bars represent SEM.

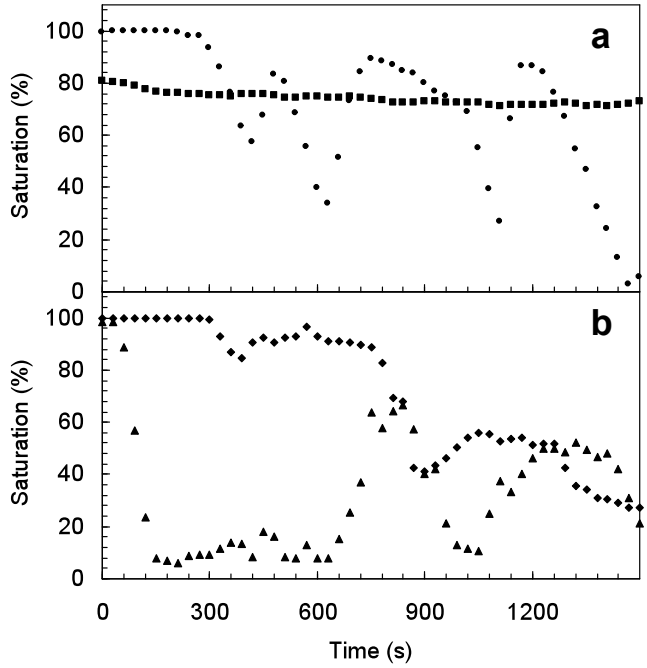

Figure 5. Saturation measured as a function of treatment time for two individual animals from the 50 mW cm^{-1} (■) and 100 mW cm^{-1} (●) m-THPC groups with similar measured fluence rates at the detection side, 19.4 ± 0.7 mW cm^{-2} and 18.7 ± 2 mW cm^{-2}, respectively. b) Saturation as function of treatment time for two individual animals from the 100 mW cm^{-1} (◆) and 250 mW cm^{-1} (▲) m-THPC groups with measured fluence rates of 52.5 ± 2 mW cm^{-2} and 49.5 ± 5 mW cm^{-2}, respectively. Error bars represent SEM.

Although we plotted the average values for the saturation per measurement group it is also instructive to investigate saturation plots of individual animals. Figure 5a shows the individual saturation profiles measured at the detection side during PDT for two animals from the 50 mW cm^{-1} and 100 mW cm^{-1} groups. The measured fluence rate at the detection sides for these animals is similar, 18.7 ± 2 and 19.4 ± 0.9 mW cm^{-2} for the 50 and 100 mW cm^{-1} animals, respectively. Though the measured fluence rates are similar a constant saturation profile is observed for the animal in the 50 mW cm^{-1} group while the animal in the 100 mW cm^{-1} group shows a periodic decrease in saturation followed by a recovery, where the saturation minimum after every successive decrease becomes lower. Different saturation profiles are also observed in animals from the 100 and 250 mW cm^{-1} treatment groups in figure 5b, where both animals also show similar measured fluence rates at the detection side, 52.5 ± 2.5 and 49.5 ± 4.5 mW cm^{-2}, respectively.

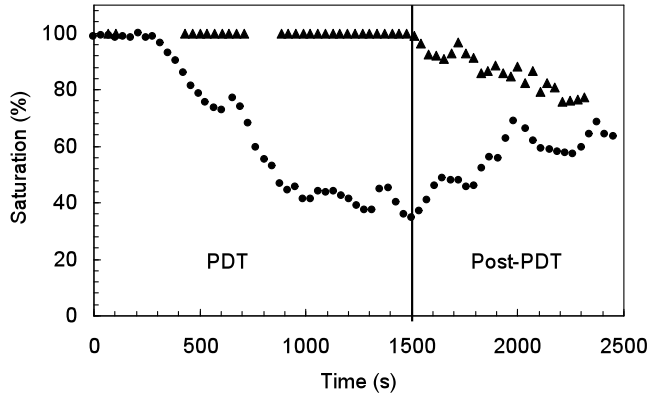

Figure 6. Saturation as function of time during and post PDT for two individual animals of the 100 mW group measured. The vertical line represents the end of therapeutic illumination.

To investigate if the saturation would return to its pre-illumination value or possibly indicate on a delayed PDT-induced vascular effect, saturation was monitored by acquiring DPS-reflectance spectra for a time period after PDT. Figure 6 shows the saturation of two individual animals from the 100 mW cm^{-1} group both during and after PDT. One animal shows constant high saturation of 100% during illumination, however directly after illumination the saturation decreases to 75%. The saturation of the second animal starts at 100% but already decreases during illumination. Directly after illumination the saturation starts to increase again, showing that both increasing and decreasing saturation are possible effects post illumination.

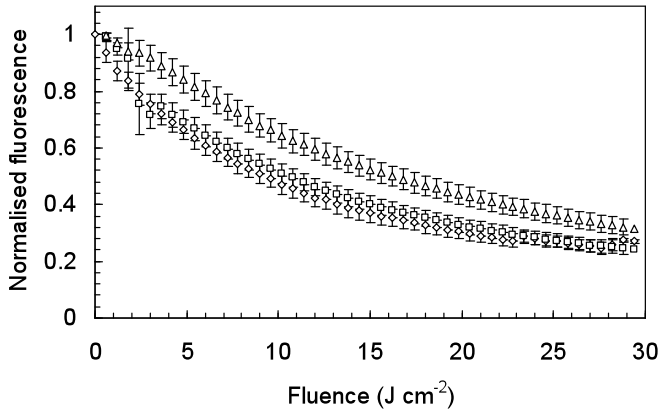

Figure 7. Normalised average fluorescence, measured at the detection side, as a function of fluence, over a range of 0 – 30 J cm^{-2} for the 50 mW cm^{-1} (◇), 100 mW cm^{-1} (□) and 250 mW cm^{-1} (△) m-THPC groups. The error bars represent SEM.

In figure 7 the average normalised m-THPC fluorescence kinetics for each of the three m-THPC-groups is plotted as a function of fluence over the range 0 - 30 J cm^{-2}. The error bars show the variation in measured fluorescence due to differences in measured fluence rates in individual animals. However it is clear that the 250 mW cm^{-1} m-THPC group has a lower rate of photobleaching than the 50 and 100 mW cm^{-1} m-THPC groups. Though not significant, the 50 mW cm^{-1} m-THPC group shows slightly faster bleaching than the 100 mW cm^{-1} m-THPC group. A lower rate of photobleaching for high fluence rates is expected since PDT performed at higher fluence rates leads to increased oxygen consumption and faster depletion of tissue-oxygen.

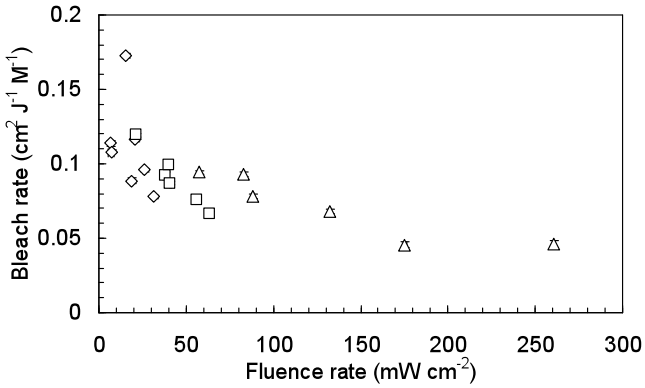

Figure 8. The bleach rate as function of fluence rate for the individual animals of the 50 mW cm^{-1} (◇), 100 mW cm^{-1} (□) and 250 mW cm^{-1} (△) m-THPC groups. The bleach rate of the individual animals are determined by fitting the measured m-THPC photobleaching characteristics using Eq.1 over the first 10 J cm^{-2}. The vertical error bars are the calculated confidence intervals of the bleach rate and the horizontal error bars show the standard deviation on the measured fluence rate over the first 10 J cm^{-2} of illumination of the individual animals.

To quantify the rate of photobleaching for the individual animals, the second order model is used to fit the bleach curves over the dose range of 0 - 10 J cm^{-2}. This under the assumption that for the first 10 J cm^{-2} m-THPC photobleaching mediates entirely via a type II reaction. An important parameter in this approach to modelling fluorescence photobleaching is a parameter that is dependent on the balance between the supply and demand of oxygen, $[^3O_2]$ in Eq. 1. Given this we refer to the term $C[^3O_2]$ in Eq. 1 as an oxygen dependent parameter. The parameter quantifying the initial photosensitizer concentration is around 1 because the normalized fluorescence is fitted. In figure 8 for every animal the fitted value for the oxygen dependent parameter from the second order model is plotted as a function of the average fluence rate per animal over the 0 – 10 J cm^{-2} fluence range. Figure 8 shows a general decrease in value of the oxygen dependent parameter at an increase in fluence rate. For fluence rates above 100 J cm^{-2} the oxygen dependent parameter is relatively constant.

DISCUSSION

The aim of this study was to investigate the potential for monitoring interstitial m-THPC-PDT by measuring the delivery of light to tissue (fluence rate) and monitoring photosensitizer fluorescence photobleaching in combination with quantitative reflectance spectroscopy during interstitial PDT without interrupting the therapeutic illumination. Our long term goal is to determine the applicability of these types of measurements in the clinical environment and potentially provide clinicians with tools to optimize and standardize clinical PDT.

So far the acquisition of reflectance spectra during PDT was limited by the therapeutic illumination which interferes with the spectroscopic measurements[4,8,9]. This means that either the acquisition of reflectance spectra are limited to directly pre and post PDT or the illumination is interrupted for the acquisition of reflectance spectra. In the latter case this also means an alteration of the intended light treatment parameters. We overcame this problem by placing a notch filter centered at the treatment wavelength in front of the spectrographs measuring reflectance spectra. This allows acquisition of differential reflectance measurements during PDT without interruptions to the illumination. Figure 3b shows the model is still able to accurately fit the reflectance data despite spectral blocking around 450 and 650 nm due to the notch filter.

Another important point is that the notch filter blocks light in the spectral region above 600 nm, which contains no distinctive spectral features of tissue absorption. Based on this approach the same method is applicable for monitoring PpIX fluorescence during illumination using a notch filter centered at 630 nm. However for therapeutic wavelengths lower than 600 nm this method can lead to inaccurate saturation values since the blocking band of the notch filter might interfere with the spectral features of hemoglobin.

In addition to quantitative reflectance spectroscopy we monitored m-THPC fluorescence using the same principle as we and others have done previously using PpIX[3,17,30]. For m-THPC we monitored long wavelength fluorescence beyond 690 nm. In this region m-THPC exhibits a (second) distinctive fluorescence peak around 720 nm. For photosensitizers that do not exhibit distinctive features in the long wavelength region the principle is still applicable though technically more challenging. The data presented in this study demonstrates the possibility of simultaneous monitoring of light treatment parameters and long wavelength fluorescence together with monitoring of blood volume and saturation during PDT without interruptions to the therapeutic illumination.

There are a number of important considerations regarding the model that we have used in the present study. It is clear that our present approach is a first step towards a true interstitial illumination geometry. A potential problem for monitoring interstitial PDT is possible bleeding due to insertion of the fiber-optic probes. Blood films covering these probes may cause artefacts in blood volume and blood saturation measurements during the course of treatment. In this case short path-length measurements of DPS will predominantly measure blood saturation and blood volume signals of blood that is not contained in the vascular system of the tissue. In the present study we have avoided possible artefacts by placing the probes between tissue layers rather than inserting them into the muscle. The influence of blood films is an important area for

further investigation. We have also chosen to first investigate monitoring normal tissue. This was done to understand our measured signals in tissue with expected normal vascular physiology. Tumor tissue is likely to be more complex in terms of both vascular physiology and oxygenation. The following step is to investigate monitoring tumour tissue using reflectance and fluorescence spectroscopy.

DPS during therapy

We began saturation and blood volume measurements directly after probe placement following surgery. These measurements before the therapeutic illumination show variations in blood volume and saturation which can be attributed to the surgical procedure (data not shown).

During illumination both control groups show a constant saturation and blood volume for both measurement locations. No change in saturation and blood volume are expected in the control groups since there is no photosensitizer present. During illumination of the m-THPC administered animals we observe an inter-individual variable attenuation in fluence rate measured at the top of the muscle which can be attributed to inter-individual variations in muscle thickness and tissue optical properties. For the majority of m-THPC administered animals we observe a gradual decrease in fluence rate during illumination, which is consistent with previous (clinical) studies monitoring fluence rate[22,31].

The saturation monitored during illumination shows a pattern where a higher percent decrease in saturation is observed for increasing applied fluence rates. This varies from random variations within 25% for the 50 mW cm^{-1} treatment group to an immediate decrease of saturation to 40% within the first 200 seconds of illumination in the 250 mW cm^{-1} treatment group. Several studies using different photosensitizers, have observed a decrease in saturation when illumination commenced[7-9,11]. In addition one of these studies using aluminium disulphonated phtalocyanine as a photosensitizer also showed a faster decrease in saturation at increasing fluence rates [7] as is observed in the current study using m-THPC. This shows that an increase in fluence rate leads to an increase in oxygen consumption or vascular response (constriction and dilatation) that can be monitored by measuring the saturation during illumination.

Although we observe trends in saturation in the three different treatment groups the relatively large error bars indicate large inter-animal variations within the treatment groups. Inter-individual differences in physiology can influence the effective local PDT dose deposited in individual animals. This might lead to inter-individual differences in vascular response during the course of treatment which might be exhibited by the measured saturation. Inter-individual variations in saturation have been reported previously and are reflected in large standard deviations between animals in the same treatment group[7] or even different locations within the tumor volume[11]. Inter-individual differences in vascular response and availability of oxygen as shown in figure 5, can be ascribed to PDT induced vascular effects, such as vasodilatation and –constriction, in combination with the vasculature responding to the extra demand of oxygen during the illumination which can be different per animal due to inter-individual biological variations.

A possible biological complication in measuring oxygen saturation of hemoglobin in muscle tissue is the presence of myoglobin. Due to the subtle spectral differences between hemoglobin and myoglobin in the visible spectrum[37,38] the DPS fitting algorithm will fit any myoglobin present as if it were hemoglobin. Depending on the amount of myoglobin present the determined value for saturation may be biased since the ratio between the 540 nm and 575 nm absorption intensities are slightly different for hemoglobin and myoglobin (1 and 0.8, respectively)[38]. However for the rat abdominal muscle we consider the contribution of myoglobin to be small compared to the hemoglobin absorption. The myoglobin content in rat abdominal muscle tissue has shown to be 0.7 ± 0.4 mg/g [39], or 0.07%, while the blood volume fraction measured using DPS was 10%. Another issue to bear in mind is that hemoglobin is tetrameric and myoglobin is monomeric, meaning that the optical measured absorbance for myoglobin is 4 times lower than for hemoglobin.
A number of other studies monitored saturation during superficial or interstitial PDT *in vivo* using diffuse reflectance spectroscopy with either visible/white light[7,8] or near infrared light[9,11]. A potential source of error in diffuse reflectance spectroscopy is that the path-length and hence the interrogated volume are strongly wavelength dependent. Thereby tissue optical properties can vary during PDT making the wavelength dependent path-length also variable in time. In contrast DPS used in this study to determine saturation and blood volume where the path-length is known and insensitive to changes in optical properties. This makes DPS more advantageous to utilize during PDT than other reflectance spectroscopy techniques.
Another important issue is that the interrogated volume in diffuse reflectance spectroscopy is larger than in DPS where it is approximately the fiber diameter used[13,14]. In large tissue volume measurements there may exist wide variations in fluence rate, dose deposition and possibly variations in photosensitizer concentration over the interrogated volume during illumination. All these variations are averaged out over the interrogated tissue volume together with potentially important local PDT-induced effects. DPS measures smaller volumes over which the variations in fluence rate, deposited dose and photosensitizer concentration are smaller. In addition DPS is able to monitor possible important local vascular effects, making DPS more suitable as a tool for understanding the mechanisms of PDT than diffuse reflectance spectroscopy. However by measuring over small volumes using DPS it will be necessary to use multiple probes to map saturation within the treated tissue volume. This can be costly and has its practical (and ethical) limitations by the amount of optic fibers to be inserted in the treatment volume.

DPS post PDT
Figure 6 shows the potential for monitoring physiological parameters directly after therapeutic illumination. Variations in these parameters monitored post-illumination can provide information on delayed vascular effects due to PDT as observed in figure 6 where the saturation during illumination is constant and decreases after illumination (closed triangles). It can also show if the saturation remains low after illumination or is able to recover (closed circles). Monitoring the vascular response after illumination may additionally provide information on the status of vascularization and possible cell

death[4,5]. For practical and ethical reasons it is often difficult to have monitoring fibers in or near the treatment volume for a period of time after PDT and surgery. Most often it will require an additional (surgical) procedure to remove the monitoring fibers with an increased risk of adverse post surgical effects, such as inflammation.

Monitoring the kinetics of m-THPC photobleaching

In addition to performing quantitative reflectance spectroscopy, we have demonstrated that it is possible to simultaneously measure m-THPC fluorescence in the long wavelength region, ranging from 690-800 nm, without interrupting therapeutic illumination at 652 nm. This approach is similar to that we and others have adopted for monitoring ALA-PDT[17,40]. While a full analysis of the relationship between these parameters is outside the scope of the present manuscript there are a number of important observations on the kinetics of photobleaching during interstitial PDT of normal muscle.

We have shown that the group average rate of m-THPC photobleaching increases as the input fluence rate of groups is reduced from 250 mW cm^{-1} to 100 mW cm^{-1} and to 50 mW cm^{-1} (figure 7). This trend is consistent with what we and others have reported for other photosensitizers that are known to undergo self-sensitized photobleaching[2,14,17,40,41]. We did not observe clear discontinuities in the kinetics of photobleaching between groups or in individual animals (data not shown). The kinetics of m-THPC fluorescence photobleaching have been measured *in vivo* in two previous studies. Forrer *et al*.[18] reported monitoring m-THPC photobleaching in clinical treatments in the esophagus and in the oral cavity and Finlay *et al*.[31] investigated m-THPC photobleaching in normal rat skin over a range of fluence rates. Both studies used a drug-light interval between 72 and 96 hours. The latter study found that the kinetics of photobleaching in rat skin are complex: at least two phases of photobleaching exist where an initial fluence-rate-independent phase is followed by a second phase that shows fluence-rate-dependent bleaching characteristics. Photobleaching in this second phase is then limited by a fraction of m-THPC that is relatively resistant to further degradation. It seems clear that the photobleaching kinetics in normal muscle are significantly different than in rat skin. It is probable that these differences are related to the differences in photosensitizer localization between the two types of tissue at the significantly different drug light intervals. In addition to the overall kinetics of photobleaching we observed a significantly lower initial rate of photobleaching in muscle. At an input fluence rate of 100 mW cm^{-1} (which results in a measured local fluence rate of 47 mW cm^{-2}) we observe a reduction in normalized m-THPC fluorescence of approximately 28% after a fluence of 4 J cm^{-2}. In skin at a fluence rate of 50 mW cm^{-2} there is a 52% decrease in m-THPC fluorescence for the same delivered fluence. This comparison between superficial illumination and detection of m-THPC fluorescence with interstitial illumination and detection and illustrates a very important phenomenon. Fluorescence collected by the isotropic probe originates from different distances within the irradiated tissue volume. This means that photobleaching signals are collected from tissues that are being illuminated with a various range of fluence rates. Clearly this is a confounding factor since these variations in kinetics will not be resolved by this type of volume averaged measurement.

To further investigate the fluence rate dependence of interstitial m-THPC photobleaching we have determined the initial rate of photobleaching with respect to fluence for individual animals (Figure 8). To determine this initial rate we have assumed that the photobleaching of m-THPC follows relatively simple kinetics[2,18]. This model is based on self-sensitized photobleaching of photosensitizer by singlet oxygen and assumes that the rate of photobleaching is predominantly dependent on the availability of oxygen. According to this model an increase in fluence rate leads to a decrease in available oxygen and hence a lower rate of photobleaching. In figure 8 we determined the rate of m-THPC photobleaching over the first 10 J cm^{-2} using the second order model and plotted these values versus the *in vivo* measured fluence rates for the individual animals. It is immediately clear that for a given input fluence rate there is a wide range of measured fluence rates, but there is a trend of increasing rate of photobleaching for decreasing measured fluence rate. The data also suggest that there may be a more complex relationship between the rate of photobleaching and fluence rate. For example we expected to observe a lower rate of photobleaching in animals with measured fluence rates above 100 mW cm^{-2}. Given the small number of data points in this part of the figure it is difficult to make strong conclusions from the results of the present study alone. Again it is important to note that these data from individual animals are also confounded by the range of fluence rates over which m-THPC fluorescence is collected. In future studies we intend to incorporate a technique that is able to monitor photosensitizer fluorescence over smaller defined volumes that can be chosen to coincide with the volume over which quantitative reflectance spectroscopy is acquired[42].

Conclusion

In conclusion we have shown that it is possible to simultaneously monitor fluence (rate), m-THPC photobleaching, saturation and blood volume during PDT without interruptions to the therapeutic illumination. We observe a decrease in saturation with increasing fluence rates. More interestingly significant differences in saturation profiles during the course of treatment between treatment groups and animals within the same treatment group are observed which indicate differences in vascular response. Furthermore the relationship between fluence rate and m-THPC photobleaching monitored using an isotropic probe is complex in an interstitial geometry. For future studies investigating the mechanisms of action of m-THPC-PDT it will be necessary to incorporate monitoring these explicit and implicit parameters during PDT in combination with determining the efficacy of therapy using clinical relevant light treatment parameters.

References

1. Wilson BC, Patterson MS and L. Lilge L. Implicit and Explicit Dosimetry in Photodynamic Therapy: A New Paradigm. Lasers Med Sci. 1997; 12:182-199.
2. Robinson DJ, de Bruijn HS, van der Veen N, Stringer MR, Brown SB, Star WM. Fluorescence photobleaching of ALA-induced protoporphyrin IX during photodynamic therapy of normal hairless mouse skin: the effect of light dose and irradiance and the resulting biological effect. Photochem Photobiol. 1998; 67:140-149.
3. Finlay JC, Conover DL, Hull EL, Foster TH. Porphyrin bleaching and PDT-induced spectral changes are irradiance dependent in ALA-sensitized normal rat skin in vivo. Photochem Photobiol. 2001; 73:54-63.
4. Wang HW, Putt ME, Emanuele MJ, Shin DB, Glatstein E, Yodh AG, Busch TM. Treatment-induced changes in tumor oxygenation predict photodynamic therapy outcome. Cancer Res. 2004; 64:7553-7561.
5. Pogue BW, Paulsen KD, O'Hara JA, Wilmot CM, Swartz HM. Estimation of oxygen distribution in RIF-1 tumors by diffusion model-based interpretation of pimonidazole hypoxia and eppendorf measurements. Radiat Res. 2001; 155:15-25
6. Curnow A, Haller JC, Bown SG. Oxygen monitoring during 5-aminolaevulinic acid induced photodynamic therapy in normal rat colon: Comparison of continuous and fractionated light regimes. J Photochem Photobiol B. 2000; 58:149-155.
7. Woodhams JH, Kunz L, Bown SG, MacRobert AJ. Correlation of real-time haemoglobin oxygen saturation monitoring during photodynamic therapy with microvascular effects and tissue necrosis in normal rat liver. Br J Cancer. 2004; 91:788-794.
8. Larsen EL, Randeberg LL, Gederaas OA, Arum CJ, Hjelde A, Zhao CM, Chen D, Krokan HE, Svaasand LO. Monitoring of hexyl 5-aminolevulinate-induced photodynamic therapy in rat bladder cancer by optical spectroscopy. J Biomed Opt. 2008;13:044031.
9. Weersink RA, Bogaards A, Gertner M, Davidson SR, Zhang K, Netchev G, Trachtenberg J, Wilson BC. Techniques for delivery and monitoring of TOOKAD (WST09)-mediated photodynamic therapy of the prostate: clinical experience and practicalities. J Photochem Photobiol B. 2005; 79:211-222.
10. Yu G, Durduran T, Zhou C, Zhu TC, Finlay JC, Busch TM, Malkowicz SB, Hahn SM, Yodh AG. Real-time in situ monitoring of human prostate photodynamic therapy with diffuse light. Photochem Photobiol. 2006; 82:1279-1284.
11. Johansson A, Johansson T, Thompson MS, Bendsoe N, Svanberg K, Svanberg S, Andersson-Engels S. In vivo measurement of parameters of dosimetric importance during interstitial photodynamic therapy of thick skin tumors. J Biomed Opt. 2006;11:34029.
12. van Veen RL, Sterenborg HJ, Marinelli AW, Menke-Pluymers M. Intraoperatively assessed optical properties of malignant and healthy breast tissue used to determine the optimum wavelength of contrast for optical mammography. J Biomed Opt. 2004; 9:1129-1136.
13. van Veen RL, Amelink A, Menke-Pluymers M, van der Pol C, Sterenborg HJ. Optical biopsy of breast tissue using differential path-length spectroscopy. Phys Med Biol. 2005; 50:2573-2581.
14. Amelink A, Sterenborg HJ. Measurement of the local optical properties of turbid media by differential path-length spectroscopy. Appl Opt. 2004; 43:3048-3054.
15. Finlay JC, Foster TH. Hemoglobin oxygen saturations in phantoms and in vivo from measurements of steady-state diffuse reflectance at a single, short source-detector separation. Med Phys. 2004; 31:1949-59.
16. Boere IA, Robinson DJ, de Bruijn HS, van den Boogert J, Tilanus HW, Sterenborg HJ, de Bruin RW. Monitoring in situ dosimetry and protoporphyrin IX fluorescence photobleaching in

the normal rat esophagus during 5-aminolevulinic acid photodynamic therapy. Photochem Photobiol. 2003; 78:271-277.
17. Kruijt B, de Bruijn HS, van der Ploeg-van den Heuvel A, de Bruin RWF, Sterenborg HJCM, Amelink A, Robinson DJ. Monitoring ALA-induced PpIX-photodynamic therapy in the rat esophagus using fluorescence and reflectance spectroscopy. Photochem Photobiol. 2008; 84:1515-1527.
18. Forrer M, Glanzmann TM, Braichotte D, Wagnieres GA, van den Bergh H, Savary JF, Monnier P. In-vivo measurement of fluorescence bleaching of meso-tetra hydroxy phenyl chlorin (m-THPC) in the esophagus and the oral cavity. Proc Soc Photo-Opt Inst Eng. 1995; 2627:33-39.
19. Copper MP, Triesscheijn M, Tan IB, Ruevekamp MC, Stewart FA. Photodynamic therapy in the treatment of multiple primary tumours in the head and neck, located to the oral cavity and oropharynx. Clin Otolaryngol. 2007; 32:185-189.
20. Copper MP, Tan IB, Oppelaar H, Ruevekamp MC, Stewart FA. Meta-tetra(hydroxyphenyl)chlorin photodynamic therapy in early-stage squamous cell carcinoma of the head and neck. Arch Otolaryngol Head Neck Surg. 2003; 129:709-711.
21. Lou PJ, Jäger HR, Jones L, Theodossy T, Bown SG, Hopper C. Interstitial photodynamic therapy as salvage treatment for recurrent head and neck cancer. Br J Cancer. 2004; 91:441-446.
22. van Veen RL, Nyst H, Rai Indrasari S, Adham Yudharto M, Robinson DJ, Tan IB, Meewis C, Peters R, Spaniol S, Stewart FA, Levendag PC, Sterenborg HJ. In vivo fluence rate measurements during Foscan-mediated photodynamic therapy of persistent and recurrent nasopharyngeal carcinomas using a dedicated light applicator. J Biomed Opt. 2006; 11:041107.
23. Moore CM, Nathan TR, Lees WR, Mosse CA, Freeman A, Emberton M, Bown SG. Photodynamic therapy using meso tetra hydroxy phenyl chlorin (m-THPC) in early prostate cancer. Lasers Surg Med. 2006; 38:356-363.
24. Campbell SM, Gould DJ, Salter L, Clifford T, Curnow A. Photodynamic therapy using meta-tetrahydroxyphenylchlorin (Foscan) for the treatment of vulval intraepithelial neoplasia. Br J Dermatol. 2004; 151:1076-1080.
25. Schouwink H, Ruevekamp M, Oppelaar H, van Veen R, Baas P, Stewart FA. Photodynamic therapy for malignant mesothelioma: preclinical studies for optimization of treatment protocols. Photochem Photobiol. 2001; 73:410-417.
26. Baas P, Saarnak AE, Oppelaar H, Neering H, Stewart FA. Photodynamic therapy with meta-tetrahydroxyphenylchlorin for basal cell carcinoma: a phase I/II study. Br J Dermatol. 2001; 145:75-78.
27. van der Snoek EM, Amelink A, van der Ende ME, den Hollander JC, den Hollander JG, Kroon FP, Vriesendorp R, Neumann HAM, Robinson DJ. Photodynamic therapy with topical metatetrahydroxychlorin (fosgel®) is ineffective for the treatment of anal intraepithelial neoplasia, grade III. J Acquir Immune Defic Syndr. 2009;52:141-3.
28. Jones HJ, Vernon DI, Brown SB. Photodynamic therapy effect of m-THPC (Foscan) in vivo: correlation with pharmacokinetics. Br J Cancer. 2003; 89:398-404.
29. Cramers P, Ruevekamp M, Oppelaar H, Dalesio O, Baas P, Stewart FA. Foscan uptake and tissue distribution in relation to photodynamic efficacy. Br J Cancer. 2003; 88:283-290.
30. Cottrell WJ, Oseroff AR, Foster TH. Portable instrument that integrates irradiation with fluorescence and reflectance spectroscopies during clinical photodynamic therapy of cutaneous disease. Rev Sci Instrum. 2006; 77:064302.
31. Finlay JC, Mitra S, Foster TH. In vivo m-THPC photobleaching in normal rat skin exhibits unique irradiance-dependent features. Photochem Photobiol. 2002; 75:282-288.
32. Hadjur C, Lange N, Rebstein J, Monnier P, van den Bergh H, Wagnieres G. Spectroscopic studies of photobleaching and photoproduct formation of

meta(tetrahydroxyphenyl)chlorin (m-THPC) used in photodynamic therapy. The production of singlet oxygen. J Photochem Photobiol B. 1998; 45:170-178.
33. Coutier S, Mitra S, Bezdetnaya LN, Parache RM, Georgakoudi I, Foster TH, Guillemin F. Effects of fluence rate on cell survival and photobleaching in meta-tetra-(hydroxyphenyl)chlorin-photosensitized Colo 26 multicell tumor spheroids. Photochem Photobiol. 2001; 73:297-303.
34. Kunz L, MacRobert AJ. Intracellular photobleaching of 5,10,15,20-tetrakis(m-hydroxyphenyl) chlorin (Foscan) exhibits a complex dependence on oxygen level and fluence rate. Photochem Photobiol. 2002; 75:28-35.
35. Dysart JS, Patterson MS, Farrell TJ, Singh G. Relationship between m-THPC fluorescence photobleaching and cell viability during in vitro photodynamic treatment of DP16 cells. Photochem Photobiol. 2002; 75:289-295.
36. Amelink A, Robinson DJ, Sterenborg HJ. Confidence intervals on fit parameters derived from optical reflectance spectroscopy measurements. J Biomed Opt. 2008; 13:054044.
37. Nighswander-Rempel SP, Kupriyanov VV, Shaw RA. Relative contributions of hemoglobin and myoglobin to near-infrared spectroscopic images of cardiac tissue. Appl Spectrosc. 2005; 59:190-193.
38. Masuda K, Truscott K, Lin PC, Kreutzer U, Chung Y, Sriram R, Jue T. Determination of myoglobin concentration in blood-perfused tissue. Eur J Appl Physiol. 2008;104:41-48
39. Pattengale PK, Holloszy JO. Augmentation of skeletal muscle myoglobin by a program of treadmill running. Am J Physiol. 1967; 213:783-785.
40. Sheng C, Hoopes JP, Hasan T, Pogue PW. Photobleaching-based Dosimetry Predicts Deposited Dose in ALA-PpIX PDT of Rodent Esophagus. Photochem Photobiol. 2007; 83:738-748.
41. Georgakoudi I, Nichols MG, Foster TH. The mechanism of Photofrin photobleaching and its consequences for photodynamic dosimetry. Photochem Photobiol. 1997; 65:135-144.
42. Amelink A, Kruijt B, Robinson DJ, Sterenborg HJ. Quantitative fluorescence spectroscopy in turbid media using fluorescence differential path length spectroscopy. J Biomed Opt. 2008; 13:054051.

8

The histological response of normal rat muscle following interstitial m-THPC-PDT

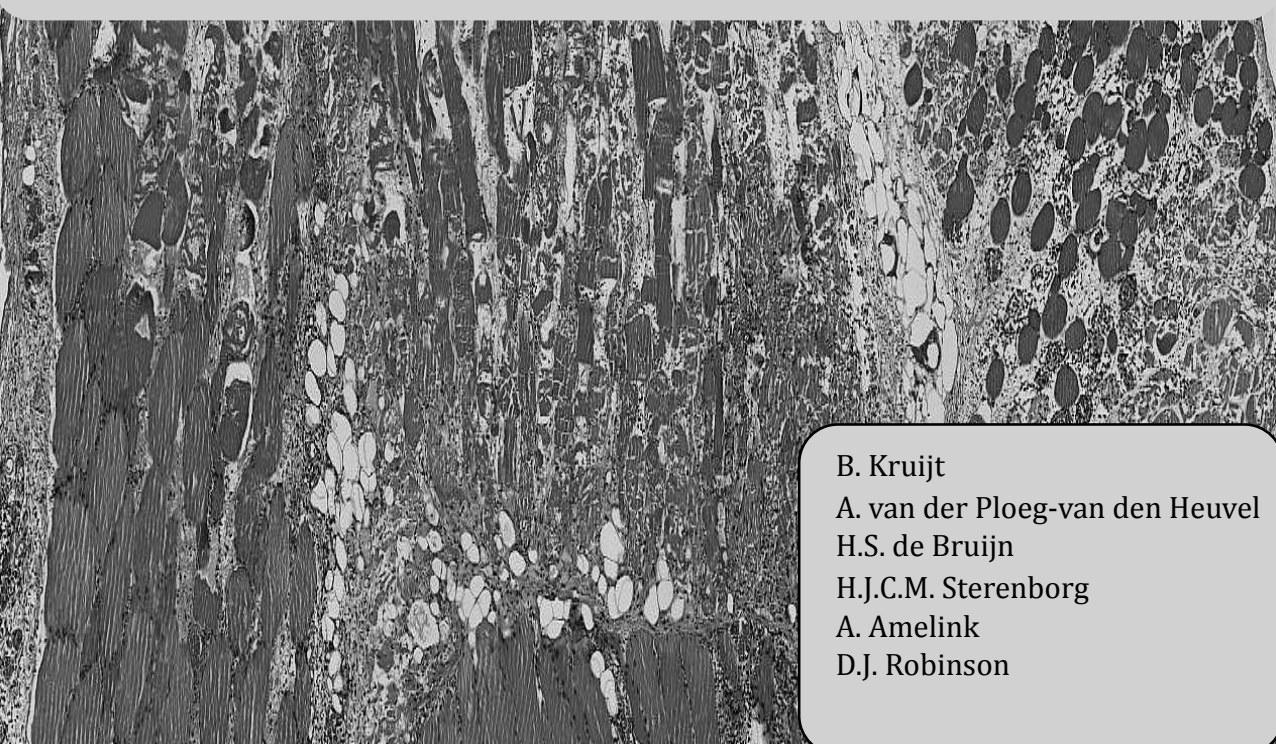

B. Kruijt
A. van der Ploeg-van den Heuvel
H.S. de Bruijn
H.J.C.M. Sterenborg
A. Amelink
D.J. Robinson

Abstract

In order to understand the mechanisms of action in m-THPC-PDT it is important to monitor parameters of importance during PDT and investigate the induced tissue response. The aim of this study is to examine PDT-induced response following PDT using clinical relevant treatment parameters. In addition several parameters such as fluence (rate), fluorescence, saturation, blood volume and differential fluorescence are monitored.

Rats were injected with 0.3 mg kg^{-1} m-THPC. Sixteen or 96 h after m-THPC administration the abdominal muscle was illuminated through a interstitial placed linear diffuser, up to a dose of 5 or 20 J cm^{-2} using clinical relevant fluence rates of 100 and 250 mW cm^{-1}. During PDT several parameters were monitored via fiber optic probes located on top and bottom of the abdominal muscle. Forty-eight hours following illumination the abdominal muscle was examined for PDT-induced response.

Response data showed higher response for necrosis in the groups with a 16 h drug light interval. An interesting observation was that no nuclei were observed in predominantly animals with a 16 h drug light interval. Despite the differences in observed tissue response, the measured parameters during PDT showed no or little variation.

We made a first step in quantification of tissue response following PDT in an interstitial treatment geometry. The response is scored both in intensity of different type of PDT-induced response and in distance from the treatment fiber. However, more investigation is necessary to relate the parameters measured during PDT with the observed response.

Cover: microscopic image of PDT induced response in muscle

Manuscript in preparation

Introduction

Meta-tetrahydroxyphenylchlorin (m-THPC) or Foscan® is a second generation photosensitizer currently under investigation as a (palliative) treatment modality for several malignancies in the head and neck region[1-3], prostate[4], vulva[5], lungs[6], skin[7], and anal cavity[8]. In many circumstances, in particular for large tumors, it is not possible to illuminate the whole of the tumor volume using superficial illumination. In these cases optical fibers are interstitially inserted into the treatment volume and used to deliver the treatment light using linear diffusing sources. This approach was adopted in some of the earliest applications of clinical PDT[9] and has been used for the treatment of a range of tumor types. In the Head and Neck interstitial m-THPC-PDT is under investigation for the palliative treatment of large tumors such as those in the tongue base[1-3]. The clinical response after interstitial PDT is encouraging but there are a significant number of tumors that show a partial or no response[3]. PDT light treatment planning and *in vivo* light dosimetry are under development in the Head and Neck[10]. The current clinical state of the art involves the manual placement of illumination fibers, fixed distances apart, using a combination of pre-treatment MR imaging and palpation of the tumor when fiber-carrying catheters are inserted immediately before therapy. All tumors including those that show complete response, partial or no response are treated using the same pre-treatment planning protocol. However, given that it is well known that there can be significant differences a range of parameters that influence the PDT dose delivered, such as tissue optical properties[11], photosensitizer pharmacokinetics[12,13] tumor vascular physiology[14] and that these can vary between patients, between tumors and potentially within tumors. It is therefore not unreasonable to assume that inter-individual differences in spatial fluence rate and the PDT-dose deposited may lead to differences in tissue response and clinical outcome. For these reasons a number of groups are pursuing strategies to measuring the magnitude of these variations and working towards techniques that are aimed at compensating for their influences so that the PDT dose is adequate within the treatment volume and is standardized between individual tumors and patients[15,16].

An important factor underlying these optimization and individualization efforts is an understanding of the mechanism(s) of action surrounding the deposition of PDT-dose and knowledge of how this relates to the PDT induced response. For mTHPC-PDT a number of pre-clinical studies have investigated the role of light fluence, photosensitizer dose, pharmacokinetics and drug light interval[17,18], relatively less attention has been given to the influence of light fluence rate and the vascular and physiological response of tissue during PDT. The aim of the present study is to investigate these later two parameters during interstitial mTHPC-PDT.

In order to investigate the relationship between the PDT-dose deposited and the PDT-induced tissue response it is necessary to quantify tissue response. Several studies have investigated response following therapeutic illumination using different photosensitizers and in different treatment geometries[19-25] Tissue response can be quantified macroscopically and/or microscopically. Macroscopic measures of tissue response, such as those used in skin response models where the severity of response is quantified[22] have the advantage that the tissue response can be followed in time. However this method is limited to exposed tissue and does not provide information on

response of deeper tissue layers. Another macroscopic quantification of response is tumor growth delay[19-21]. In these types of experiments a relatively large volume of tissue (on the order of 2-5 cm^3) is illuminated using either a superficial or interstitial illumination and the response to PDT is determined measuring the growth of the tumor in time after illumination compared to the growth of an untreated tumor. One potential confounding factor in these types of studies is that it can be difficult to deliver the same PDT-dose throughout the whole treatment volume. In these circumstances the spatial distribution of PDT dose deposited in the treatment volume is not taken into account in the overall quantification of response. Histological measures of PDT response make it possible to quantify response based on the mode of PDT cell death, i.e. necrosis and/ or apoptosis and combine this with an assessment of the induction of an immunological response to PDT[25]. Here it is also possible to quantify the response with respect to different tissue structures such as layers and investigate boundaries between tumor and normal tissue. One disadvantage of these approaches is that in most circumstances microscopic quantification of response does not allow for temporal quantification of response in a single animal, it is often preferred in situations where the tissue is not already exposed. One notable exception is the use of intra-vital methods[26] here however most treatment geometries mean that it is difficult to combine interstitial light delivery with intra-vital models.

In the present study we have therefore chosen to deliver PDT using an interstitial geometry and investigate the histological response to PDT. In this type of approach there is a spatial distribution of PDT dose deposited that is dependent on the fluence rate, the availability of oxygen and photosensitizer concentration but also from the distance from the illumination source. As a result we expect to find a spatial distribution of microscopic response.

In combination with this investigation of the microscopic response following mTHPC-PDT we have also extended our previous dosimetric and monitoring techniques; monitoring fluence (rate), fluorescence photobleaching, blood saturation and blood volume during illumination to this true interstitial geometry using clinically relevant light treatment parameters.

2 Materials and Methods

Animal and treatment procedure

The animal experiment committee of the Erasmus University Medical Center approved the experimental design for this study. Two weeks prior to the experiments 45 normal adult male Wistar rats were placed on a diet of chlorophyll free food to minimize the influence on autofluorescence centred at 675 nm due to pheophorbide-α. All animals were injected with 0.3 mg kg^{-1} m-THPC i.v., dissolved in PEG400:ethanol:water with a ration of 3: 2: 5, except for five control animals which were injected with the control-solution not containing m-THPC. The m-THPC administered animals were divided into 8 PDT-groups as shown in table 1.

Table 1. Illumination groups (n=5 animals in each).

Group	Drug light interval/h	Incident fluence rate/mW cm^{-1}	Flunece/J cm^{-1}
1	16	100	5
2	16	100	20
3	16	250	5
4	16	250	20
5	96	100	5
6	96	100	20
7	96	250	5
8	96	250	20

After a drug-light interval of either 16 or 96 hours, animals received a light dose of 5 or 20 J cm^{-1}, at a fluence rate of 100 or 250 mW cm^{-1} diffuser length. The remaining 5 animals received a light dose of 20 J at 250 mW cm^{-1} diffuser length 96 h after injection with the control solution not containing any m-THPC. Two different incubation times were chosen to investigate possible differences in PDT induced damage due to different compartmental localizations of m-THPC.

At the time of treatment a vertical incision was made through the skin and the abdominal muscle layer at the *linea alba*. Skin overlying the muscle layer was separated from the muscle structure for probe placement. Figure 1 shows a schematic outline of the probe placement between the different tissue layers. To prevent PDT induced damage to the intestines located directly underneath the muscle layer, a black plastic sheet was placed between the muscle layer and the intestines. A polyurethane catheter (BD Venflon pro 18GA, Helsingborg, Sweden) was placed perpendicular from the incision at the *linea alba* through the muscle layers towards the *linea semilunaris*. The linear diffuser, with a length of 2 cm and diameter of 500 micron (MedSpecLab, Toronto, Canada) was placed into the catheter. On both top and bottom side of the muscle FDPS and isotropic probes (Cardiofocus, formerly Rare Earth Medical, West Yarmouth MA, USA) were positioned at the centre of the linear diffuser and as close to it as possible. FDPS probes were used to locally monitor saturation, blood volume and

fluorescence. The two isotropic probes located at the bottom and top of the muscle are both bifurcated to monitor fluence (rate) and long wavelength fluorescence with the same probe.

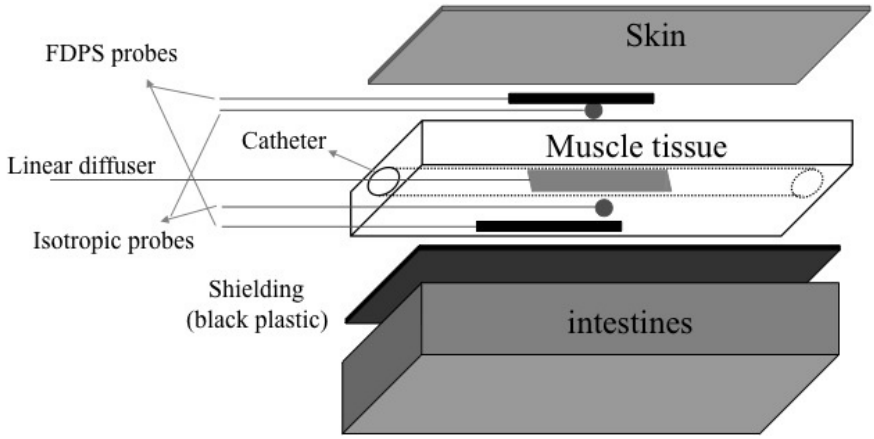

Figure 1. Schematic detailed outline of the placements of the linear diffuser to deliver the treatment light to the tissue, and the measurement probes (FDPS and isotropic probes) on top and bottom of the muscle tissue.

We had previously observed significant variations in blood volume and saturation for a period of time directly after surgery and probe placement. Therefore these physiological parameters were allowed to stabilize in each animal before the start of illumination. On average it took 10-15 minutes for the blood volume and saturation to stabilize. Therapeutic illumination was performed using 652 nm light from a diode laser (CeramOptec, Jena, Germany). During the course of treatment light dosimetry, fluorescence spectroscopy and FDPS were measured continuously without disturbing the light treatment protocol. After the end of the illumination PDT-induced vascular effects were monitored by measuring blood volume and saturation for a period of 300 seconds. After these post illumination measurements the optical fibers were removed and the muscle layer was sutured together. For orientation during histology the polyurethane catheter was left in the muscle structure after illumination. To minimize discomfort at possible disfunctionality of muscle tissue during the 48 hour post treatment period, Premilene® mesh (Braun Medical, Oss, the Netherlands), normally used in the clinic for treatment of *hernia inguinalis*, was sutured on top of the illuminated muscle tissue.

Light dosimetry and fluorescence spectroscopy

Fluence rate and photosensitizer fluorescence above 690 nm were measured at both top and bottom side of the abdominal muscle structure, using an 1 mm isotropic probe at the distal end of a 400 micron fiber. The fiber-probes were then coupled into a 200-400 micron bifurcated fibers to give optimal signal for the fluorescence

measurements measured with the larger fiber diameter while still having sufficient light for accurate fluence rate measurements. The 200 micron arms were coupled directly in a modular-based multi-channel dosimetry device[27]. Both 400 micron arms were coupled into a two-channel spectrograph controlled by the dosimetry device. In front of this spectrograph a 690 nm long pass filter was placed enabling measurements of long wavelength m-THPC fluorescence during PDT without interruption to the treatment light. After every fluence rate measurement fluorescence spectra were acquired. The integration times used for the two-channel spectrograph varied between the 2000 and 4000 milliseconds, allowing a maximum sampling rate of 15 measurements per minute at an integration time of 2000 milliseconds for a two-channel spectrograph.

Fluorescence differential pathlength spectroscopy

Fluorescence differential pathlength spectroscopy (FDPS) is used to acquire local information on physiological parameters, such as saturation and blood volume[28], tissue optical characteristics and fluorescence all over the same tissue volume. FDPS was measured at both top and bottom side of the muscle tissue using a fiber probe containing two 600 micron fibers placed at a core-to-core distance of 660 micron and polished under an angle of 15 degrees to minimize specular reflection at the probe-tissue interface. Excitation light for the fluorescence measurements was split out from the treatment laser using a tri-furcated fiber of which a 600 micron leg lead to the treatment fiber and the two 200 micron legs lead to two individual 150 micron bifurcated fibers of the two FDPS probes. The second leg of this 150 micron bifurcated fiber was coupled into a white light source for DPS measurements. The distal end of the 150 micron bifurcated fiber was coupled into one of the arms of a 300 micron bifurcated fiber, the other arm is coupled into a channel of the 4-channel spectrograph. The distal end of the 300 micron bifurcated fiber is coupled into one of the 600 micron fibers of the FDPS-probe which forms the delivery and collection (dc) fiber. The second 600 micron fiber of the FDPS probe, the collection (c) fiber, was coupled directly into the 4-channel spectrograph. To enable measurements during the therapeutic illumination a 4-channel filter-block containing a notch filter centered on 650 nm was placed directly in front of the spectrographs. Differential fluorescence measurements were acquired directly after differential reflectance measurements. Integration times for the differential fluorescence measurements varied between the 250 and 1000 milliseconds. To maximize the temporal resolution low integration times were used for PDT with high fluence rate and low dose. Since the white light used for acquiring reflectance spectra can interfere with the fluorescence signal measured using the isotropic probe the sampling rate for FDPS was set at 2 measurements/min.

Histology and PDT response

Forty-eight hours after illumination the animals were sacrificed after which the muscle tissue on both the right and left side of the *linea alba* (treated and untreated, respectively) were excised and fixed in formalin. This provided histological sections of both normal and PDT-treated muscle tissue for each animal. Before embedding the tissue in paraffin the polyurethane catheter and Premilene® mesh were removed from the treated tissue side to prevent artifacts when sectioning the tissue. Sections were

stained with hematoxylin and eosin and subsequently scanned at 40x magnification using a digital scanning microscope (Nanozoomer digital pathology, Hamamatsu).
From the center of treatment concentric circles with 1 mm intervals up to 7 mm were drawn in the tissue sections. Within these 1 mm successive circular bands the tissue damage was scored for three PDT induced responses of tissue; (a) tissue edema, (b) inflammation and (c) necrosis. The presence of edema was scored based on the separation between muscle fibers due to presence of intercellular fluids. The presence of an inflammatory infiltrate (mainly neutrophils) was used to score the severity of inflammatory response in and around the muscle fibers. Non-viable muscle fibers were scored as necrosis. The viability of muscle tissue was assessed according to their morphology. In normal viable muscle 'fiber striping' is observed due to the myofibrilles. Absence of this striping indicates non-viable muscle fiber and was considered necrotic. The severity of each response was scored on a scale of 0 – 3 corresponding to the percentage of the tissue that exhibited the score within each 1 mm concentric ring where 0 corresponds to no response; 1 for 10-40%; 2 for 40-70%; and 3 for over 70% response. For each circular ring three scores are given for necrosis, inflammation and edema respectively. The values per ring were averaged for each treatment group. Tissue sections were scored by two investigators blinded from the drug light interval and light treatment parameters.

Data processing

Fluorescence spectroscopy

As we and others described previously long wavelength fluorescence spectra acquired by the isotropic probe were analyzed as a linear combination of basis spectra using a singular value decomposition (SVD) algorithm[29,30]. The fluorescence signal was described by a combination autofluorescence, m-THPC fluorescence and residual laser light. Due to the width of the laser peak some fraction of laser light was attenuated but not completely filtered out. This made it necessary to incorporate an additional component in the fit. Basis spectra for the components were extracted from *in vivo* measured spectra. The basis spectrum for the autofluorescence is the average from fluorescence spectra acquired in the control animals corrected for the residual laser light. The basis spectrum for m-THPC is extracted from the m-THPC injected animals with subtraction of the autofluorescence signal and correction for the residual laser light.

Fluorescence differential path-length spectroscopy

Before every experiment the FDPS system was calibrated as described previously[31]. A differential reflectance spectrum was acquired before every fluorescence measurement by subtraction of the signals acquired by the dc- and c-fibers. Values on blood volume and saturation were acquired by fitting the DPS spectrum according to the same model as described previously[18]. A differential fluorescence spectrum (DF_{meas}) is obtained by subtraction of the fluorescence spectral signal measured by the c-fiber from the fluorescence spectral signal measured by the dc-fiber. The measured differential fluorescence signal is corrected for day-to-day variations in laser output. Furthermore the differential fluorescence signal is corrected for absorption by multiplying DF_{meas} by

the ratio of the reflectance at the excitation wavelength without and with absorption present. At the excitation wavelength, 652 nm, there are no significant absorption artifacts in the measured reflectance, hence the ratio between reflectance signal without and with absorption present at this particular wavelength equals 1. The differential fluorescence signal is relatively insensitive to variations in tissue scattering. For this reason no corrections were made to account for variations scattering. The absorption-corrected differential fluorescence spectra were analyzed using the same SVD algorithm as for the long wavelength-fluorescence measurements. Here the fluorescence was described by a combination of m-THPC fluorescence and autofluorescence.

Statistics

Confidence intervals on fit parameters were determined based on the covariance matrix as described previously[32]. Differences between animals and groups were tested using the non-parametric Mann-Whitney test.

Results

General observations and histological response to PDT

In all animals, the right side of the abdominal muscle was treated and the left side served as a m-THPC no-light and no-catheter control. For the majority of m-THPC PDT animals the illuminated tissue was more rigid and thicker than the control tissue. Macroscopically the average thickness of the illuminated tissue per treatment group was measured by measuring the width of the fixed and stained sections. On average the PDT treated sections were 14.6 mm long and 4.2 mm thick, the control sections 13.8 mm and 3.9 mm, respectively. There was no significant change in thickness due to PDT treatment between the sections of the different PDT groups or within the control groups.

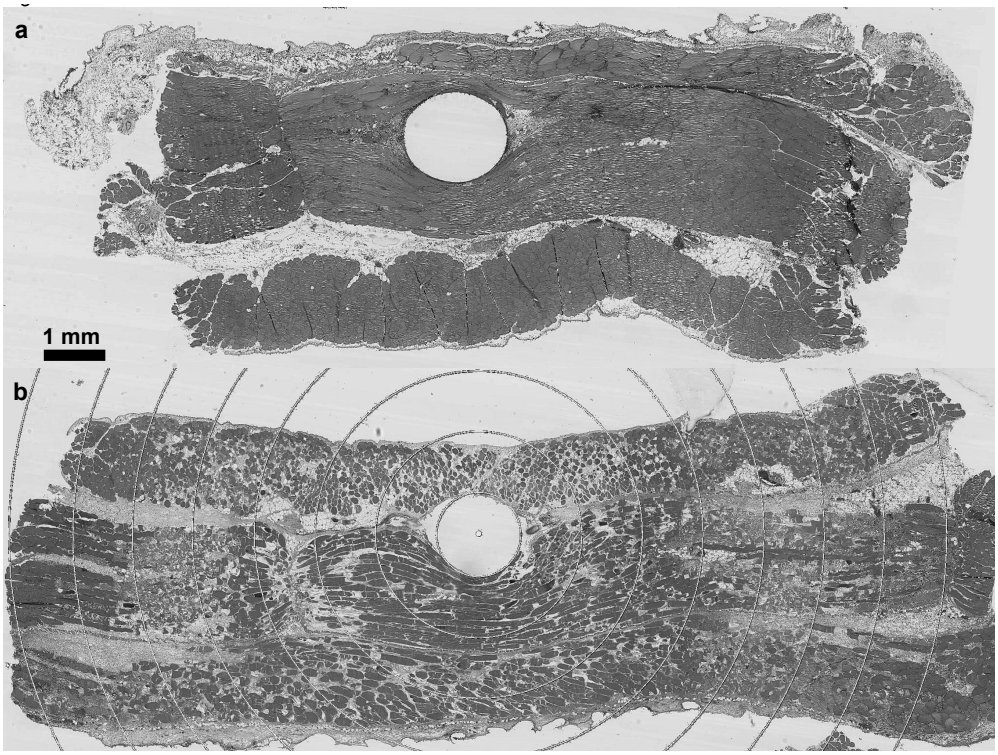

Figure 2. a) abdominal muscle cross-section of a control animal (no m-THPC) which received 20 J at 250 mW cm^{-1} at a magnification of 25X. The open circular shape in the center is the place where the treatment fiber was located during illumination; b) abdominal muscle cross-section of a PDT treated animal, 20 J at 100 mW cm^{-1}. The concentric lines with 1 mm separation around the location of the treatment fiber are the regions within which tissue response was scored.

We observed no PDT-induced effects in the untreated side of the muscle. Figure 2a shows a tissue section at a 25x magnification of an animal that was injected with the control solution not containing m-THPC that received 20 J cm^{-1} at a fluence rate of 250 mW cm^{-1} per length of diffuser. For the animals in this control group we observed

edema formation, inflammation and sometimes necrosis close to the location of the catheter (and treatment fiber) due to the insertion of the catheter. Figure 2b shows a typical tissue section at a 25x magnification of a PDT treated m-THPC animal with a drug light interval of 16 h and a dose of 20 J cm^{-1} at a fluence rate of 100 mW cm^{-1}. In sections of the treatment groups also edema formation, inflammatory response and necrosis were observed. The extent (distance from the treatment fiber) and intensity of damage was different depending on the drug light interval, delivered dose and fluence rate. An additional interesting observation was the loss of nuclei in muscle cells. This was apparent in all animals with a 16 h drug light interval and only in two out of 20 animals with a 96 h drug light interval.

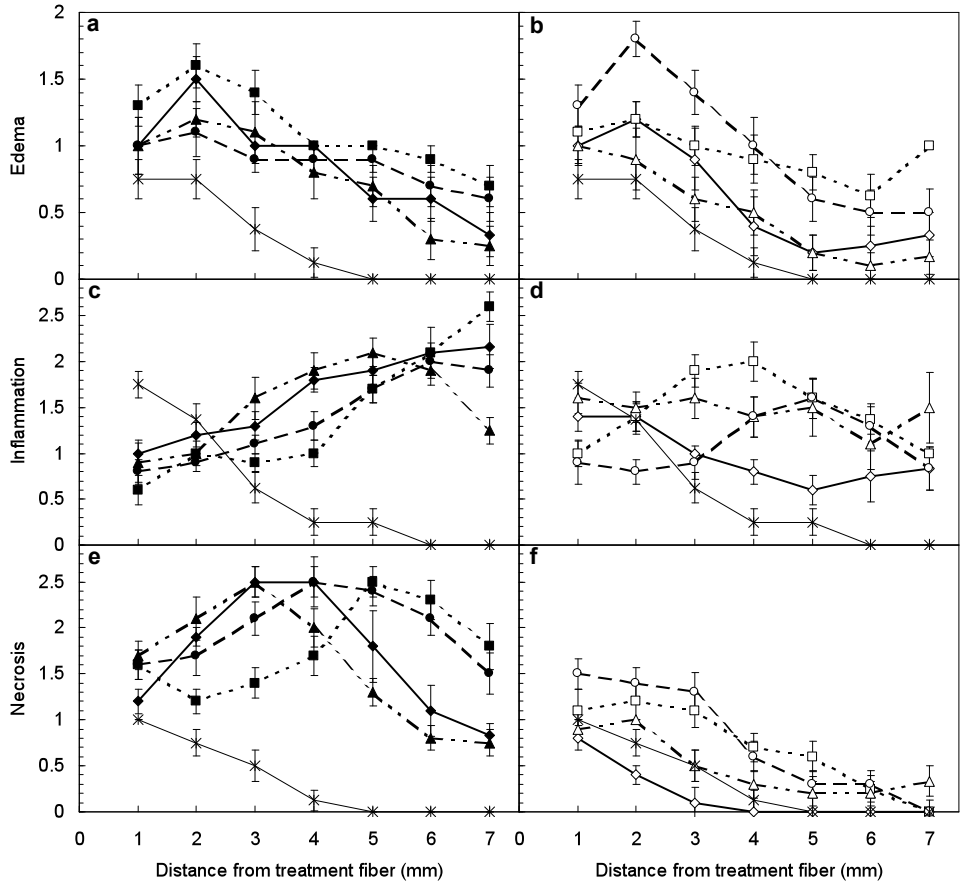

Figure 3. Quantatively scored tissue response differentiated between 16 h (closed symbols) and 96 h (open symbols) and type of response, for all groups; 5 J at 100 mW cm^{-1} (◆, ◇) and 250 mW cm^{-1} (▲, △); 20 J at 100 mW cm^{-1} (■, □) and 250 mW cm^{-1} (●, ○); and the control group (X). Average score on edema as function of distance from the treatment fiber for the 16 h (a) and 96 h (b) treatment groups. Average score on the inflammatory response as function of distance from the treatment fiber for the 16 h (c) and 96 h (d) treatment groups. Average score on the necrosis as function of distance from the treatment fiber for the 16 h (e) and 96 h (f) treatment groups.

Figure 3 shows the values scored for edema (a, b), inflammation (c, d) and necrosis (e, f) as a function of distance from the treatment fiber for the control group and the eight treatment groups. Overall the control group shows mild edema formation, inflammation and sometimes necrosis close to the treatment fiber that all decreases as a function of distance from the treatment fiber. Figures 3a and b show the values scored for edema for the 16 h and 96 h treatment groups, respectively. For all treatment groups a similar decrease in edema formation as a function of distance from the treatment fiber are observed as for the control group. However the scores for edema in the treatment groups are higher than for the control group. Figures 3c and d show the inflammatory response for 16 h and 96 h treatment groups. While the control group shows a decrease in inflammatory response as function of distance of the treatment fiber, the 16 h treatment groups show an increase in inflammatory response as a function of distance. The 96-hour treatment groups show a relative constant inflammatory response as function of distance from the illumination fiber. An interesting observation is that close to the treatment fiber the average score on inflammation is lower in the both 16 h and 96 h treatment groups than in the control group. Figure 3c shows the average score for necrosis for all groups as a function of distance from the treatment fiber. Figures 3e and f show the score on necrosis for the 16 h and 96 h treatment groups, respectively. There is a clear difference in spatial distribution of necrosis is observed between the two different drug-light intervals. For the treatment groups with a 16 h drug light interval there is an increase in necrosis up to 5 mm from the treatment fiber after which it starts to decrease. An interesting observation is that in these treatment groups the groups which received a dose of 5 J cm^{-1} reach a maximum score for necrosis approximately 1 mm closer to the treatment fiber than the groups receiving 20 J cm^{-1}. The 16 h drug light interval and 20 J cm^{-1} groups show a higher score for necrosis over the over the first 5 mm from the illumination fiber for the 250 mW cm^{-1} treatment group than for the 100 mW cm^{-1} treatment group.
In the treatment groups with a drug light interval of 96 h a similar decrease in necrosis as function of distance from the treatment fiber is observed as in the control groups. The treatment groups that received 20 J cm^{-1} show higher scores for necrosis than the 5 J cm^{-1}groups. The scores for necrosis in the 5 J cm^{-1} treatment groups are within the standard deviations of the control group. It is noteworthy that differences in necrosis score between groups with the same fluence but different fluence rates are within standard deviations of the measurements.

Light Dosimetry and Optical Spectroscopy
Optical measurements; fluence rate, reflectance, and fluorescence spectroscopy were acquired at two locations, on top of and beneath the illuminated abominable muscle. Since the exact distance between the therapeutic light source and the linear diffuser are important considerations for the measured fluence rate and the interrogation volume of the optical spectroscopy the location of the catheter (linear diffuser) was determined in control animals at the time of sacrifice. Due to the unknown distance between the measurement probes above and below the muscle regarding the linear diffuser for illumination it was assumed that the average distance for each of measurement probes regarding the linear diffuser is on average the same. For this

reason optical measurements above and below the muscle were averaged. It is important to distinguish between the input fluence rate, defined by the calibrated output of the linear diffuser prior to the insertion of the fiber into the animal (either 100 or 250 mW cm^{-1}) from the measured fluence rate in the measured in tissue. The average measured fluence rate was 81 ± 44 mW cm^{-2} and 149 ± 75 mW cm^{-2} for 100 and 250 mW cm^{-1}, respectively. The measured average fluence rate was relatively constant throughout PDT in the majority of animals, with variations of less than 10%. In two animals we observed an increase of 29% and 40% for the isotropic probe located at the top of the muscle.

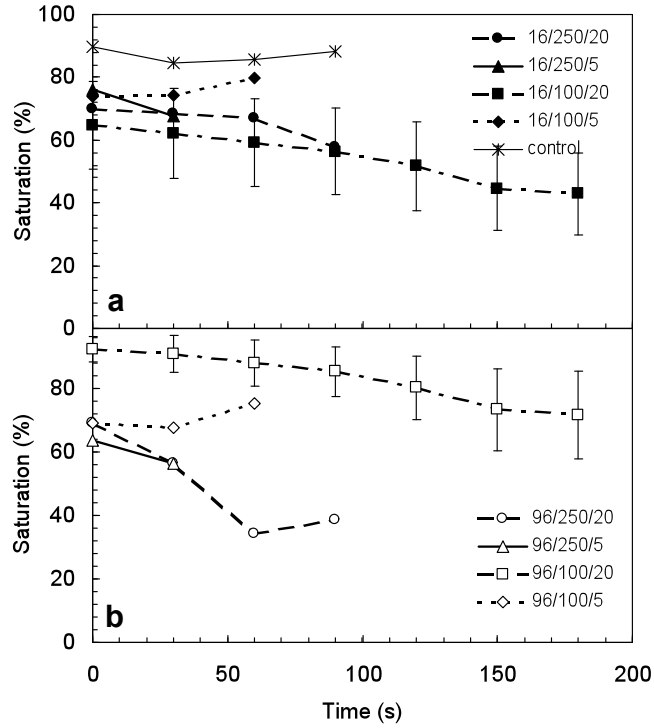

Figure 4. The measured saturation as function of treatment time for the 16 h (a) and 96 h (b) treatment groups depicted in the legend as follows: DLI\fluence rate\dose.

FDPS

Fluorescence differential path length spectroscopy was used to monitor blood saturation, blood volume and m-THPC fluorescence using 652 nm excitation. Figure 4 shows the average saturation during PDT as a function of treatment time for the 16 h (a) and 96 h (b) treatment groups and the control group. The saturation of the control group remains constant during illumination, whereas a decrease in saturation is observed in the 16 h treatment groups (Fig 4a) except in the group that received 5 J cm^{-1} at 100 mW cm^{-1} length of diffuser. This treatment group shows an increase in saturation during illumination. For the 96 h treatment groups (Fig 4b) we also observe

a decrease in saturation in all groups except the group that received 5 J cm^{-1} at 100 mW cm^{-1}. Both groups that were illuminated with a fluence rate of 250 mW cm^{-1} show a steeper decrease in saturation than the other 96 h treatment group and the corresponding 16 h treatment groups. The measured blood volume in all treatment groups remained constant during illumination and was on average 4% ± 2. During the period immediately after the illumination (300 seconds) the measured blood volume remained constant for all groups. In figure 5 the saturation post illumination as a function of time is shown for the 16 h (a) and 96 h treatment groups (b). In three out of four 16 h treatment groups (fig 4a) show an increase in saturation post illumination sometimes increasing above initial pre-illumination saturation values. The 16 h group that received 5 J cm^{-1} at 250 mW cm^{-1} showed a decrease in saturation down to 40% 100 seconds after the end of illumination. For the 96 h treatment groups also an increase in saturation is observed post illumination increasing up to the pre-illumination saturation values for all but the group that received 20 J cm^{-1} at 250 mW cm^{-1}. Both the 100 and 250 mW cm^{-1} groups that received 5 J show a steep increase 50 seconds after the end of illumination. Whereas the group receiving 20 J cm^{-1} at 250 mw cm^{-1} shows a decrease after 50 seconds.

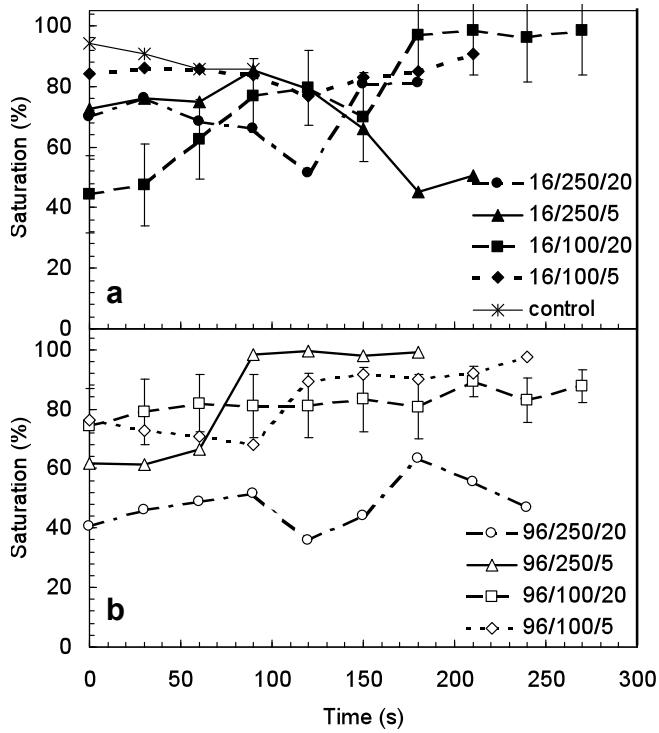

Figure 5. The measured saturation function of time post illumination for the 16 h (a) and 96 h (b) treatment groups depicted in the legend as follows: DLI\fluence rate\dose.

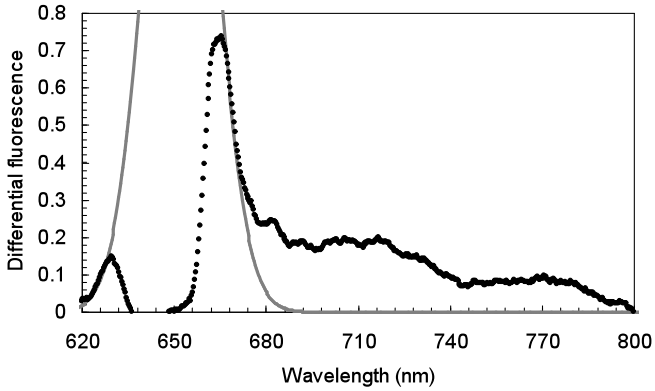

Figure 6. Measured differential fluorescence signal (●) consisting of autofluorescence, m-THPC fluorescence and contribution from the therapeutic laser peak. Clearly the blocking effect of the notch filter is observed around 650 nm. The profile of the laser peak is also shown (solid gray line).

Figure 6 shows a differential fluorescence spectrum (closed circles) and the peak position of the laser (grey solid line). The differential fluorescence spectrum contains a small fraction of laser light of the tail of the laser emission that is only partially filtered by the notch filter. The signal above 690 nm is predominantly fluorescence measured in the animal.

Fluorescence spectroscopy

Long wavelength fluorescence and fluence rate were measured using the same isotropic probe at both locations on the muscle. These data were used to (i) calculate the average initial intensity of m-THPC fluorescence before the start of therapy between animals in groups with a drug light interval of 16 and 96 hours and (ii) investigate the kinetics of photobleaching during illumination. The intensity of m-THPC fluorescence was 59 ± 57 and 20 ± 13 for the 16 h and 96 h treatment groups, respectively. Despite the high standard deviation the non-parametric Mann-Whitney test show a significant difference in the amount of fluorescence between the 16 h and 96 h treatment groups ($P<0.00006$). To investigate the fluence rate dependence of m-THPC photobleaching we averaged m-THPC fluorescence signals within pre-defined fluence rate ranges based on the accompanied measured fluence rate. Four ranges of fluence rate were defined to average corresponding photobleaching signals; 0-49, 50-99, 100-149, >150 mW cm^{-2}.

Figure 7 shows the m-THPC photobleaching characteristics over a fluence range of 15 J cm^{-2} for the 16 h (a) and 96 h treatment groups (b). The mean measured fluence rate within the 0-49, 50-99, 100-149 and <150 mW cm^{-2} fluence rate ranges for the 16 h DLI animals were 30 ± 9 (n=5), 73 ± 17 (n=13), 126 ± 13 (n=11) and 201 ± 31 mW cm^{-2} (n=8), respectively. It is important to note that it was not possible to acquire adequate signals in 8 animals. For these four fluence rate ranges we observe fluence rate dependent rate of m-THPC photobleaching where the highest rate of photobleaching is

observed for animals in the lowest fluence rate range (0-49 mW cm^{-2}). The difference in rate of photobleaching for fluence rates above 50 mW cm^{-2} are small and within the standard errors of the mean. For the 96 h DLI animals the mean measured fluence rate within the 0-49, 50-99, 100-149 and <150 mW cm^{-2} fluence rate ranges were 34 ± 15 (n=6), 73 ± 14 (n=13), 114 ± 9 (n=8) and 211 ± 53 mW cm^{-2} (n=13), respectively. Here we also observe fluence rate dependent m-THPC photobleaching with the highest rate of photobleaching for animals in lowest fluorescence rate range. Again, small differences in rate of photobleaching are observed for fluence rates above 50 mW cm^{-2}.

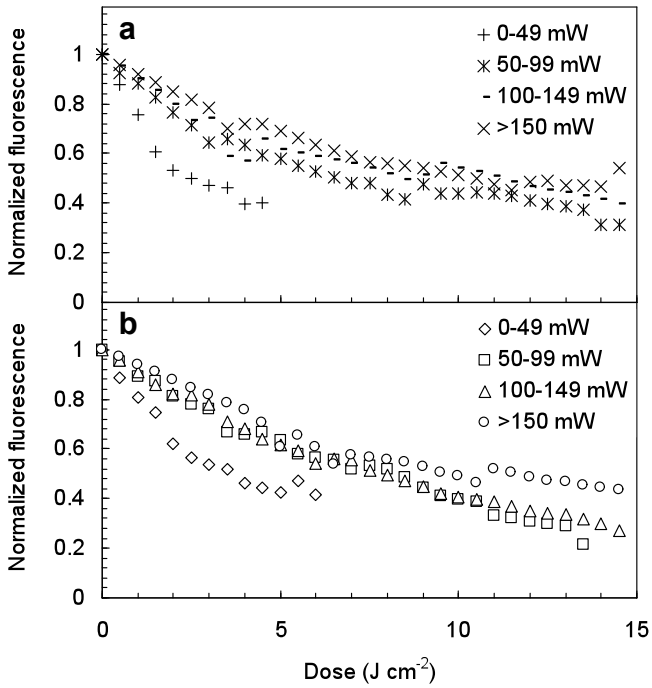

Figure 7. The m-THPC fluorescence photobleaching characteristics measured using the isotropic probes for animals with a 16 h (a) and 96 h (b) DLI. Photobleaching characteristics were categorized and averaged within 4 fluence rate ranges as depicted in the legends based on the in vivo measured fluence rate accompanying every individual photobleaching profile.

Discussion

The aims of this study were to investigate the therapeutic response following interstitial m-THPC-PDT using clinical light treatment parameters and combine this with optical monitoring of the therapy. To our knowledge this is the first study quantifying the microscopic tissue response in optically thick tissues using a linear diffuser to deliver the therapeutic illumination. We have shown that the determination of the volume averaged microscopic response in tissues of the order of 1 cm is complex: In optically thick tissue the depth dependence or spatial distribution of fluence rate distribution is dependent on the optical properties in combination with the distance from the treatment fiber. At different distances a different dose is delivered at a different fluence rate in the tissue. For this reason differences in tissue response can be expected based on distance from the treatment fiber. A small number of studies for example Rovers et al have investigated the response of thick tissues such as liver to m-THPC PDT. This study was only focused on tumor response and the illumination was not performed interstitially using a linear diffuser. In the rat-esophagus depth dependent response was observed and quantitatively assessed for different tissue layers (epithelium, submucosa and muscularis propria)[25,33]. However the total thickness of the rat-esophagus is approximately 800 micron[28] and over this thickness the spatial fluence rate distribution can be regarded constant. In the case of the esophagus the difference in response was determined by a combination of spatial distribution of photosensitizer and tissue oxygen[28].

Our approach in quantifying tissue response was to score on PDT induced effects such as edema formation, inflammatory response and necrosis, as a function of distance from the interstitial fiber. Differences in inflammatory response and necrosis as a function of distance from the treatment fiber are observed between the treatment groups with a drug light interval of 16 and 96 h. The 16 h groups generally show an increase in inflammatory response in distance and an overall higher necrosis score than the 96 h groups. According to pharmacokinetic studies[12,13] the concentration of m-THPC is relatively constant in muscle tissue for these drug light intervals. However this does not take into account of the m-THPC present in the vasculature. Serum values for m-THPC have been shown to be higher for a 16 h than for a 96 h drug light interval. So based on this the overall concentration of m-THPC present in both muscle and vascular compartment is higher for the 16 h drug light interval than for the 96 hour drug light interval. This is confirmed by the fluorescence measurements which shows a higher m-THPC fluorescence intensity at the start of treatment for the 16 h drug light interval. The difference in total m-THPC concentration between the two drug light intervals may account for the difference in response.

Another interesting result of the present study is the fact that the observed necrosis in the 96 h treatment groups is low and not significantly higher than necrosis observed in the control. It is important to note that we have treated normal muscle tissue and pharmacokinetic studies show low accumulation of m-THPC in normal muscle tissue which accounts for the relatively low score on necrosis for the 96 h groups.

An interesting observation regarding the inflammatory response is that all treatment groups show lower scores on inflammation close to the fiber compared to the control group (Fig. 3b&d). Henderson et al. investigated the PDT-induced inflammatory

response in tumors at different fluence rates and doses. They observe more inflammation for low fluence rate PDT and subscribe this to a longer survival period of the (micro) vasculature. This allows cells of the immune system to infiltrate the treatment volume in which the surviving cells exhibit increased expression of inflammatory mediators[34]. This mechanism can be a possible explanation for the fact that we observe more inflammation in the control group (no m-THPC) compared to the treatment groups treated with relatively high fluence rates of 100 and 250 mW cm^{-2}.
In addition to the three types of PDT-induced response (edema formation, inflammation and necrosis), we also observe the absence of cell nuclei. This effect has not been reported previously *in vivo*. It is also interesting that the absence of nuclei is predominantly observed after PDT in the treatment groups with a 16 h DLI (n=20 and n=2 for DLI's of 16 h and 96 h, respectively). Several in vitro studies show sub-cellular localisation and accumulation of m-THPC within the perinuclear region[35] predominantly in the endoplasmatic reticulum and Golgi aparatus after an incubation time of 3 h [36]. Incubation times longer than 24 h show a decrease of m-THPC accumulation in the Golgi apparatus and an enhanced presence of m-THPC in the endoplasmatic reticulum[37]. For the *in vivo* situation it may be that at the relatively short *in vivo* incubation time of 16 h m-THPC on even sub-cellular level is predominantly localised in the peri-nuclear region, inducing photodynamic damage within this region upon illumination. For longer *in vivo* incubation times the amount of m-THPC present in the peri-nuclear region might decrease and be distributed in other subcellular regions. This may explain the absence of cell nuclei in the treatment volume of animals with a 16 h DLI.

For the difference in response between the 5 and 20 J cm^{-1} groups a similar spatial distribution, at lower scores for the low dose group, up to a certain distance from the treatment fiber was expected after which the amount of response would decrease for the low dose group. This is observed for necrosis in the 96 h group. However in the 16 h group we observe a different spatial distribution in necrosis between the groups treated with a dose of 5 and 20 J cm^{-1}. For the different fluence groups the maximum score of necrosis occur 1 mm closer to the treatment fiber for the low dose, 5 J cm^{-1}, groups. The overall extent of necrosis in the 5 J cm^{-1} group is less than in the 20 J cm^{-1} group. Also a slightly lower inflammatory response is observed for the 20 J cm^{-1} group 2-6 mm distance from the treatment fiber. Again the higher inflammatory response in the low dose groups, 5 J cm^{-1}, can be subscribed to a longer survival period of the vasculature[34] at a low dose compared to the high dose. Inflammatory can be a reversible effect but also can lead to irreversible damage to tissue. The difference in inflammatory response in combination with spatial difference in PDT-dose deposited may also account for the different spatial distribution of necrosis between the 5 and 20 J cm^{-1} groups at a 16 h drug light interval

A potential weakness in our current method of assessing the microscopic response to PDT is that we have not considered boundary effects in tissue response at the start and end regions of the linear diffuser delivering the treatment light. Although the position of the linear diffuser in the tissue is clearly marked and visible after

histopathological processes, it is more difficult to demarcate start and end of the diffuser.

FDPS during illumination

As we have reported previously, variations in measured saturation and blood volume values are observed in the measurements following probe placement after surgery and before starting illumination in all groups (both treatment and control groups). These variations can be attributed to the surgical procedure. For this reason illumination was started when saturation and blood volume values had stabilized, which took between 10-15 minutes.

During illumination the control group show constant values for saturation and blood volume. Since the control group was administered with the control-solution not containing m-THPC, no variations in saturation and blood volume were expected. Also the fluence rate during illumination is constant for the control group. However in the treatment groups the fluence rate was relatively constant over the treatment time with a measured variation of 10%. This is in agreement with our previous study considering a same time period after the onset of illumination. In the current study there are no significant variations in decrease of measured fluence rate between the different fluence rate regimes within the applied treatment times.

However, in all but two treatment groups a decrease in saturation is observed for both 16 h and 96 h drug light interval. For a delivered fluence of 20 J cm^{-1} a different decrease in saturation is observed in the 96 h groups but not in the 16 h group. Whereas in our previous study different saturation profiles were observed at a drug light interval of 16 h between the 100 and 250 mW cm^{-1} groups. However these differences were observed over a longer treatment time, 1500 seconds (and thus higher delivered dose) than in the current study. Notwithstanding the difference in decrease between 100 and 250 mW cm^{-1} is observed in the 96 h group. It might be that due to the difference in m-THPC localisation that the effect of fluence rate on saturation is more apparent for a 96 h compared to the 16 h drug light interval.

There are two groups that show an increase in saturation during illumination, these groups with a 16 h and 96 h drug light interval both had a delivered dose of 5 J cm^{-1} at 100 mW cm^{-1}. We did not observe an increase in saturation anywhere during the illumination in the other treatment groups. A possible explanation is that the last saturation measurement for some animals might be after therapeutic illumination ended. At this time a recovery or a delayed vascular response to increase the supply of oxygen to overcome the extra demand of oxygen due to PDT can lead to the increase in saturation. In the future for these short treatment times the temporal resolution for measuring saturation should be increased. This was not possible with the current setup due to additional differential fluorescence measurements.

The differential fluorescence signal in the present study was hampered by a low signal to noise ratio, which made determination of m-THPC fluorescence unreliable. Optimizing the system for fluorescence by increasing signal to noise ratio and reducing exposure times will also be beneficial for the temporal resolution of saturation and blood volume measurements done with the same system. The first step in improving

the signal to noise ratio is to replace the current grating which is inefficient in the high wavelength regions, for a grating with improved efficiency in the high wavelength region.

DPS post illumination

In a previous study we showed delayed PDT-induced vascular effects and recovery directly after the end of illumination. Monitoring saturation post illumination may additionally provide information on vascular response[38,39]. In the current study it was not possible to measure for a long time period post-illumination since the animal needed to recover and survive for 48 hours. Despite the relatively short measurement time-period post illumination we observe recovery of saturation sometimes above the initial pre-illumination saturation values after illumination in the majority of treatment groups. As soon as the therapeutic light is switched off there is no extra demand for oxygen anymore for the PDT mechanism. Assuming that the vasculature is intact the saturation has the ability to recover to its initial values. A recovery above the initial saturation value might be explained by vasodilitation in combination with increased blood flow.

Monitoring m-THPC photobleaching

In addition to monitor FDPS we also monitored fluorescence using an isotropic probe in the same way as we did before[18]. In every animal the fluorescence and fluence rate were measured using the same isotropic probe at two locations, top and bottom of the muscle. We and others showed fluence rate dependent m-THPC photobleaching characteristics were high fluence rates show a lower rate of photobleaching than for low fluence rates due to the fast depletion of tissue oxygen. In this study due to the variation in thickness of muscle tissue means there are 80 different measured fluence rates accompanied by 80 possible different rates of m-THPC photobleaching. For this reason we averaged the m-THPC photobleaching characteristics within pre-determined fluence rate ranges based on the measured *in vivo* fluence rate. For both 16 and 96 h groups fluence rate dependent m-THPC photobleaching is observed, where on average a decrease in rate of m-THPC photobleaching is observed for increasing fluence rates. However for the three fluence rates above 50 mW cm^{-2} the differences in rate of m-THPC photobleaching are surprisingly small and within standard error of the means. In our previous study we used the second order model, under the assumption that during the first 10 J cm^{-2} m-THPC photobleaching mediated predominantly through singlet oxygen, to quantify the rate of m-THPC photobleaching. This showed a relative constant rate of m-THPC photobleaching beyond 75 mW cm^{-2}. This implies that the rate of m-THPC photobleaching is partially independent on fluence rate above a certain value and might indicate that m-THPC photobleaching mediates via other photochemical mechanisms than singlet oxygen alone. Further studies should investigate the paths via which m-THPC photobleaches to understand the relation between fluence rate, photobleaching and oxygen availability.

The next step in a interstitial pre-clinical model is move towards a tumor model. Where the tumor is induced in the tissue. An issue to consider is that the m-THPC

concentration, vascularity and the demand for oxygen is different for tumors. For this reason the kinetics of photobleaching are potentially very different from normal tissue.

Conclusion

We have made the first step into quantification of tissue response in optically thick tissue undergoing interstitial m-THPC-PDT using a linear diffuser to deliver the treatment light. In addition we measured several parameters, such as fluence (rate), fluorescence, saturation and blood volume, during the course of treatment. The relation of the measured parameters regarding the observed response is complex due to the treatment geometry, a three dimensional geometry with spatial distribution of fluence rate and PDT-dose deposition, in combination with the interrogation volumes of the various measurement techniques. The response is assessed over a cross-section while it is difficult to determine exactly at what distance *in vivo* the measurement probes were located. In the clinic this problem can be overcome by marking the probes with something that can be imaged under CT or MR imaging. On the other hand this study is one out of two studies investigating the possibility of measuring parameters during the course of treatment and assessing PDT induced response. More investigation is necessary for understanding the mechanisms underlying m-THPC-PDT but also more investigation into the relation between measured explicit and implicit (dose metric) parameters, and their interrogation volumes, and response in a three dimensional treatment geometry. For a following study these measurements need to be repeated in a pre-clinical tumor model.

References

1. Copper MP, Triesscheijn M, Tan IB, Ruevekamp MC, Stewart FA. Photodynamic therapy in the treatment of multiple primary tumours in the head and neck, located to the oral cavity and oropharynx. Clin Otolaryngol. 2007; 32:185-189.
2. Copper MP, Tan IB, Oppelaar H, Ruevekamp MC, Stewart FA. Meta-tetra(hydroxyphenyl)chlorin photodynamic therapy in early-stage squamous cell carcinoma of the head and neck. Arch Otolaryngol Head Neck Surg. 2003; 129:709-711.
3. Lou PJ, Jäger HR, Jones L, Theodossy T, Bown SG, Hopper C. Interstitial photodynamic therapy as salvage treatment for recurrent head and neck cancer. Br J Cancer. 2004; 91:441-446.
4. Moore CM, Nathan TR, Lees WR, Mosse CA, Freeman A, Emberton M, Bown SG. Photodynamic therapy using meso tetra hydroxy phenyl chlorin (m-THPC) in early prostate cancer. Lasers Surg Med. 2006; 38:356-363.
5. Campbell SM, Gould DJ, Salter L, Clifford T, Curnow A. Photodynamic therapy using meta-tetrahydroxyphenylchlorin (Foscan) for the treatment of vulval intraepithelial neoplasia. Br J Dermatol. 2004; 151:1076-1080.
6. Schouwink H, Ruevekamp M, Oppelaar H, van Veen R, Baas P, Stewart FA. Photodynamic therapy for malignant mesothelioma: preclinical studies for optimization of treatment protocols. Photochem Photobiol. 2001; 73:410-417.
7. Baas P, Saarnak AE, Oppelaar H, Neering H, Stewart FA. Photodynamic therapy with meta-tetrahydroxyphenylchlorin for basal cell carcinoma: a phase I/II study. Br J Dermatol. 2001; 145:75-78.
8. van der Snoek EM, Amelink A, van der Ende ME, den Hollander JC, den Hollander JG, Kroon FP, Vriesendorp R, Neumann HAM, Robinson DJ. Photodynamic therapy with topical metatetrahydroxychlorin (fosgel®) is ineffective for the treatment of anal intraepithelial neoplasia, grade III. J Acquir Immune Defic Syndr. 2009;52:141-3.
9. Lowdell CP, Ash DV, Brown SB. Interstitial photodynamic therapy: Clinical experience with diffusing fibres in the treatment of cutaneous and subcutaneous tumours. British J.Cancer 1993; 67:1398-1403.
10. Personal communication with dr. RLP van Veen.
11. van Veen RL, Nyst H, Rai Indrasari S, Adham Yudharto M, Robinson DJ, Tan IB, Meewis C, Peters R, Spaniol S, Stewart FA, Levendag PC, Sterenborg HJ. In vivo fluence rate measurements during Foscan-mediated photodynamic therapy of persistent and recurrent nasopharyngeal carcinomas using a dedicated light applicator. J Biomed Opt. 2006; 11:041107.
12. Jones HJ, Vernon DI, Brown SB. Photodynamic therapy effect of m-THPC (Foscan) in vivo: correlation with pharmacokinetics. Br J Cancer. 2003; 89:398-404.
13. Cramers P, Ruevekamp M, Oppelaar H, Dalesio O, Baas P, Stewart FA. Foscan uptake and tissue distribution in relation to photodynamic efficacy. Br J Cancer. 2003; 88:283-290.
14. Mitra S, Maugain E, Bolotine L, Guillemin F, Foster TH. Temporally and spatially heterogeneous distribution of mTHPC in a murine tumor observed by two-color confocal fluorescence imaging and spectroscopy in a whole-mount model. Photochem Photobiol. 2005;81:1123-30.
15. Davidson SR, Weersink RA, Haider MA, Gertner MR, Bogaards A, Giewercer D, Scherz A, Sherar MD, Elhilali M, Chin JL, Trachtenberg J, Wilson BC. Treatment planning and dose analysis for interstitial photodynamic therapy of prostate cancer. Phys Med Biol. 2009; 54:2293-313.
16. Johansson A, Axelsson J, Andersson-Engels S, Swartling J. Realtime light dosimetry software tools for interstitial photodynamic therapy of the human prostate. Med Phys. 2007;34:4309-21.

17. Finlay JC, Mitra S, Foster TH. In vivo m-THPC photobleaching in normal rat skin exhibits unique irradiance-dependent features. Photochem Photobiol. 2002; 75:282-288.
18. Kruijt B, van der Ploeg-van den Heuvel A, de Bruijn HS, Sterenborg HJCM, Amelink A, Robinson DJ. Monitoring interstitial m-THPC-PDT in vivo using fluorescence and reflectance spectroscopy. Submitted to lasers surg med.
19. Sitnik TM, Henderson BW. The effect of fluence rate on tumor and normal tissue responses to photodynamic therapy. Photochem Photobiol. 1998 Apr;67(4):462-6
20. Veenhuizen R, Oppelaar H, Ruevekamp M, Schellens J, Dalesio O, Stewart F. Does tumour uptake of Foscan determine PDT efficacy? Int J Cancer. 1997 Oct 9;73(2):236-9
21. Bai L, Guo J, Bontempo FA 3rd, Eiseman JL. The relationship of phthalocyanine 4 (pc 4) concentrations measured noninvasively to outcome of pc 4 photodynamic therapy in mice. Photochem Photobiol. 2009 Jul-Aug;85(4):1011-9
22. de Bruijn HS, van der Ploeg-van den Heuvel A, Sterenborg HJ, Robinson DJ. Fractionated illumination after topical application of 5-aminolevulinic acid on normal skin of hairless mice: the influence of the dark interval. J Photochem Photobiol B. 2006 Dec 1;85(3): 184-90.
23. Rovers JP, Saarnak AE, Molina A, Schuitmaker JJ, Sterenborg HJ, Terpstra OT. Effective treatment of liver metastases with photodynamic therapy, using the second-generation photosensitizer meta-tetra(hydroxyphenyl)chlorin (mTHPC), in a rat model. Br J Cancer. 1999 Oct;81(4):600-8.
24. Sheng C, Hoopes PJ, Hasan T, Pogue BW. Photobleaching-based dosimetry predicts deposited dose in ALA-PpIX PDT of rodent esophagus. Photochem Photobiol. 2007 May-Jun; 83(3):738-48.
25. Boere IA, Robinson DJ, de Bruijn HS, Kluin J, Tilanus HW, Sterenborg HJ, de Bruin RW. Protoporphyrin IX fluorescence photobleaching and the response of rat Barrett's esophagus following 5-aminolevulinic acid photodynamic therapy. Photochem Photobiol. 2006 Nov-Dec; 82(6):1638-44.
26. de Bruijn HS, Kruijt B, van der Ploeg-van den Heuvel A, Sterenborg HJ, Robinson DJ. Increase in protoporphyrin IX after 5-aminolevulinic acid based photodynamic therapy is due to local re-synthesis. Photochem Photobiol Sci. 2007;6:857-64.
27. Nyst HJ, van Veen RL, Tan IB, Peters R, Spaniol S, Robinson DJ, Stewart FA, Levendag PC, Sterenborg HJ. Performance of a dedicated light delivery and dosimetry device for photodynamic therapy of nasopharyngeal carcinoma: phantom and volunteer experiments. Lasers Surg Med. 2007 Sep;39(8):647-53.
28. Kruijt B, de Bruijn HS, van der Ploeg-van den Heuvel A, de Bruin RWF, Sterenborg HJCM, Amelink A, Robinson DJ. Monitoring ALA-induced PpIX-photodynamic therapy in the rat esophagus using fluorescence and reflectance spectroscopy. Photochem Photobiol. 2008; 84:1515-1527.
29. Finlay JC, Conover DL, Hull EL, Foster TH. Porphyrin bleaching and PDT-induced spectral changes are irradiance dependent in ALA-sensitized normal rat skin in vivo. Photochem Photobiol. 2001; 73:54-63.
30. Cottrell WJ, Oseroff AR, Foster TH. Portable instrument that integrates irradiation with fluorescence and reflectance spectroscopies during clinical photodynamic therapy of cutaneous disease. Rev Sci Instrum. 2006; 77:064302.
31. Amelink A, Kruijt B, Robinson DJ, Sterenborg HJ. Quantitative fluorescence spectroscopy in turbid media using fluorescence differential path length spectroscopy. J Biomed Opt. 2008; 13:054051.
32. Amelink A, Robinson DJ, Sterenborg HJ. Confidence intervals on fit parameters derived from optical reflectance spectroscopy measurements. J Biomed Opt. 2008; 13:054044

33. Boere IA, Robinson DJ, de Bruijn HS, van den Boogert J, Tilanus HW, Sterenborg HJ, de Bruin RW. Monitoring in situ dosimetry and protoporphyrin IX fluorescence photobleaching in the normal rat esophagus during 5-aminolevulinic acid photodynamic therapy. Photochem Photobiol. 2003 Sep;78(3):271-7.
34. Henderson BW, Gollnick SO, Snyder JW, Busch TM, Kousis PC, Cheney RT, Morgan J. Choice of oxygen-conserving treatment regimen determines the inflammatory response and outcome of photodynamic therapy of tumors. Cancer Res. 2004;64(6):2120-6.
35. Foster TH, Pearson BD, Mitra S, Bigelow CE. Fluorescence anisotropy imaging reveals localization of meso-tetrahydroxyphenyl chlorin in the nuclear envelope. Photochem Photobiol. 2005;81(6):1544-7.
36. Teiten MH, Bezdetnaya L, Morlière P, Santus R, Guillemin F. Endoplasmic reticulum and Golgi apparatus are the preferential sites of Foscan localisation in cultured tumour cells. Br J Cancer. 2003;88(1):146-52.
37. Marchal S, François A, Dumas D, Guillemin F, Bezdetnaya L. Relationship between subcellular localisation of Foscan and caspase activation in photosensitised MCF-7 cells. Br J Cancer. 2007 Mar 26;96(6):944-51.
38. Wang HW, Putt ME, Emanuele MJ, Shin DB, Glatstein E, Yodh AG, Busch TM. Treatment-induced changes in tumor oxygenation predict photodynamic therapy outcome. Cancer Res. 2004; 64:7553-7561.
39. Pogue BW, Paulsen KD, O'Hara JA, Wilmot CM, Swartz HM. Estimation of oxygen distribution in RIF-1 tumors by diffusion model-based interpretation of pimonidazole hypoxia and eppendorf measurements. Radiat Res. 2001; 155:15-25.

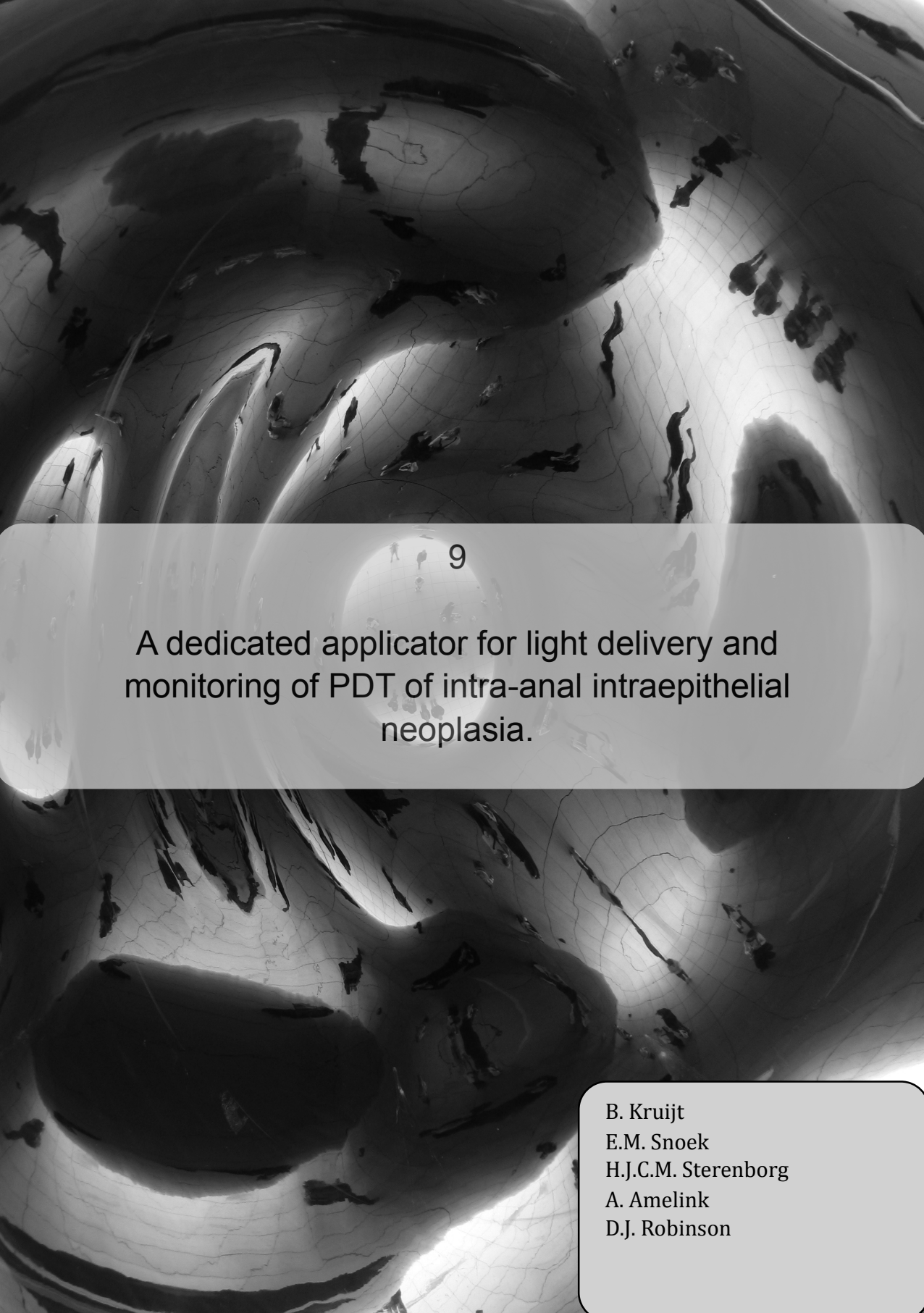

9

A dedicated applicator for light delivery and monitoring of PDT of intra-anal intraepithelial neoplasia.

B. Kruijt
E.M. Snoek
H.J.C.M. Sterenborg
A. Amelink
D.J. Robinson

ABSTRACT

The objective of this study was to develop an applicator for delivery of light and monitoring of photodynamic therapy (PDT) in the anal cavity for treatment of anal intraepithelial neoplasia grade III (AIN III), which can progress to invasive anal cancer.

Forty-eight hours before treatment, patients participating in the study were injected with 0.03 (n=2) or 0.075 (n=2) mg kg^{-1} m-THPC. For light delivery and monitoring of PDT, an applicator based on standard anoscopy equipment was developed which facilitates, in addition to a light treatment fiber, fiber optic probes to monitor blood saturation, blood volume, fluorescence and fluence (rate) at two different locations *in situ*. Patients were given a light dose of 10-17 J cm^{-2} at a fluence rate of 45-50 mW cm^{-2} based on *in situ* measured light treatment parameters.

We demonstrate that the applicator does not influence the fluence rate profile of the light treatment fiber. Furthermore this study shows the possibility of monitoring blood saturation, blood volume, fluorescence and fluence (rate) during therapeutic illumination without changing the light treatment protocol.

Cover: 'underneath the shiny thing,' Chicago 2007.

Manuscript submitted to photodiagnosis and photodynamic therapy

INTRODUCTION

Currently, we are investigating the feasibility of m-THPC mediated photodynamic therapy (PDT) as a treatment modality for perianal and intra-anal, anal intraepithelial neoplasia grade 3 (AIN III), which can progress to invasive anal cancer. Our goal is to screen for AIN III and treat it before it can progress to invasive anal cancer.

To date the management of AIN III is unclear and lacks accepted treatment protocols. Current treatment modalities for AIN III are immunomodulation[1], laser ablation[2,3], and excision[4,5]. However the latter treatment modality can have severe long-term side effects, such as strictures, faecal incontinence and colostomy[4] while laser ablation can only be used to treat small lesions. Currently there is little long-term data on therapies based on immunomodulation. Another possible treatment modality, that has the potential for curative treatment of AIN III with less long-term side effects, is PDT[6,7,8]. An additional and significant advantage of PDT is that it allows therapeutic illumination of the whole surface of the anal cavity in a single treatment session. This is of importance since other treatment modalities show, based on their high recurrence rates of up to 50% [6], that it is difficult to determine exactly where to treat for AIN III in the anal cavity.

Photodynamic therapy has been successfully used for superficial, intraluminal and interstitial treatment of (pre) malignant lesions in among others skin[9], esophagus[10], lung[11], head and neck[12,13], prostate[14] and vulva[15]. There are a small number of clinical reports on PDT in the anal region for treatment of perianal AIN III [6] and carcinoma *in situ*[7] using topical or systemically administered ALA. Light delivery for perianal lesions was done using a light delivery device that uses a mirror to direct treatment light onto the treatment area[6]. For intra-anal treatment of carcinoma *in situ* a rectal speculum was used to expose the mucosa[7]. Subsequently a linear diffuser was placed in the center of the speculum for therapeutic illumination. Since the speculum shields half of the tissue, two illuminations are necessary with the speculum rotated 90 degrees for the second illumination. Recently we reported a clinical study performed in patients with AIN III using m-THPC in a gel based solution, Fosgel ®, which can be applied topically[8]. Light delivery was done either superficially (perianal lesions) or using a transparent inflatable balloon (intra-anal) as previously used for ALA-PDT of the esophagus[10].

Currently applicators used for PDT of the anal cavity only facilitate the delivery of light to either the perianal or intra-anal region and do not facilitate (fiber-optic) probes to monitor explicit parameters (fluence (rate), photosensitizer concentration, tissue oxygenation) and/or implicit parameters (fluorescence photobleaching). Since the deposited PDT dose depends on the concentration of photosensitizer, light treatment parameters and the tissue oxygen concentration, monitoring these parameters can give information not only on delivered PDT dose but also provide insight into the relationship between PDT dose and tissue response. For this reason monitoring of explicit and implicit parameters can aid in optimizing and standardizing PDT.

In this study, we demonstrate the clinical use of a dedicated light applicator for treatment of perianal and intra-anal AIN III using m-THPC. For convenience of both patient and doctor, this light applicator is based on standard anoscopy equipment. A phantom study shows homogeneous light distribution along the applicator for the length of diffuser used for treatment. Furthermore we show it is possible to monitor

fluence (rate), fluorescence, saturation and blood volume at two different locations without changes to the clinical light treatment protocol. For treatment of the patients light treatment parameters were standardized based on the measured fluence (rate) at the treatment location.

MATERIALS AND METHODS

Treatment procedure

Only patients with biopsy proven clinical intra-anal AIN III were included in this study. Patients gave written informed consent to participate in the study. Local hospital ethics committee approved the study.

Forty-eight hours before illumination patients (n=4) were administered with 0.03 or 0.075 mg kg^{-1} intravenous m-THPC (Biolitec AG, Jena, Germany). The low drug dose was used in the first two patients, and based on their results the drug dose was increased to 0.075 mg kg^{-1}. During the 48 hours between administration and therapeutic illumination, patients were send home with a lux meter (Voltcraft, Oldenzaal, the Netherlands) and instructions to maintain under subdued light conditions. At the time of treatment a special designed applicator was placed in the anal cavity. Figure 1 shows the applicator (a) and a schematic cross section of the applicator (b) showing the channels for the fiber optics. During treatment this applicator contains the treatment fiber, in this case a 5 cm linear diffuser (CeramOptec, Jena, Germany), and four fiber optic probes, 1 cm linear diffusers (CeramOptec, Jena, Germany) and fluorescence differential pathlength spectroscopy (FDPS) probes. The 1 cm linear diffusers are used to monitor fluence (rate) and fluorescence and the FDPS probes are used to monitor saturation, blood volume, and local quantitive fluorescence during therapeutic illumination. The applicator is placed with the treatment fiber and the two linear diffusers to measure fluence (rate). After placement of the applicator FDPS probes were placed to prevent damage or perforation of the anal mucosa upon insertion due to the steel casing of these probes. Finally an occluding cloth was applied at the base of the applicator to prevent illumination of normal skin around the perianal region.

Before illumination saturation and blood volume were measured to acquire pre-illumination values. Based on the size of the lesion, a linear diffuser of appropriate length was chosen to insert in the treatment channel of the applicator, in this case a linear diffuser with a length of 5 cm . The fluence rate was measured *in situ* at the anal wall and adjusted to 45-50 mW cm^{-2} which took on average 10 seconds. Illumination was stopped when the desired dose, measured *in situ* at the anal wall, had been delivered. Based on the response in these patients the delivered dose was increased from 10 to 17 J cm^{-2}. Fluence (rate) is measured at two opposite locations; treatment was stopped as soon as with one of the probes the desired fluence was reached. This to prevent possible overtreatment of tissue which can possibly lead to negative side effects, such as perforations or anal dysfunction. After illumination the applicator was removed and as a precaution the patient stayed in overnight to monitor response. The acute response and the side effects associated by PDT were assessed in the days following therapy.

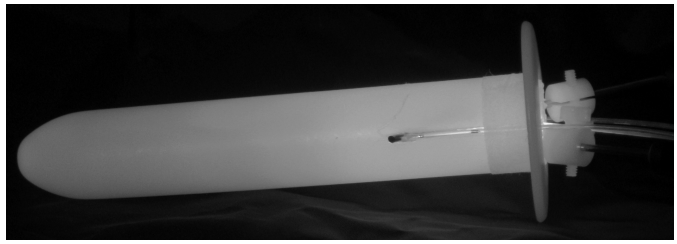

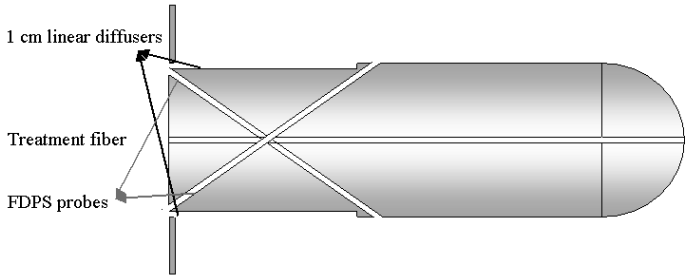

Figure 1. a) Picture of the applicator with all fiber optics in place. The notch in longitudinal direction is used to position the 1 cm linear diffusers to monitor fluence (rate) and fluorescence. At the end of this notch the FDPS needle probe protrudes from the applicator under an angle of 35 degrees. At the base of the probe clearly the cylindrical spacers are seen used to set the insertion depth of the FDPS needle probes. b) shows a schematic longitudinal cross section of the applicator showing all fiber optic channels in the applicator.

Applicator

The applicator used to deliver treatment light and to monitor PDT was based on a clinical anoscope. The white diffusing plastic hollow cylinder of an anoscope with a total length of 13 cm. (Sapimed, Alessandria, Italy) was filled with medical grade silicone leaving a 1 mm channel in the center for the light delivery fiber and 4 additional channels for measurement probes. Figure 1a shows a schematic cross-section of the applicator with all channels and figure 1b shows an image of the applicator together with all fiber optic probes. Two measurement channels are opposite each other at the surface of the applicator and parallel to the treatment channel. These two channels or notches are used to place small 1 cm linear diffusers (CeramOptec, Jena, Germany) to measure fluence rate and fluence at the anal mucosa. The other two measurement channels are under a slope of 35 degrees to facilitate contact of the FDPS measurement probes with the anal wall. The distal ends of the FDPS probes are polished under an angle of 35 degrees to minimize specular reflection between the probe-tissue interface. Adjustable spacers were placed on the FDPS needle probes to prevent damage to the anal mucosa by inserting the FDPS-probes too far.

Light dosimetry and long wavelength fluorescence

Light dosimetry and long wavelength fluorescence were measured as described before (16,17) with the difference that here linear diffusing tips of 1 cm were used instead of an isotropic tip at the distal end of a 400 micron fiber. The other end of the fiber was split using a 200/400 micron bifurcated fiber for acquiring optimal fluorescence signal through the 400 micron fiber while still collect sufficient signal through the 200 micron fiber to accurately monitor fluence (rate). The 200 micron arm of the bifurcated fiber was coupled into a modular based multichannel dosimetry device[18]. The 400 micron arm was coupled into a long pass filtered, >690 nm, channel of a two-channel spectrograph (Ocean Optics, Duiven, the Netherlands).

FDPS

Two FDPS needle probes were designed for this application. The stainless steel needles contained two 400 micron fibers placed at a core-to-core distance of 440 micron and polished under an angle of 35 degrees to minimize specular reflection at the probe-tissue interface. This angle was chosen to optimize probe-tissue contact in the current measurement/treatment geometry in combination with the used treatment applicator.

Excitation light from a 650 nm diode laser (Diomed, Cambridge, United Kingdom), for fluorescence measurements was split to deliver light to both FDPS probes. Shutters (Ocean Optics, Duiven, the Netherlands) in the individual light tracts allowed control of the excitation light for each probes. The excitation light was then coupled into a 100 micron bifurcated fiber, the other arm was coupled into a white light source for DPS measurements. The distal end of the 100 micron bifurcated fiber was coupled into a 200 micron bifurcated fiber of which the other arm was coupled into the first channel of a 650 nm notch filtered (03FIN149, Melles Griot, Didam, the Netherlands) two-channel spectrograph. The distal end of the 200 micron bifurcated fiber was coupled into the light delivery and collection (dc) fiber of the FDPS needle. The collection (c) fiber was coupled directly into the second channel of the 650 nm notch filtered two-channel spectrograph. During illumination FDPS spectra were acquired with an interval of 2-10 seconds.

Data processing

Fluorescence spectroscopy

Long wavelength fluorescence spectra were analyzed as a linear combination of basis spectra using a singular value decomposition (SVD) algorithm as we and others described previously[16,17,19]. The fluorescence was described by a combination of autofluorescence and m-THPC fluorescence. The autofluorescence basisspectrum is the average of acquired spectra measured in a patient before m-THPC was administered. The m-THPC basisspectrum is the average of spectra acquired in m-THPC administered patients with subtraction of the autofluorescence signal.

Fluorescence differential path-length spectroscopy

Differential fluorescence spectra were analyzed using the same SVD as for the long wavelength fluorescence with the addition of a third component. The differential fluorescence spectra contain a contribution from the therapeutic laser. The residual laser light in the fluorescence spectra were described by a Gaussian, peak at 648 nm width 12.3 nm. The autofluorescence basisspectrum is the average of spectra acquired in a patient before m-THPC was administered. The m-THPC basisspectrum is the average of spectra acquired in m-THPC administered patients with subtraction of the autofluorescence and residual laser light. The differential reflectance signal was fitted using the same model as described previously (16,17) to obtain values on saturation and blood volume.

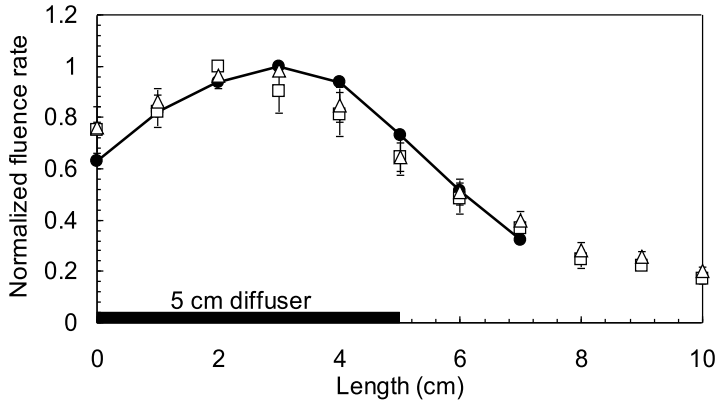

Figure 2. The normalized fluence rate as a function of length is shown for measurements along the applicator with all fiber optics at the correct position (open triangles and squares). measurements were done on the side were the measurement fiber optics were located (open squares) and on a side where no measurement fiber optics were located (open triangles). The solid line represents the fluence rate profile of the linear diffuser, used for treatment, itself (i.e. measured outside the applicator).

RESULTS

Reponse

To prevent potential strictures or anal dysfunction, the first two patients were treated using a drug dose of 0.03 mg kg^{-1}. Based on the low to non response of the tissue after therapeutic illumination it was decided to increase the drug dose to 0.075 mg kg^{-1}. This drug dose was used in combination with a light dose between 10 and 17 J cm^{-2}. The acute response following PDT, the side effects of therapy and the long-term response of AIN III are being evaluated and will be presented elsewhere.

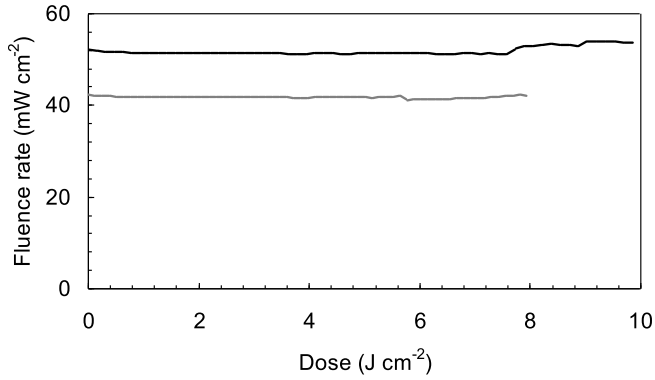

Figure 3. The measured fluence rate as a function of delivered dose measured in situ at two locations (black and gray lines) in a single patient.

Light distribution of the applicator

The light distribution of the applicator was investigated by measuring along the applicator when immersed in scattering phantom (100 ml intralipid 20% diluted in 25 L water), with all measurement and treatment fibers inserted. Figure 2 shows the normalized measured fluence rate as function of distance along the applicator, with the linear diffuser located in the center channel of the applicator. Fluence rate was measured in a longitudinal direction along the applicator at two sides, one side where no measurement probes are located (open triangles) and one side where measurement probes were located (open squares). The filled circles represents the profile of the linear diffuser itself (i.e. profile of the linear diffuser outside the applicator in the same phantom). The two fluence rate profiles measured at the surface of the applicator at two different sides both overlap with the fluence rate profile of the linear diffuser on itself. Figure 2 shows that the applicator has little influence on the fluence rate profile of the linear diffuser used for delivering the therapeutic light.

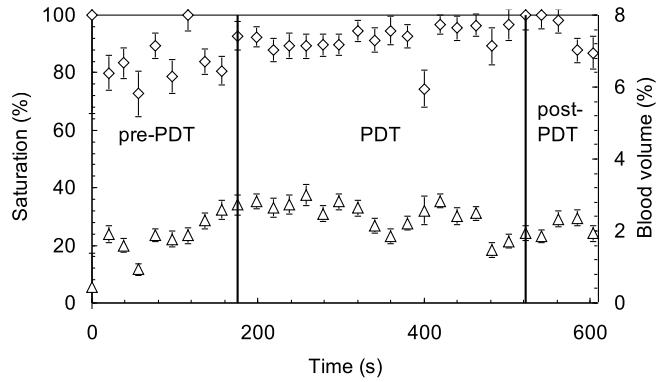

Figure 4. Saturation (open diamonds) and blood volume (open triangles) as a function of time measured during the course of treatment in a patient. The vertical lines indicate start and end of therapeutic illumination. In this patient the delivered dose was 17 J cm^{-2}.

Light dosimetry

Figure 3 shows the measured fluence rate as a function of delivered light dose for two opposite locations (black and gray lines) in a single patient. In all patients and locations, the fluence rate was found to be constant, or gradually increasing or decreasing during therapeutic illumination. However the amounts of increase or decrease in fluence rate were within 10% in all locations except at one location in a single patient, where a decrease in fluence rate of 17% was observed.

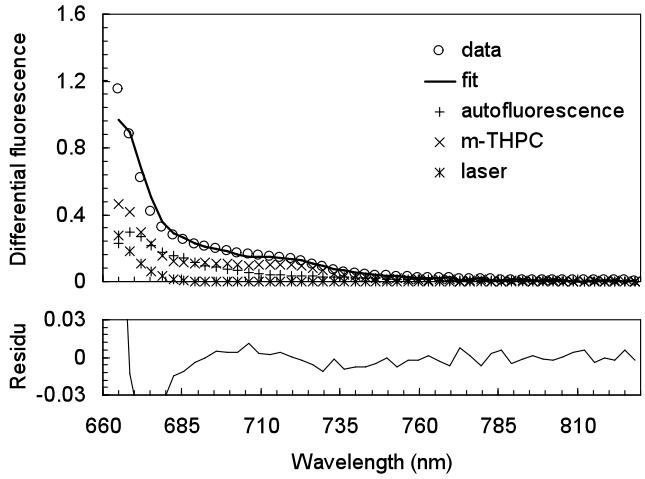

Figure 5. Differential fluorescence spectrum (open circles) with its fit (solid line) and residual. Also the individual components are shown.

FDPS during illumination

FDPS allows monitoring of saturation, blood volume and fluorescence over the same volume. Figure 4 shows the measured saturation (open diamonds) and blood volume (open triangles) at a single location during the course of treatment, i.e. before, during, and after therapeutic illumination. The vertical lines indicate start and end of therapeutic illumination. This particular patient received a light dose of 17 J cm^{-2}. The saturation shows to be relatively constant during illumination for this patient while the blood volume shows oscillating behavior.

Figure 5 shows the fit and components of a measured differential fluorescence spectrum and its residual. The shallow peak at 720 nm is due to the presence of m-THPC.

Long wavelength fluorescence

Figure 6 shows a fluorescence spectrum and its fit with the individual components and the residual, acquired with the 1 cm linear diffusers on the opposite sides of the applicator. In contrast to the differential fluorescence, the long wavelength fluorescence measured by the linear diffusers interrogates an unknown but larger volume than the FDPS signal. Since a different optical filter was used in this setup it was not necessary to include a component for the laser light in the SVD. The Gaussian estimate for the

autofluorescence component shows to yield a good fit in combination with the *in vivo* measured m-THPC component.

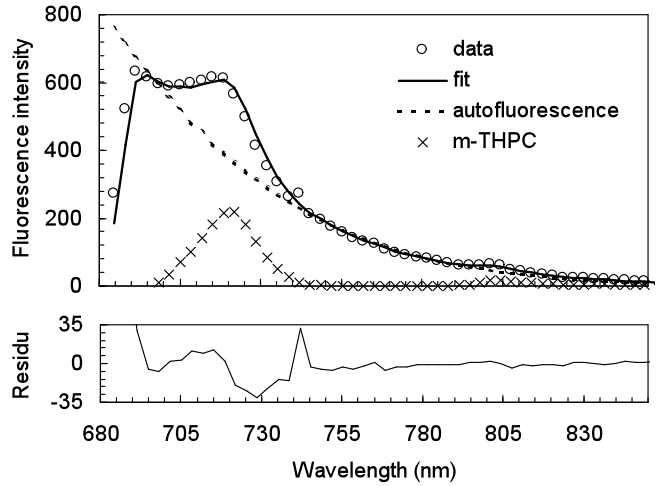

Figure 6. A long wavelength fluorescence spectrum acquired by a 1 cm linear diffuser (open circles), used for monitoring fluence (rate) and fluorescence, with its fit (solid line) and residual. Also the individual components are shown.

Discussion

Fluence rate

The designed applicator for PDT-treatment of anal intraepithelial neoplasia grade III, facilitates fibers for therapeutic illumination and monitoring of fluence (rate), fluorescence, saturation and blood volume. The ability of measuring fluence rate at the treatment location allows for *in situ* setting of the treatment fluence rate. Currently the applied fluence rate is based on the setting of the treatment laser which is set the same for all treated patients. Several studies have shown that the actual measured fluence rate at the treatment location can vary up to a factor 4 between different individuals while the intended fluence rate according to the pre-determined laser settings was kept constant. These inter-individual variations in fluence rate are caused by inter-individual variations in tissue optical properties[20]. These inter-individual variations in light treatment parameters can lead to variations in deposited dose and with that variations in tissue response and treatment outcome. By standardizing light treatment parameters based on fluence (rate) measurements *in situ*, inter-individual variations in deposited dose and tissue response are minimized. Standardizing light treatment parameters based on *in vivo* measured fluence rate has been done before in pre-clinical models such as the rat esophagus[16,21].

The applicator itself shows to have no significant influence on the fluence rate profile of the linear diffuser that is inserted into the applicator for treatment. Potentially the fluence rate profile can be more evenly distributed in length by using better or custom made linear diffusers.

During illumination the fluence rate showed to be relatively constant, the observed gradual increase or decrease in fluence rate were usually within 10%. Other (pre) clinical studies, where the fluence rate was monitored at the treatment location in (pre) clinical studies also show, for some individuals, constant fluence rate during illumination using m-THPC or ALA induced PpIX[16,20]. However, a decrease of over 30% in fluence rate during illumination has also been reported in these studies. Variations in fluence rate are attributed to changes in predominantly tissue absorption which is mainly affected by changes in the amount of hemoglobin present and the saturation (ratio between oxy and deoxyhemoglobin)[20,22]. The saturation is influenced by the amount of oxygen consumed during illumination and is dependent on the fluence rate (increase in fluence rate means an increase in oxygen consumption). In addition PDT-induced vascular responses (vasodilation and vasoconstriction) influence the amount of blood present. Using a relatively low fluence rate, 45-50 mW cm^{-2}, compared to other clinical studies, 100-245 mW cm^{-2}, might prevent rapid oxygen depletion and low blood saturations during illumination. This in combination with less severe vascular effects at lower fluence rates, this might explain the relatively constant measured fluence rates observed in this study.

FDPS

In addition to measuring light treatment parameters we have also shown the potential for monitoring saturation, and blood volume during illumination without changing the therapeutic light treatment protocol. The applied notch filter in front of the spectrographs blocks all light at the treatment wavelength and prevents overexposure due to the treatment light. A previous study showed that the region of the light that is blocked by the notch filter in the differential reflectance spectra has no significant influence on the fit which is used to determine blood saturation and blood volume.

Knowledge of these parameters during illumination can provide real time feed-back on oxygen consumption and vascular response during PDT. These parameters can give insight in the mechanisms of response in m-THPC-PDT. In addition pressure exerted from the applicator on the anal mucosa can have an influence on the saturation and blood volume in the mucosa. In the rat esophagus we observed significant variations in blood volume due to the pressure exerted on the esophageal wall by the treatment balloon[16]. For this reason it is also important to monitor saturation and blood volume directly after insertion of the applicator and before illumination to determine if there are pressure induced changes in saturation and blood volume.

The setup used for monitoring saturation and blood volume also allowed measuring fluorescence over the same volume using 652 nm excitation light. By monitoring m-THPC fluorescence during illumination it is possible to monitor photobleaching of m-THPC. For PpIX the photobleaching characteristics can be used as an implicit dose metric parameter indicative for deposited PDT-dose[16,21,23]. Photobleaching of m-THPC may also contain information indicative of PDT dose deposited, although several studies have shown that photobleaching characteristics of m-THPC are more complicated than PpIX[17,24,25]. The differential spectra clearly show a fluorescence contribution due to m-THPC which is possible to fit with a SVD algorithm (fig 5). However, the fit ting procedure can be improved by the addition of *in vivo* measured

autofluorescence. The current data set is relatively small and does not contain a control group (i.e. spectra without contributions due to m-THPC). This makes it difficult to extract individual components from the *in vivo* measured fluorescence spectra. In the future we will acquire fluorescence spectra in patients that will undergo anoscopy before m-THPC is administered.
For measuring saturation, blood volume and differential fluorescence the FDPS fiber optic needle probes need to be in contact with the tissue. The risk of causing perforation to the anal cavity means that the FDPS needle should not protrude significantly beyond the surface of the applicator. This procedure makes it slightly more difficult to ensure probe-tissue contact than in other studies were we utilized the (F)DPS technique.

Although this applicator is designed for intra-anal treatment of AIN III, it might also be utilized for treatment of AIN III in the perianal region. Currently an occluding cloth is used to prevent PDT-induced response of normal skin around the perianal region. In addition by removing the occluding cloth the perianal region can also be treated. For AIN III limited to the perianal region the intra-anal region can be shielded from the treatment light for an appropriate length of the applicator. In this case the risk for a possible short-term side effect is the treatment of normal skin in a small region around the perianal region.

Conclusion
In conclusion, we demonstrate that the light distribution along the applicator is the same as the linear diffuser applied in the applicator.
Furthermore we demonstrate the possibility of monitoring fluence (rate), fluorescence, saturation and blood volume during therapeutic illumination without changing the light treatment protocol by using, where necessary, a notch filter in front of the spectrographs to block light at the treatment wavelength. By monitoring fluence (rate) at the treatment location we standardized light treatment parameters based on *in situ* measured fluence rate and delivered dose. This is a first step in optimizing and standardizing clinical PDT.

References

1. Kreuter A, Potthoff A, Brockmeyer NH, Gambichler T, Stücker M, Altmeyer P, Swoboda J, Pfister H, Wieland U; German Competence Network HIV/AIDS. Imiquimod leads to a decrease of human papillomavirus DNA and to a sustained clearance of anal intraepithelial neoplasia in HIV-infected men. J Invest Dermatol 2008;128(8):2078-83

2. Cranston RD, Hirschowitz SL, Cortina G, Moe AA. A retrospective clinical study of the treatment of high-grade anal dysplasia by infrared coagulation in a population of HIV-positive men who have sex with men. Int J STD AIDS 2008;19(2):118-20.

3. Nathan M, Hickey N, Mayuranathan L, Vowler SL, Singh N. Treatment of anal human papillomavirus-associated disease: a long-term outcome study. Int J STD AIDS 2008;19(7): 445-9.

4. Brown SR, Skinner P, Tidy J, Smith JH, Sharp F, Hosie KB. Outcome after surgical resection for high-grade anal intraepithelial neoplasia (Bowen's disease). Br J Surg. 1999;86(8): 1063-6.

5. Lyons M, Francis N, Allen-Mersh TG. Treatment of grade 3 anal intraepithelial neoplasia by complete anal mucosal excision without fecal diversion: report of a case. Dis Colon Rectum. 1999 Oct;42(10):1342-4.

6. Hamdan KA, Tait IS, Nadeau V, Padgett M, Carey F, Steele RJ. Treatment of grade III anal intraepithelial neoplasia with photodynamic therapy: report of a case. Dis Colon Rectum. 2003; 46:1555-9.

7. Webber J, Fromm D. Photodynamic therapy for carcinoma in situ of the anus. Arch Surg. 2004; 139:259-61.

8. van der Snoek EM, Amelink A, van der Ende ME, den Hollander JC, den Hollander JG, Kroon FP, Vriesendorp R, Neumann HAM, Robinson DJ. Photodynamic therapy with topical metatetrahydroxychlorin (Fosgel®) is ineffective for the treatment of anal intraepithelial neoplasia, grade III. J Acquir Immune Defic Syndr. 2009;52:141-3.

9. de Haas ER, Kruijt B, Sterenborg HJ, Martino Neumann HA, Robinson DJ. Fractionated illumination significantly improves the response of superficial basal cell carcinoma to aminolevulinic acid photodynamic therapy. J Invest Dermatol. 2006; 126:2679-86.

10. Van Veen RL, Aalders MC, Pasma KL, Siersema PD, Haringsma J, van de Vrie W, Gabeler EE, Robinson DJ, Sterenborg HJ. In situ light dosimetry during photodynamic therapy of Barrett's esophagus with 5-aminolevulinic acid. Lasers Surg Med 2002;31:299-304.

11. Schouwink H, Ruevekamp M, Oppelaar H, van Veen R, Baas P, Stewart FA. Photodynamic therapy for malignant mesothelioma: preclinical studies for optimization of treatment protocols. Photochem Photobiol. 2001; 73:410-417.

12. Copper MP, Tan IB, Oppelaar H, Ruevekamp MC, Stewart FA. Meta-tetra(hydroxyphenyl)chlorin photodynamic therapy in early-stage squamous cell carcinoma of the head and neck. Arch Otolaryngol Head Neck Surg. 2003; 129:709-711.

13. Lou PJ, Jäger HR, Jones L, Theodossy T, Bown SG, Hopper C. Interstitial photodynamic therapy as salvage treatment for recurrent head and neck cancer. Br J Cancer. 2004; 91:441-446.

14. Moore CM, Nathan TR, Lees WR, Mosse CA, Freeman A, Emberton M, Bown SG. Photodynamic therapy using meso tetra hydroxy phenyl chlorin (m-THPC) in early prostate cancer. Lasers Surg Med. 2006; 38:356-363.

15. Campbell SM, Gould DJ, Salter L, Clifford T, Curnow A. Photodynamic therapy using meta-tetrahydroxyphenylchlorin (Foscan) for the treatment of vulval intraepithelial neoplasia. Br J Dermatol. 2004; 151:1076-1080.

16. Kruijt B, de Bruijn HS, van der Ploeg-van den Heuvel A, de Bruin RWF, Sterenborg HJCM, Amelink A, Robinson DJ. Monitoring ALA-induced PpIX-photodynamic therapy in the rat

esophagus using fluorescence and reflectance spectroscopy. Photochem Photobiol. 2008; 84:1515-1527.
17. Kruijt B, van der Ploeg-van den Heuvel A, de Bruijn HS, Sterenborg HJCM, Amelink A, Robinson DJ. Monitoring interstitial m-THPC-PDT in vivo using fluorescence and reflectance spectroscopy. Submitted to lasers surg med.
18. Nyst HJ, van Veen RL, Tan IB, Peters R, Spaniol S, Robinson DJ, Stewart FA, Levendag PC, Sterenborg HJ. Performance of a dedicated light delivery and dosimetry device for photodynamic therapy of nasopharyngeal carcinoma: phantom and volunteer experiments. Lasers Surg Med. 2007; 39:647-53.
19. Finlay JC, Conover DL, Hull EL, Foster TH. Porphyrin bleaching and PDT-induced spectral changes are irradiance dependent in ALA-sensitized normal rat skin in vivo. Photochem Photobiol. 2001; 73:54-63.
20. van Veen RL, Nyst H, Rai Indrasari S, Adham Yudharto M, Robinson DJ, Tan IB, Meewis C, Peters R, Spaniol S, Stewart FA, Levendag PC, Sterenborg HJ. In vivo fluence rate measurements during Foscan-mediated photodynamic therapy of persistent and recurrent nasopharyngeal carcinomas using a dedicated light applicator. J Biomed Opt. 2006; 11:041107.
21. Boere IA, Robinson DJ, de Bruijn HS, van den Boogert J, Tilanus HW, Sterenborg HJ, de Bruin RW. Monitoring in situ dosimetry and protoporphyrin IX fluorescence photobleaching in the normal rat esophagus during 5-aminolevulinic acid photodynamic therapy. Photochem Photobiol. 2003; 78:271-7.
22. Amelink A, van der Ploeg van den Heuvel A, de Wolf WJ, Robinson DJ, Sterenborg HJ. Monitoring PDT by means of superficial reflectance spectroscopy. J Photochem Photobiol B. 2005; 79:243-51.
23. Robinson DJ, de Bruijn HS, van der Veen N, Stringer MR, Brown SB, Star WM. Fluorescence photobleaching of ALA-induced protoporphyrin IX during photodynamic therapy of normal hairless mouse skin: the effect of light dose and irradiance and the resulting biological effect. Photochem Photobiol. 1998; 67:140-149.
24. Forrer M, Glanzmann TM, Braichotte D, Wagnieres GA, van den Bergh H, Savary JF, Monnier P. In-vivo measurement of fluorescence bleaching of meso-tetra hydroxy phenyl chlorin (m-THPC) in the esophagus and the oral cavity. Proc Soc Photo-Opt Inst Eng. 1995; 2627:33-39.
25. Finlay JC, Mitra S, Foster TH. In vivo m-THPC photobleaching in normal rat skin exhibits unique irradiance-dependent features. Photochem Photobiol. 2002; 75:282-288.
26. de Veld DC, Skurichina M, Witjes MJ, Duin RP, Sterenborg HJ, Roodenburg JL. Clinical study for classification of benign, dysplastic, and malignant oral lesions using autofluorescence spectroscopy. J Biomed Opt. 2004; 9:940-50.
27. Zellweger M, Grosjean P, Goujon D, Monnier P, van den Bergh H, Wagnières G. In vivo autofluorescence spectroscopy of human bronchial tissue to optimize the detection and imaging of early cancers. J Biomed Opt. 2001; 6:41-51.

10

General discussion

General discussion

The aim of this thesis was to investigate methods for monitoring photosensitizer pharmacokinetics, performing PDT dosimetry and monitoring therapy without interrupting the therapeutic illumination. This required the development and investigation of techniques such as fluorescence differential path length spectroscopy (FDPS) and laser speckle imaging. This thesis includes several studies investigating the mechanisms of action in PDT and the relationship between parameters measured during illumination and the therapeutic response following PDT. An understanding of these mechanisms may in the future give insight into the reasons why in clinical PDT some individuals do not or partially respond to therapy. This may allow for the optimization of PDT to induce an optimal response in all individuals.

Chapter 2 investigates the possibility of monitoring relative blood flow during PDT. Monitoring of blood flow possibly in addition to measurements on blood volume and blood saturation can provide an estimate of oxygen consumption during therapeutic illumination. Information on oxygen consumption provides information on reactive oxygen species produced during PDT and this may contribute to the determination of deposited PDT dose. The rat window chamber model was used to investigate the full field laser speckle imaging technique which utilizes the variations in the laser speckle pattern induced by scattering erythrocytes to determine relative blood flow. Since the laser speckle pattern of the treatment laser can be used the technique can be applied during therapeutic illumination. This study showed that the variation in speckle pattern, induced by variations in optical path length of light scattering from erythrocytes, is influenced by variations in optical path length due to variations in tissue optical properties during therapeutic illumination. Hence the variations in tissue optical properties have an unknown contribution to the relative estimate of flow, which is not related to blood flow. Another confounding factor in this type of approach is that in tissue it is difficult to determine the contribution to the relative flow from individual vessels when multiple vessels are present in depth. Until these issues are solved, laser speckle imaging is of limited value for blood flow monitoring during therapeutic illumination.

Chapters 3, 4, and 5 describe the process of validation from a phantom study to an *in vivo* model for a technique that allows quantitative fluorescence spectroscopy, namely fluorescence differential pathlength spectroscopy (FDPS), which is based on differential path length spectroscopy. Quantitative fluorescence spectroscopy allows for inter-individual comparison of fluorescence data since these are corrected for tissue optical properties and the optical transmission of the measurement setup. In addition they can give quantitative information on photosensitizer concentration for fluorescing photosensitizers, such as PpIX and m-THPC.
The FDPS concept and its ability to measure fluorescence quantitatively was first validated in a series of phantom experiments in which the absorption, scattering and the concentration of the fluorescing agent were controlled and varied (chapter 3). This study showed that within the expected variation of tissue optical properties, tissue

scattering had no significant influence on the acquired fluorescence. It was necessary to correct the fluorescence signal for the tissue absorption at the excitation wavelength. The step to validate the FDPS concept *in vivo* requires an additional measurement technique to determine true photosensitizer concentration in tissue. With these measurements a calibration curve can be obtained from which it is possible to relate the measured fluorescence to actual photosensitizer concentration. This step is required only once to determine the calibration curve for a certain type of tissue. However, small differences in environment in different types of tissue can affect the fluorescence quantum yield and may require to repeat this step for each individual tissue type in which the photosensitizer concentration is to be measured. An accurate method of determining true photosensitizer concentration in tissue is through chemical extraction. This method determines the photosensitizer concentration by chemically dissolving the tissue and acquiring a fluorescence spectrum in a dilute solution. Although the different steps in chemical extraction process are relatively simple, variations in the concentration of solvent and the duration of incubation between photosensitizer and solvent can influence outcome. Chapter 4 investigated the different steps in the chemical extraction process and its influence on the determination of the photosensitizer concentration. This study showed that accurate and reproducible measurements of photosensitizer concentration can be obtained when solvent concentrations are kept constant and when the procedure is performed within a specific time frame.

In chapter 5 FDPS was used to determine m-THPC pharmacokinetics in the rat liver. FDPS measured photosensitizer fluorescence was then compared to true photosensitizer concentration determined using chemical extraction. According to m-THPC pharmacokinetics of the liver, different m-THPC concentrations were obtained by measuring at 4 different drug light intervals. A correlation coefficient of 0.87 was found between the actual *in vivo* m-THPC concentration and the measured quantitative fluorescence measurements. More interesting was that for the short drug light intervals the measured differential fluorescence showed strong correlation with the measured blood volume fraction. For longer drug light intervals there was a decrease in correlation coefficient between measured differential fluorescence and the blood volume fraction. This is in agreement with the pharmacokinetics of m-THPC which show that m-THPC is primarily localized in the vascular compartment for short drug light intervals and diffuses from the vascular compartment to the cellular compartment for longer drug light intervals. Variations in standard deviations between the differential fluorescence and the m-THPC concentration determined by chemical extraction were attributed to the intra-animal microscopic variations in m-THPC distribution and the difference in interrogation volumes of both methods (0.2 mm^3 and 10^2 mm^3 for FDPS and chemical extraction, respectively). This intra-animal microscopic variation in m-THPC distribution was confirmed by fluorescence microscopy.

Quantitative fluorescence measurements allow non-invasive concentration measurements of fluorophores *in vivo*. Another potential field of interest is to monitor quantitative fluorescence photobleaching of photosensitizers during therapeutic

illumination. During therapy the tissue optical properties can vary significantly. This can strongly influence standard methods of acquiring fluorescence and fluorescence photobleaching kinetics *in vivo*. Measuring quantitative fluorescence allows more accurate bleaching profiles that may aid the understanding of the mechanisms via which photosensitizers photobleach during illumination.

Chapter 6 investigates the phased photobleaching characteristics that are observed in ALA-PDT of the rat esophagus. In this study fluence rate and long wavelength fluorescence, i.e. fluorescence measured in the wavelength region beyond the therapeutic wavelength, were monitored during therapeutic illumination. Differential fluorescence, blood saturation and blood volume fraction were acquired during regular short interruptions to the therapeutic illumination. Monitoring saturation in combination with fluorescence should indicate if phased photobleaching characteristics can be ascribed to variations in oxygen availability during therapeutic illumination. Whereas the comparison between the long wavelength fluorescence and differential fluorescence can show depth related fluorescence information since these methods have different interrogation volumes. In addition the histological response of the esophagus to PDT is examined to investigate whether there is a difference in response between animals that do or do not exhibit phased photobleaching characteristics. Finally fluorescence microscopy of the esophagus was performed to investigate the PpIX distribution and relate this to the treatment outcome and the measured parameters during PDT.
The histological response of this study showed similar severe response of the deeper muscle layers in all animals but variations in the epithelial response. Fluorescence spectroscopy showed that PpIX predominantly accumulates in the epithelial layer and part of the submucosa in the esophagus. However PpIX was present at lower concentrations in the deeper layers of which the muscle layer. In addition the morphology of the esophagus showed that the epithelial layer is dependent on oxygen diffusion from vasculature that is located on average 100 microns below the esophageal lumen. The muscle layers showed high vascular density. The distribution of PpIX and oxygen can explain the observed response and phased photobleaching characteristics.
In the epithelial layer with its high concentrations of PpIX and its dependence on oxygen from deeper vessels there is an increased risk of oxygen depletion during PDT decreasing the treatment efficacy and increasing the risk of incomplete treatment. Whereas in the deeper layers there is less PpIX and sufficient oxygen, here there is no risk of oxygen depletion and the response is determined by the amount of PpIX present. In terms of fluorescence it can be that the rate of photobleaching is different for each esophageal layer. Monitoring fluorescence over all esophageal layers with different PpIX and oxygen distributions may result in photobleaching characteristics with multiple rates of photobleaching. This is observed in the long wavelength fluorescence data in all animals. Furthermore, as expected the differential fluorescence which measures fluorescence predominantly over the epithelial layer and part of the submucosa does not show these phased photobleaching characteristics. Based on the measurements during PDT, fluorescence microscopy and histological examination it

was concluded that phased photobleaching characteristics in the esophagus originates from a complex interrelationship between photosensitizer distribution and oxygen supply to the illuminated volume.
A potential weakness of this study is the regular interruptions to PDT to monitor blood saturation, blood volume and differential fluorescence. For clinical PDT it would mean a change in the light treatment protocol and it is unclear whether regular interruptions to the therapeutic light significantly influence the treatment outcome. It would therefore be an advantage to investigate if it is possible to monitor blood saturation, blood volume and differential fluorescence during PDT without interruptions to the therapeutic illumination.

Chapter 7, illustrates the possibility of monitoring fluence rate, fluorescence, blood saturation and blood volume during PDT without changing the light treatment parameters. The study presented in Chapter 6 demonstrated the possibility of monitoring photosensitizer fluorescence in the long wavelength region beyond the therapeutic wavelength for PpIX. Since m-THPC has a similar characteristic second fluorescence peak beyond the therapeutic wavelength this could be repeated with slight modifications to the filter settings. To monitor DPS, which provides information on the blood saturation and blood volume, during PDT a notch filter was placed before the detectors to filter out light at the therapeutic wavelength to allow differential reflectance measurements when the treatment light is on. This pre-clinical study was designed as a first step to monitor these parameters in an interstitial m-THPC PDT environment. This is important because interstitial PDT using m-THPC is gaining acceptance in the clinic and to date there have been very few studies investigating mechanisms of action of PDT and the difficulties of in particular an interstitial setting. These studies focusing on monitoring interstitial PDT are necessary to explain variations in response encountered in clinical PDT and understand the mechanisms of action in PDT in order to optimize and standardize clinical PDT.

This study showed variations in vascular response during the course of treatment both between different fluence rate groups and animals within the same fluence rate group. For this reason it may be useful for following (pre) clinical studies to monitor the vascular response during the course of treatment and compare this to PDT induced tissue response. Another interesting observation was significant photobleaching at very low measured saturations. In addition fitting of the photobleaching curves of all animals suggest fluence rate independent photobleaching for fluence rates higher than 100 mW cm^{-2}. These observations indicate that m-THPC may bleach via other mechanisms than those mediated by the generation of singlet oxygen (type II) alone. A limitation of this study was that the treatment fiber that delivers the therapeutic light was not interstitially inserted in tissue but it was completely ‘surrounded’ by tissue. In the following study (chapter 8) the treatment fiber was inserted in the abdominal tissue to have a more realistic interstitial model. In addition differential fluorescence was incorporated by including a notch filter to allow fluorescence measurements during therapeutic illumination.

The emphasis of this study lay in quantitatively determining PDT induced response after interstitial m-THPC-PDT using clinical relevant fluence (rates) Interstitial PDT in this pre-clinical model was performed according to the general accepted protocols for clinical PDT. Despite the fact that clinical interstitial PDT using linear diffusers has been applied for many years, prior to this study there were no investigations regarding PDT-induced histological tissue response following interstitial PDT using linear diffusers to deliver the treatment light. Clinically the locations of the treatment fibers within the treatment volume in clinical PDT are based on an assumed necrosis area to be induced around the treatment fiber. However, in large interstitial treatment volumes fluence rate and therefore PDT-induced response, become dependent on distance from the treatment fiber. It seems essential to take this in to account to prevent possible over- or under treatment.

Chapter 8 shows different types of PDT-induced histological response as a function of distance from the treatment fiber. In general the necrosis data shows more severe and extended necrosis profiles for the short drug light interval of 16 hours compared to the long drug light interval of 96 hours. There is no significant difference in m-THPC concentration in muscle according to the pharmacokinetics. However plasma values for m-THPC between these two drug light intervals are significantly higher at 16 hours than at 96 hours, which may explain the differences in response between these two drug light intervals.

Despite the significant variations in response observed between the two drug light intervals and the two fluence rate regimes the blood volume and blood saturation measured during therapeutic illumination in these groups do not show significant variations. In addition the m-THPC photobleaching characteristics, based on the long wavelength fluorescence, show no significant differences in rate of photobleaching for measured fluence rate ranges over 50 mW cm^{-2}. Unfortunately the differential fluorescence could not be used due to the poor signal to noise ratio of the detectors in the wavelength range above 690 nm. The complex mechanisms of action in m-THPC PDT especially combined with the interstitial geometry requires further investigation to relate the observed response to the parameters monitored during PDT. This requires passive monitoring of m-THPC-PDT in (pre-) clinical settings where possible preferably with quantitative determination of induced response following PDT.

Chapter 9 illustrates that monitoring during PDT can be implemented during clinical PDT In this study m-THPC-PDT of anal intraepithelial neoplasia grade III (AINIII) is monitored using the techniques developed, validated and utilized as described in previous chapters. In contrast to the previous chapter for this study different spectrographs with better signal to noise ratio for the higher wavelengths were used to acquire FDPS signals.
Since the treatment geometry differs from the interstitial or superficial skin illuminations a dedicated light delivery and monitoring applicator was developed in order to circumferentially treat AINIII in the anal cavity. This applicator was able to hold the fiber to deliver the treatment light and several fiber optic probes for monitoring PDT.

By monitoring fluence (rate), among other parameters, during PDT it was possible to standardize light treatment parameters *in situ*. This ensures the same fluence rate and light dose is delivered *in situ* to all individuals.
Although we monitored parameters such as fluorescence, blood volume, blood saturation and differential fluorescence it is currently too early to be able to relate these parameters to the long term response.

In summary, this thesis shows the possibility of monitoring several explicit and implicit parameters of potential importance to PDT. These parameters can be monitored during therapeutic illumination without changing the light treatment protocol. However, the FDPS technique needs further investigation and development for application during PDT to yield good signal to noise ratio and accurate differential fluorescence measurements.
Monitoring PDT is necessary to understand mechanisms of action in PDT as shown in chapter 3 where monitoring PDT led to understanding of phased photobleaching characteristics in ALA-PpIX PDT. For m-THPC-PDT relating the induced response with parameters monitored during PDT is more complex due to the mechanisms via which m-THPC-PDT relates to response. This necessitates further investigation into the mechanisms of m-THPC-PDT especially considering the expanding clinical application and investigation of m-THPC-PDT for superficial, intra-luminal and interstitial treatment geometries.
Based on the results of the studies in this thesis it can be concluded that:

1. Monitoring during the course of treatment in PDT is necessary for better understanding mechanisms of action in PDT.
2. Further work is needed to develop new techniques to monitor parameters of importance in PDT and to enhance current techniques such as FDPS and possibly laser speckle imaging.
3. Further work is needed on clinical implementation of monitoring techniques.

Clinical monitoring will aid in the understanding of the mechanisms of action in PDT and in addition may give an explanation for the variable response in patients undergoing PDT. In the future passive monitoring as done currently may become more active, where monitored parameters can provide real-time feed-back on variable treatment parameters such as the light treatment parameters. For example fluence rate might be adjusted if the monitored parameters indicate premature oxygen depletion.
The ultimate goal for PDT monitoring and understanding its mechanisms of action is to yield maximum treatment outcome while minimizing (long term) side effects. It is not unthinkable that for some malignancies, such as those in the Head and Neck region, PDT could become a first line treatment modality in addition to surgery and radiotherapy.

11

Summary-Samenvatting

Curriculum Vitae, Scientific output

PhD portfolio summary

Dankwoord - Acknowledgements

SUMMARY

Chapter 2 describes a full field imaging technique, laser speckle imaging, to monitor relative blood flow during therapeutic illumination. This technique uses the variation in the laser speckle pattern, induced by moving scattering particles (erythrocytes), to determine relative blood flow. Laser speckle imaging was used in the rat skin-fold observation chamber, a model suitable to investigate vascular changes during the course of treatment. This study illustrates the potential of monitoring blood flow during therapeutic illumination. However, the unknown variations in optical path-length during illumination also contribute to the variation in laser speckle pattern. Based on this it can be concluded that the information provided by laser speckle imaging is of limited value until changes in blood flow and variations in optical path-length can be separated.

Chapters 3, 4, and 5 shows the development of a new quantitative fluorescence spectroscopy technique, fluorescence differential path length spectroscopy (FDPS). Quantitative fluorescence spectroscopy allows absolute estimates on fluorophore concentrations in solutions and tissue. In chapter 3 the concept of the FDPS technique is investigated in a series of optical phantoms. In these series the scattering and absorption properties of the phantoms are varied at different fluorophore concentrations. The next step to investigate FDPS in vivo requires a standard to determine the actual fluorophore concentration in the interrogated tissue.
Chapter 4 describes an adapted chemical extraction method to determine actual fluorophore concentrations in tissue. For this method the tissue containing the fluorophore is completely dissolved using the substance Solvable. In a following step the optical density of the liquefied tissue solution is decreased to <0.1 to minimize self-absorption effects. This study demonstrated that for the photosensitizer m-THPC current chemical extraction methods can be improved by accounting for the tissue/ solvent fluorescence background using spectroscopy and by keeping the same environment by diluting solutions with Solvable in stead of water.
In chapter 5 the FDPS technique is investigated in vivo in the rat liver using m-THPC. Different m-THPC concentrations are obtained by measuring FDPS at different time points after m-THPC administration based on the m-THPC pharmacokinetics in rat liver. The method of chemical extraction, described in chapter 4, was used to determine true in vivo m-THPC concentrations in the liver. FDPS measured m-THPC fluorescence was then compared to the true measured m-THPC concentration. This study showed a R^2 value of 0.87 between the FDPS measured m-THPC fluorescence and true m-THPC concentration in liver. Furthermore m-THPC concentrations as low as 169 ng g^{-1} could be measured. An interesting observation was that there was a strong correlation between blood volume and m-THPC fluorescence for short drug light intervals and there was a decrease in correlation coefficient for longer drug light intervals.

In chapter 6 ALA-PpIX PDT in the rat esophagus is monitored using reflectance and fluorescence spectroscopy to investigate the phased photobleaching characteristics and where it originates from. Another aim of this study was to compare the reflectance

and fluorescence spectroscopy techniques used to monitor monitor ALA-PpIX PDT in the rat-esophagus, with histological observed response.
ALA was orally administered to the animals and two hours after administration they were illuminated to a dose of 54 J cm^{-2} at a fluence rate of 75 mW cm^{-2}. Fluence (rate) and fluorescence were measured during therapeutic illumination. Blood saturation, blood volume and quantitative fluorescence were measured during short interruptions to the therapeutic illuminations at regular intervals. 48 hours after illumination the esophagus was histologically examined and scored for PDT-induced damage. In contradiction to previous studies, no clear correlation was found between phased photobleaching and histologic tissue response. Based on the results it can be concluded that the phased photobleaching is related to a complex interrelationship between PpIX distribution and the supply of oxygen to the illuminated volume.

Chapter 7 investigates the possibility of monitoring reflectance and fluorescence spectroscopy without interruptions to the therapeutic illumination in a pre-clinical interstitial treatment geometry using m-THPC. For this normal muscle tissue was treated using clinical relevant fluence rates of 50, 100 and 250 mW cm^{-1} sixteen hours after m-THPC administration. This study showed the possibility to monitor fluence rate, fluorescence, blood saturation and blood volume in vivo during PDT. Differences in vascular response during the course of treatment were observed between treatment groups and between animals of the same treatment group. Fluence rate dependent m-THPC photobleaching was observed up to a measured fluence rate of 100 mW cm^{-1}. This shows that the relationship between fluence rate and m-THPC photobleaching is complex in an interstitial environment.

In chapter 8 the pre-clinical interstitial model as described in chapter 7 is extended. In addition to the previous study, it incorporates differential fluorescence measurements by FDPS during illumination and investigating histologic PDT-induced response after therapeutic illumination using clinical relevant fluence rates and dose. In addition to different fluence (rate) groups also two different drug-light intervals of 16 and 96 hours were investigated. For histologic examination of response the treated muscle was excised and assessed 48 hours after therapeutic illumination. The PDT-induced response showed to be significantly greater in groups with a drug light interval of 16 h than groups with a drug light interval of 96 h. An interesting observation was the absence of nuclei in muscle cells in predominantly individuals with a 16 h drug light interval. Despite the variation in observed response, blood saturation and blood volume monitored during therapeutic illumination remained relatively constant. Photobleaching characteristics of m-THPC at different measured fluence rates showed little difference in rate of photobleaching for fluence rates higher than 50 mW cm^{-1}.

In chapter 9 the reflectance and fluorescence spectroscopy techniques are incorporated in a dedicated light delivery applicator for clinical treatment of AIN III. To date there are no accepted treatment protocols for AIN III which is a pre-malignant condition and can progress to invasive anal cancer.

Forty-eight hours before therapeutic illumination m-THPC is administered to the patients. In this study the light treatment parameters are standardized by adjusting the fluence rate in situ to 45-50 mW cm^{-2}. The treatment is stopped when the desired light dose, measured in situ, has been delivered. Initial results are promising, however, further monitoring is required to understand the mechanisms of action in m-THPC-PDT.

Chapter 10 the results of these studies are discussed and future perspectives are presented.

SAMENVATTING

Hoofdstuk 2 beschrijft een beeldtechniek, laser speckle imaging, voor het monitoren van de relatieve stroomsnelheid van bloed gedurende therapeutische belichting. Deze techniek gebruikt de variatie in het laser speckle patroon, welke wordt geïnduceerd door bewegende verstrooiende deeltjes (erytrocyten), om de relatieve stroomsnelheid van het bloed te bepalen. Laser speckle imaging is hier gebruikt in het zogenaamde kamertjes model, welke geschikt is om variaties in vascularisatie gedurende de PDT behandeling te onderzoeken. De studie illustreert het potentiaal van het monitoren van de stroomsnelheid van bloed gedurende de behandeling. Echter, onbekende variaties in optische pad lengte dragen ook bij aan de variatie in het laser speckle patroon en hebben dus invloed op de relatieve waarde voor de stroomsnelheid. Gebaseerd op deze resultaten kan worden geconcludeerd dat de informatie gegeven door laser speckle imaging beperkende waardevolle bijdrage kan leveren, totdat variaties in optische pad lengte en veranderingen in de stroomsnelheid van het bloed gescheiden kunnen worden.

Hoofdstukken 3, 4 en 5 laten de ontwikkeling zien van een nieuwe quantitatieve fluorescentie spectroscopie techniek, fluorescentie differentiële pad lengte spectroscopie (FDPS). Quantitatieve fluorescentie spectroscopie maakt het mogelijk om absolute waarden te bepalen van concentraties van fluorophoren in oplossingen en weefsel. In hoofdstuk 3 wordt het concept van FDPS onderzocht in een serie optische fantomen. In deze fantoomseries worden de verstrooiende en absorberende eigenschappen van het fantoom gevarieerd bij verschillende fluorophor concentraties. De volgende stap om het FDPS concept *in vivo* te onderzoeken vereist een standaard om de daadwerkelijke fluorophor concentratie in weefsel te bepalen.
Hoofdstuk 4 beschrijft een aangepaste chemische extractie methode om de daadwerkelijke fluorophor concentratie in weefsel te bepalen. Bij deze methode wordt het weefsel dat het fluorophor bevat volledig opgelost gebruikmakend van het oplosmiddel Solvable. In een volgende stap wordt de weefseloplossing dusdanig verdund zodat de optische dichtheid van de oplossing <0.1, dit om effecten zelfabsorptie te reduceren. Deze studie liet zien dat voor de lichtgevoelige stof meta-tetrahydroxyphenylchloride (m-THPC) de huidige chemische extractie methoden verbeterd konden worden door rekening te houden met de fluorescentie achtegronden van het weefsel/oplosmiddel gebruikmakend van spectroscopie en door de chemische

omgeving gelijk te houden door oplossingen te verdunnen met Solvable in plaats van water.
In hoofdstuk 5 wordt de FDPS techniek in vivo in de lever van de rat toegepast en onderzocht gebruikmakend van de lichtgevoelige stof m-THPC. Verschillende m-THPC concentraties werden verkregen door op verschillende tijdsintervallen na injectie, gebaseerd op de farmacokinetiek van m-THPC in lever, met de FDPS methode te meten. De methode van chemische extractie, zoals beschreven in hoofdstuk 4, werd gebruikt om de daadwerkelijke m-THPC concentratie in de lever te bepalen. De waarden voor m-THPC fluorescentie gemeten met FDPS werden vervolgens vergeleken met de daadwerkelijke m-THPC concentratie. Dit onderzoek liet een R^2 waarde zien van 0.87 tussen de FDPS gemeten fluorescentie en daadwerkelijke m-THPC concentratie. Daarnaast was het mogelijk om concentraties tot 160 ng g^{-1} te meten met FDPS. Een interessante observatie was dat er een sterke correlatie bestond tussen het gemeten bloed volume en m-THPC fluorescentie voor de korte tijdsintervallen en deze correlatie nam af naarmate het tijdinterval langer werd.

In Hoofdstuk 6 wordt ALA-PpIX-PDT in de ratten oesophagus geobserveerd middels reflectantie en fluorescentie spectroscopie teneinde het fenomeen van de gefaseerd bleken van PpIX te onderzoeken en waar de grondslag van het gefaseerd bleken van PpIX ligt. Een tweede doel van dit onderzoek was om de gegevens van de gemeten reflectantie en fluorescentie spectroscopie in de ratten oesophagus te vergelijken met de histologische respons op de behandeling.
ALA werd oraal toegediend bij de dieren en twee uur na toediening werden zij belicht tot een lichtdosis van 54 J cm^{-2} bij een fluence rate van 75 mW cm^{-2}. De fluence (rate) en fluorescentie werden gemeten tijdens de belichting. Bloed saturatie, bloed volume en quantitatieve fluorescentie werden gemeten tijdens regelmatig korte intervallen van de therapeutische belichting. Achtenveertig uur na de belichting werd de behandelde oesophagus histologisch onderzocht en quantitatief beoordeeld op PDT-geïnduceerde weefselschade. In tegenstelling tot voorgaande studies, was er geen heldere correlatie tussen het gefaseerd bleken van PpIX en de histologische respons. Gebaseerd op de resultaten van dit onderzoek kan worden geconcludeerd dat het gefaseerd bleken van PpIX is gerelateerd aan een complexe afhankelijke verhouding tussen PpIX distributie en de aanvoer van zuurstof binnen het belichtte weefsel volume.

Hoofdstuk 7 onderzoekt de mogelijkheden van het monitoren van reflectantie en fluorescentie spectroscopie tijdens therapeutische belichting, zonder deze te onderbreken, in een pre-klinisch interstitiële belichtingsgeometrie gebruikmakend van de lichtgevoelige stof m-THPC. In deze studie werd normaal spierweefsel behandeld 16 uur na m-THPC toediening gebruikmakend van klinisch relevante fluence rates van 50, 100 en 250 mW cm^{-1}. Deze studie demonstreert de mogelijkheid om fluence (rate), fluorescentie, bloed saturatie en bloed volume *in vivo* gedurende PDT. Verschillen in vasculaire respons werden geobserveerd tussen en binnen de verschillende fluence rate groepen. Fluence rate afhankelijke m-THPC bleking werd geobserveerd tot een fluence rate van 100 mW cm^{-1}. Dit laat zien dat de relatie tussen fluence rate en m-THPC bleking complex is in een interstitiële belichtingsgeometrie.

In hoofdstuk 8 wordt het pre-klinische model zoals beschreven in hoofdstuk 7 verder uitgebreid. Als aanvulling op de voorgaande studie wordt nu ook quantitatieve fluorescentie gemeten tijdens de behandeling en wordt de histologische respons onderzocht na een PDT behandeling waarbij gebruik gemaakt wordt van klinisch relevante fluence rates en licht dosis. Hierbij werd ook gekeken naar twee verschillende tijdsintervallen tussen administratie van m-THPC en belichting, van 16 en 96 uur. Voor het histologisch onderzoek werd de behandelde spier 48 uur na PDT verwijderd en beoordeeld. Het histologisch onderzoek liet zien dat de schade door behandeling significant groter was in de groepen met het 16 uur tijdsinterval dan in de groepen met het 96 uur tijdsinterval. Een interessante observatie was het afwezig zijn van celkernen in voornamelijk individuen behandeld 16 uur na m-THPC toediening. Ondanks de variatie in histologische respons, bleven de gemeten waarden voor bloed saturatie en bloed volume tijdens de behandeling relatief constant. De bleking karakteristieken van m-THPC bij verschillende gemeten fluence rates lieten weinig verschil zien in snelheid van bleking voor fluence rates hoger dan 50 mW cm^{-1}.

In hoofdstuk 9 worden de reflectantie en fluorescentie spectroscopie technieken toegepast in een speciale ontwikkelde applicator voor het toedienen van therapeutisch licht voor het behandelen van AIN III. Tot op heden zijn er geen geaccepteerde behandelprotocollen voor AIN III, terwijl AIN III kan leiden tot invasieve anale kanker.
Achtenveertig uur voor therapeutische belichting kregen de patienten m-THPC toegediend. In deze studie werden de belichtingsparameters gestandaardiseerd door de fluence rate *in situ* bij te stellen tot een waarden tussen de 45 en 50 mW cm^{-2}. De behandeling werd gestopt zodra de vooraf vastgestelde lichtdosis, ook gemeten *in situ*, was afgeleverd. De voorlopige resultaten zijn veelbelovend. Echter, verder onderzoek en monitoren is nodig om de mechanismen van m-THPC-PDT te begrijpen.

In hoofdstuk 10 worden de resultaten van de bovenstaande studies bediscussieerd en toekomstige perspectieven worden gepresenteerd.

Curriculum Vitae

Bastiaan Kruijt, born on 28 September 1978, Rotterdam.

I attended primary school at the Kolom (Oude Noorden, Rotterdam) and later at the Jan Prins (Rotterdam-Centrum). After finishing primary school in 1990 at the age of 11 I started secondary school at the Libanon Lyceum (Rotterdam-Kralingen), the first three years at building located at the Mecklenburglaan and the remaining years at the main building located at the Ramlehweg. After graduation in 1995 for HAVO and in 1997 for VWO, I started studying applied physics. The first year of applied physics I attended at the Technical University Delft (Delft). However the second year I continued the study applied physics in a more practical and less theoretical manner at the technical school in Rijswijk, the TH Rijswijk. In my first traineeship at the lung department of Dijkzigt (Erasmus medical center, Rotterdam) I investigated the possibility of differentiating between different lung diseases based on the quantification of the capnogram (this shows the expired CO_2 as a function of the expired volume). After this traineeship I functioned as a technical assistant, employed by the ErasmusMC, at the lung department to determine the bronchial dead space for different lung diseases using capnography.
The second traineeship was at the photodynamic therapy and optical spectroscopy program led by Dick Sterenborg at the Daniel den Hoed kliniek (nowadays merged with the Raman-group of Gerwin Puppels into the center for optical diagnostics and therapy (CODT) located on the 16th floor of the faculty building). Here I investigated the possibility of performing single point spectroscopy of frozen tissue slices using a fluorescence microscopy system and a spectrograph. After this second traineeship I graduated for my Bachelor in Science degree at the TH Rijswijk in 2002.
From 2002 to 2005 I worked at the CODT on several projects. These projects were mostly focused on imaging (fluorescence, laser speckle) and image processing, this involved constructing dedicated imaging setups both hardware and software. From May to Oktober 2005 I was on a stipend in Lund, Sweden, at the medical physics group of Stefan Andersson-Engels. Here I investigated the application of wide field structured illumination microscopy. Following in December 2005 I started research at the CODT under the supervision of Dominic Robinson and Arjen Amelink, which has resulted into the thesis '*in vivo monitoring of photodynamic therapy; from lab to clinic*' that now lies in front of you.

Scientific output

Publications:

Sterenborg HJCM, de Wolf JW, Koning M, **Kruijt B**, van den Heuvel A, Robinson DJ. Phosphoresence-fluorescence ratio imaging for monitoring the oxygen status during photodynamic therapy. Optics Express 12(9), 1873-78 (2004).

Kruijt B, de Bruijn HS, van der Ploeg-van den Heuvel A, Sterenborg HJ, Robinson DJ. Laser speckle imaging of dynamic changes in flow during photodynamic therapy. Lasers Med. Sci. 21(4), 208-212 (2006). *This thesis.*

de Haas ER, **Kruijt B**, Sterenborg HJ, Neumann HA, Robinson DJ. Fractionated illumination significantly improves the response of superficial basal cell carcinoma to aminolevulinic acid photodynamic therapy. J. Invest. Dermatol. 126(12), 2679-86 (2006).

de Bruijn HS, **Kruijt B**, van der Ploeg – van den Heuvel A, Sterenborg HJCM, Robinson DJ. Increase in protoporphyrin IX after 5-aminolevulinic acid based photodynamic therapy is due to local re-synthesis. Photochem. Photobiol. Sci. 6, 857-864 (2007).

Kruijt B, de Bruijn HS, van der Ploeg-van den Heuvel A, de Bruin RWF, Sterenborg HJ, Amelink A, Robinson DJ. Monitoring ALA-induced PpIX-photodynamic therapy in the rat esophagus using fluorescence and reflectance spectroscopy. Photochem. Photobiol. 84(6), 1515-1527 (2008). *This thesis.*

Kaščáková S, **Kruijt B**, de Bruijn HS, van der Ploeg-van den Heuvel A, Robinson DJ, Sterenborg HJ, Amelink A. Ex vivo quantification of mTHPC concentration in tissue: Influence of chemical extraction on the optical properties. J. Photochem. Photobiol. B. 91(2-3), 99-107 (2008). *This thesis.*

Amelink A, **Kruijt B**, Robinson DJ, Sterenborg HJ. Quantitative fluorescence spectroscopy in turbid media using fluorescence differential path length spectroscopy. J. Biomed. Opt. 13(5), 054051 (2008). *This thesis.*

Kruijt B, Kaščáková S, de Bruijn HS, van der Ploeg-van den Heuvel A, Sterenborg HJ, Robinson DJ, Amelink A. In vivo quantification of chromophore concentration using fluorescence differential path length spectroscopy (FDPS). J biomed. opt. 14, 034022 (2009). *This thesis.*

Kruijt B, van der Ploeg-van den Heuvel A, de Bruijn HS, Sterenborg HJ, Amelink A, Robinson DJ. Monitoring interstitial m-THPC-PDT in vivo using fluorescence and reflectance spectroscopy. submitted to lasers in surg med. *This thesis.*

Kruijt B, van der Snoek EM, Sterenborg HJCM, Amelink A, Robinson DJ. A dedicated applicator for light delivery and monitoring of m-THPC-PDT of intra-anal intraepithelial neoplasia grade 3. manuscript in preparation. *This thesis.*

Kruijt B, van der Ploeg-van den Heuvel A, de Bruijn HS, Sterenborg HJ, Amelink A, Robinson DJ. Tissue response after interstitial m-THPC-PDT. manuscript in preparation. *This thesis.*

Presentations:

Kruijt B, Amelink A, de Bruijn HS, Robinson DJ, Sterenborg HJCM. Ratio fluorescence imaging of ALA induced PpIX fluorescence of the skin. Biophotonics 2002, 18-20 October 2002 Crete, Greece (poster).

Kruijt B, Robinson DJ, Sterenborg HJCM, Imaging PpIX fluorescence photobleaching during ALA-PDT of basal cell carcinoma. Biophotonics 2003 graduate summer school, 15-21 June 2003 Ven, Sweden (*poster*).

Kruijt B, Sterenborg HJCM, Robinson DJ. Monitoring capillary blood flow during photodynamic therapy (PDT) of superficial basal cell carcinoma with laser speckle perfusion imaging: a validation of method, molecular medicine day. 21 January 2004, Erasmus MC Rotterdam, the Netherlands (*poster*).

Kruijt B, van den Heuvel A, de Bruijn HS, Sterenborg HJCM, Robinson DJ. Laser speckle imaging of microvascular flow during photodynamic therapy, molecular medicine day. 9 February 2005, Erasmus MC Rotterdam, the Netherlands (*poster*).

Kruijt B, de Bruijn HS, van der Ploeg-van den Heuvel A, Sterenborg HJCM, Robinson DJ. Photobleaching of Foscan at 720nm as possible real-time dose metric parameter during PDT: a feasibility study. Annual symposium UCL, 18 & 19 September 2006, University College London, England (*poster*).

Kruijt B, Kaščáková S, van der Ploeg-van den Heuvel A, de Bruijn HS, Sterenborg HJCM, Robinson DJ, Amelink A. Validation of two optical concentration measurement techniques in vivo on the rat liver," NTROI 2007, Boston, United States (*presentation*).

Kruijt B, de Bruijn HS, van der Ploeg-van den Heuvel A, de Bruin RWF, Sterenborg HJCM, Amelink A, Robinson DJ. Monitoring ALA-induced PpIX-photodynamic therapy in the rat esophagus using fluorescence and reflectance spectroscopy. BIOS SPIE Photonics West 2008, San Jose, United States (*presentation*).

Kruijt B, van der Ploeg-van den Heuvel A, de Bruijn HS, Sterenborg HJCM, Amelink A, Robinson DJ. Monitoring mTHPC (Foscan®) interstitial photodynamic therapy in the rat abdominal muscle using fluorescence and reflectance spectroscopy. IPA 2009, Seattle, United States (*presentation*).

PhD Portfolio Summary

1. PhD training	Year
General academic skills:	
Biomedical english writing and communication	2005 - 2009
Research integrity	2005 - 2009
Research skills:	
Statistics	2005 - 2009
Methodology	2005 - 2009
In-depth courses:	
Biophotonics 2003 graduate summer school	2003
Presentations:	
Posters:	
Biophotonics 2002, Crete, Greece	2002
Biophotonics 2003, Ven, Sweden - Denmark	2003
Molecular medicine day 2004, Rotterdam, the Netherlands	2004
Molecular medicine day 2005, Rotterdam, the Netherlands	2005
Annual symposium, London, England	2006
Presentations:	
Annual symposium, Boston, US	2007
BIOS SPIE Photonics West, San Jose, US	2008
IPA 2009, Seattle, US	2009
International conferences:	
Biophotonics 2002, Crete, Greece	2002
Annual symposium UCL, London, England	2006
Current indications for PDT, Amsterdam, The Netherlands	2006
Annual symposium, Boston, US	2007
BIOS SPIE Photonics West, San Jose, US	2008
IPA 2009, Seattle, US	2009
Seminars and workshops	
Molecular medicine day 2004	2004
Molecular medicine day 2005	2005

Other:

Stipend for 6 months of research at the medical physics group of prof. S. Andersson-Engels, Lund, Sweden (during this time not employed by the ErasmusMC).	2005
Pathology skills (embedding, sectioning, evaluation of tissue)	2006 - 2009
Lasers: maintenance, safety and handling.	2002 - 2006
Development of fiber optics.	2003 - 2009

2. Teaching actvities

(Co-) supervising theses:

Co-supervising thesis: laser speckle imaging
Supervising thesis: detectie van singlet zuurstof luminescentie bij fotodynamische therapie (detection of singlet oxygen luminescence in PDT)

Other:

Transferring knowledge to colleagues/students:	
on construction of fiber-optics	2003 - 2009
on specific (solid) tissue optical phantoms	2003 - 2008
on LabView (programming and controlling hardware)	2004 - 2009

Dankwoord - Acknowledgements

Aangekomen bij de laatste pagina's van welgeteld 47 maanden onderzoek en schrijven. Dit traject heb ik niet alleen afgelegd en mijn dank gaat dan ook uit naar de mensen die mij gedurende dit traject begeleid, geholpen en gesteund hebben op welke wijze dan ook. Mijn dank gaat ook uit naar enkele mensen die mij (on) bewust geholpen hebben keuzes te maken in aanloop naar dit traject.

Een proefschrift schrijven doe je uiteindelijk niet alleen, getuige de co-auteurs op de diverse wetenschappelijke artikelen. Het is uiteindelijk een team van mensen die jou motiveren en waardoor je gemotiveerd wordt tot hetgeen wat nu concreet op tafel ligt.
Dominic Robinson. Dear Dom, you dared to be one of my supervisors from day one. I appreciate your trust in me from the beginning in, apparently, the capacity to write a thesis. I liked the discussions on the sometimes enormous experiments that led to even so elaborate articles. Arjen Amelink. Beste Arjen, jij was mijn begeleider tijdens mijn afstudeer periode en ik vond het geweldig dat jij nu ook co-promotor wilde zijn. Meer dan eens met je scherpe opmerkingen doet mij vermoeden dat je mij soms beter kent dan ik mijzelf. Dick Sterenborg. Beste Dick, het waren drukke tijden voor de groep de afgelopen jaren met onder andere de verhuizing, een nieuw lab en jouw benoeming tot professor. Dit laatste maakt dat jij nu de promotor bent voor dit proefschrift. Bedankt voor de afgelopen jaren.

Hierbij wil ik ook de leden van de kleine commissie bedanken, prof. Peter Levendag, prof. Ben Heijmen en dr. Gerard van Rhoon, voor het willen plaatsnemen in de commissie en het beoordelen van het proefschrift.
Ook wil ik de overige leden bedanken, prof Neumann, dr Witjes en prof Tan, die samen met de kleine commissie de grote commissie vormen.

Natuurlijk zijn er velen mensen met wie ik heb samengewerkt om tot dit geheel te komen. Heel erg belangrijk voor dit proefschrift waren Riette en Lique. Jullie inzet met betrekking tot het dierexperimentele gebeuren is enorm geweest. Niet alleen bij het uitvoeren, maar ook bij het bedenken van de experimenten hebben jullie een grote bijdrage geleverd. Daarnaast was het altijd gezellig om met jullie in het lab te zitten, bedankt voor dit alles, ik ga het erg missen. Lique, naast dat ik altijd ontzettend heb kunnen lachen met jou, vond ik bij jou ook een luisterend oor wanneer ik in een dipje zat. Ik ben erg blij dat jij paranimf wilde zijn.
Hier moet ik ook een ex-collega en vriendin bedanken. Diana, onze uurtjes achter de microscoop tijdens mijn stage, zijn uiteindelijk uitgelopen tot een vriendschap. Ik waardeer dit enorm samen met de gesprekken die we hebben gehad, al laat ik dit misschien niet altijd even goed blijken. Floor, je bent een gezellige kamergenote. De Seattle reis was een erg leuke onderneming na een vermoeiend congres. Succes met je onderzoek. Ute, my other room mate, just started your PhD, good luck and have fun. Slavka, we always seem to have interesting non-work-related funny conversations, I am going to miss that. Good luck with your future. Chad, thanks for the nice discussions, your interest and the occasional drinking, it is always fun. Robert van

‘Veni’, beste Robert ik denk dat je in Jan-Bonne een goede technicus hebt voor het Veni-project, veel succes beiden de komende jaren.
Sinds onze eerste verhuizing naar de centrum lokatie zijn wij gefuseerd met de Raman groep tot het CODT. Kees, Diana, Tom, Peter, Gerwin, Jan-Willem, jullie natuurlijk ook bedankt voor de gezelligheid op de werkvloer.

Veel konden we altijd zelf maken op de afdeling met wat improviseren. Maar als het echt serieus werd en we de middelen zelf niet meer hadden waren daar de collega’s van de medische instrumentatie op de Daniel den Hoed kliniek. Later toen we verhuisden naar de centrum lokatie spraken we de experimentele medische instrumentatie dienst aan onder leiding van Wouter Sjoerdsma. Je kan een ontwerp zo gek niet bedenken of deze mensen vinden een manier om het te realiseren. Bedankt voor jullie hulp bij de diverse ontwerpen die ik door de jaren heen bedacht heb.

Sport is voor mij erg belangrijk, het fungeert als een uitlaatklep en geeft veel nieuwe energie. Het wordt nog leuker als je kan sporten binnen een vereniging en leuke activiteiten kan ondernemen met gezellige mensen zoals bij Euroturn, bedankt! Ik denk dat maar weinigen van jullie echt weten dat dit voor mij een positieve ommekeer was. Trouwens een bijzonder bedankje voor Anneloes, Dineke, Niki, Thomas en Oliver voor het poseren, de cover van hoofdstuk 7. Siske, enorm bedankt voor het ontwerpen van de cover. Mijn tweede paranimf bedank ik ook hierbij, Astrid, ik ben erg blij dat ook jij paranimf wilde zijn bij deze gelegenheid.

Door bezig te zijn met auto’s ben ik al tijden geleden in aanraking gekomen met Tom en Olav. Die-hard auto-hobbyisten waarbij ieder serieus gesprek kan eindigen in de grootste hilariteit waardoor je ook weer even alles relativeert, bedankt. Norman bedankt voor het zo nu en dan even de Irish pub induiken waar onder het genot van een goede whisky we weer even bijpraten over van alles en nog wat. Marc en Mark, dan te bedenken dat we elkaar nog kennen sinds de middelbare school, bedankt voor de uitjes zo nu en dan als we weer allen in 1 land of stad waren.

In preparation for this PhD track, I spend several months doing research in the medical physics group of the Lund laser center. Tack so mycket, Stefan Andersson-Engels, Christoffer Abrahamsson, Johan Axelsson, Thomas Svensson, Jenny Svensson, Nazila Yavira and Florian Forster for your hospitality at work and the activities after work. Ann (Johansson), needless to say but I really enjoyed our conversations and hanging out. The trigger for me, that you partially started, in running resulted in over 280 km of travelled distance in official running events of which 2 complete marathons in the last 4 years. Tack so mycket.

Dan heb ik ook nog Maarten rondlopen, bijna elkaars tegenpolen in veel zaken, maar over 1 ding zijn we het gezamenlijk eens: mensen die vinden dat we qua uiterlijk op elkaar lijken zijn gek. Ondanks alles blijf jij toch mijn broertje, bedankt.

Tenslotte mijn ouders, Kar en Leny, die je toch altijd steunen zolang je maar doet waar je voor staat en er plezier in kan hebben. De steun die ze je geven, zoals na mijn terugkomst uit Zweden. Dankzij jullie steun en motivatie zijn we (Maarten en ik) met plezier toch best goed terechtgekomen. Ik hoop dat ik het later minstens zo goed mag doen als jullie.

q.e.d.